



논문개요집

ISSN 2233-9485(Print)
ISSN 2233-9574(Online)

2021년 한국자기학회 하계학술대회

2021 KMS Summer Conference

논문개요집



일시 2021. 7. 21(수) ~ 23(금)

장소 강릉 세인트존스호텔

주최 한국자기학회

후원     한국재료연구원  파워유닛스마트제조센터

Digests of the 2021 KMS Summer Conference
The Korean Magnetics Society

사단법인 한국자기학회

2021년 한국자기학회 하계학술대회

2021 KMS Summer Conference

논문개요집



일시 2021. 7. 21(수) ~ 23(금)

장소 강릉 세인트존스호텔

주최 한국자기학회

후원 **KOFST** 한국과학기술단체총연합회 **GWTO** 강원도관광재단 **GS/PA** (주)강릉과학산업진흥원 **KIMS** 한국재료연구원 **epU** 파워유닛스마트제조센터

“이 발표논문집은 정부재원(과학기술진흥기금 및 복권기금)으로 한국과학기술단체총연합회의 지원을 받아 발간되었음”

공지사항

1. 포스터발표를 하시는 회원은 아래의 사항을 지켜주시기 바랍니다.

- 1) 포스터보드 크기는 한 명당 가로 100cm X 세로 200cm 사용할 수 있습니다.
- 2) 포스터발표자료는 아래 해당 시간까지 행사장 로비에 설치된 포스터 판넬에 부착해 주시면 됩니다.
[포스터발표 1] 7월 21일(수) 13:00 까지 / [포스터발표 2] 7월 22일(목) 09:00 까지
- 3) 포스터발표 질의응답(Q&A)은 코로나19 확산 방지를 위해 7월 21일(수) 18:00~18:30, 7월 22일(목) 17:30~18:00 사이에 대면이 아닌 온라인 홈페이지를 통해 댓글 형태로 진행됩니다.

2. 일정

7월 21일(수)	08:30~	참가자 등록			
	09:00~12:00	Symposium 1 (Antigua1)			
	13:00~18:00	포스터발표1 (로비)			
	13:00~14:00	과학기술문화 대중화를 위한 프로그램 (Antigua1)			
	14:30~18:00	강습회 (Antigua1)			
	18:00~18:30	포스터발표 Discussion (온라인Q&A)			
7월 22일(목)	08:30~	참가자 등록			
	09:00~18:00	포스터발표2 (로비)			
	09:00~12:30	Symposium 2 (Antigua1)	Symposium 3 (Antigua2)	Symposium 4 (Barbuda1)	Symposium 5 (Barbuda2)
	12:30~14:00	점심식사			
	14:00~17:30	Symposium 6 (Antigua1)	Symposium 3 (Antigua2)	Symposium 7 (Barbuda1)	Symposium 8 (Barbuda2)
	17:30~18:00	포스터발표 Discussion (온라인Q&A)			
	18:00~18:30	한국자기학회 임시총회 및 시상식 (Antigua1)			
	18:30~	저녁식사 (취소)			
7월 23일(금)	08:30~	참가자 등록			
	09:00~12:00	Symposium 9 (Antigua1)	Session 1 (Antigua2)	Symposium 10 (Barbuda1)	
	12:00~	폐회 및 포스터 시상식 (Antigua1)			

3. 7월 22일(목) 저녁 만찬은 코로나19 확산에 따른 영향으로 부득이하게 취소되었습니다.

7월 21일[수]

시간	프로그램
08:30 ~	참가자 등록
	<p>Symposium 1 'Bio-Convergence Magnetics cooperation with M-care center - 자성기반 라이프케어 연구센터 협력 세션' (Antigua1) 좌장 : 김철기(DGIST)</p>
09:00 ~ 09:30	<p>초S-1-1. COVID-19 면역치료제용 항-CD3 단클론항체와 자성나노입자 접합체 개발 및 자기적 특성 연구 이상석(상지대)</p>
09:30 ~ 10:00	<p>초S-1-2. 자성기반 맥박 패턴 측정시스템 오선종(한국기계연구원)</p>
10:00 ~ 10:30	<p>초S-1-3. Magnetic-based Pressure Sensor and its applications for health monitoring 이성원(DGIST)</p>
10:30 ~ 11:00	<p>초S-1-4. Double Hall bar 를 이용한 마이크로 온도계 개발 유천열(DGIST)</p>
11:00 ~ 11:30	<p>초S-1-5. Noise reduction method for PHMR bridge sensor by resistance compensator 임병화(DGIST)</p>
11:30 ~ 12:00	<p>초S-1-6. Real time monitoring of temperature/impedance variations for cell-drug reaction monitoring using semiconductor processed biosensor 장문규(한림대)</p>
13:00 ~ 18:00	<p>포스터발표 1 (로비)</p> <p>[1] Electro-Magnetic Energy Conversion [2] Bio-Convergence Magnetics [3] Magnetics in Medical Science [4] Mössbauer Magnetics [5] Spintronics [6] Magnetization Dynamics [7] Permanent Magnetics</p>
	<p>과학기술문화 대중화를 위한 프로그램 (Antigua1) 좌장 : 정종율(충남대)</p>
13:00 ~ 14:00	<p>O-1. 자석 -마법에서 과학으로- 김갑진(KAIST)</p>
	<p>강습회 '대학원생 진행세션' (Antigua1)</p>
14:30 ~ 16:10	<p>T-1. Introduction to spin Hall effect 이현우(포항공대) 좌장 : 손정훈(포항공대)</p>
16:10 ~ 16:20	Coffee Break
16:20 ~ 18:00	<p>T-2. Spin-transfer torque and current-induced magnetization dynamics 이경진(KAIST) 좌장 : 박은상(고려대)</p>
18:00 ~ 18:30	<p>포스터 발표 discussion (온라인 Q&A) 좌장 : 김상훈(울산대)</p>



7월 22일[목]

시간	프로그램			
08:30 ~	참가자 등록			
09:00 ~ 18:00	포스터발표 2 (로비)			
	Symposium 2 'Spintronics' (Antigua1) 좌장 : 박병국(KAIST)	Symposium 3 'Permanent Magnetics' & 'Electro-Magnetic Energy Conversion' 공동세션 (Antigua2)	Symposium 4 'Quantum Magnetism' 좌장 : 문은국(KAIST) / 손창희(UNIST) (Barbuda1)	Symposium 5 'Magnetic Sensors and Micro-Devices' (Barbuda2)
09:00 ~ 09:20	초S-2-1. Antiferromagnetic Insulatronics: Spintronics without magnetic fields Mathias Kläui (Johannes Gutenberg-University Mainz)	09:00 ~ 09:05 개회사 이우영(연세대) 좌장 : 이정구(KIMS)	09:00 ~ 09:25 초S-4-1. Quantum entangled magnetic exciton in magnetic van der Waals NiPS3 박제근(서울대)	좌장 : 윤석수(안동대) 초S-5-1. 자기 저항 신호를 이용한 저주파수 와전류 센서 개발 연구 김동영(안동대)
09:20 ~ 09:40	초S-2-2. Electrical Spin Current Generation in Ferromagnets and Antiferromagnets Vivek Amin(Purdue University)	09:05 ~ 09:30 초S-3-1. Nd가 저장된 영구자석 회전자와 자유형상 연자성분말 고정자를 활용한 로봇용 서모터 개발에 관한 연구 양상선(KIMS)	09:25 ~ 09:50 초S-4-2. Ferromagnetic spin waves of Cr-based van der Waals honeycomb materials 정재호(고려대)	초S-5-2. 자기센서를 이용한 비파괴 결함탐상 및 인공지능을 이용한 결함 평가 박덕근(㈜아이피트)
09:40 ~ 10:00	초S-2-3. Two-dimensional magnetism and its spintronic device applications 김현호(금오공대)	09:30 ~ 09:55 초S-3-2. MR(자기유변)유체의 차량용 부품 적용 사례 및 기술 동향 이은준(현대로템)	09:50 ~ 10:15 초S-4-3. Noncollinear magnetic order of a new magnetoelectric material determined by single-crystal neutron diffraction 최성균(성균관대)	초S-5-3. 3-축 자기장 gradiometer를 사용한 지하 매설물의 깊이와 크기의 추정 김은애(㈜센서피아)
10:00 ~ 10:20	초S-2-4. Out-of-plane spin polarization and antiferromagnetic spin Hall effect Cheng Song(Tsinghua University)	09:55 ~ 10:20 초S-3-3. 희토자석 최근 시장 및 연구동향 김동환(성림첨단산업)		
10:20 ~ 10:40	초S-2-5. Electrical manipulation of non-collinear antiferromagnet Shunsuke Fukami(Tohoku University)	10:20 ~ 10:45 초S-3-4. 스마트 절연 방법을 이용한 고온 초전도 전자석의 안정성 및 운전 특성 향상 김형욱(한국전기연구원)	10:15 ~ 10:40 초S-4-4. Thermal Hall Transport in Spiral Magnet and Spin Liquid 한정훈(성균관대)	초S-5-4. Carbon fiber 및 Ag/AgCl 전극에 기반한 고감도 수중 전기장 센서 정현주(국방과학연구소)
10:40 ~ 10:50	Coffee Break	10:45 ~ 10:55 Coffee Break	10:40 ~ 10:50 Coffee Break	Coffee Break
10:50 ~ 11:10	초S-2-6. Novel Spintronic Responses of Novel Materials: A Tale of Two Systems Paul Haney(National Institute of Standards and Technology)	좌장 : 이정중(한국전자기술연구원) 10:55 ~ 11:20 초S-3-5. Development Status of Permanent magnets For Vehicle Motor 이형주(현대자동차)	10:50 ~ 11:15 초S-4-5. Deconfinement and hidden phases of U(1) quantum spin liquids 이성빈(KAIST)	좌장 : 신광호(경성대) 초S-5-5. Study on the Possibility of Magnetic Field Communication for High-Sensitivity GMI Sensor 김장열 (한국전자통신연구원)

7월 22일[목]

시간	프로그램						
11:10 ~ 11:30	초S-2-7. Electrically switching ferromagnets by spin orbit torques Kaiyou Wang(CAS)	11:20 ~ 11:45	초S-3-6. Electrical and Mechanical Characteristics Comparison of EV Traction Motor According to Electrical Steel Sheet 정영훈(현대자동차)	11:15 ~ 11:40	초S-4-6. Composite Spin Construction of a Topological Order 황규성(고등과학원)	초S-5-6. Mechanism and manipulation of magnetic microrobot for medical applications 김성훈(원광대)	
11:30 ~ 11:50	초S-2-8. Dynamics of orbital angular momentum in centrosymmetric systems 김경환(KIST)	11:45 ~ 12:10	초S-3-7. 열간-변형 영구자석(hot deformed magnet)기술 동향 및 연구방향 안종빈(㈜디아이씨)	11:40 ~ 12:05	초S-4-7. Field-angle anisotropy of magnetic excitation and specific heat in proximate Kitaev systems under an in- plane magnetic field 김범현(고등과학원)	초S-5-7. 친환경자동차(xEV)용 전류센서의 기술동향 박종민(㈜TNC)	
11:50 ~ 12:10	초S-2-9. Direct Observation of Fe- Ge ordering in Fe5-xGeTe2 Crystals and Resultant Helimagnetism 박정민(KBSI)	12:10 ~ 12:35	초S-3-8. Characteristics of Slotless Motor according to Electrical Steel and Bulk Core Materials 이호영(한국생산기술연구원)			12:05 ~ 12:30	초S-5-8. Development of pin-type magnetic sensing probe with PHR of the 10nT resolution targeting for highly integrated PCB analysis 이남영(디엔제이테크)
12:10 ~ 12:30	초S-2-10. Spin Rotation in Magnetic Metals Xin Fan(University of Denver)						
12:30 ~ 14:00	점심식사						

시간	프로그램						
Symposium 6 'Magnetization Dynamics'		Symposium 3 'Permanent Magnetics' & 'Electro-Magnetic Energy Conversion' 공동세션		Symposium 7 'Mössbauer Magnetics'		Symposium 8 'Theory and Computational Magnetics'	
(Antigua1) 작장 : 김준서(DGIST)		(Antigua2)		(Barbuda1) 작장 : 윤성현(군산대)		(Barbuda2) 작장 : 이관우(고려대)	
14:00 ~ 14:30	초S-6-1. Observation of strong bulk spin-orbit torques in the van der Waals ferromagnet Fe3GeTe2 이규준(고려대)	작장 : 김동환(성림첨단산업)		14:00 ~ 14:25	초S-7-1. Activation Study of Precipitated Iron-Based Catalysts for Fischer-Tropsch Synthesis using Mössbauer Spectroscopy 천동현(한국에너지기술연구원)	14:00 ~ 14:30	초S-8-1. Anomalous exciton and magneto-electric effect in a layered antiferromagnet 손영우(KIAS)
		14:00 ~ 14:25	초S-3-9. Current Research and Challenges of Magnet Additive Manufacturing 하태호(한국기계연구원)				
14:30 ~ 15:00	초S-6-2. Observation of Correlation Between Unidirectional Spin Hall and Magnon Magnetoresistances 김상훈(울산대)	14:25 ~ 14:50	초S-3-10. 전기장만 포화도를 고려한 비대칭 형상을 적용 전동기 토크 특성 연구 윤명환(한국전자기술연구원)	14:25 ~ 14:50	초S-7-2. 철계코어셸 촉매가 적용된 연료 전지용 막전극접합체의 촉매-이온노드 나노계면 제어를 위한 잉크 구조 연구 임성대(한국에너지기술연구원)	14:30 ~ 15:00	초S-8-2. Anomalous Hall effect in compensated collinear ferrimagnet: Symmetry analysis in Mn3Al 박민규(울산대)
15:00 ~ 15:30	초S-6-3. Current and Future Prospect of MRAM technology in Semiconductor Industry 백승현(KIST)	14:50 ~ 15:15	초S-3-11. Toward Development of Grain Boundary Diffusion Process for High-performance Nd-Fe-B Sintered Magnets 김태훈(KIMS)	14:50 ~ 15:15	초S-7-3. The Quantum Theory of Recoilless in Mössbauer Effect 서정철(원광대)	15:00 ~ 15:30	초S-8-3. Terahertz field-induced phase transition via nonlinear phonon interaction 신동빈(Max Planck연구소)
15:30 ~ 15:40	Coffee Break	15:15 ~ 15:40	초S-3-12. 코어 조립공차에 따른 로봇용 액추에이터 특성분석 박민로(한국로봇융합연구원)	15:15 ~ 15:40	초S-7-4. Study on cathode materials using Mössbauer spectroscopy 최현경(국민대)	15:30 ~ 16:00	초S-8-4. All-optical fast control of band topology by exploiting the correlation between Berry curvature and magnetic anisotropy 박노정(UNIST)
15:40 ~ 16:10	초S-6-4. Photoinduced ultrafast magnetization dynamics in ferromagnetic thin films 김동현(충북대)						
		작장 : 임명섭(한양대)					
16:10 ~ 16:40	초S-6-5. The interfacial Dzyaloshinskii-Moriya interaction in the heavy metal/Co/heavy metal sandwiched structure 조재훈(DGIST)	15:50 ~ 16:15	초S-3-13. Fabrication and Magnetic Properties of ThMn12-type Sm(Fe0.8Co0.2)11Ti Bulk 박지훈(KIMS)	15:50 ~ 16:15	초S-7-5. Introduction of Precise Nuclear Measurements and Geostandards 선광민(한국원자력연구원)		
		16:15 ~ 16:40	초S-3-14. 해석적 기법과 PSO알고리즘을 이용한 SPM 전동기의 초기설계 자동화 기법 김우현(충남대)	16:15 ~ 16:40	초S-7-6. Proposals to extending Mössbauer study for the Korean cultural properties 문동혁(국립문화재연구소)		
16:40 ~ 17:10	초S-6-6. Quasi-Static Strain Effect on Ultrafast Magnetization Dynamics 김지완(군산대)	16:40 ~ 17:05	초S-3-15. Grain Boundary Diffusion of La Based Low-melting Alloy to Nd-Fe-B Sintered Magnets 장예령(연세대)	16:40 ~ 17:05	초S-7-7. Facile Synthesis of Fe@Pt Core-Shell Nanoparticles and Their Electrocatalytic Activity for Oxygen Reduction Reaction 이은직(한국에너지기술연구원)		
		17:05 ~ 17:30	초S-3-16. 해석적 방법을 이용한 영구자석 전동기의 특성 해석 이훈기(충남대)				
17:30 ~ 18:00	포스터발표 Discussion (온라인 Q&A) 작장 : 박지훈(KIMS)						
18:00 ~ 18:30	한국자기학회 임시총회 및 시상식 (Antigua1)						
18:30 ~	만찬취소						

7월 23일[금]

시간	프로그램					
08:30 ~	참가자 등록					
Symposium 9 'Low Dimensional Magnetics' (Antigua1) 좌장 : 유정우(UNIST)			Session 1 '신진과학자 콜로키움' (Antigua2) 좌장 : 민병철(KIST)		Symposium 10 'Magnetics in Medical Science' (Barbuda1) 좌장 : 한만석(강원대) / 안우상(울산의대)	
09:00 ~ 09:25	초S-9-1. Controlling the Magnetic Properties of the Van der Waals Ferromagnet Fe3GeTe2 <div>류혜진(KIST)</div>	09:00 ~ 09:15	초O-1-1. Spin wave non-reciprocity in spin superfluids 고경춘(KAIST)	09:00 ~ 09:20	초S-10-1. The Effect of Somatosensory Training in Combination with Low-Frequency Repetitive Transcranial Magnetic Stimulation on Functional Improvement in Stroke Patients <div>한소영(보바스기념병원)</div>	
		09:15 ~ 09:30	초O-1-2. Long-range Spin Transport using Magnon Phonon Coupling 안경모(KRISS)			
09:25 ~ 09:50	초S-9-2. Engineering ferromagnetic lines in graphene by local functionalization using AFM lithography <div>박배호(건국대)</div>	09:30 ~ 09:45	초O-1-3. Demonstration of Core Operations for Skyrmion Racetrack Memory Device 양승모(KRISS)	09:20 ~ 09:40	초S-10-2. Scalability evaluation of resistor charge division circuit for PET detector based on GAPD <div>양진규(전남대)</div>	
		09:45 ~ 10:00	초O-1-4. Spin dependent light emission in organic light emitting diodes with single ferromagnetic electrode 이년중(울산대)			
09:50 ~ 10:15	초S-9-3. Exchange bias effect in van der Waals magnetic materials <div>최준우(KIST)</div>	10:00 ~ 10:15	초O-1-5. Reconfigurable spintronic physical unclonable functions based on spin-orbit torques in ferromagnet/nonmagnet/ferromagnet trilayer structures 이수길(KAIST)	09:40 ~ 10:00	초S-10-3. Optimization of Diverging Collimator for Radiation Monitoring Imaging using Monte Carlo Simulation <div>한동희(강원대)</div>	
10:15 ~ 10:40	초S-9-4. Robust quantum oscillation of Dirac fermions in a single-defect resonant transistor <div>양희준(KAIST)</div>	10:15 ~ 10:30	초O-1-6. Tunable dynamics of exchange-biased domain wall via spin-current-induced antiferromagnet switching 김현중(KRISS)	10:00 ~ 10:20	Coffee Break	
10:40 ~ 10:45	Coffee Break	10:30 ~ 10:45	Coffee Break	10:20 ~ 10:50	초S-10-4. A Review on the Disposal of Radioactive Waste in the Radio-iodine Ward 김정호(선린대)	
10:45 ~ 11:10	초S-9-5. Dirac Fluid Tesla Valves in Graphene <div>김영덕(경희대)</div>	10:45 ~ 11:00	초O-1-7. Effect of post-sintering annealing temperature on the magnetic and microstructural properties of multi-main phase Nd-Ce-Fe-B with high Ce-content 배경훈(KIMS)	10:50 ~ 11:25	초S-10-5. Monte Carlo project of carbon-ion radiation therapy at Yonsei Cancer Center: Present and future <div>한민철(연세대)</div>	
11:10 ~ 11:35	초S-9-6. Ferroelectricity-driven angular momentum textures: from spins and orbitals to Berry curvature <div>진호섭(UNIST)</div>	11:00 ~ 11:15	초O-1-8. Thermal Plasma Synthesis of FexCo1-x Nano-Chained Particles with High Permeability for GHz-band Electromagnetic Wave Absorption 장민선(KIMS)			
11:35 ~ 12:00	초S-9-7. Rashba effects on the transport properties of low-dimensional systems <div>유정우(UNIST)</div>	11:15 ~ 11:30	초O-1-9. Magnetic State Generation using Hamiltonian Guided Variational Autoencoder with Spin Structure Stabilization 권희영(KIST)	11:25 ~ 12:00	초S-10-6. The review of the Task Group 284 report: Magnetic resonance imaging simulation in radiotherapy <div>안소현(연세대)</div>	
		11:30 ~ 11:45	초O-1-10. Role of Demagnetization Field on Permanent Magnet 김남규(KIMS)			
		11:45 ~ 12:00	초O-1-11. Higher-order Topological Magnons in Honeycomb Antiferromagnet 박문집(기초과학연구원)			
12:00 ~	폐회 및 포스터 시상식 (Antigua1)					

CONTENTS

2021 KMS Summer Conference

7월 21일(수) 09:00~12:00

Symposium 1 'Bio - Convergence Magnetics cooperation with
M - care center - 자성기반 라이프케어 연구센터 협력 세션'

Antigua1

✿ 좌 장 : 김철기(DGIST)

초S-1-1	09:00	COVID-19 면역치료제용 항-CD3 단클론항체와 자성나노입자 접합체 개발 및 자기적 특성 연구 3
		최유경, 최상헌, 이보람, 이현숙, 이상석*
초S-1-2	09:30	자성기반 맥박 패턴 측정시스템 4
		오선종*, 김미진, 정영도, 이보연, 김성기, 김철기
초S-1-3	10:00	Magnetic-based Pressure Sensor and its applications for health monitoring 5
		Sungwon Lee*
초S-1-4	10:30	Development micro-thermometer using dual Hall cross bars 6
		Dongryul Kim, Chun-Yeol You*
초S-1-5	11:00	Noise reduction method for PHMR bridge sensor by resistance compensator ... 7
		byeonghwa Lim*, Jaehoon Lee, Changyeop Jeon, Cheol Gi Kim
초S-1-6	11:30	Real time monitoring of temperature/impedance variations for cell-drug reaction monitoring using semiconductor processed biosensor 8
		Gayoung Lee, Jaehun Jeong, Jisu Choi, Yeyeon Kim, Sooyong Shin, Sungho Jeon and Moongyu Jang*

7월 21일(수) 13:00~14:00

과학기술문화 대중화를 위한 프로그램 자석 - 마법에서 과학으로 -

Antigua1

✿ 좌 장 : 정종율(충남대)

O-1	13:00	자석 - 마법에서 과학으로- 11
		김갑진*

7월 21일(수) 14:30~18:00

강습회

Antigua1

✿ 좌 장 : 손정훈(포항공대) / 박은상(고려대)

T-1	14:30	Introduction to spin Hall effect 15
		Hyun-Woo Lee*
T-2	16:20	Spin-transfer torque and current-induced magnetization dynamics 16
		Kyung-Jin Lee*

○ Session EM [Electro-Magnetic Energy Conversion]

- EM01 Poster Coil Arrangement to Reduce AC Copper Loss by Applying Strand and Transposition of Ultra-high-speed Motor for Air Compressor of Fuel Cell Vehicle 19
Sun-Yong Shin*, Jin-Cheol Park, Jun-Woo Chin, Myung-Seop Lim

○ Session MS [Magnetics in Medical Science]

- MS01 Poster Digital Coordinate Determination of 29 x 29 Scintillation Array Detector using Simulated LUT and MLPE 21
Seung-Jae Lee*, Cheol-Ha Baek†
- MS02 Poster Synthesis and Magnetic Characteristics of Gamma Phase Iron oxide and Magnesium Iron oxide Nanoplates for Magnetic Hyperthermia Therapy 22
Pyung Won Im*, Man Seung Heo, Hyung Woo Park, Yona Kim and Sun Ha Paek
- MS03 Poster Use of fast non-local means approach for noise reduction in diffusion weighted magnetic resonance imaging with high b-value 23
Jaeyoung Park, Chang-Ki Kang, Seong-Hyeon Kang, Youngjin Lee*

○ Session MM [Mössbauer Magnetics]

- MM01 Poster 뢰스바우어 분광학을 이용한 $\text{Ba}_2\text{Co}_{1.7}\text{Mg}_{0.3}\text{Fe}_{12}\text{O}_{22}$ 의 자기적 특성 연구 24
백재성*, 심인보, 김철성†
- MM02 Poster Crystal structure and Mössbauer studies of $\alpha\text{-NaFeO}_2$ 26
Jin Gyo Jung*, Hyunkyung Choi, In-Bo Shim, Chul Sung Kim†
- MM03 Poster Synthesis and magnetic properties of iron catalyst $\text{Fe}_{1.5}\text{@Pt/C}$ (Fresh) 28
Hyunkyung Choi*, Jin Gyo Jung, Hyun-Uk Park, Eunjik Lee, Gu-Gon Park, Sung-Dae Yim and Chul Sung Kim†
- MM04 Poster Mössbauer studies on core-shell $\text{Fe}_{1.5}\text{@Pt/C}$ nanoparticles post-heated in NH_3 gas atmosphere 30
Hyunkyung Choi*, Jae Sung Baik, Hyun-Uk Park, Eunjik Lee, Gu-Gon Park, Sung-Dae Yim and Chul Sung Kim†
- MM05 Poster Investigation for Manufacture of the Portable Backscattering Mössbauer Spectrometer 32
Mingi Eom*, Young Rang Uhm, Jaegi Lee, Gwang-Min Sun

○ Session SS [Spintronics]

- SS01 Poster Orbital angular momentum of a domain wall and geometrically twisted magnons 34
Seungho Lee* and Se Kwon Kim

SS02	Poster	Enhanced functionalities in Ruddlesden-Popper oxide thin films employing single-terminated substrate surfaces	35
		Jinkwon Kim*, Youngdo Kim, Junsik Mun, Jeong Rae Kim, Miyoung Kim, Changyoung Kim and Tae Won Noh	
SS03	Poster	Dynamics of a ferrimagnetic domain wall by a rotating field	36
		Munsu Jin*, Ik-Sun Hong, Duck-Ho Kim, Kyung-Jin Lee and Se Kwon Kim	
SS04	Poster	Probing fundamental transport parameters during the phase transition of FeRh by terahertz time domain spectroscopy	38
		Ji-Ho Park*, Yu June Jang, Min Tae Park, Se Kwon Kim, Kyung-Jin Lee, Myung Hwa Jung, Kab-Jin Kim	
SS05	Poster	Valley splitting and enhanced anomalous Hall effect in Mn impurity doped WS ₂ /CrGeSe ₃ heterostructure	39
		Brahim Marfoua* and Jisang Hong [†]	
SS06	Poster	Electric field dependent valley polarization in 2D ferromagnetic WSe ₂ /CrSnSe ₃ heterostructure	40
		Brahim Marfoua* and Jisang Hong [†]	
SS07	Poster	Phase Transition-induced spin pumping in FeRh/Pt	41
		Taekhyeon Lee*, Min Tae Park, Se Kwon Kim, Kyung-Jin Lee, Myung Hwa Jung and Kab-Jin Kim	
SS08	Poster	Unconventional spin-orbit torques arising from 3d/transition metal with an ultrathin Pt insertion layer	42
		Jun-Ho Kang*, Soogil Lee, Woon-Jae Won, Min-Gu Kang, Byong-Guk Park and Kab-Jin Kim [†]	
SS09	Poster	Boron concentration dependence of magnetic properties and structural characteristics of MgO/CoFeB/MgO	43
		Jun-Su Kim*, Gukcheon Kim, Jinwon Jung, Jaehun Cho, Woo-Yeong Kim, Chun-Yeol You [†]	
SS10	Poster	Improved Spin-Orbit Torque Switching Efficiency by He ⁺ Ion Irradiation	45
		Suhyeok An*, Eunchong Baek, Jin-A Kim, Ki-Seung Lee*, Chun-Yeol You [†]	
SS11	Poster	Static and time-resolved optical detection of magnetization vectors by spin Hall effect	46
		Young-Gwan Choi* and Gyung-Min Choi [†]	
SS12	Poster	Investigation of current-induced spin-orbit torques in Pt _x Mn _{1-x} /ferromagnetic heterostructures	47
		Pham Ngoc Luu Ly*, Kyun-Hun Ko and Gyung-Min Choi [†]	
SS13	Poster	Direct Observation of Current-induced Spin Accumulation in InAs Two-dimensional Electron Gas (2DEG) Structure	48
		Won-Bin Lee*, Seong-Been Kim, Kyung-Jin Lee, Kyoung-Whan Kim, Hyun-Cheol Koo and Gyung-Min Choi	
SS14	Poster	Reduced spin-orbit torque switching current by voltage-controlled magnetic easy-cone states	49
		Jimin Jeong*, Min-Gu Kang, Soogil Lee, Byong-Guk Park	

SS15	Poster	Unconventional angle dependence of magnetoresistance in GdO_x 50 Woon-Jae Won*, Jun-Ho Kang, Soogil Lee, Young-Hun Cho, Byong-Guk Park and Kab-Jin Kim
SS16	Poster	Multi-level States of GaMnAsP Single Layer Induced by Spin-orbit Torque 51 Kyung Jae Lee*, Seongjin Park, Phunvira Chongthanaphisut, Sanghoon Lee [†] , X. Liu, M. Dobrowolska and J. K. Furdyna
SS17	Poster	Ruderman-Kittel-Kasuya-Yosida-type interfacial Dzyaloshinskii-Moriya interaction in heavy metal/ferromagnet heterostructures 52 Taehyun Kim*, In Ho Cha, Yong Jin Kim, Gyu Won Kim, Andrey Stashkevich, Yves Roussigné, Mohamed Belmeguenai, Salim M. Chérif, Alexander S. Samardak and Young Keun Kim
SS18	Poster	Current induced magnetization switching in GaMnAsP film with Perpendicular Magnetic Anisotropy 54 Seongjin Park, Kyung Jae Lee*, Phunvira Chongthanaphisut, Sanghoon Lee [†] , X. Liu, M. Dobrowolska and J. K. Furdyna
SS19	Poster	Gigahertz frequency modulation of spin Hall oscillator via voltage controlled magnetic anisotropy engineering 55 Jong-Guk Choi*, Jaehyeon Park, Kab-Jin Kim and Byong-Guk Park
SS20	Poster	Observation of Quantum-like Interference Effect in Graphene-based Devices with Random Co Clusters 56 Thi-Nga Do*, Sehee Lee, Chanyong Hwang, Tae Hee Kim [†]
SS21	Poster	Gate voltage control of spin Seebeck effect 57 Jeong-Mok Kim*, Mingu Kang, Cao-Van Phouc, Jong-Ryul Jeong and Byong-Guk Park
SS22	Poster	Control of magnetization compensation temperature in ferrimagnetic GdCo thin films by He^+ irradiation 59 Jisu Kim*, Seyeop Jeong, Donghyeon Lee, Taekhyeon Lee, Suhyeok An, Kab-Jin Kim, Ki-Seung Lee, Chun-Yeol You, Sanghoon Kim [†]
SS23	Poster	Anomalous Hall effect in a quaternary compensated ferrimagnetic spin gapless semiconductor Heusler compound TiZrMnAl 60 T. Thuy Hoang*, Minkyu Park, Do Duc Cuong, S. H. Rhim and S. C. Hong
SS24	Poster	Observation of spin-current transport in normal metal/Nb/ferromagnet tri-layers 62 Min Hyeok Lee*, Gyungchoon Go, Yong Jin Kim, In Ho Cha, Gyu Won Kim, Taehyun Kim, Kyung-Jin Lee and Young Keun Kim [†]
SS25	Poster	A Spin-Orbit Torque efficiency in W/CoFeB heterostructures with W-Nb alloys insertion layers 63 Seok In Yoon*, Min Hyeok Lee and Young Keun Kim [†]
SS26	Poster	Analysis of magnetic and crystallographic properties of Mn-Ga thin films 64 Jeong Kyu Lee*, Gyu Won Kim, Taehyun Kim, Young Keun Kim
SS27	Poster	Electrical manipulation of exchange bias in IrMn/NiFe heterostructures 65 Jaimin Kang*, Jeongchun Ryu [†] , Jong-Guk Choi, Taekhyeon Lee, Jaehyeon Park, Soogil Lee, Kab-Jin Kim and Byong-Guk Park [†]

SS28	Poster	Thin-film study of molecular spin qubits using a surface-sensitive electron spin resonance spectrometer 67
		Jisoo Yu*, Franklin H. Cho, Luciano Colazzo, Yejin Jeong, Juyoung Park, Junjie Liu, Arzhang Ardavan, Giovanni Boero, Andreas J. Heinrich, Fabio Donati*

○ Session MD [Magnetization Dynamics]

MD01	Poster	Demonstration of the current-driven Bloch line motion for novel magnetic memory operation 68
		Jiseok Yang*, Kyoung-Woong Moon, Min Gyu Park, Soogil Lee, Sanghoon Kim, Mincheol Shin and Kab-Jin Kim
MD02	Poster	Double Walker Breakdown of Ultrathin Magnetic Double Layers 69
		Jaesung Yoon*, Joon Moon, Kitae Kim, Seong-Hyub Lee, Sug-Bong Choe*
MD03	Poster	A 3-dimensional control of exchange bias by spin orbit torque in Pt/Co/IrMn heterostructure 70
		Eunchong Baek*, Suhyeok An, Woo-Yeong Kim, Ki-Seung Lee and Chun-Yeol You†
MD04	Poster	The trapezoidal shaped wire driven Domain wall dynamics under perpendicular magnetic anisotropy system 71
		Dongryul Kim*, Woo-Yeong Kim, Suhyeok An, Eunchong Baek, Ki-Seung Lee, Chun-Yeol You†
MD05	Poster	Scaling law of magnetic skyrmion motion in the creep regime 72
		Moojune Song*, Mujin You, Seungmo Yang, Min Gyu Park, Kab-Jin Kim
MD06	Poster	Theoretical finding of robust dynamics of spin waves channeled in antiferromagnetic domain walls 73
		Hyeon-Kyu Park* and Sang-Koog Kim†
MD07	Poster	Highly efficient heat-dissipation power driven by ferromagnetic resonance in superparamagnetic nanoparticles of ferrimagnetic MFe_2O_4 ($M = Fe, Mn, Ni$) 74
		Jae-Hyeok Lee, Yongsu Kim* and Sang-Koog Kim†
MD08	Poster	Split-gap orientation dependence of photon-magnon coupling strength in two inverted split ring resonators 75
		Haechan Jeon*, Biswanath Bhoi, Bosung Kim, Loïc Millet and Sang-Koog Kim†
MD09	Poster	Broadband photon-magnon coupling using multiple photon resonators 77
		Seung-Hun Jang*, Biswanath Bhoi, Bosung Kim and Sang-Koog Kim†
MD10	Poster	The change of interfacial magnetic properties depends on the stacking order in magnetic tri-layer systems 78
		Jinyong Jung*, Jaehun Cho, Hyeok-Cheol Choi, Kwang Hyun Lee, Chun-Yeol You†, Sug-Bong Choe, June-Seo Kim
MD11	Poster	Conceptual design of time- and frequency-division demultiplexer: Coupled-gyration-propagation signal in arrays of vortex-state circular and chopped disks 79
		Bosung Kim*, Young-Jun Cho and Sang-Koog Kim†

MD12	Poster	Effect of controlled stoichiometric vanadium oxide with respect to magnetic properties in Pt/Co/VO _x heterostructure	81
		Kwonjin Park*, Jae-Hyun Ha, Jinyong Jung, Jaehun Cho, Jung-Il Hong*, Chun-Yeol You†	
MD13	Poster	Coupling induced transparency and absorption in photon-magnon coupling	83
		Biswanath Bhoi*, Bosung Kim, Haechan Jeon and Sang-Koog Kim†	
MD14	Poster	Magneto-Optical Kerr Measurement using Ultrafast Sagnac Interferometer	84
		Yooleemi Shin and Ji-Wan Kim*	
MD15	Poster	Dynamics of magnetic skyrmion bags induced by spin-transfer torques	85
		Suyeong Jeong*, Hee-Sung Han, Dae-Han Jung, Ganghwi Kim and Ki-Suk Lee	
MD16	Poster	Magnetic field tunability of a skyrmion diode	86
		Dae-Han Jung*, Hee-Sung Han, Ganghwi Kim, Suyeon Jeong and Ki-Suk Lee*	
MD17	Poster	Symmetry-breakings for unidirectional skyrmion motions under spin-orbit and -transfer torques	88
		Dae-Han Jung*, Hee-Sung Han, Ganghwi Kim, Suyeon Jeong and Ki-Suk Lee*	

○ Session PM [Permanent Magnetics]

PM01	Poster	Compositional development of M-type hexaferrite magnet without sintering additives	89
		Jin-Young You, Ji-Hye Lee, Jun-Pyo Lim, Min-Ho Kim, Young-Min Kang*	
PM02	Poster	HDDR 처리된 Nd-Fe-계 소결자석의 미세구조 변화가 자기적 특성에 미치는 영향	90
		노태성*, 차희령, 김태훈, 김양도†, 이정구†	
PM03	Poster	Structure and magnetic properties of BaFe ₁₂ O ₁₉ Nanoparticles	91
		Jae-Young Choi*, Jeong-Min Lee, Youn-Kyung Baek, Jung-Goo Lee, Young Kuk Kim†	
PM04	Poster	Na-La-Co계 M형 페라이트의 합성과 자기적 특성	92
		손성우*, 김부안†, 권해웅†, 최재영, 이정구	
PM05	Poster	Coercivity improvement in Nd-Cu infiltrated Nd-Fe-B hot-deformed magnets by controlling microstructure of initial HDDR powders	93
		Jae-Gyeong Yoo*, Tae-Hoon Kim, Hee-Ryoung Cha, Yang-Do Kim*, Jung-Goo Lee†	
PM06	Poster	Systematic process control for high performance MnBi magnets	95
		Su Yeon Ahn*, Yang Yang, Jung Tae Lim, Jihoon Park, Jong-Woo Kim, Soon Chul Hong, Chul-Jin Choi	
PM07	Poster	Effects of Sn Addition on the Microstructure and Magnetic Properties of MnBi Bulk Magnets	96
		Yang Yang*, Jung Tae Lim, Jihoon Park, Hui-Dong Qian, Oi Lun Li, Jong-Woo Kim*, Chul-Jin Choi†	
PM08	Poster	Influence of grain boundary diffusion process on grain alignment and magnetic properties of Nd lean Nd-Fe-B hot-deformed magnets	98
		Ga-Yeong Kim*, Tae-Hoon Kim, Hee-Ryoung Cha, Yang-Do Kim* and Jung-Goo Lee†	

PM09	Poster	Phase transformation and magnetic properties of ThMn_{12} structure Sm-Fe-Co-Ti-Si magnetic ribbons 99 Hui-Dong Qian*, Jung Tae Lim, Yang Yang, Jong-Woo Kim, Su Yeon Ahn, Hankuk Jeon, Tian Hong Zhou, Kyung Mox Cho, Jihoon Park*, Chul-Jin Choi [†]
PM10	Poster	Effect of Ti and V content on the magnetic properties of $\text{Sm}(\text{FeCo})_{12}$ -based magnets produced by melt-spinning method 101 Tianhong Zhou*, Hui-Dong Qian, Jihoon Park, Yong-Rae Cho, Chul-Jin Choi [†]
PM11	Poster	Magnetic properties and microstructure evaluation of $(\text{Sm}_{0.9}\text{Zr}_{0.1})$ $(\text{Fe}_{0.75}\text{Co}_{0.25})_{11.35}\text{Ti}_{0.65}$ particles with ThMn_{12} structure produced by reduction diffusion process 103 Hankuk Jeon*, Jung Tae Lim, Hui-Dong Qian, Jihoon Park, Hyo-Jun Ahn and Chul-Jin Choi
PM12	Poster	Melt-spinning 법을 이용한 Nd-Fe-B분말의 전열처리에 따른 열간 변형 영구자석의 입자거동 및 자기특성 변화 104 황진성*, 안종빈, 최판규
PM13	Poster	머신 러닝 기반 High Br 54SH Grade 영구자석 입계확산 최적 공정 도출 연구 105 임현석*, 이철희, 나현민, 배석, 김동환
PM14	Poster	The effect of iron deficiency and additives of La-Co substituted Sr M-type hexaferrites on the Magnetic properties 106 Kanghyuk Lee*, Junho Park, SungJoon Choi and Sang-Im Yoo [†]
PM15	Poster	Synthesis and Characterization of SmFe_{12} -based compounds prepared by reaction-diffusion reaction 107 Kang-Hyuk Lee*, SungJoon Cho and Sang-Im Yoo [†]
PM16	Poster	Enhancing magnetic and structural properties of chemically prepared Nd-Fe-B particles by reduction- diffusion method through optimization of heat treatments 108 Rambabu Kuchi*, Seunghyun Kim, Vitalii Galkin, Dongsoo Kim [†]
PM17	Poster	Chemical synthesis of NdFeB particles with enhanced magnetic properties through planetary ball milling process of oxide powders 109 Seunghyun Kim*, Rambabu Kuchi, Vitalli Galkin, Dongsoo Kim [†]
PM18	Poster	Intrinsic Hard Magnetism and Thermal Stability of ThMn_{12} -Type Permanent Magnet: Density Functional Theory and Monte Carlo Simulation 110 Tumentsereg Ochirkhuyag*, Soon Cheol Hong* and Dorj Odkhuu [†]
PM19	Poster	Micromagnetic Studies on the Enhancement of the Coercivity of B-doped $\text{Sm}(\text{Fe}_{0.8}\text{Co}_{0.2})_{12}$ Thin Film by Forming Amorphous Grain Boundary 112 Ganghwi Kim*, Dae-Han Jung, Suyeong Jeong, Namkyu Kim and Ki-Suk Lee
PM20	Poster	First principles studies of new type of rare-earth free permanent magnet: $\text{Co}_3\text{Mn}_2\text{Al}$ 113 Dorjsuren Tuvshin*, Tumentsereg Ochirkhuyag, Soon Cheol Hong [†] and Dorj Odkhuu [†]

○ Session SM [Soft Magnetics]

SM01	Poster	Electromagnetic wave absorption properties of M-type hexaferrite-perovskite manganese composites and bilayers	114
		Jae-Hee Heo, Young-Min Kang*	
SM02	Poster	Electromagnetic wave absorption properties of multistacked hexaferrite-epoxy composites	115
		Jae-Uk Kim, Young-Min Kang*	
SM03	Poster	Electromagnetic microwave absorption properties of Mn-Ti substituted M-type Ba hexaferrite-epoxy composites	116
		Su-Mi Lee, Min-Gu Kang, Young-Min Kang*	
SM04	Poster	Coercive field variation of Co/Pt multilayer depending on Co thickness and annealing temperature	117
		Seungha Yoon*	
SM05	Poster	Metal FDM 공정으로 제작된 등방성 미세조직의 17-4PH 스테인리스 강의 기계적 및 자성 특성 분석	118
		Kwangsue Choi*, Seonghoon Yi, Hyo Yun Jung†	
SM06	Poster	Comparison of structural, microstructure, and magnetic properties of nickel nanowires according to the shape of the magnetic field	119
		Min Ji Shin*, Su Jeong Park, Akshay Kumar, Kavita Kumari, Seok Hwan Huh* and Bon Heun Koo†	
SM07	Poster	Excellent absorption properties of Zn-substituted SrW-type hexaferrites in Ka-band for 5G application	120
		Sungjoon Choi*, Seung-Young Park and Sang-Im Yoo	
SM08	Poster	Curvature-Induced symmetry breaking of Néel Caps in asymmetric ferromagnetic disk	121
		Myeonghwan Kang*, Hee-Sung Han, Sooseok Lee, Young-Sang Yu, Soong-Geun Je, Hye-Jin Ok, Weilun Chao, Mi-Young Im and Ki-Suk Lee†	
SM09	Poster	Silane 첨가량에 따른 Fe-Ni 코어 효율 향상에 관한 연구	122
		김예래*, 안지훈, 이민영, 이보화	
SM10	Poster	BiFeO ₃ 의 전자기파 차폐가능한 주파수 이동에 관한 특성 연구	123
		정우현*, 이민영, 김상우, 유성초, 이보화	
SM11	Poster	Enhanced microwave absorption properties of La-doping Ba ₃ Co ₂ Fe ₂₄ O ₄₁ hexaferrite in the frequency range of 2-18 GHz	124
		W.H. Jeong*, N. Tran and B.W. Lee	
SM12	Poster	Spin-wave multiplets excited in Sierpiński-like fractals	125
		Gyuyoung Park* and Sang-Koog Kim	

SM13	Poster	NiCuZn-ferrite코팅에 따른 Fe-Si-Al의 자기적 특성 연구 126 김대유*, 안지훈, 박봉태, 우혁준, 이보화
SM14	Poster	FeCo@MnO ₂ with a high microwave absorption and wide bandwidth using two-step method: Effect of MnO ₂ layer thickness on magnetic/ electromagnetic properties 127 Yeong Jun Park*, Jong Hwan Park, Su Jeong Suh, Byeong Sun Cho
SM15	Poster	Effect of P addition on the Microstructure and Magnetic Properties of Fe _{83.2} Si _{5.33-0.33x} B _{10.67-0.67x} P _x Cu _{0.8} Nanocrystalline Soft Magnetic Alloys 128 Hyun Ah Im*, Subong An, Kyoung-Hoon Bae, Sangsun Yang, Jung Woo Lee and Jae Won Jeong [†]
SM16	Poster	Characteristics of crystalline and amorphous soft magnetic cores from Fe-based soft magnetic powders 129 Minwoo Lee*, Yeonjoo Lee, Dohoon Kwon, Eunji Cha, Sungmin Kim, Daewon Jung, Hwijun Kim [†]
SM17	Poster	졸-겔법으로 형성된 분말 표면 SiO _x 절연층이 연자성 복합체의 고온 열처리 후 자기적 특성에 미치는 영향 130 박종민*, 장민선, 구본욱, 김혜란, 권영태, 양상선, 이정우, 정재원
SM18	Poster	Effect of Ce/La addition on the soft magnetic properties in Fe-Si-B-P amorphous alloys 132 Young-Sin Choi*, Min-Woo Lee, Do-Hun Kwon, Eun-Ji Cha, Jong-Ryoul Kim and Hwi-Jun Kim [†]
SM19	Poster	충진율에 따른 Ni-Zn 페라이트의 차폐특성 향상 133 김상우*, 이민영, 우혁준, 이보화
SM20	Poster	Magnetic Properties as Fe/Co Ratio Variation in Fe-Co-V Alloy System 134 Hyunsol Son*, Haein Choi-Yim [†]
SM21	Poster	Thermal and Soft Magnetic Properties of Fe-Co-B-Si-Nb Amorphous Ribbons as Fe/Co Ratio Variation 135 Hyunsol Son*, Haein Choi-Yim [†]

○ Session TC [Theory and Computational Magnetism]

TC01	Poster	Understanding of magnetic cobalt spinel: A first-principles study 136 Inseo Kim*, Hyungwoo Lee, Ho-Hyun Nahm, Minseok Choi
TC02	Poster	First-principles study of two dimensional magnetic oxides 137 Hyungwoo Lee*, Minseok Choi
TC03	Poster	Strain effect on magnetic properties of atomically thin Fe ₃ GeTe ₂ 138 Gyeonghye Kim*, Qurat ul Ain, Soon Cheol Hong and S. H. Rhim
TC04	Poster	Spin Hall Conductivities of W-N Alloys 139 Quynh Anh T. Nguyen*, D. D. Cuong, S. C. Hong and Sonny H. Rhim
TC05	Poster	Anomalous Hall and Nernst Effect in Mn ₃ Al under Volume Change 140 Guihyun Han*, Minkyu Park, Soon Cheol Hong and S. H. Rhim

TC06	Poster	Anomalous Hall signatures of nonsymmorphic nodal lines in doped chromium chalcospinel CuCr_2Se_4 141 Subhasis Samanta, Gang Chen and Heung-Sik Kim*
TC07	Poster	Symmetry Effects on Magnetocrystalline Anisotropy of hcp and fcc Cobalt: a First-principles Study 142 Thi H. Ho*, Sonny H. Rhim and S. C. Hong
TC08	Poster	Role of Fe intercalation in bilayer MoS_2 143 Jin Jae Park*, G. Hye Kim, Soon Cheol Hong and S. H. Rhim
TC09	Poster	정방 왜곡에 따른 덩치 Mn_4C 의 스핀 구조 : 제일원리 계산 144 이준규*, 웬 티 꾸인 안, 호 후인 티, 임성현, 홍순철*

○ Session QM [Quantum Magnetism]

QM01	Poster	Tunable Two-channel Magnetotransport in SrRuO_3 Ultrathin Films Achieved by Controlling the Kinetics of Heterostructure Deposition 146 Eun Kyo Ko*, Han Gyeol Lee [†] , Sangmin Lee, Junsik Mun, Jinkwon Kim, Ji Hye Lee, Tae Heon Kim, Jin-Seok Chung, Suk Bum Chung, Miyoung Kim, Seo Hyoung Chang* and Tae Won Noh [†]
QM02	Poster	Anomalous Hall Effect in (111)- LaNiO_3 Thin Films with CaTiO_3 Capping Layer 147 Ji Hye Lee*, Hongjoon Kim, Jeong Rae Kim, Tae Won Noh
QM03	Poster	Investigation of ferromagnetic state of SrRuO_3 thin films by optical second harmonic generation 148 Chang Jae Roh*, Jeong Rae Kim, Jong Seok Lee and Tae Won Noh
QM04	Poster	Non-BCS-type Superconductivity and its Correlation to Ferromagnetism in $\text{SrTiO}_3/\text{LaAlO}_3/\text{SrTiO}_3$ trilayer heterostructure 149 Yongsu Kwak [†] , Woojoo Han, Jinhee Kim, Jonghyun Song*

○ Session LM [Low Dimensional Magnetism]

LM01	Poster	Switching behaviors of NiFe nanorings on carbon nanotubes 150 Seungha Yoon*
LM02	Poster	Comparison of Coercivity and Ferromagnetic resonance frequency of Ferrites that Absorb Millimeter Waves 151 Gi-Ryeon Jo*, Min-Ji Pyo, Young-Guk Son, Youn-Kyoung Baek [†]
LM03	Poster	Single atomic spin sensing of magnetic interactions in a tunnel junction 152 Jinkyung Kim*, Won-jun Jang, Thi Hong Bui, Deung-Jang Choi, Christoph Wolf, Fernando Delgado, Yi Chen, Denis Krylov, Soonhyeong Lee, Sangwon Yoon, Christopher P. Lutz, Andreas J. Heinrich* and Yujeong Bae*
LM04	Poster	Home-built sub-Kelvin scanning tunneling microscope with electron spin resonance capability 153 Jiyeon Hwang*, Denis Krylov, Taehong Ahn, Lei Fang, Kyungju Noh, Andreas J. Heinrich [†] and Yujeong Bae [†]

LM05	Poster	Investigating the structural, magnetic and magnetocaloric properties in B-site Mo-doped $\text{La}_{1.4}\text{Ca}_{1.6}\text{Mn}_{2-x}\text{Mo}_x\text{O}_7$ ($0 \leq x \leq 0.3$) bilayer manganites	154
		Akshay Kumar*, Kavita Kumari, Minji Shin, Seok Hwan Huh and Bon Heun Koo†	
LM06	Poster	Magnetic properties of LDH based low temperature synthesis of spinel oxide nanoparticle	155
		Jun Han Lee*, Jaejung Song, Jae Won Jeong, Seungho Cho and Yoon Seok Oh	
LM07	Poster	Effect of reaction time on the structural, morphological and magnetic properties of Fe ₃₀ Co ₇₀ nanoparticles	156
		Kavita Kumari*, Akshay Kumar, Minji Shin, Huh Seok Hwan and Bon Heun Koo†	
LM08	Poster	Electron Spin Resonance of Atoms on a Surface	157
		Yujeong Bae*	
LM09	Poster	CoFe/MnIr박막의 투자율 스펙트럼 분석	158
		김동영*, 윤석수	
LM10	Poster	Charge Trapping Memory Device Based on MoS ₂ FET with CrPS ₄	159
		Minjeong Shin*, Mi Jung Lee, Chansoo Yoon, Gwangtak Oh, Woohyeon Ryu, Sungmin Lee, Je-Geun Park, Bea Ho Park*	
LM11	Poster	Effect of Underlayer, CoFeB Composition and Annealing Temperature on Perpendicular Magnetic Anisotropy of CoFeB	160
		Han Seok Ko*, Taehyun Kim, Jiyoung Lee, Young Keun Kim	
LM12	Poster	Stoner-Wohlfarth Model with Standard Deviation of Magnetic Easy Axis to Understand Magnetization Switching of Granular Films	162
		Donghyeon Lee*, Donghyeon Han, Seyeop Jung, Nyunjong Lee, Suzuki Ippei, Takahashi Yukiko, Sanghoon Kim*	
LM13	Poster	Magnetic difference with MoS ₂ and Oxidized MoS ₂ fabricated by Local chemical modification	163
		DaYea Oh*, Duk Hyun Lee, Won Dong Kim, Woo Hyeon Ryu, Gwang Taek Oh, Jong Wan Son, Bae Ho Park*	
LM14	Poster	Manipulation of Magnetic Skyrmion by Localized Magnetic Field	164
		Sooseok Lee*, Hee-Sung Han, Dae-Han Jung, Myeonghwan Kang, Hye-Jin Ok, Namkyu Kim and Ki-Suk Lee†	
LM15	Poster	Stochastic Switching in Array of Co/Pt Nanodisks	165
		Hee-Sung Han*, Sooseok Lee, Soong-Geun Je, Myeonghwan Kang, Hye-Jin Ok, Namkyu Kim, Weilun Chao, Mi-Young Im* and Ki-Suk Lee†	
LM16	Poster	Optimization of spin Seebeck properties in YIG thin film by tuning the PVP concentration in MOD solution	166
		Trinh Nguyen Thi, Phuoc Cao Van, Jong-Ryul Jeong*	

○ Session SD [Magnetic Sensors and Micro-Devices]

SD01	Poster	Majority gate logic using current-induced magnetic domain wall motion	167
		San Ko*, Geun-Hee Lee, Byong-Guk Park and Kab-Jin Kim	
SD02	Poster	TMR sensor development for ultra-high frequency field applications	168
		Seungha Yoon*	

SD03	Poster	Individual and Collective Locomotion Control of Magnetic Microrobots Using a Single Electromagnet System	169
		Seungchan Hwang, Armando Ramos Sebastian*, Minseo Goo, Changho Yu, Sung Hoon Kim [†]	
SD04	Poster	Using Amorphous CoB Alloy as Transducer to Detect Acoustic Propagation and Heat Transport at Interface	170
		Liu Jina*, Gyung-Min Choi	
SD05	Poster	Modified torque magnetometry to determine magnetic anisotropy	171
		Joonyoung Choi, In Hyuk Jo, Younjung Jo*	
SD06	Poster	Machine learning based Human Activity Recognition with mobile 3-axis magnetometers	172
		Chunghee Nam*	

○ Session OS [Others]

OS01	Poster	A New Strategy of Finger Rehabilitation: Wireless Magnetic Actuation for Pinch motion	173
		지동민*, 송원일, 김성훈	
OS02	Poster	Optimization of Polycrystalline-YIG with a High Magnetization <i>via</i> the Correlation Between Mechanical Compression and Heat-Treatment in the Sol-Gel Synthesis	174
		Hye-Jin Ok*, Min-Sun Jang, Inseon Oh, Jung-Woo Yoo and Ki-Suk Lee	
OS03	Poster	Landau Level Tomography, Valley Chern Number, Nernst Effect in Moiré Superlattices	176
		J. A. Crosse and Pilkyung Moon*	
OS04	Poster	The effects of spin-Peierls distortion on thermoelectric properties: a first principle study of TiPO_4	177
		Changhoon Lee*, Taesu Park, Ji Hoon Shim	
OS05	Poster	희토류 자석합금의 균질화 및 HDDR 처리에 관한 연구	178
		김상욱*, 김인호, 송창빈	

7월 22일(목) 09:00~12:30
Symposium 2 'Spintronics'

Antigua1

✿ 좌 장 : 박병국(KAIST)

초S-2-1	09:00	Antiferromagnetic Insulatronics: Spintronics without magnetic fields	181
		Mathias Kläui*	
초S-2-2	09:20	Electrical Spin Current Generation in Ferromagnets and Antiferromagnets ..	183
		Vivek Amin*, Fei Xue, Paul Haney, Mark Stiles	
초S-2-3	09:40	Two-dimensional magnetism and its spintronic device applications	184
		Hyun Ho Kim*	

초S-2-4	10:00	Out-of-plane spin polarization and antiferromagnetic spin Hall effect 185 Cheng Song*, Xianzhe Chen, Xiaofeng Zhou, Hyunsoo Yang, Feng Pan
초S-2-5	10:20	Electrical manipulation of non-collinear antiferromagnet 186 Shunsuke Fukami*
초S-2-6	10:50	Novel Spintronic Responses of Novel Materials: A Tale of Two Systems 188 Paul Haney*, Fei Xue, Duarte Pereira de Sousa, Jian-Ping Wang, Tony Low
초S-2-7	11:10	Electrically switching ferromagnets by spin orbit torques 189 Kaiyou Wang*
초S-2-8	11:30	Dynamics of orbital angular momentum in centrosymmetric systems 190 Seungyun Han, Kyoung-Whan Kim*, Hyun-Woo Lee
초S-2-9	11:50	Direct Observation of Fe-Ge ordering in Fe _{5-x} GeTe ₂ Crystals and Resultant Helimagnetism 191 Trinh Thi Ly, Jungmin Park*, Kyoo Kim, Hyo-Bin Ahn, Nyun Jong Lee, Kwangsu Kim, Tae-Eon Park, Ganbat Duvjir, Nguyen Huu Lam, Kyuha Jang, Chun-Yeol You, Younghun Jo, Se Kwon Kim, Changgu Lee, Sanghoon Kim, Jungdae Kim
초S-2-10	12:10	Spin Rotation in Magnetic Metals 192 Xin Fan*

7월 22일(목) 09:00~17:30

Symposium 3 'Permanent Magnetics' & 'Electro - Magnetic Energy Conversion' 공동세션

Antigua2

❀ 좌 장 : 이정구(KIMS) / 이정종(한국전자기술연구원) / 김동환(성림첨단산업) / 임명섭(한양대)

초S-3-1	09:05	Nd가 저감된 영구자석 회전자와 자유형상 연자성분말 고정자를 활용한 로봇용 서모보터 개발에 관한 연구 195 양상선*, 김용진, 정재원, 권영태, 차희령, 김태훈, 이정구
초S-3-2	09:30	MR유체의 차량용 부품 적용사례 및 기술동향 196 Eunjun Rhee*, Kyongho Kang
초S-3-3	09:55	희토자석 최근 시장 및 연구동향 197 김동환*
초S-3-4	10:20	스마트 절연 방법을 이용한 고온 초전도 전자석의 안정성 및 운전 특성 향상 198 김형욱*, 조영식, 김석환
초S-3-5	10:55	Development Status of Permanent magnets for Vehicle Motor 200 Hyungju Lee*
초S-3-6	11:20	Electrical and Mechanical Characteristics Comparison of EV Traction Motor According to Electrical Steel Sheet 201 Young-Hoon Jung*, Jin-Cheol Park, Myung-Seop Lim
초S-3-7	11:45	열간-변형 영구자석(hot deformed magnet)기술 동향 및 연구방향 203 안종빈*, 황진성, 최판규

초S-3-8	12:10	Characteristics of Slotless Motor according to Electrical Steel and Bulk Core Materials 204 Ho-Young Lee*, Gi-Ju Lee, Jin-Yeong Shin, Seung-Young Yoon, Myeong-Sik Jeong and Soon-O Kwon
초S-3-9	14:00	Current Research and Challenges of Magnet Additive Manufacturing 206 Taeho Ha*, Joon Phil Choi, Hakseuon Lee
초S-3-10	14:25	전기강판 포화도를 고려한 비대칭 형상을 적용 전동기 토크 특성 연구 207 윤명환*, 이기덕, 이정중
초S-3-11	14:50	Toward Development of Grain Boundary Diffusion Process for High-performance Nd-Fe-B Sintered Magnets 208 Tae-Hoon Kim* and Jung-Goo Lee
초S-3-12	15:15	코어 조립공차에 따른 로봇용 액추에이터 특성분석 209 박민로*, 박진철, 신선용, 이수경, 임명섭
초S-3-13	15:50	Fabrication and Magnetic Properties of ThMn ₁₂ -type Sm(Fe _{0.8} Co _{0.2}) ₁₁ Ti Bulk 211 Jihoon Park*, Hui-Dong Qian, Jung Tae Lim, Jong-Woo Kim and Chul-Jin Choi
초S-3-14	16:15	해석적 기법과 PSO알고리즘을 이용한 SPM 전동기의 초기설계 자동화 기법 212 Woo-Hyeon Kim*, Kyung-Hun Shin, Gang-Hyeon Jang, Hoon-Ki Lee, Jang-Young Choi
초S-3-15	16:40	Grain Boundary Diffusion of La Based Low-melting Alloy to Nd-Fe-B Sintered Magnets 213 Ye Ryeong Jang*, Hyungju Lee, Jaeryung Lee, Hyun-Sook Lee [†] and Wooyoung Lee [†]
초S-3-16	17:05	해석적 방법을 이용한 영구자석 전동기의 특성 해석 215 이훈기*, 최장영 [†]

7월 22일(목) 09:00~12:05

Symposium 4 'Quantum Magnetism'

Barbuda1

✿ 좌 장 : 문은국(KAIST) / 손창희(UNIST)

초S-4-1	09:00	Quantum entangled magnetic exciton in magnetic van der Waals NiPS ₃ ... 219 Je-Geun Park*
초S-4-2	09:25	Ferromagnetic spin waves of Cr-based van der Waals honeycomb materials ... 220 Jae-Ho Chung*, Lebing Chen and Pengcheng Dai
초S-4-3	09:50	Noncollinear magnetic order of a new magnetoelectric material determined by single-crystal neutron diffraction 222 Sungkyun Choi*
초S-4-4	10:15	Thermal Hall Transport in Spiral Magnet and Spin Liquid 224 Jung Hoon Han*
초S-4-5	10:50	Deconfinement and hidden phases of U(1) quantum spin liquids 225 SungBin Lee*

초S-4-6	11:15	Composite Spin Construction of a Topological Order 226 Kyusung Hwang*
초S-4-7	11:40	Field-angle anisotropy of magnetic excitation and specific heat in proximate Kitaev systems under an in-plane magnetic field 227 Beom Hyun Kim*

7월 22일(목) 09:00~12:30

Symposium 5 'Magnetic Sensors and Micro - Devices'

Barbuda2

✿ 좌 장 : 윤석수(안동대) / 신광호(경성대)

초S-5-1	09:00	자기 저항 신호를 이용한 저주파수 와전류 센서 개발 연구 231 김동영*, 윤석수
초S-5-2	09:25	자기센서를 이용한 비파괴 결함탐상 및 인공지능을 이용한 결함 평가 232 박덕근*, 김재민, 서호건, 이진이
초S-5-3	09:50	3-축 자기장 gradiometer를 사용한 지하 매설물의 깊이와 크기의 추정 233 김은애*, 손대락, 류권상
초S-5-4	10:15	Carbon fiber 및 Ag/AgCl 전극에 기반한 고감도 수중 전기장 센서 234 정현주*, 이상규, 배기웅, 양창섭
초S-5-5	10:50	Study on the Possibility of Magnetic Field Communication for High-Sensitivity GMI Sensor 236 Jang-Yeol Kim*, Hyun Joon Lee, Jae-Ho Lee, Jung Hoon Oh and In-Kui Cho
초S-5-6	11:15	Mechanism and manipulation of magnetic microrobot for medical applications 237 Sung Hoon Kim*
초S-5-7	11:40	친환경자동차(xEV)용 전류센서의 기술동향 238 박종민*, 황병봉, 이희성, 김대원, 조준호
초S-5-8	12:05	Development of pin-type magnetic sensing probe with PHR of the 10nT resolution targeting for highly integrated PCB analysis 239 Nam Young Lee*, Dal Ho Lee, Dae Sung Lee

7월 22일(목) 14:00~17:10

Symposium 6 'Magnetization Dynamics'

Antigua1

✿ 좌 장 : 김준서(DGIST)

초S-6-1	14:00	Observation of strong bulk spin-orbit torques in the van der Waals ferromagnet Fe_3GeTe_2 243 Franziska Martin, Kyujoon Lee*, Maurice Schmitt, Anna Liedtke, Aga Shahee, Haakon Thømt Simensen, Tanja Scholz, Tom G. Saunderson, Dongwook Go, Martin Gradhand, Yuriy Mokrousov, Thibaud Denneulin, András Kovács, Bettina Lotsch, Arne Brataas, Mathias Kläui
--------	-------	--

초S-6-2	14:30	Observation of Correlation Between Unidirectional Spin Hall and Magnon Magnetoresistances	244
		Sanghoon Kim*	
초S-6-3	15:00	Current and Future Prospect of MRAM technology in Semiconductor Industry	245
		Seung-heon Chris Baek*	
초S-6-4	15:40	Photoinduced ultrafast magnetization dynamics in ferromagnetic thin films	246
		Dong-Hyun Kim*	
초S-6-5	16:10	The interfacial Dzyaloshinskii-Moriya interaction in the heavy metal/Co/heavy metal sandwiched structure	247
		Jaehun Cho*, June-Seo Kim	
초S-6-6	16:40	Quasi-Static Strain Effect on Ultrafast Magnetization Dynamics	248
		Yooleemi Shin, Mircea Vomir, Dong-Hyun Kim, Phuoc Cao Van, Jong-Ryul Jeong and Ji-Wan Kim*	

7월 22일(목) 14:00~17:05

Symposium 7 'Mössbauer Magnetics'

Barbuda1

✿ 좌 장 : 윤성현(군산대)

초S-7-1	14:00	Activation Study of Precipitated Iron-Based Catalysts for Fischer-Tropsch Synthesis using Mössbauer Spectroscopy	251
		Dong Hyun Chun*	
초S-7-2	14:25	철계코어셸 촉매가 적용된 연료전지용 막전극접합체의 촉매-이오노머 나노계면 제어를 위한 잉크 구조 연구	252
		임성대*, 김성민, 박현욱, 우승희, 강윤식, 이은직, 박구곤, 박석희	
초S-7-3	14:50	The Quantum Theory of Recoilless in Mössbauer Effect	253
		Jong Woan Choi, Hyun Suk Kim, Jung Chul Sur*	
초S-7-4	15:15	Study on cathode materials using Mössbauer spectroscopy	254
		Hyunkyung Choi* and Chul Sung Kim†	
초S-7-5	15:50	Introduction of Precise Nuclear Measurements and Geostandards	255
		Gwang-Min Sun*, Young Rang Uhm and Jaegi Lee	
초S-7-6	16:15	Proposals to extending Mössbauer study for the Korean cultural properties	256
		Dong Hyeok Moon*, Eun Woo Lee†, Ji Hyeon Yoon, Young Rang Uhm, Chul Sung Kim	
초S-7-7	16:40	Facile Synthesis of Fe@Pt Core-Shell Nanoparticles and Their Electrocatalytic Activity for Oxygen Reduction Reaction	257
		Hyun-Uk Park†, Eunjik Lee*, Jeongyun Jang, Min Ho Seo, Gu-Gon Park†	

7월 22일(목) 14:00~16:00

Symposium 8 'Theory and Computational Magnetism'

Barbuda2

✿ 좌 장 : 이관우(고려대)

초S-8-1	14:00	Anomalous exciton and magneto-electric effect in a layered antiferromagnet	261
		Young-Woo Son*	
초S-8-2	14:30	Anomalous Hall effect in compensated collinear ferrimagnet: Symmetry analysis in Mn_3Al	262
		Minkyu Park*, Guihyun Han, S. H. Rhim	
초S-8-3	15:00	Terahertz field-induced phase transition via nonlinear phonon interaction ...	263
		Dongbin Shin*, Angel Rubio	
초S-8-4	15:30	All-optical fast control of band topology by exploiting the correlation between Berry curvature and magnetic anisotropy	264
		Bumseop Kim, Mahmut Sait Okyay, Noejung Park*	

7월 23일(금) 09:00~12:00

Symposium 9 'Low Dimensional Magnetism'

Antigua1

✿ 좌 장 : 유정우(UNIST)

초S-9-1	09:00	Controlling the Magnetic Properties of the Van der Waals Ferromagnet Fe_3GeTe_2	267
		Hyejin Ryu*, Se Young Park, Dong Seob Kim, Yu Liu, Jinwoong Hwang, Younghak Kim, Wondong Kim, Jae-Young Kim, Cedomir Petrovic, Choongyu Hwang, Sung-Kwan Mo, Hyung-jun Kim, Byoung-Chul Min, Hyun Cheol Koo, Joonyeon Chang, Chaun Jang and Jun Woo Choi	
초S-9-2	09:25	Engineering ferromagnetic lines in graphene by local functionalization using AFM lithography	268
		Bae Ho Park*, Ik-Su Byun, Danil W. Boukhvalov, Duk Hyun Lee, Wondong Kim, Jaeyoon Baik, Hyun-Joon Shin and Young-Woo Son	
초S-9-3	09:50	Exchange bias effect in van der Waals magnetic materials	269
		Jun Woo Choi*, Hyung Keun Gweon, Hee Young Kwon, Kyoung-Whan Kim, Zi Qiang Qiu, Hyejin Ryu, Chaun Jang	
초S-9-4	10:15	Robust quantum oscillation of Dirac fermions in a single-defect resonant transistor	270
		Heejun Yang*	
초S-9-5	10:45	Dirac Fluid Tesla Valves in Graphene	271
		Young Duck Kim*	
초S-9-6	11:10	Ferroelectricity-driven angular momentum textures: from spins and orbitals to Berry curvatures	272
		Hosub Jin*	

초S-9-7	11:35	Rashba effects on the transport properties of low-dimensional systems 273
		Jung-Woo Yoo*

7월 23일(금) 09:00~12:00

Session 1 ‘신진과학자 콜로키움’

Antigua2

✿ 작 장 : 민병철(KIST)

초O-1-1	09:00	Spin wave non-reciprocity in spin superfluids 277
		Gyungchoon Go and Se Kwon Kim*
초O-1-2	09:15	Long-range Spin Transport using Magnon Phonon Coupling 278
		Kyongmo An*, Li Shi, Xiaoqin Li, Olivier Klein
초O-1-3	09:30	Demonstration of Core Operations for Skyrmion Racetrack Memory Device 279
		Seungmo Yang*, Kyoung-Woong Moon, Tae-Seong Ju, Changsoo Kim, Hyun-Joong Kim, Juran Kim, Bao Xuan Tran, Jung-Il Hong and Chanyong Hwang†
초O-1-4	09:45	Spin dependent light emission in organic light emitting diodes with single ferromagnetic electrode 280
		Nyun Jong Lee*, Yu Jeong Bae, Heeyoung Jung, Changhee Lee and Tae Hee Kim†
초O-1-5	10:00	Reconfigurable spintronic physical unclonable functions based on spin-orbit torques in ferromagnet/ nonmagnet/ferromagnet trilayer structures 281
		Soogil Lee*, Jaimin Kang, Jeong-Mok Kim, Taek-Hyeon Lee, Sungjun Lee, Donghyeon Han, Sanghwa Lee, Kab-Jin Kim and Byong-Guk Park
초O-1-6	10:15	Tunable dynamics of exchange-biased domain wall via spin-current-induced antiferromagnet switching 282
		Hyun-Joong Kim*, Soong-Geun Je, Jung-Il Hong, Chanyong Hwang
초O-1-7	10:45	Effect of post-sintering annealing temperature on the magnetic and microstructural properties of multi-main phase Nd-Ce-Fe-B with high Ce content 284
		Kyoung-Hoon Bae*, Tae-Hoon Kim, Jung-Goo Lee, Sang-Hyup Lee, Dong-Hwan Kim
초O-1-8	11:00	Thermal Plasma Synthesis of Fe _x Co _{1-x} Nano-Chained Particles with High Permeability for GHz-band Electromagnetic Wave Absorption 286
		Min-Sun Jang*, Mi Se Chang, Young-tae Kwon, Sangsun Yang, Jina Gwak, Suk Jin Kwon, Joonsik Lee, Sang Bok Lee, Byeongjin Park, Jae Won Jeong
초O-1-9	11:15	Magnetic State Generation using Hamiltonian Guided Variational Autoencoder with Spin Structure Stabilization 288
		H. Y. Kwon*, H. G. Yoon, S. M. Park, D. B. Lee, J. W. Choi and C. Won
초O-1-10	11:30	Role of Demagnetization Field on Permanent Magnet 289
		Namkyu Kim*, Jihoon Park, Ki-Suk Lee, Chul-Jin Choi
초O-1-11	11:45	Higher-order Topological Magnons in Honeycomb Antiferromagnet 291
		Moon Jip Park*, SungBin Lee, Yong Baek Kim

✿ 좌 장 : 한만석(강원대) / 안우상(울산의대)

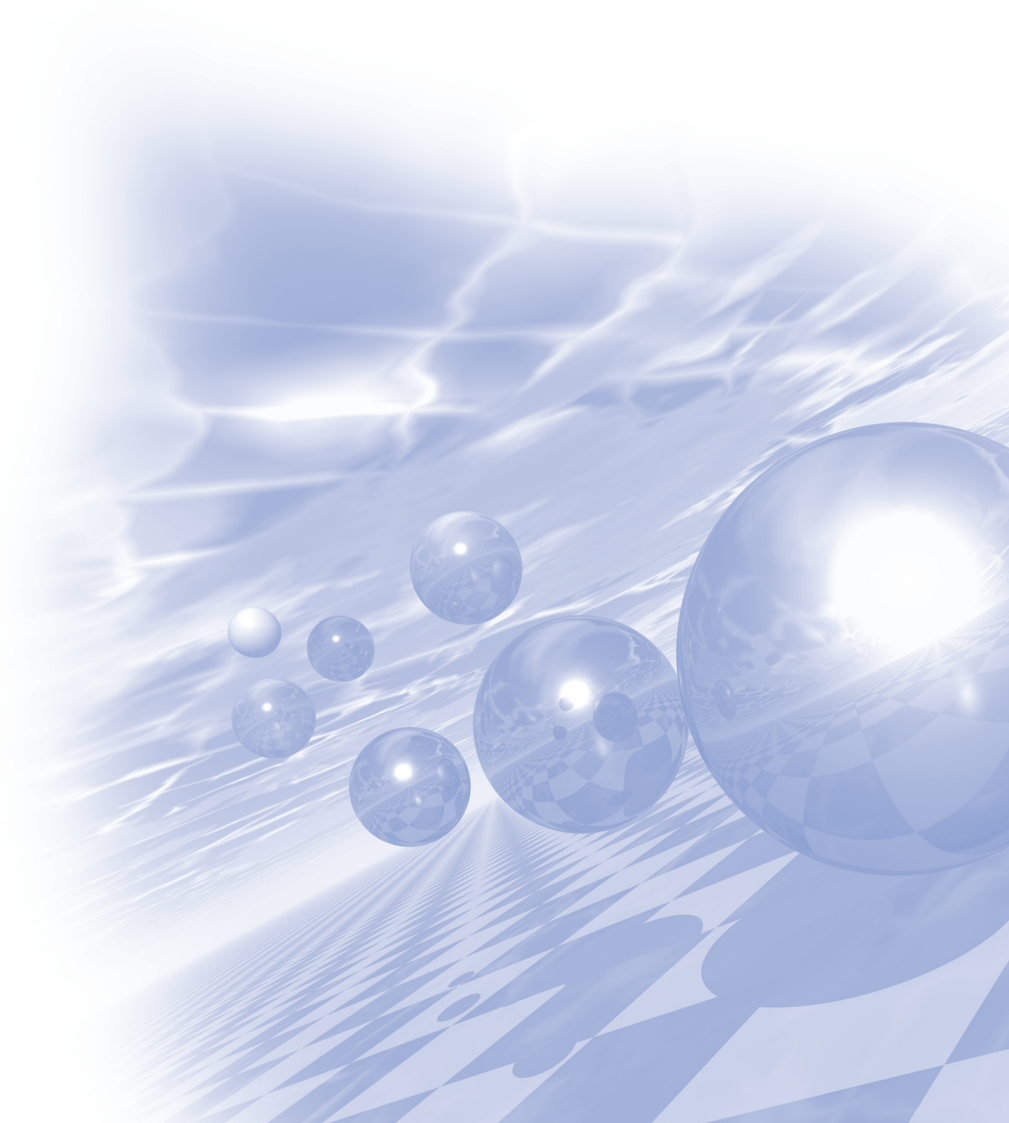
초S-10-1	09:00	The Effect of Somatosensory Training in Combination with Low-Frequency Repetitive Transcranial Magnetic Stimulation on Functional Improvement in Stroke Patients	295
So-Young Han*, Byung Il Yang, Bo-Kyoung Song			
초S-10-2	09:20	Scalability evaluation of resistor charge division circuit for PET detector based on GAPD	297
Jingyu Yang*, Hea Ryeong Lee and Jihoon Kang			
초S-10-3	09:40	Optimization of Diverging Collimator for Radiation Monitoring Imaging using Monte Carlo Simulation	298
Dong-Hee Han*, Da-Eun Kwon, Kyung-Hwan Jung, Seung-Jae Lee, Cheol-Ha Baek†			
초S-10-4	10:20	A Review on the Disposal of Radioactive Waste in the Radio-iodine Ward ...	299
Kim Jeong Ho*			
초S-10-5	10:50	Monte Carlo project of carbon-ion radiation therapy at Yonsei Cancer Center: Present and future	300
Min Cheol Han*			
초S-10-6	11:25	Review of the Task Group 284 Report: Magnetic Resonance Imaging Simulation in Radiotherapy	301
So Hyun Ahn*			



2021 KMS Summer Conference

Symposium 1

**‘Bio-Convergence Magnetics
cooperation with M-care center
– 자성기반 라이프케어 연구센터 협력 세션’**



COVID-19 면역치료제용 항-CD3 단클론항체와 자성나노입자 접합체 개발 및 자기적 특성 연구

최유경, 최상현, 이보람, 이현숙, 이상석*

상지대학교 한방의료공학과, 원주 26339

이전에는 정맥으로 전달되는 면역치료제용으로 항-CD3 단클론항체가 부정적인 부작용으로 알려져 있다. 본 연구에서는 최적의 조건에서 자성나노입자에 접합된 항-CD3 단클론항체의 정제 전달을 위한 마이크로니들형 패치 개발에 필요한 연구 기반 기술을 확보하고 치료 효능 결과를 얻는다. 궁극적으로 연구목표는 피부에 붙이는 마이크로니들 패치를 통해 자성나노입자에 접합된 항-CD3 단클론항체의 국소 면역치료 약물전달을 사용하여 과도한 T 세포 활성화를 억제하여 사이토카인의 과잉분비를 제어함으로써 COVID-19로 인한 사망률을 줄이는 것이다. 실험방법으로는, 최적의 액상 생산을 위한 조건은 항-CD3 단클론항체와 자성나노입자의 Fc 지향적 접합으로부터 유도한다. 항-CD3 단클론항체는 SiteClick 항체 라벨링 키트를 사용하여 자성나노입자와의 접합을 위해 준비하였다. Fig. 1에서 보인 바와 같이 일단 접합되면, 항-CD3 단클론항체와 자성나노입자 혼합물의 자기적 특성이 액상의 최적화를 위해 분석하였다. 또한 항-CD3 단클론항체와 자성나노입자의 성공적인 접합의 자기적 물성은 초상자성체 자성비드와 자성나노입자들의 크기와 분포에 따른 자기저항 특성으로 조사하였다. 부피 10 μ l 만큼 들어가는 플라스틱 수조 중앙에 2개의 원통형 Cu 전극 그리고 균일한 외부자기장이 Cu 전극 두 면 사이 공간을 가로지르게 인가하도록 측정장치를 제작하였다. 1 mm 공간 내 존재하는 크기가 다른 입자들이 분포가 되도록 CD3 단클론항체와 자성나노입자가 접합한 용액을 통과하는 외부자기장 세기에 따라 측정된 전압곡선로부터 얻은 최저 자기저항값, 자기저항비, 그리고 용액보자력을 비교하였다. 이후 비임상 동물실험을 통해 정맥주사를 통한 직접 약물전달과 마이크로니들 패치를 통한 간접 약물전달 전과 후 차이의 효과를 림프관내 프리모관의 형태학적 변화를 관찰하였다. 다음으로, 항-CD3 단클론항체-자성나노입자 처리 패치에 의한 T-세포 (CD3) 활성화의 억제를 통한 IFN- γ 및 인터루킨 분비 감소를 확인하기 위한 토끼 동물혈장을 조사하는 ELISA 실험도 진행된다. 동물의 대정맥에서 혈청 샘플을 추출하여 과도한 염증성 사이토카인 분비의 주산물 중 하나인 IFN- γ 의 양과 인터루킨 분비의 변화를 확인하는 토끼와 마우스 동물 실험을 실시한다. T-세포의 과잉 활성화 억제를 위해 항-CD3 단클론항체-자성나노입자들을 혈액으로 전달하는 필름형 마이크로니들 패치 기술을 적용하여 피부로 통과되는 액상의 양이 조절되도록 펄스형 자기장 자극을 가한다. 또한 혈액으로 들어간 항-CD3 단클론항체-자성나노입자들을 상체의 부분에 자성패드를 붙여서 효율성을 높인다.

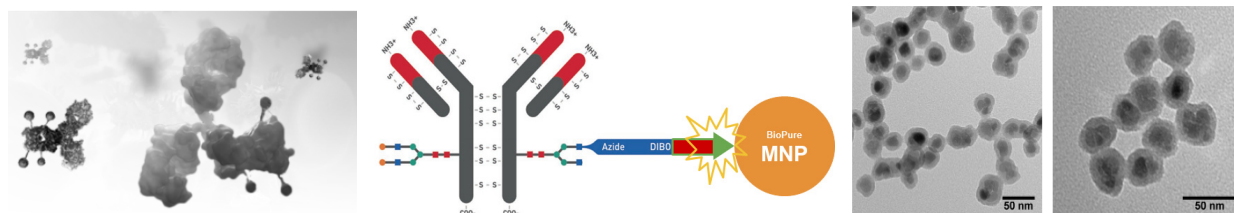


Fig. 1. The used shape of anti-CD3 monoclonal antibody and magnetic nanoparticles, and the schematic diagram of conjugation between monoclonal antibody and magnetic nanoparticles.

Acknowledgment: This research was supported by Basic Science Research Program through the National Research Foundation of Korea(NRF) funded by the Ministry of Education(2021R1I1A3054773).

자성기반 맥박 패턴 측정시스템

오선종^{1*}, 김미진², 정영도¹, 이보연¹, 김성기¹, 김철기²

¹한국기계연구원, 자연모사응용연구실

²대구경북과학기술원, 나노소자연구실

동맥혈관은 노화, 심혈관 질환 등에 의한 질병 및 흡연, 당뇨 등의 이유로 혈관의 탄력조직이 감소 또는 파괴가 발생하는 것으로 보고되고 있다. 맥박패턴은 진행파와 반사파의 중첩으로 나타나는데, 탄력조직의 감소로 혈관의 경직도가 커지게 되면 반사파 속도가 상승하게 되어 진행파와 중첩되는 심장의 수축기 때 최대 혈압이 상승하게 된다. 최대 혈압 상승은 심혈관, 뇌혈관, 관상동맥, 말초혈관 등에 영향을 주어 혈관건강에 문제가 발생하게 된다. 혈관건강은 초기 전조증상을 감지하기 어렵고 골든타임이 매우 짧아 정밀한 분석 장치를 통한 지속적인 맥박 패턴 측정시스템이 필요하다.

개발된 자성기반 맥박 패턴 측정시스템은 혈관에 접촉하는 센싱부와 물리적 힘을 전기적 신호로 변환해주는 신호변환 센서부로 구성되어 있다. 신호변환 센서부는 자기저항 센서와 영구자석의 거리 변화를 예측하여 최적 설계 및 제작을 하였다. 측정시스템은 혈관에 가해지는 인가압력을 달리하면서 맥박 패턴을 정밀하게 감지할 수 있어 혈관 경직도를 예측할 수 있으며 어레이로 구성하면 맥파전달 속도 측정도 가능하여 환자의 혈관 건강상태에 따른 정확한 물리적 혈관특성을 모니터링 할 수 있는 측정시스템을 개발 하였다.

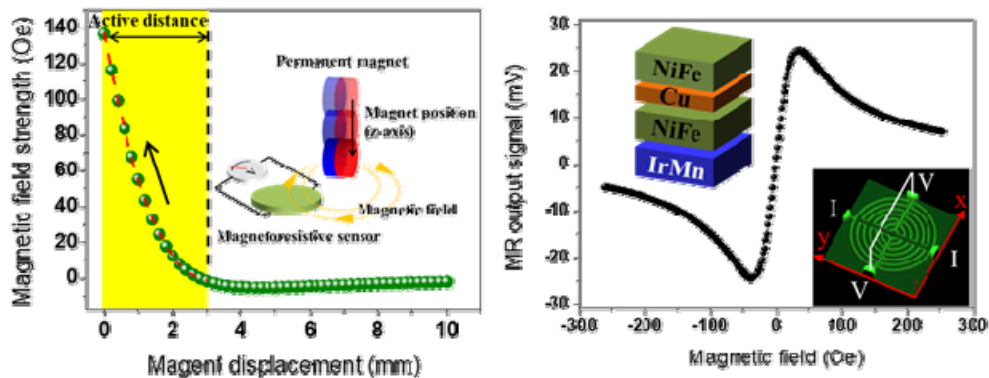


그림 1. 신호변환 센서부 최적 설계

Magnetic-based Pressure Sensor and its applications for health monitoring

Sungwon Lee^{*}

Department of Emerging Materials Science, Daegu Gyeongbuk Institute of Science & Technology (DGIST), 333,
Techno Jungang-daero, Hyeonpung-myeon, Dalseong-gun, Daegu 711-873, Korea

Pressure sensors have been integral in the development of biomedical industry and health monitoring devices. Their versatility in applications as well as their simple, straightforward mechanisms have led to massive production of sensors which are typically based on the electrical properties of the active materials. This, however, introduces some risks in sensor reliability due to difficulties in maintaining the materials' uniformity. To address this issue, a unique magnetic-based pressure sensor is fabricated utilizing a planar Hall resistive sensor. The stability of the magnetic sensor and its small hysteresis value ensures high reproducibility. The successful integration of the magnetic-based pressure sensor into health monitoring processes such as pulse monitoring, respiration and phonetic recognition also promises its wide expanse of possibilities as a wearable diagnostic device.

Development micro-thermometer using dual Hall cross bars

Dongryul Kim, Chun-Yeol You^{*}

Department of Emerging Materials Science, DGIST, Daegu, Korea

Any kind of chemical reaction is accompanied inevitable heat process. During chemical reactions, heat will be generated or absorbed, as results the temperature will be changed. Therefore, measuring the temperature variation of a living cell, where many chemical reactions occur, is scientifically important and technically challenging. In order to measure the temperature of the individual living cell, which is order of a few micrometers, many novel techniques are suggested. Here, we proposed a new technique, by using dual Hall cross bars. The magnetization of a ferromagnetic substance is a function of the temperature, it decreases with increasing the temperature. Furthermore, it is well-known that the Curie temperature of ultra-thin (< 1 nm) ferromagnetic layer is much lower than its bulk value. The temperature dependent magnetization becomes more sensitive around the Curie temperature. The magnetization of optimized ferromagnetic ultra-thin film can be very sensitive function of the desired temperature range. Since the anomalous Hall signal is proportional to the magnetization of the ferromagnetic materials, the anomalous Hall signal of ultra-thin ferromagnetic layer can be a sensitive temperature sensor. The Hall bar can be easily miniaturized of sub-micro-meter size by conventional photo-lithography process, and the Hall signal detect only Hall cross bar area which can be much smaller than typical cells. Furthermore, it consists of ultra-thin metal film, the heat capacity is much smaller than the cells, so the Hall cross bar micro-thermometer does not disturb the cell temperature. In order to improve the signal to noise ratio, we employed dual Hall cross bar system. One Hall cross bar acts as a reference, while the other detect cell temperature. We will discuss more details of the dual Hall cross bar micro-thermometer for the living cell temperature measurement.

Noise reduction method for PHMR bridge sensor by resistance compensator

byeonghwa Lim^{*}, Jaehoon Lee, Changyeop Jeon, Cheol Gi Kim
DGIST, Daegu, Korea

MR sensors are of great interest in industrial and medical applications due to their high sensitivity, portable size, and low cost. However, the noise of the MR sensor limits the sensitivity and requires complex signal processing, which limits the utilization of the sensor. To utilize the MR sensor effectively, it is necessary to increase the sensitivity of the sensor and reduce the noise. For this purpose, a self-balancing bridge type sensor with integrated resistance compensator for noise reduction in the frequency range from 0.5 Hz to 200 Hz has been devised. The proposed resistance compensator integrated with the self-bridge sensor architecture adjusted the offset voltage compensation at the Wafer level and significantly improved the sensor noise level. As a result, we achieved the lowest noise of $3.34\text{nV}/\sqrt{\text{Hz}}$ at about 100Hz. It was also confirmed that thermal drift was significantly reduced through offset voltage compensation. Therefore, the developed sensor can be used in various industrial and medical applications.

Real time monitoring of temperature/impedance variations for cell-drug reaction monitoring using semiconductor processed biosensor

Gayoung Lee¹, Jaehun Jeong¹, Jisu Choi¹, Yeyeon Kim¹,
Sooyong Shin², Sungho Jeon² and Moongyu Jang^{1*}

¹School of Nano Convergence Technology, Hallym University, Chuncheon, 24252, Korea

²Department of Life Science, Hallym University, Chuncheon, 24252, Korea

e-mail: jangmg@hallym.ac.kr

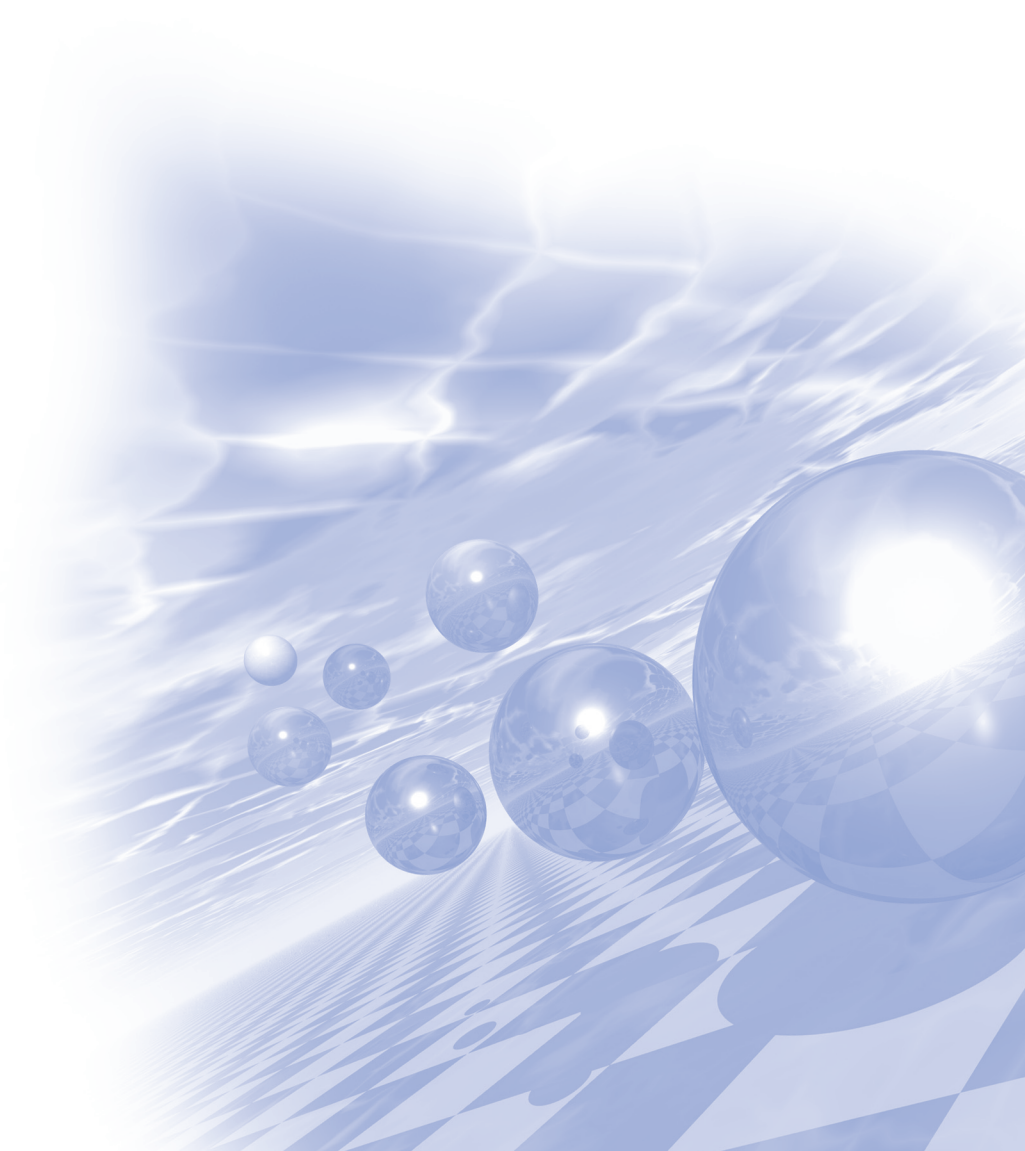
Electrical Cell-substrate Impedance System and Electrical Impedance Spectroscopy are the widely used methods in the field of biosensors for the monitoring of the status of cell. On the contrary, the usually used biosensors are bulky and hard to monitor in real time.

In this work, temperature/impedance integrated sensors are manufactured using semiconductor process for the simultaneous monitoring of the temperature and impedance variations during the cell-drug reactions. The developed platinum thin film temperature sensor showed the inaccuracy less than ± 0.05 °C and the MEMS process is adopted to enhance the temperature sensitivity. HeLa cancer cells and NIH 3T3 cells are grown on the biosensors and the drug reactions are monitored as a function of time and frequency. The impedance rapidly increase at the early stage and gradually decreased with time as a results of cell-drug reactions. Also, the temperature variations are monitored during the cell-drug reactions. The results are compared with the results by biological cell viability test on the conventional culture plates. The time and frequency dependent impedance signals are analysed in detail with the comparison between biological results.



2021 KMS Summer Conference

과학기술문화 대중화를 위한 프로그램



자석

- 마법에서 과학으로-

김갑진*

Department of Physics, Korea Advanced Institute of Science and Technology

흔히 자석이라고 하면 아이들이 가지고 노는 막대자석이나 말굽자석, 혹은 냉장고에 붙어 있는 자석을 떠올릴 테지만, 우리가 생활하는 주변에는 생각보다 많은 자석이 존재한다. 아침에 일어나서 비몽사몽간에 냉장고 문을 열고 또 닫을 수 있는 이유는 냉장고 문에 자석이 있기 때문이고, 세탁기로 빨래를 하고 헤어드라이어로 머리를 말릴 수 있는 이유는 회전하는 모터에 자석이 있기 때문이다. 이어폰으로 노래를 들을 수 있는 것도 자석이 있기 때문이고, 자동차나 지하철이 움직이는 것도 모터나 센서에 자석이 있기 때문이고, 컴퓨터로 작업한 데이터를 저장할 수 있는 것도 자석으로 된 메모리가 있기 때문이다. 신용카드도 돈을 지불하는 것도 카드에 자석으로 된 센서가 있기 때문이고, 가게에서 계산하지 않은 물건을 갖고 밖으로 나오면 경보음이 울리는 것도 물건에 부착된 자석에 센서가 반응하기 때문이다. 어디 그뿐인가? 우리의 일상생활에 없어서는 안되는 전기를 만들어내는 발전소에도 자석이 반드시 필요하니, 실로 자석이 없다면 세상이 돌아가지 않는다 해도 지나친 말이 아닐 것이다.

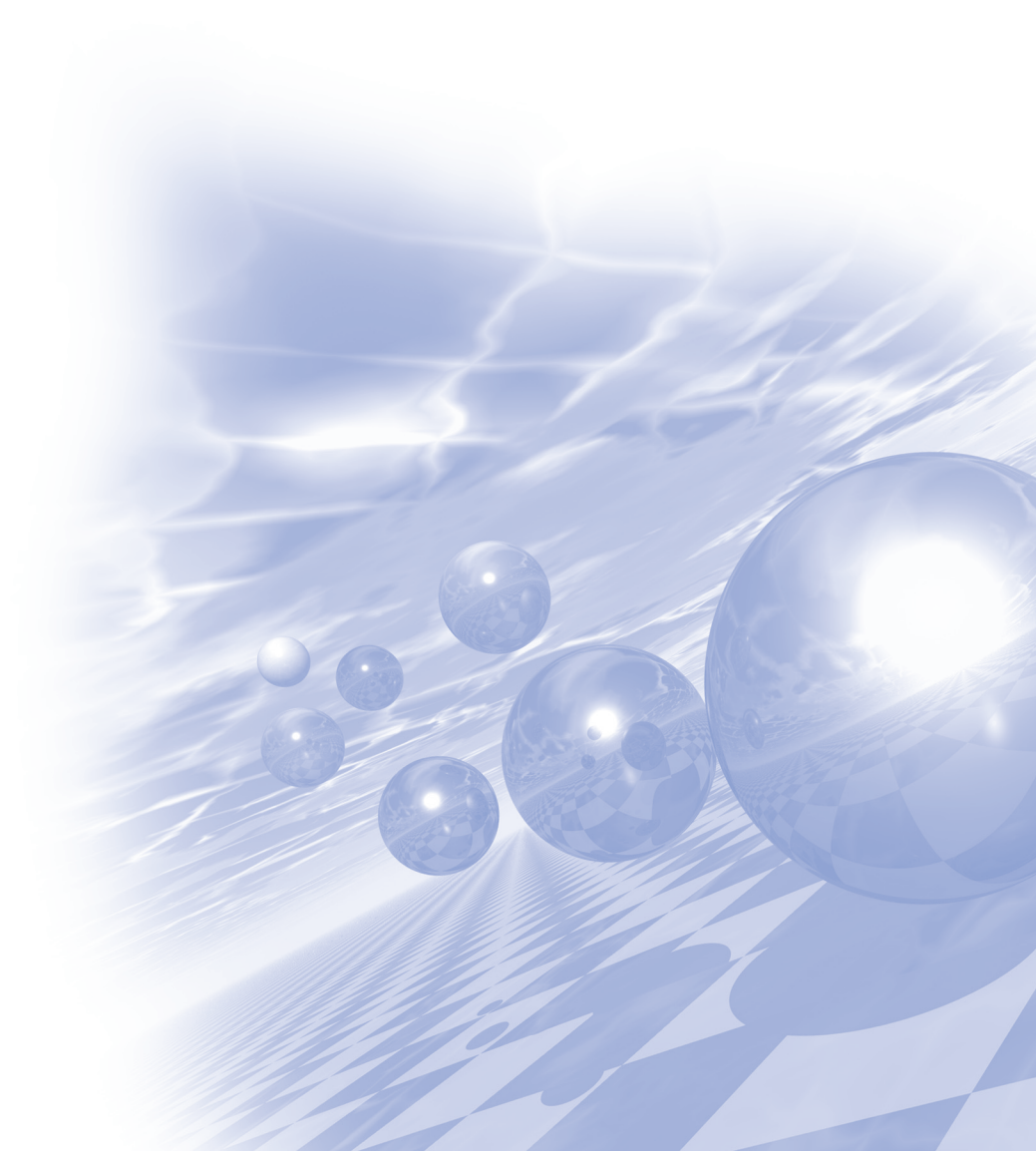
널리고 널린 게 자석인데 뭐 그리 신기할 게 있을까 싶지만, 곰곰이 생각해보면 자석은 정말 신기하다. 신기하다는 건 예상하지 못했다는 말인데, 예상하지 못했다는 건 질문하지 않았다는 뜻이다. 몇 가지 간단한 질문부터 시작해 보자. “자석의 N극과 S극은 도대체 어디에서 나올까?” “자석끼리는 왜 밀고 당기는 힘을 주는 걸까?” “철은 자석에 붙는데 알루미늄은 왜 자석에 붙지 않을까?” 쉬운 질문처럼 보이지만, 아마 쉽게 답하기는 어려울 것이다. 이런 질문이 다소 근원적이기도 하지만, 우리가 이런 질문을 제대로 해본 적이 없기 때문이다. 매일 생활하면서 자석을 보고 만지고 이용하며, 그 덕에 편리하게 생활하고 있는데도 말이다.

자석의 근원을 찾아 여행을 떠나보자. 질문을 던지고 그 질문에 답을 해 나가 보자. 꼬리에 꼬리를 무는 질문은 우리가 계속 여행을 이어가게 해줄 것이고, 더 이상 질문이 이어지지 않을 때, 여행은 거기서 끝나게 될 것이다. 자, 그럼 함께 출발해 보자.



2021 KMS Summer Conference

강습회 프로그램



Introduction to spin Hall effect

Hyun-Woo Lee^{*}

Department of Physics, POSTECH, Pohang, Korea

The spin Hall effect is an important element of spintronics. The tutorial will begin with a very introductory discussion of a spin current and the spin Hall effect, followed by a brief summary of historical development. Mechanisms of the spin Hall effect will be also discussed including the skew scattering, anomalous velocity.

Spin-transfer torque and current-induced magnetization dynamics

Kyung-Jin Lee^{*}

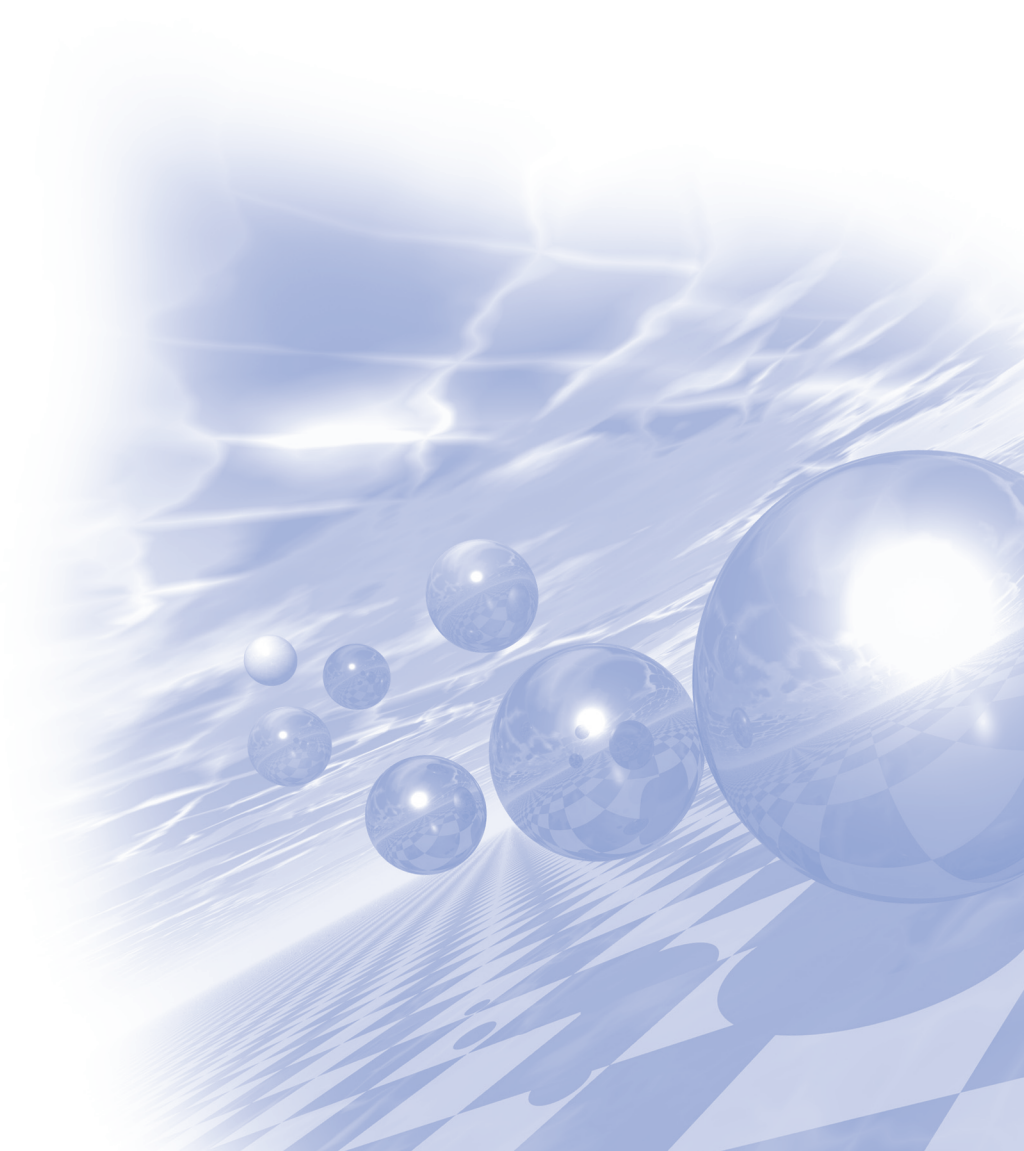
Department of Physics, KAIST, Daejeon, Korea

이번 강습회에서는 스핀전달토크 및 스핀궤도토크의 기초원리와 이의 응용을 소개하고자 한다. 이와 함께 최근 학계에서 많은 관심을 받고 있는 반강자성 스핀트로닉스에 대한 개괄과 페리자성체를 이용하여 반강자성체의 자화거동 및 스핀 전달특성을 조사한 최근 연구결과를 소개하고자 한다.



2021 KMS Summer Conference

포스터발표



Coil Arrangement to Reduce AC Copper Loss by Applying Strand and Transposition of Ultra-high-speed Motor for Air Compressor of Fuel Cell Vehicle

Sun-Yong Shin^{1*}, Jin-Cheol Park², Jun-Woo Chin², Myung-Seop Lim²

¹Department of Automotive Engineering(Automotive-Computer Convergence), Hanyang University, 222 Wangsimni-ro, Sungdong-gu, Seoul 04763, Korea

² Department of Automotive Engineering, Hanyang University, 222 Wangsimni-ro, Sungdong-gu, Seoul 04763, Korea

An internal combustion engine vehicle emits various harmful gases and causes environmental problems such as global warming. Therefore, research and development of eco-friendly vehicles have been actively conducted in recent years. An air compressor that intakes and compresses air from the atmosphere at an appropriate pressure and flow rate is used to drive a fuel cell vehicle among various eco-friendly vehicles. Air compressors are required to be high efficiency and power density due to size constraints. It is powered by an ultra-high-speed motor with small volume, weight and high energy density [1]. Ultra-high-speed motor is driven by high-frequency current. However, owing to the high current frequency, the AC copper loss in the stator winding is large which affects the efficiency of the motor [2].

This paper proposes a coil arrangement method for reducing copper loss occurring in the motor by applying strand and transposition. The target motor is 2-pole, 6-slot, ultra-high-speed motor and was designed considering the slot liner and the copper insulation. The AC copper losses that occur in no strand, strand and strand transposition are compared and analyzed under the same conditions of current density and fill factor. In the slot of the motor, the magnetic field distribution imbalance due to the leakage magnetic flux causes the skin effect and the proximity effect. When the winding of the motor is no strand, the AC copper loss occurs the most. When a strand was applied, AC copper loss decreased by increasing the total effective cross-sectional area of the coil compared to no strand. Additionally, AC copper loss was reduced by reducing the impedance difference between strands by applying a transposition [3]. As a result, AC copper losses are smallest at the strand potential.

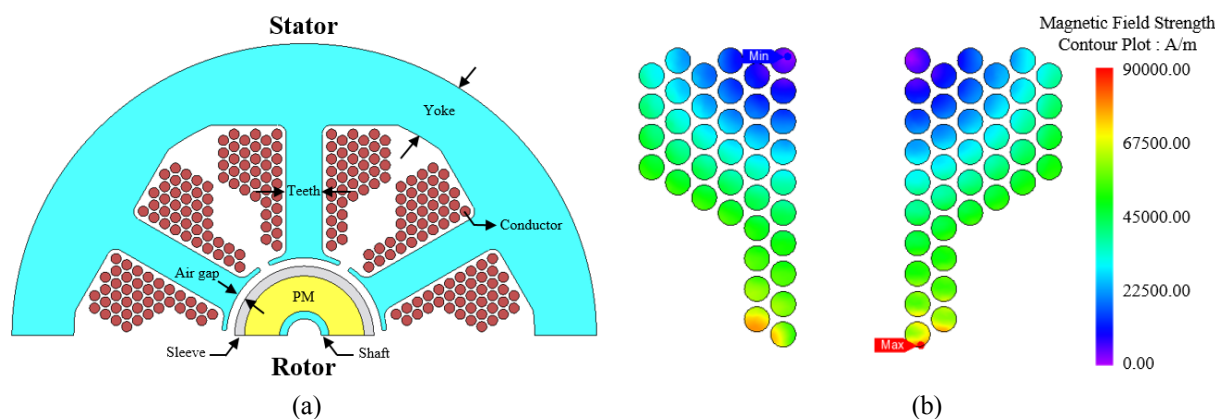


Fig. 1. (a) Ultra-high-speed motor (b) Unbalance of magnetic field distribution due to leakage flux in the slot

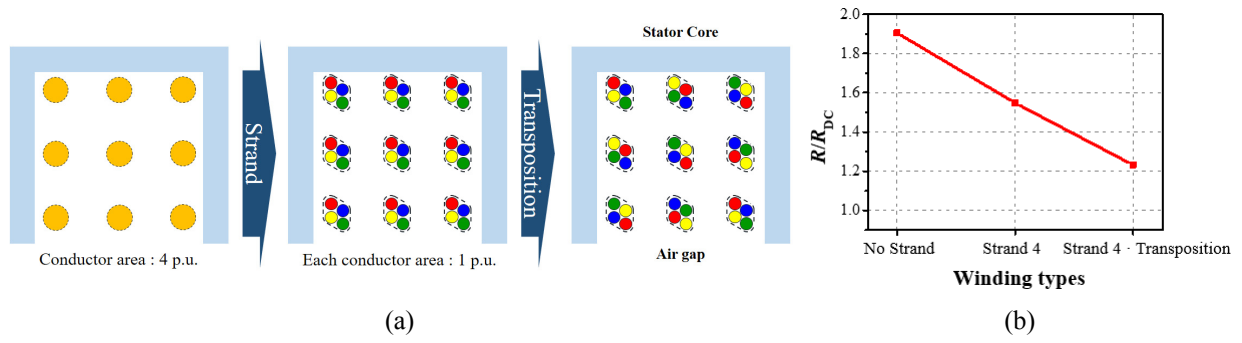


Fig. 2. (a) No strand, strand, strand transposition applied winding arrangement
(b) Ratio of AC resistance to DC resistance according to stator winding arrangement

References

- [1] Min-gyu Park, Kyu-sung Choi, Hyun-sup Yang, Kyung-hun Jung. Analysis of AC copper loss of Air Compressor Ultra-high-speed Permanent Magnet Synchronous Motor for Hydrogen Fuel Cell Electric Vehicle. *KSAE* (2020), 971-974.
- [2] Ki-O Kim, Dae-Kee Kim, Jin-Cheol Park, Sung-Woo Hwang, Myung-Seop Lim. Efficiency Analysis according to the Shape of the Rectangular Wire of a Hybrid Vehicle Traction Motor Considering AC Resistance Effect. *KSAE* (2020), 880-883.
- [3] J. -W. Chin, K. -S. Cha, J. -C. Park, D. -M. Kim, J. -P. Hong and M. -S. Lim, "Investigation of AC Resistance on Winding Conductors in Slot According to Strands Configuration," in *IEEE Transactions on Industry Applications*, vol. 57, no. 1, pp. 316-326, Jan.-Feb. 2021, doi: 10.1109/TIA.2020.3033815.

Digital Coordinate Determination of 29 x 29 Scintillation Array Detector using Simulated LUT and MLPE

Seung-Jae Lee^{1*}, Cheol-Ha Baek^{2†}

¹Department of Radiological Science, Dongseo University, Korea

²Department of Radiological Science, Kangwon National University, Korea

In order to obtain the position of the scintillation pixel for the PET detector in digital coordinates, it goes through a complicated process. In this study, the location of the scintillation pixel was simply obtained as digital coordinates using the simulation look-up table and the maximum likelihood position estimation method. After configuring a 29 x 29 scintillation array detector using the DETECT2000 simulation tool, a gamma-ray interaction was generated at the center position of each scintillation pixel. The signal obtained from the photo sensor was reduced to 4channels using the Anger equation, and the average value and standard deviation of each channel were obtained, and a look-up table was created. In order to evaluate the accuracy of digital coordinate acquisition, gamma-ray interaction were generated at 0.03 mm intervals in the range of 0.01 mm to 2.98 mm in the Z-axis direction of all scintillation pixels. As a result, it showed an accuracy of 98%. If the results of this study are applied to a PET system, it will be possible to more conveniently obtain digital coordinate values.

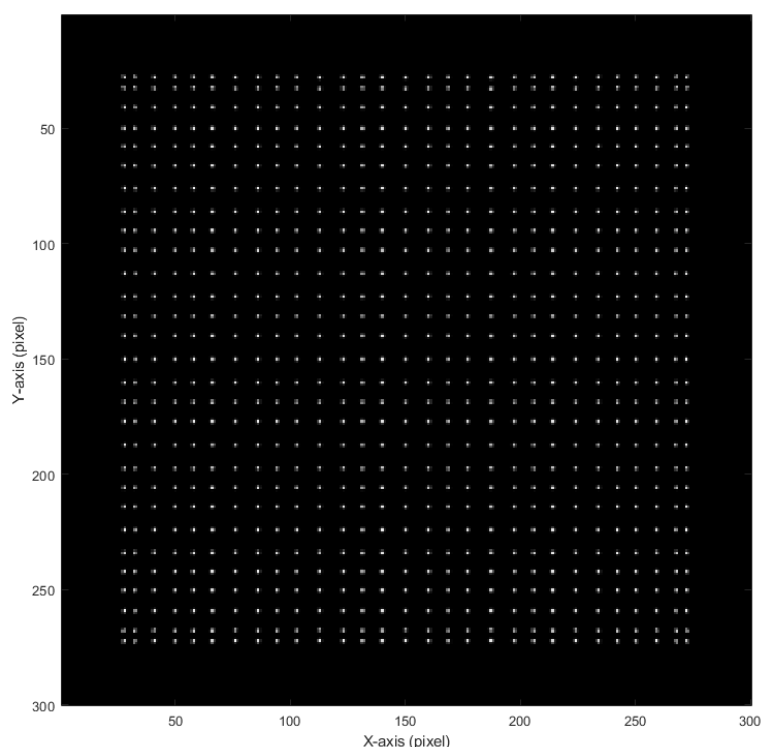


Fig. 1. Flood image of a 29 x 29 scintillator array detector acquired through DETECT2000 simulation

Synthesis and Magnetic Characteristics of Gamma Phase Iron oxide and Magnesium Iron oxide Nanoplates for Magnetic Hyperthermia Therapy

Pyung Won Im^{2,3*}, Man Seung Heo^{1,2,3}, Hyung Woo Park^{1,2,3}, Yona Kim^{1,2} and Sun Ha Paek^{1,2,3}

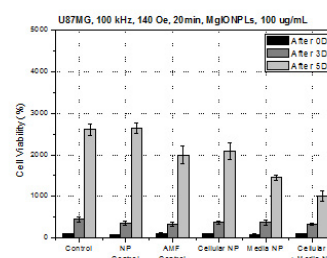
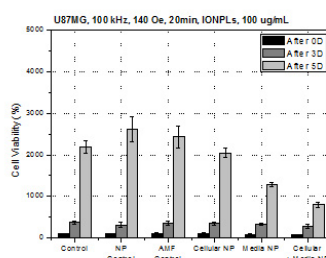
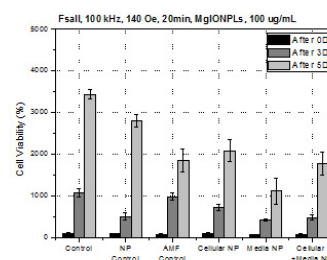
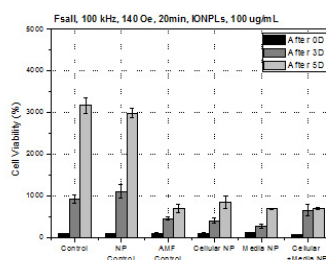
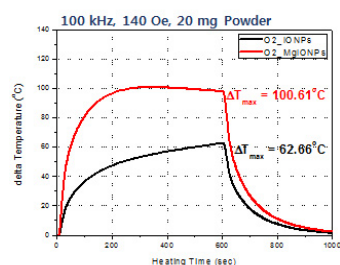
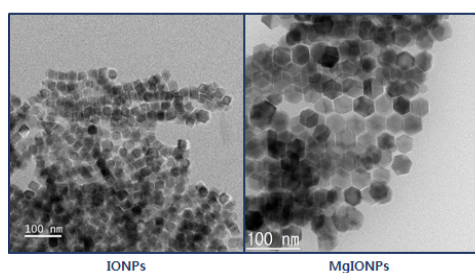
¹Department of Neurosurgery, Clinical Research Institute Seoul National University Hospital, South Korea

²Department of Neurosurgery, Cancer Research Institute Ischemia/Hypoxia Disease Institute

Seoul National University College of Medicine, Seoul, Republic of Korea

³Advanced Institutes of Convergence Technology (AICT), Seoul National University, Suwon, Korea

We report magnetic nanomaterials for magnetic hyperthermia therapy. We successfully synthesis gamma phase iron oxide nanoplates (gIONPLs) using thermal decomposition method and ‘O₂ adding’ to helped oxidation of nanomaterials. Normally, synthesis method of iron oxide nanoparticles (IONPs) is 2 temperature steps for reaction and we followed same temperature steps. One of added method ‘O₂ adding’ help oxidation of IONPs to formed gamma phase. AMF generator induced mild frequency and magnetic field (100 kHz and 140 Oe) for harmless to human body generally used range of hyperthermia therapy. Gamma phase IONPLs are usually formed spinel structure. Alkali and alkali earth metals can doped on spinel structure. Magnesium is one of the alkali earth metal that can doped on gIONPs. We used U87MG, FsaII and HFB cells to *in vitro*, hyperthermia test and observed greatly therapeutic effects. Our gIONPLs and Mg-gIONPLs have potential therapeutic effects on cancer in human body by high temperature magnetic hyperthermia therapy.



Use of fast non-local means approach for noise reduction in diffusion weighted magnetic resonance imaging with high b-value

Jaeyoung Park, Chang-Ki Kang, Seong-Hyeon Kang, Youngjin Lee*

Department of Radiological Science, Gachon University, Korea

In this study, we designed a fast non-local means (FNLN) noise reduction approach and evaluated its effectiveness for denoising brain images with high b-values. This study was performed at 3 T MRI (Verio, Siemens, Germany). Diffusion-weighted image (DWI) with a spin-echo echo planar imaging pulse sequence, which is the fastest imaging method currently available, was used to produce the images. In the process of denoising, the NLM algorithm has the advantage of minimizing blurring and artifacts after image processing, as it is calculated in reference to the surrounding pixels in the region of interest (ROI). However, the process of calculating the weight is difficult to apply in a clinical setting due to the length of time required. Therefore, this study has changed the process of calculating the weight from 2D to 1D. To demonstrate the effectiveness of the algorithm, we compared the qualities of the images obtained using FNLN with those obtained using previously developed algorithms using noise reduction performance and no-reference image quality assessment parameters. A visual inspection of the images indicates that our proposed algorithm achieved better denoising efficiency compared with conventional methods. In particular, upon observing the enlarged image, we confirmed that the noise was reliably reduced, as shown by the red arrow, by applying the proposed algorithm. In particular, the results of applying the FNLN noise reduction algorithm to DWI images obtained at high b-values indicated superior quantitative characteristics. In this study, we investigated and analyzed the proposed FNLN noise reduction algorithm in high b-value images with DWI.

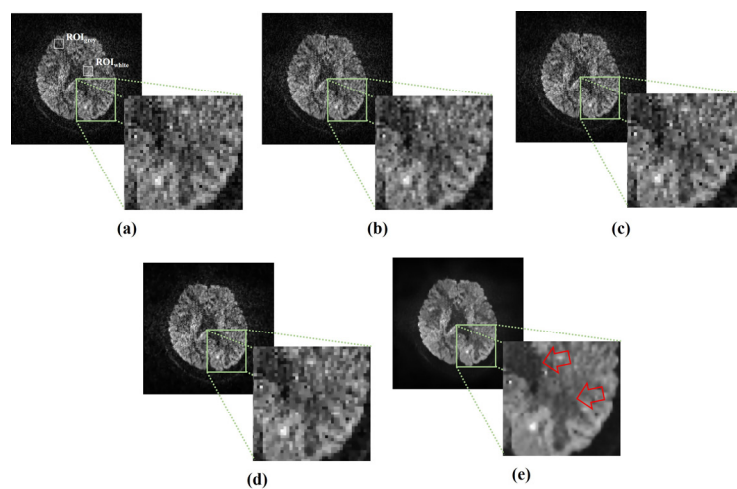


Fig. 1. Resultant diffusion-weighted images with b-values of 1400 s/mm^2 obtained using (a) non-algorithm (noisy image), (b) median filter, (c) improved median filter, (d) total variation approach, and (e) fast nonlocal means noise reduction algorithm.

뮌스바우어 분광학을 이용한 $\text{Ba}_2\text{Co}_{1.7}\text{Mg}_{0.3}\text{Fe}_{12}\text{O}_{22}$ 의 자기적 특성 연구

백재성*, 심인보, 김철성†

국민대학교 물리학과

1. 서론

헥사페라이트는 RF 디바이스, 고집적 메모리 등에 사용되는 다강성 물질로 오랜 시간동안 많은 관심을 끌고 있는 소재이다. 또한 최근 많은 이슈가 되고 있는 Magnetoelectric(ME)효과가 여러 화합물에서 발견되고 있으며, 상온에서 활용이 가능할 수 있는 수준의 ME효과가 발현된 경우도 관찰되었다. 헥사페라이트 중에서도 Y-type의 경우 ME효과를 나타내며 여러 물질의 치환 연구를 통해 변화하는 특성 변화에 대한 연구가 활발하다. 본 연구에서는 $\text{Ba}_2\text{Co}_{1.7}\text{Mg}_{0.3}\text{Fe}_{12}\text{O}_{22}$ 의 자기적특성에 대한 연구를 진행하였다.

2. 실험방법

출발물질로 고순도의 BaCO_3 (99.98%), CoO (99.99%), MgO (99.999%), Fe_2O_3 (99%)를 사용하였다. 준비된 앞의 시료들을 화학양론적 당량비에 맞게 마노에 넣어준 뒤 1시간동안 곱게 갈아주었다. 그 후 앞에 갈아준 시료들을 $4\text{ }^\circ\text{C/min}$ 의 속도로 $1000\text{ }^\circ\text{C}$ 까지 승온하여 10시간 동안 하소하였다. 하소된 분말 시료를 1시간동안 곱게 갈아준 뒤, 약 1 mm 의 두께로 압축 성형 해주었다. 압축 성형된 시료를 $2\text{ }^\circ\text{C/min}$ 의 속도로 $1100\text{ }^\circ\text{C}$ 까지 승온하여 10시간 동안 1차 소결을 진행하였다. 바륨헥사페라이트 제조 시 빈번하게 생성되는 2차상인 BaFe_2O_4 를 제거하기 위해 $2\text{ }^\circ\text{C/min}$ 의 속도로 $1150\text{ }^\circ\text{C}$ 까지 승온하여 10시간 동안 2차 소결을 진행하여 단일상의 $\text{Ba}_2\text{Co}_{1.7}\text{Mg}_{0.3}\text{Fe}_{12}\text{O}_{22}$ 를 얻었다. 시료의 결정학적 특성을 분석하기 위해 X-ray diffraction (XRD)를 이용하여 측정하였고, Rietveld 분석기법을 이용하여 결정구조를 분석하였다. 또한 등가속도형 Mössbauer 분광기와 Vibrating sample magnetometer (VSM)을 이용하여 자기적 특성을 확인하였다.

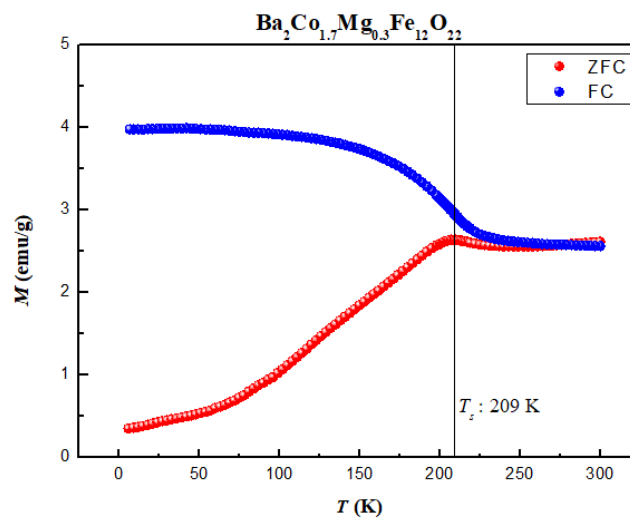


Fig. 1. ZFC-FC magnetization measured from 4.2 to 300 K for $\text{Ba}_2\text{Co}_{1.7}\text{Mg}_{0.3}\text{Fe}_{12}\text{O}_{22}$

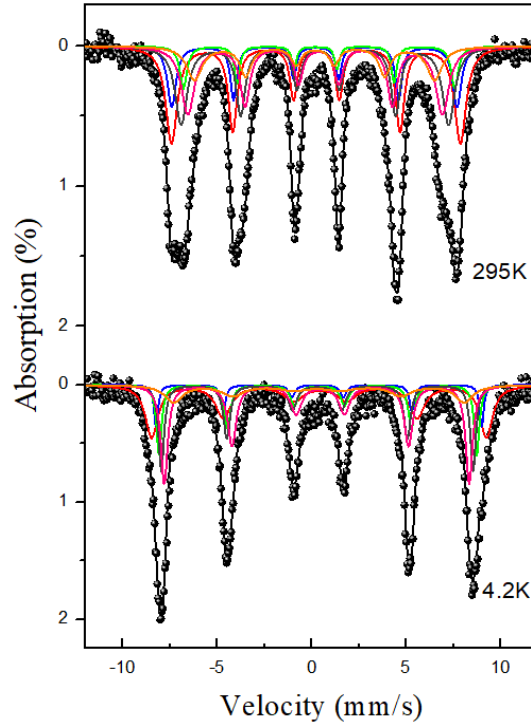


Fig. 2. Mössbauer spectra of $\text{Ba}_2\text{Co}_{1.7}\text{Mg}_{0.3}\text{Fe}_{12}\text{O}_{22}$ at 4.2 and 295K

3. 실험결과 및 고찰

X-ray Diffraction을 통해 얻어낸 데이터 분석을 통해 해당 물질이 R-3m 공간군의 Hexagonal 구조를 가지고 있는 것으로 확인되었다. VSM을 이용하여 온도에 따른 자화율 실험 결과 ZFC곡선의 209K에서 변곡점을 관찰하였다. Mössbauer 분광기를 이용하여 4.2 K 부터 295 K까지 온도실험을 진행한 결과 209K에서 사중극자 분열치의 값이 급격하게 변화하는 변곡점을 관찰하였으며, 그 결과를 통해 해당 209K를 T_s 로 결정하였다. 또한 실험을 진행한 모든 온도에서 6site의 이성질체 이동치가 0.1~0.4 mm/s 사이의 값으로 분석되어 철의 이온가가 Fe^{3+} 임을 확인하였다. 초미세 자기장의 경우 4.2K 에서 $H_{\text{hf}}(18h_{\text{VI}}) = 518.57$ kOe, $H_{\text{hf}}(3b_{\text{VI}}) = 508.40$ kOe, $H_{\text{hf}}(6c_{\text{IV}}) = 502.56$ kOe, $H_{\text{hf}}(6c_{\text{IV}}^*) = 491.62$ kOe, $H_{\text{hf}}(6c_{\text{VI}}) = 476.86$ kOe, $H_{\text{hf}}(3a_{\text{VI}}) = 462.91$ kOe로 분석되었으며, 295K 에서, $H_{\text{hf}}(18h_{\text{VI}}) = 474.83$ kOe, $H_{\text{hf}}(3b_{\text{VI}}) = 468.97$ kOe, $H_{\text{hf}}(6c_{\text{IV}}) = 445.88$ kOe, $H_{\text{hf}}(6c_{\text{IV}}^*) = 439.68$ kOe, $H_{\text{hf}}(6c_{\text{VI}}) = 418.27$ kOe, $H_{\text{hf}}(3a_{\text{VI}}) = 394.78$ kOe 로 분석되었다.

Crystal structure and Mössbauer studies of α -NaFeO₂

Jin Gyo Jung^{*}, Hyunkyung Choi, In-Bo Shim, Chul Sung Kim[†]

Department of Physics, Kookmin University, Seoul 02707, Korea

Lithium – ion batteries (LIBs) have excellent electrochemical performance. However, lithium's price is increased due to the low reserves all over the world. As the alternative cathode material of lithium, sodium has attracted attention. It is environmentally friendly, and it is cost-advantage because of the abundance worldwide. Also, the de-intercalation/intercalation properties of sodium-ion batteries (SIBs) are similar to those of LIBs. However, sodium has the disadvantage of being heavy and has a lower energy density than lithium. To solve this problem, sodium layered oxide is recently being studied. NaMO₂ (M = Fe, Co, Ti, Mn, Ni, etc.) has high volume and gravitational density. In this study, the crystal structure, and magnetic properties of NaFeO₂ materials were characterized by X-ray diffraction (XRD), vibrating sample magnetometry (VSM), and Mössbauer spectra measurements.

NaFeO₂ was synthesized using the solid reaction method from Na₂CO₃ (99.5%) and Fe₃O₄ (99%) as starting materials. The mixture mixed at a ratio of 1:1. After grinding the mixture in an agate mortar, there was calcined at 300 °C for 5 h. The calcined mixture was ground again in an agate mortar and compressed using a disk-shaped pellet. The compressed mixture was sintered to 650 °C for 12 h. To confirm the crystal structure of NaFeO₂, it was measured by XRD with Cu-K α radiation ($\lambda = 1.5406$ Å). Mössbauer spectra measured from 4.2 K to 295 K on a Mössbauer spectrometer, and the VSM measured magnetic properties through the zero-field-cooled (ZFC) and field-cooled (FC) measurements from 4.2 K to 295 K with magnetic fields of 0.1 kOe and 1 kOe.

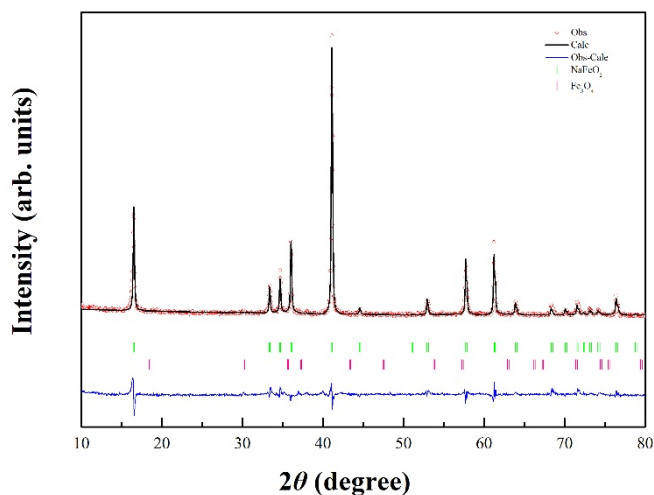


Fig. 1. Refined XRD patterns of NaFeO₂

The crystal structure of NaFeO₂ samples were analyzed using the FULLPROF program after XRD experiment at room temperature. As a result of the analysis, it was found that 5.37% of Fe₃O₄ was present in NaFeO₂ sample. it has a trigonal structure with space group of R-3m. The lattice constants were analyzed as $a = b = 3.0251$ Å, $c = 16.0983$ Å. To know the magnetic properties, VSM was experimented from low to room temperature at 0.1

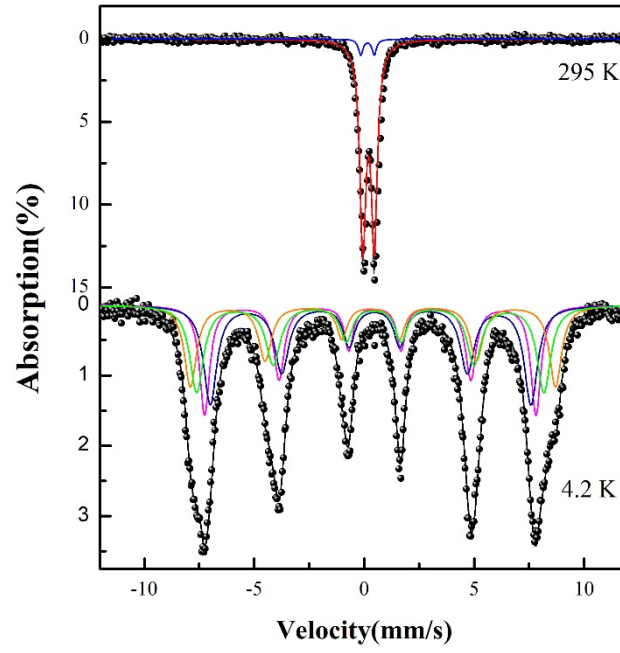


Fig. 2. Mössbauer spectra of NaFeO₂ at 4.2 and 295 K

kOe. it was shown through ZFC-FC data that the Néel temperature (T_N) of NaFeO₂ is 11 K. As a result of Mössbauer spectroscopy analysis from 4.2 K to 295 K, the values of magnetic hyperfine field (H_{hf}) at 4.2 K are $H_{hf}(1) = 468.31$ kOe, $H_{hf}(2) = 453.41$ kOe, $H_{hf}(3) = 516.00$ kOe, $H_{hf}(4) = 490.79$ kOe, and the electric quadrupole splitting and isomer shift of NaFeO₂ at 11 K are measured to be 0.51 mm/s, and 0.37 mm/s.

Synthesis and magnetic properties of iron catalyst $\text{Fe}_{1.5}@\text{Pt}/\text{C}$ (Fresh)

Hyunkyung Choi^{1*}, Jin Gyo Jung¹, Hyun-Uk Park², Eunjik Lee²,
Gu-Gon Park², Sung-Dae Yim² and Chul Sung Kim^{1†}

¹Department of Physics, Kookmin University, Seoul 02707, Korea

²Fuel Cell Laboratory, Korea Institute of Energy Research, Daejeon 34129, Korea

The slow oxygen reduction reaction movement of hydrogen fuel cells is one of the challenges to be solved, and one of the electrode catalysts that has solved this problem is platinum. However, as the price of platinum rises, research on core-shell structure electrode catalysts to reduce platinum usage and increase electrochemical performance are actively underway. Among them, iron-platinum nanoalloy catalysts are in the spotlight. The use of an iron-containing core as a catalyst has the advantage of low cost by reducing the amount of platinum used, and it is expected that such an iron-platinum core shell can improve catalytic activity. Therefore, $\text{Fe}_{1.5}@\text{Pt}/\text{C}$ (Fresh) catalyst was prepared using sonochemical method, and crystallographic and magnetic properties of the synthesized catalyst were studied.

$\text{Fe}_{1.5}@\text{Pt}/\text{C}$ (Fresh) used $\text{Pt}(\text{acac})_2$, $\text{Fe}(\text{acac})_3$, ethylene glycol, and Vulcan XC-72 carbon black as starting materials. After all the starting materials were mixed, it was placed in a horn sonicator and then was irradiated with an amplitude of 40 % (300 W) over 3 h. After the reaction, it was filtered and dried using distilled water and ethanol. Crystallographic properties of the obtained sample were analyzed using X-ray diffraction (XRD) using $\text{Cu-K}\alpha$ rays ($\lambda = 1.5406 \text{ \AA}$) and a scanning transmission electron microscope (STEM). To investigate the magnetic properties, the M-H curve was measured at room temperature using vibrating sample magnetometer, and Mössbauer spectroscopy experiment was performed at 4.2 and 295 K.

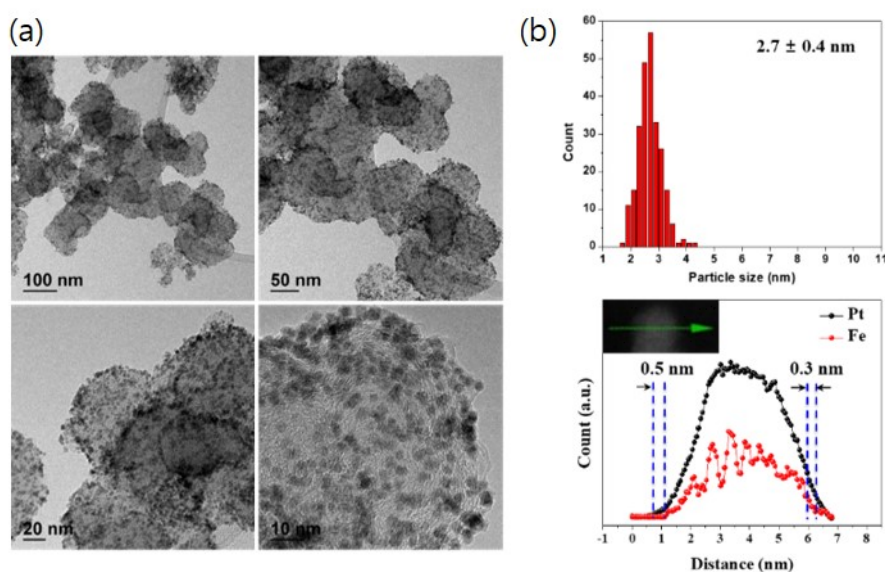


Fig. 1. (a) STEM images, (b) particle size histogram and graphs of line scan profile analysis of $\text{Fe}_{1.5}@\text{Pt}/\text{C}$ (Fresh)

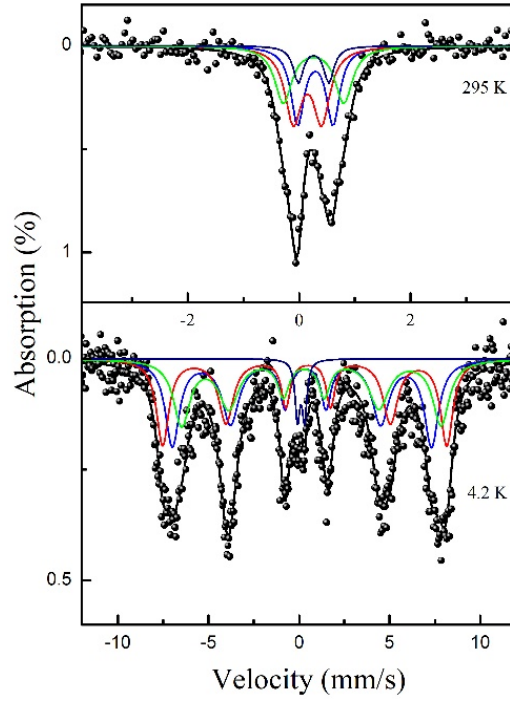


Fig. 2. Mössbauer spectra of Fe_{1.5}@Pt/C (Fresh) at 4.2 and 295 K.

From the XRD analysis results and the TEM images, it was confirmed that the size of the sample was 2.7 ± 0.4 nm. In addition, as a result of comparing the distribution and intensity of Pt and Fe using the line scan profile analysis of the STEM mode, it was confirmed that the Pt shell was coated on the Fe core by about 0.3-0.5 nm. From the M-H curve, the coercivity was measured to be 90.7 Oe, and the magnetization of the sample at 1.5 T was confirmed to be 0.58 emu/g. The Mössbauer spectra of Fe_{1.5}@Pt/C (Fresh) were analyzed in order to verify the hyperfine interaction and state in terms of the Fe nucleus. The spectrum at 295 K was analyzed with 4-sets of doublet and it was confirmed that all of them were in the Fe³⁺ ion state. The magnetic hyperfine field (H_{hf}) at 4.2 K of magnetically ordered each sextets were measured to be $H_{\text{hf}(1)} = 445.6$ kOe, $H_{\text{hf}(2)} = 487.3$ kOe, and $H_{\text{hf}(3)} = 444.9$ kOe. And one doublet was still observed in the spectrum at 4.2 K.

Mössbauer studies on core-shell $\text{Fe}_{1.5}\text{@Pt/C}$ nanoparticles post-heated in NH_3 gas atmosphere

Hyunkyung Choi^{1*}, Jae Sung Baik¹, Hyun-Uk Park², Eunjik Lee²,
Gu-Gon Park², Sung-Dae Yim² and Chul Sung Kim^{1†}

¹Department of Physics, Kookmin University, Seoul 02707, Korea

²Fuel Cell Laboratory, Korea Institute of Energy Research, Daejeon 34129, Korea

$\text{Fe}_{1.5}\text{@Pt/C}$ core-shell is used as an electrode catalyst for fuel cells, and research has been conducted to reduce costs and improve performance for application to fuel cells. In this study, the structural and magnetic properties of the $\text{Fe}_{1.5}\text{@Pt/C}$ core-shell heat treated in an NH_3 gas atmosphere were investigated.

The $\text{Fe}_{1.5}\text{@Pt/C}$ core-shell was prepared using the sonochemical method. $\text{Fe}(\text{acac})_3$, $\text{Pt}(\text{acac})_2$, and carbon support (Vulcan XC-72R) were dispersed in ethylene glycol. The mixture was placed in a girb0type sonicator and then it was irradiated over 3 h. To remove residual ethylene glycol, the obtained black slurry was filtered and washed with ethanol and DI water. The sample was dried in a vacuum oven at 70 °C for 12 h. Then, the post-heat treated $\text{Fe}_{1.5}\text{@Pt/C}$ samples in an NH_3 gas atmosphere were annealed at 510 °C for 2 h. To remove iron oxides and other residues from the heat-treated sample, the sample was acid-treated in 0.1M HClO_4 at 85 °C for 2 h. In order to obtain a clear core-shell structure, the sample was additionally annealed at a temperature of 300 °C in an H_2/N_2 atmosphere for 2 h. And finally, $\text{Fe}_{1.5}\text{@Pt/C}$ with a core-shell structure was obtained. The sample was denoted as $\text{Fe}_{1.5}\text{@Pt/C_NH}_3$.

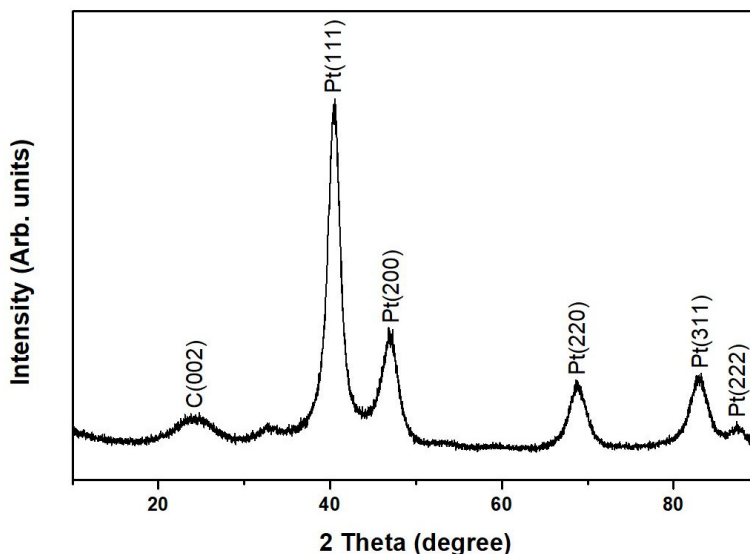


Fig. 1. XRD patterns of $\text{Fe}_{1.5}\text{@Pt/C_NH}_3$

The crystallographic properties and core-shell structure of the $\text{Fe}_{1.5}\text{@Pt/C_NH}_3$ core-shell were confirmed through X-ray diffraction (XRD), transmission electron microscopy (TEM), and scanning transmission electron microscopy–energy dispersive spectroscopy (EDS). In addition, in order to investigate the magnetic properties of

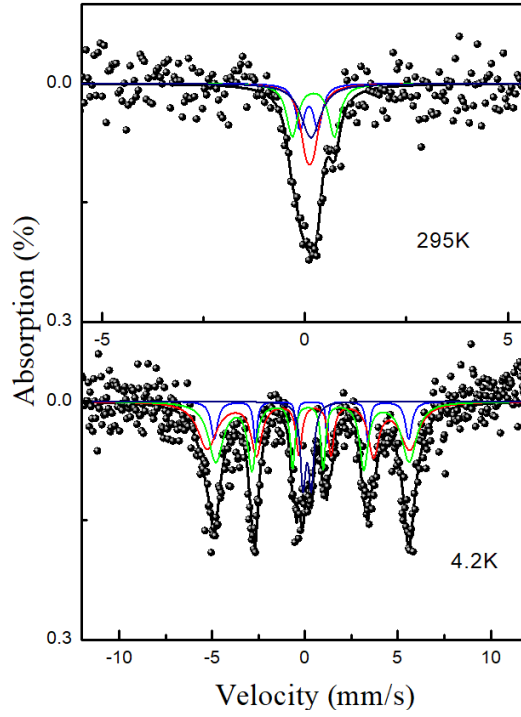


Fig. 2. Mössbauer spectra of $\text{Fe}_{1.5}@\text{Pt/C_NH}_3$ at 4.2 and 295K

the sample, the Mössbauer spectra were observed at 4.2 and 295 K and the M-H curve was measured using a vibrating sample magnetometer (VSM). Pt peaks were confirmed from the XRD patterns and the average crystallite sizes of the sample was confirmed to be 4.9 ± 1.4 nm using TEM image. The EDS line profile of $\text{Fe}_{1.5}@\text{Pt/C_NH}_3$ revealed a core-shell structure with a Pt skin layer (0.3 nm). The saturation magnetization and coercivity at 295 K were 7.1 emu/g and 134.5 Oe, respectively. The Mössbauer spectrum of the $\text{Fe}_{1.5}@\text{Pt/C_NH}_3$ at 295 K were analyzed with 4 sets of doublets and the electric quadrupole splitting (ΔE_Q) values were $\Delta E_{Q,1} = 0.44$ mm/s, $\Delta E_{Q,2} = 0.17$ mm/s, $\Delta E_{Q,3} = 1.04$ mm/s, and $\Delta E_{Q,4} = 0.07$ mm/s, respectively. Also, the spectrum at 4.2K was measured with 3 sets of sextet and one doublet and the magnetic hyperfine field (H_{hf}) values were analyzed as $H_{\text{hf},1} = 325.2$ kOe, $H_{\text{hf},2} = 339.7$ kOe, and $H_{\text{hf},3} = 323.6$ kOe, respectively. From the isomeric shift values, all Fe valence states was determined to be ferric.

Investigation for Manufacture of the Portable Backscattering Mössbauer Spectrometer

Mingi Eom^{1,2*}, Young Rang Uhm¹, Jaegi Lee¹, Gwang-Min Sun¹

¹HANARO Utilization Division, Korea Atomic Energy Research Institute, Daejeon, 34057, Republic of Korea

²Department of Transdisciplinary Studies, Seoul National University Graduate School of Convergence and Technology, Seoul, 08826, Republic of Korea

Mössbauer spectroscopy is one of the most powerful methods for the analysis of hyperfine interactions in materials. The most widely used target material is ^{57}Fe , of which the natural abundance is 2.12 % [1]. As the γ -ray emitted from the first excited state of ^{57}Fe has too low energy (14.4 keV) to penetrate a thick sample, the transmission Mössbauer spectrometer can analyze the only artificial thin samples. To analyze cultural heritages or relics, non-destructive (without sampling) and *in situ* inspection is required. The backscattering Mössbauer spectrometer detects the backscattered γ -rays from the surface of the materials, so the additional sampling is unnecessary. An example of this type of Mössbauer spectrometer is shown in **Figure 1**. For the *in situ* measurement, miniaturized devices, including a velocity drive and detectors, should be developed. The Miniaturized Mössbauer Spectrometer (MIMOS II) was developed and sent to MARS by NASA, which was the type of backscattering Mössbauer spectrometer [2]. In the first step of developing the velocity transducer, the interested velocity range is from -10 to 10 mm/s with a triangular waveform. Then the time term per signal will be set constant so that the whole channel number becomes 1,024. As shown in **Figure 1**, detectors should be attached to the head of the spectrometer, and more than one detector is required to get a higher count rate. The previous detectors for the transmission Mössbauer spectrometer were gas detectors or scintillators, which are not suitable for portable devices. The first prototype is shown in **Figure 2**. The Si-PIN detectors, also used in the MIMOS II, were equipped in the front line of the velocity transducer. Our new spectrometer will be equipped with cadmium telluride (CdTe) semiconductor detectors. The CdTe detectors can detect 6.3 and 14.4 keV photons from ^{57}Fe atoms with the full width at half maximum (FWHM) of 500 eV at 14.4 keV and have higher sensitivity than Si-PIN detectors at energies above 20 keV [3]. A newly developed Mössbauer spectrometer will be applied to the investigation of metal and ceramic relics.

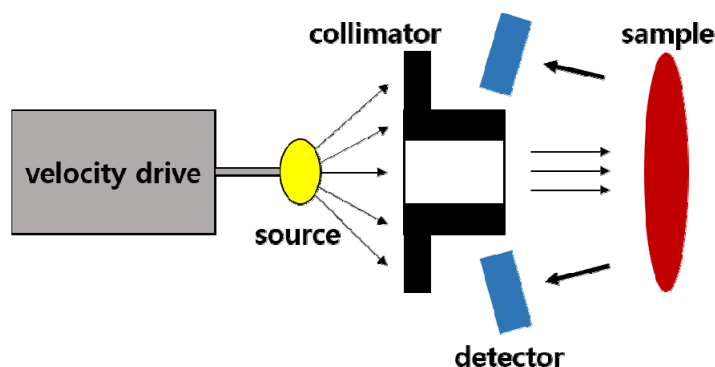


Figure 1. The scheme of the backscattering Mössbauer spectrometer

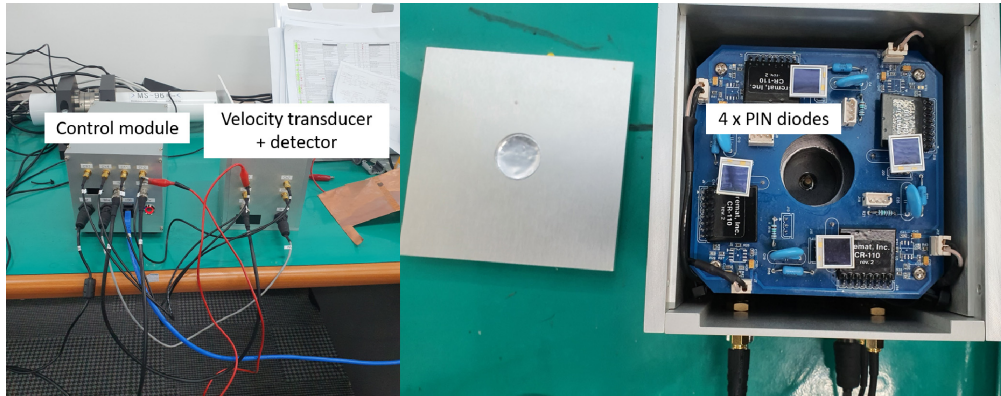


Figure 2. The first prototype of the newly developed spectrometer.
4 Si-PIN detectors were attached to the front line of the velocity transducer.

References

- [1] Philipp Gülich, Eckhard Bill, and Alfred X. Trautwein, Mössbauer Spectroscopy and Transition Metal Chemistry, Springer (2011)
- [2] G. Klingelhöfer, R. V. Morris, B. Bernhardt, D. Rodionov, P. A. de Souza Jr., S. W. Squyres, J. Foh, E. Kankeleit, U. Bonnes, R. Gellert, C. Schröder, S. Linkin, E. Evlanov, B. Zubkov, and O. Prilutski, Athena MIMOS II Mössbauer spectrometer investigation, J. Geophys. Res. **108** E12, 8067 (2003)
- [3] R. Redus, Member, IEEE, J. Pantazis, T. Pantazis, A. Huber, and B. Cross, Characterization of CdTe Detectors for Quantitative X-ray Spectroscopy, IEEE **56** 4 (2009)

Orbital angular momentum of a domain wall and geometrically twisted magnons

Seungho Lee^{*} and Se Kwon Kim

Department of Physics, Korea Advanced Institute of Science and Technology, Daejeon 34141, Republic of Korea

We theoretically study the dynamics of a domain wall in a ferromagnetic nanotube driven by electrons and magnons by investigating the electron-domain-wall and magnon-domain-wall interactions. Due to the geometry of the sample, domain walls are classified by the Skyrmion charge which counts the winding number of magnetic textures on the domain wall [1]. The domain wall with a non-zero Skyrmion charge generates an emergent magnetic field for interacting particles, which exerts the Lorentz force on moving electrons and magnons and thereby deflects their trajectories. This deflection is manifested as generation of the finite orbital angular momenta of the electrons and magnons that traverse the domain wall [2,3]. For the case of electrons, we can interpret the exchange of orbital angular momenta between electrons and the domain wall as a current-induced torque. From this peculiar torque, the domain wall with the non-zero Skyrmion charge can be driven by an arbitrary small current without the Walker breakdown. For the case of magnons, we obtain the exact solution for the magnon on the Skyrmion-textured domain wall and also their scattering properties with the domain wall with the aid of supersymmetric quantum mechanics (SUSY QM). We also show that there is a critical wavenumber for the total reflection and it is discretized by the Skyrmion charge of the domain wall. Our results show that orbital angular momenta of magnetic systems and quasi-particles can be intertwined in the curved geometry.

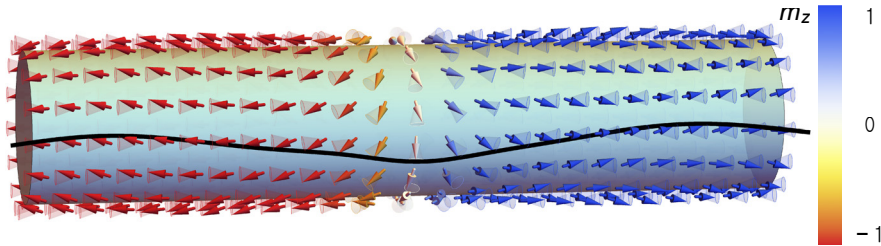


Fig. 1. A ferromagnetic nanotube with a domain wall possessing finite Skyrmion charge.

The arrows represent magnetizations of spin-wave excitations.

The black curve lines the heads of the arrows. The axis of the nanotube is z -axis.

References

- [1] S. Lee and S. K. Kim, Orbital angular momentum and current-induced motion of a Skyrmion-textured domain wall in a ferromagnetic nanotube, arXiv:2102.08405.
- [2] C. Jia, D. Ma, A. F. Schäffer, and J. Berakdar, Twisted magnon beams carrying orbital angular momentum, Nat. Commun. 10, 2077 (2019).
- [3] Y. Jiang, H. Y. Yuan, Z.-X. Li, Z. Wang, H. W. Zhang, Y. Cao, and P. Yan, Twisted Magnon as a Magnetic Tweezer., Phys. Rev. Lett. 124, 217204 (2020).

Enhanced functionalities in Ruddlesden-Popper oxide thin films employing single-terminated substrate surfaces

Jinkwon Kim^{*}, Youngdo Kim, Junsik Mun, Jeong Rae Kim,
Miyoung Kim, Changyoung Kim and Tae Won Noh

¹Center for Correlated Electron Systems, Institute for Basic Science, Seoul 08826, Republic of Korea

²Department of Physics and Astronomy, Seoul National University, Seoul 08826, Republic of Korea

³Department of Materials Science and Engineering and Research Institute of Advanced Materials, Seoul National University, Seoul 08826, Republic of Korea

Over the past decades, Ruddlesden-Popper (RP) phase oxides ($A_{n+1}B_nO_{3n+1}$, $n = 1, 2, \dots$) have been spotlighted with advantageous physical properties such as high-temperature superconductivity, giant magnetoresistance. ^[1-2] These emergent phenomena provide a platform for novel oxide-based electronic devices including spintronics application. However, high-quality RP-phase thin film growth has been disturbed by extended structural defects, so-called out-of-phase boundaries (OPBs).^[3] OPB is a translational boundary between neighboring unit cells, shifted in a specific crystallographic direction. For instance, if RP-phase thin films grown on ABO_3 perovskite substrates, the structural mismatch between film and substrates induces a crystallographic shift in the c -axis direction, thus OPBs form at the film-substrate interface. Since OPB formation hampers the physical properties of RP-phase thin films, the suppression of the structural defects is highly required to carry out the high-performance RP-phase based functional devices.^[4-5]

In this study, we suppressed OPB suppression in RP-phase oxide thin films by using single-terminated LaSrAlO_4 substrate ($n = 1$ RP phase, $a = b = 3.756 \text{ \AA}$ and $c = 12.636 \text{ \AA}$). As a model system, the high- T_c cuprates superconductor $\text{La}_{1.85}\text{Sr}_{0.15}\text{CuO}_4$ thin film ($n = 1$ RP phase, $a = b = 3.777 \text{ \AA}$ and $c = 13.226 \text{ \AA}$) was employed. Despite the structural similarities between films and substrates, the $\text{La}_{2-x}\text{Sr}_x\text{CuO}_4$ films exhibited huge OPB formations when deposited on mixed-terminated LaSrAlO_4 substrate. In contrast, when the $\text{La}_{2-x}\text{Sr}_x\text{CuO}_4$ films were deposited on single-terminated LaSrAlO_4 substrates, the OPBs were significantly suppressed in the film structure. Notably, these OPB-free $\text{La}_{2-x}\text{Sr}_x\text{CuO}_4$ films exhibited highly enhanced superconductivity ($T_c^{\text{zero}} \sim 30 \text{ K}$) than the film with huge OPB formation ($T_c^{\text{zero}} \sim 5 \text{ K}$) under the same thickness ($\sim 6.5 \text{ nm}$). Our study suggests a comprehensive method to suppress OPB formation in RP thin films, enabling superconducting spintronics devices based on RP-phase high- T_c superconductors.^[5-6]

References

- [1] J. G. Bednorz *et al.*, *Science* **236**, 73 (1987).
- [2] Y. Moritomo *et al.*, *Nature* **380**, 141 (1996).
- [3] M. A. Zurbuchen *et al.*, *J. Mater. Res.*, **22**, 1439 (2007).
- [4] A. Tsurumaki-Fukuchi *et al.*, *ACS Appl. Mater. Interfaces* **12**, 28368 (2020).
- [5] J. Kim *et al.*, *Nano Lett.* **21**, 4185 (2021).
- [6] S. B. Chung *et al.*, *Phys. Rev. Lett.* **121**, 167001 (2018).

Dynamics of a ferrimagnetic domain wall by a rotating field

Munsu Jin^{1*}, Ik-Sun Hong², Duck-Ho Kim³, Kyung-Jin Lee¹ and Se Kwon Kim¹

¹Department of Physics, Korea Advanced Institute of Science and Technology, Daejeon 34141, Republic of Korea

²KU-KIST Graduate School of Converging Science and Technology,
Korea University, Seoul 02841, Republic of Korea

³Center for Spintronics, Korea Institute of Science and Technology, Seoul 136-791, Republic of Korea

A magnetic domain wall is a topological defect between two uniform states, which is stable against local perturbations due to the topological nature [1]. For this robustness, a domain wall has been proposed as central units in spintronic devices such as magnetic domain-wall racetrack memory and domain-wall logic devices [2, 3]. Due to this utility, it is important to find efficient means to drive a domain wall. For example, it has been recently reported that a domain-wall in a ferromagnet can be driven by an AC-field and AC-current and a domain wall in a ferrimagnet can be driven by spin-transfer-torque [4, 5]. Here, we theoretically and numerically study a domain-wall motion in a ferrimagnet by a rotating field. Depending on the magnitude and the frequency of the rotating field, the dynamics of a ferrimagnetic domain wall can be classified into two regimes. First, the stationary solution corresponding to the low frequency can be interpreted to belong to a phase-locking regime, where a domain-wall angle rotates in-phase with an external field. Second, the non-linear solution corresponding to the high frequency can be interpreted as a phase-unlocking regime [6-8], where a domain-wall angle is not synchronous with the applied field. In the phase locking regime, the domain-wall velocity is proportional to the field frequency, which implies that the velocity of the domain wall can be controlled by the rotating-field frequency. Once the frequency is over the critical frequency (set by the field magnitude), the domain-wall

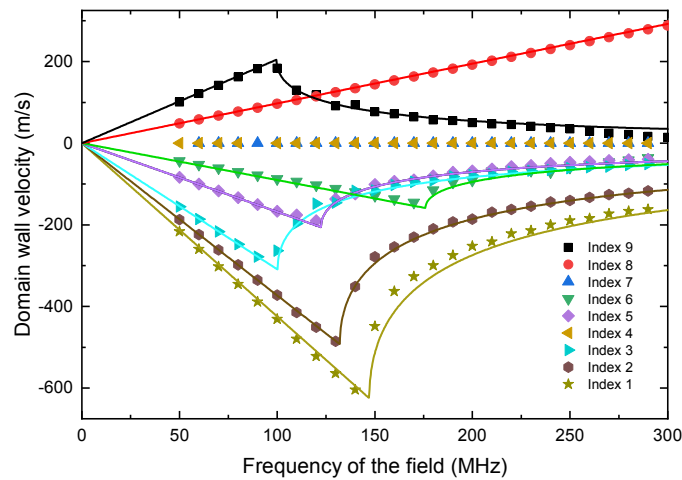


Figure 1. Domain-wall velocity in a ferrimagnet by a rotating field at various temperatures (denoted by indices) including the angular momentum compensation point (corresponding to index 7) and the magnetization compensation point (corresponding to index 4).

Dots represent our simulation results. Lines represent our analytic results.

dynamics enters the phase-unlocking regime where the domain wall velocity decreases due to the incoherent precessional motion of a domain wall. Moreover, the sign of the domain-wall velocity is flipped across the angular compensation point where the net spin density of the ferromagnets changes its sign. Considering that there have been experimental demonstrations of the effect of rotating magnetic field on the dynamics of a magnetic vortex domain-wall chirality reversal [9], we believe that our setup is experimentally feasible. Our work reports not only the novel critical phenomenon associated with the dynamics of a ferrimagnetic domain-wall by a rotating field, but also a new way to detect the angular momentum compensation point of ferrimagnets.

References

- [1] A. M. Kosevich, B. Ivanov, and A. Kovalev, *Phys. Rep.* **194**, 117 (1990).
- [2] D. A. Allwood, G. Xiong, C. Faulkner, D. Atkinson, D. Petit, and R. Cowburn, *Science* **309**, 1688 (2005).
- [3] S. S. Parkin, M. Hayashi, and L. Thomas, *Science* **320**, 190 (2008).
- [4] D.-H. Kim, D.-H. Kim, D.-Y. Kim, S.-B. Choe, T. Ono, K.-J. Lee, and S. K. Kim, *Phys. Rev. B* **102**, 184430 (2020).
- [5] D.-H. Kim, D.-H. Kim, K.-J. Kim, K.-W. Moon, S. Yang, K.-J. Kim, S. K. Kim, *J. Magn. Magn. Mater.* **514**, 167237 (2020).
- [6] W. H. Rippard, M. R. Pufall, S. Kaka, T. J. Silva, S. E. Russek, and J. A. Katine, *Phys. Rev. Lett.* **95**, 067203 (2005).
- [7] B. Georges, J. Grollier, M. Darques, V. Cros, C. Deranlot, B. Marciilhac, G. Faini, and A. Fert, *Phys. Rev. Lett.* **101**, 017201 (2008).
- [8] S. Urazhdin, P. Tabor, V. Tiberkevich, and A. Slavin, *Phys. Rev. Lett.* **105**, 104101 (2010).
- [9] A. Bisig, M.-A. Mawass, M. Sta'rk, C. Moutafis, J. Rhen- sius, J. Heidler, S. Gliga, M. Weigand, T. Tyliczszak, B. Van Waeyenberge, et al., *Appl. Phys. Lett.* **106**, 122401 (2015).

Probing fundamental transport parameters during the phase transition of FeRh by terahertz time domain spectroscopy

Ji-Ho Park^{1*}, Yu June Jang¹, Min Tae Park², Se Kwon Kim¹,
Kyung-Jin Lee¹, Myung Hwa Jung², Kab-Jin Kim¹

¹Department of Physics, Korea Advanced Institute of Science and Technology, Daejeon, Republic of Korea

²Department of Physics, Sogang University, Seoul, Republic of Korea

FeRh exhibits magnetic phase transition from antiferromagnetic to ferromagnetic near room temperature [1]. Along with the change of magnetic ordering, the phase transition also accompanies a significant change of electrical resistivity which can be modulated by magnetic field or doping, making FeRh very attractive for future applications, such as thermally assisted memory devices [2] and spin valve-based devices [3]. However, the origin of resistivity variation during phase transition is still unclear because the experimental verification of fundamental transport parameters, such as charge density(n), effective mass(m^*) and scattering time(τ) is lacking. Here we experimentally identify the fundamental transport parameters using terahertz time domain spectroscopy and ordinary Hall measurement. The n , m^* and τ are found to vary significantly during phase transition, which is consistent with the theoretical prediction [4]. Interestingly, the effective mass of electrons in FeRh is much larger than that of typical ferromagnetic metals such as Permalloy, which implies the large electron-phonon coupling in FeRh,[5]. Further analysis on the THz spectra reveals that the large electron-phonon coupling in FeRh triggers the THz-wave-driven phonon resonance. Our results not only quantify the fundamental transport parameters but also provide a novel way to generate phonon resonance in metallic sample.

References

- [1] M. Fallot, Ann. Phys. **10**, 291 (1938).
- [2] J. U. Thiele *et al.* Appl. Phys. Lett. **82**, 2859 (2003).
- [3] S. Yuasa *et al.* J. Appl. Phys. **83**, 6813 (1998).
- [4] S. Mankovsky *et al.* Phys. Rev. B **95**, 155139 (2017).
- [5] A.Szajekand J.A.Morkowski, Physica B **193**, 81 (1994).

Valley splitting and enhanced anomalous Hall effect in Mn impurity doped WS₂/CrGeSe₃ heterostructure

Brahim Marfoua^{*} and Jisang Hong[†]

Department of Physics, Pukyong National University, Busan 48513, Korea

Valleytronics (valley-dependent electronics) is attracting extensive research effort for next generation potential device applications [1-3]. Mostly, the lifting of valley degeneracy was achieved by the incorporation of the magnetic layer induced the proximity effect or the magnetic impurity doping effect. However, it is rare to find reports regarding the valley splitting induced by impurity doping combined with the proximity effect. Thus, we investigated the possibility of enhancing the valley splitting and anomalous Hall conductivity by the combination of two methods in WS₂/CrGeSe₃ heterostructure. In the pure WS₂/CrGeSe₃ heterostructure, we obtained a small valley splitting of 1 meV at K⁺ and K⁻ valleys due to the weak hybridization between the WS₂ and CrGeSe₃ layers. However, we obtained a large valley splitting of 68 meV in the Mn impurity doped WS₂/CrGeSe₃ heterostructure owing to the Mn doping effect and also the K valley dependent proximity effect. Consequently, this led to a sizable difference in the out-of-plan Berry curvature. We obtained anomalous Hall conductivity (AHC) of 110 S/cm in the Mn doped WS₂/CrGeSe₃ system, and this is 20 times larger than that found in the pristine WS₂/CrGeSe₃ heterostructure. Our results may provide a new platform through the combination of the two approaches for potential valleytronics applications.

Acknowledgment :This research was supported by the Basic Science Research Program through the National Research Foundation of Korea (NRF) funded by the Ministry of Science, ICT and Future Planning (2019RA21B5B01069807).

References

- [1] Cao, T. *et al.* Valley-selective circular dichroism of monolayer molybdenum disulphide. *Nat. Commun.* **3**, 1–5 (2012).
- [2] Sanchez, O. L., Ovchinnikov, D., Misra, S., Allain, A. & Kis, A. Valley Polarization by Spin Injection in a Light-Emitting van der Waals Heterojunction. *Nano Lett.* **16**, 5792–5797 (2016).
- [3] Mak, K. F., McGill, K. L., Park, J. & McEuen, P. L. The valley Hall effect in MoS₂ transistors. *Science* **344**, 1489–1492 (2014).

Electric field dependent valley polarization in 2D ferromagnetic WSe₂/CrSnSe₃ heterostructure

Brahim Marfoua^{*} and Jisang Hong[†]

Department of Physics, Pukyong National University, Busan 48513, Korea

Along with the traditional charge and spin degree of freedom physical quantities, another physical quantity namely valley state has been introduced as a new degree of freedom that can be utilized for future quantum information storage devices [1]. The valleytronics (valley-dependent electronics) in van der Waals two-dimensional (2D) heterostructures is receiving extensive research efforts. Thus, we investigated the electric field-induced valley polarization in the WSe₂/CrSnSe₃ heterostructures by varying the stacking order. The heterostructure shows indirect band gaps of 270 and 330 meV in the two most stable structures. The WSe₂/CrSnSe₃ heterostructure displays a ferromagnetic ground state with out-of-plane anisotropy (0.02 meV) in one stable stacking (S-1) while a small in-plane anisotropy (-0.01 meV) is found in other stacking (S-2). The Curie temperature is slightly enhanced to 73 K compared to the monolayer CrSnSe₃. We have found the valley splitting of 4 meV in S-1 whereas it became 9 meV in the S-2 system. The valley splitting is further enhanced if an electric field is applied from CrSnSe₃ to the WSe₂ layer whereas it is suppressed in the reversed electric field. Particularly, the S-2 structure shows a giant valley splitting of 67 meV at an electric field of 0.6 V/Å. We attribute this electric field-dependency to the dipolar effect. Overall, our findings may imply that the WSe₂/CrSnSe₃ heterostructure can be a potential structure for obtaining a giant valley splitting.

Reference

- [1] Yu, Z.-M., Guan, S., Sheng, X.-L., Gao, W. & Yang, S. A. Valley-Layer Coupling: A New Design Principle for Valleytronics. *Phys. Rev. Lett.* **124**, 037701 (2020).

Phase Transition-induced spin pumping in FeRh/Pt

Taekhyeon Lee^{1*}, Min Tae Park², Se Kwon Kim¹, Kyung-Jin Lee¹,
Myung Hwa Jung² and Kab-Jin Kim¹

¹Department of Physics, Korea Advanced Institute of Science and Technology, Daejeon, Republic of Korea

²Department of Physics, Sogang University, Seoul, Republic of Korea

Spin pumping is a phenomenon in which precessing magnetization injects a spin current into an adjacent non-magnetic layer.[1] So far, the majority of the studies have used the small angle precession of ferromagnet, known as ferromagnetic resonance (FMR), to pump spins into the neighboring non-magnet (spin detecting layer), resulting in a steady spin pumping signal.[2] Here we report a novel spin pumping mechanism by which a phase transition pumps spins into adjacent non-magnetic layer. Using real-time electrical detection technique, we observe a transient spin pumping signal in FeRh/Pt where FeRh undergoes phase transition from an antiferromagnet to a ferromagnet around 370 K.[3] The spin pumping signal appears during the phase transition of FeRh, and is found to be about 3 orders of magnitude larger than that found previously for FMR-induced spin pumping. The result can be explained by exchange field-induced large angle and high frequency spin pumping. Our work provides a novel way to generate a spin current, which could lead further studies on a spin pumping induced by other magnetic phase transitions.

References

- [1] Y. Tserkovnyak, A. Brataas, and G. E. W. Bauer, Phys. Rev. B - Condens. Matter Mater. Phys. 66, 1 (2002).
- [2] O. Mosendz, V. Vlaminck, J. E. Pearson, F. Y. Fradin, G. E. W. Bauer, S. D. Bader, and A. Hoffmann, Phys. Rev. B - Condens. Matter Mater. Phys. 82, 1 (2010).
- [3] S. Maat, J. U. Thiele, and E. E. Fullerton, Phys. Rev. B - Condens. Matter Mater. Phys. 72, 1 (2005).

Unconventional spin-orbit torques arising from 3d transition metal with an ultrathin Pt insertion layer

Jun-Ho Kang^{1*}, Soogil Lee², Woon-Jae Won¹, Min-Gu Kang²,
Byong-Guk Park² and Kab-Jin Kim¹

¹Department of Physics, KAIST, Daejeon 34141, Korea

²Department of Materials Science and Engineering, KAIST, Daejeon 34141, Korea

Current-induced spin orbit torque (SOT) in normal metal (NM)/ferromagnet (FM) hetero-structures has been a central theme in spintronic research [1]. The orthodox SOT theory states that the spin current generated in the NM layer due to the large spin orbit coupling (SOC) is injected into the FM layer, resulting in a torque in magnetic moments of FM. Therefore, materials having a large SOC, e.g., heavy metals, have usually been used in NM layer. However, recent discoveries about non-trivial SOT in light metal/ferromagnet imply that the torque can be generated not only by the SOC-mediated spin current but also by the orbital current itself [1-3]. This suggests that we can efficiently generate a torque by using orbital current, known as orbital torque, even with light metals having a weak SOC.

In this presentation, we provide an experimental evidence for the large orbital torque. We prepared Co/Pt($t = 0 \sim 5$ nm)/Cr layer in which thickness-varied Pt layer is inserted between Co and Cr layer. We found that the SOT is weak without Pt layer, implying that the orbital current generated from Cr layer is hardly exert a torque to Co layer. However, we found that the SOT is significantly enhanced when we insert ultrathin Pt layer. This suggests that the orbital current is converted into the spin current in Pt insertion layer due to the large SOC of Pt, followed by the injection of converted spin into the adjacent Co layer. The orbital origin is further studied by varying the thickness of Cr or by varying the light metals, e.g., Cu and Ti. Our results provide a new way to generate SOT, which opens a possibility for the efficient manipulation of spintronic devices.

References

- [1] A. Manchon, et al, Rev. Mod. Phys. 91, 035004 (2019)
- [2] Shilei Ding, et al, Phys. Rev. Lett, 125, 177201 (2020)
- [3] Junyeon Kim, et al, Phys. Rev. B, 103, L020407 (2021).
- [4] Dongwook Go, et al, Phys. Rev. Lett, 121, 086602 (2018)

Boron concentration dependence of magnetic properties and structural characteristics of MgO/CoFeB/MgO

Jun-Su Kim^{1*}, Gukcheon Kim², Jinwon Jung², Jaehun Cho³, Woo-Yeong Kim⁴, Chun-Yeol You^{1†}

¹Department of Emerging Materials Science, DGIST, Daegu, Republic of Korea

²SK hynix Inc., Icheon, Republic of Korea

³Convergence Research Institute, DGIST, Daegu, Republic of Korea

⁴Department of Materials Science and Engineering, Korea University, Seoul, Republic of Korea

*Corresponding Author email: cyyou@dgist.ac.kr

CoFeB-MgO system has been established as a representative ferromagnetic layer of spin based memory devices since the discovery of high TMR and interfacial perpendicular magnetic anisotropy (iPMA) characteristics. To secure the two major properties, control of CoFeB layer crystallinity is an important theme. And it is well known that the crystallinity of CoFeB is closely linked with the boron concentration. However, many previous works have not touched how the amount of boron affect the overall crystallinity of CoFeB. Here, we present three conclusions. First is a critical boron concentration at which CoFeB abruptly crystallizes. And the second highlights remained boron effect in crystallized CoFeB. Lastly, the third one provides the obvious causal effect that the

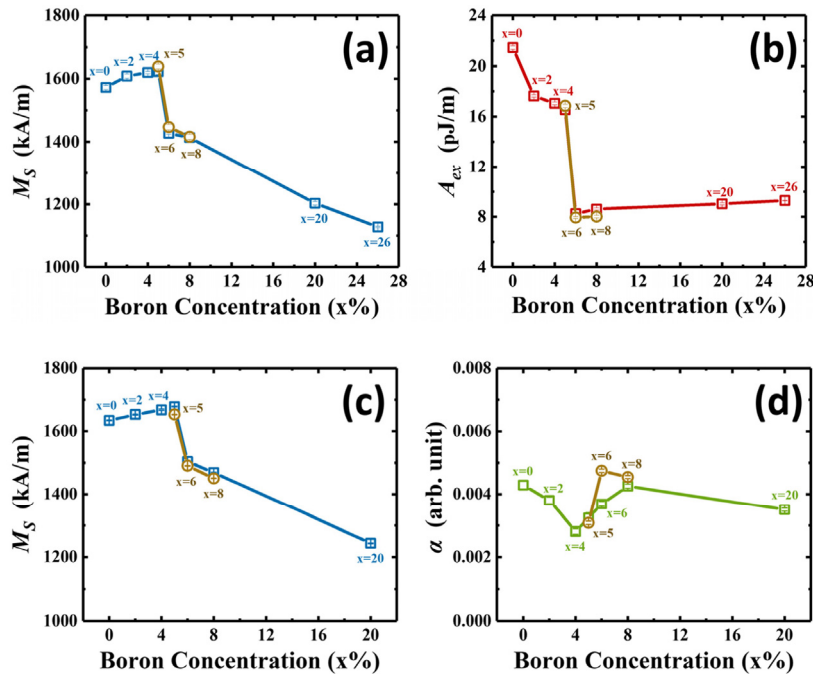


Fig. 1. Brillouin light scattering (BLS) and ferromagnetic resonance (FMR) results. BLS results for the (a) saturation magnetization and (b) exchange stiffness constant (A_{ex}) following to boron concentration. FMR results for the (c) saturation magnetization and (d) Gilbert damping constant regarding to boron concentration.

Brown disks shows the evaluated properties of 18nm CoFeB for trend confirmation

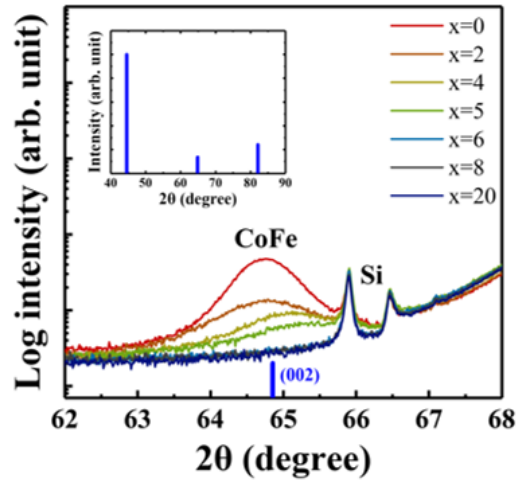


Fig. 2. X-ray diffraction (XRD) theta-2theta scan. XRD spectra shows bcc (002) CoFe peak in crystallized boron concentration section (0~ 5%). With increasing boron concentration, the peak intensity decreases, and peak linewidth is broaden.

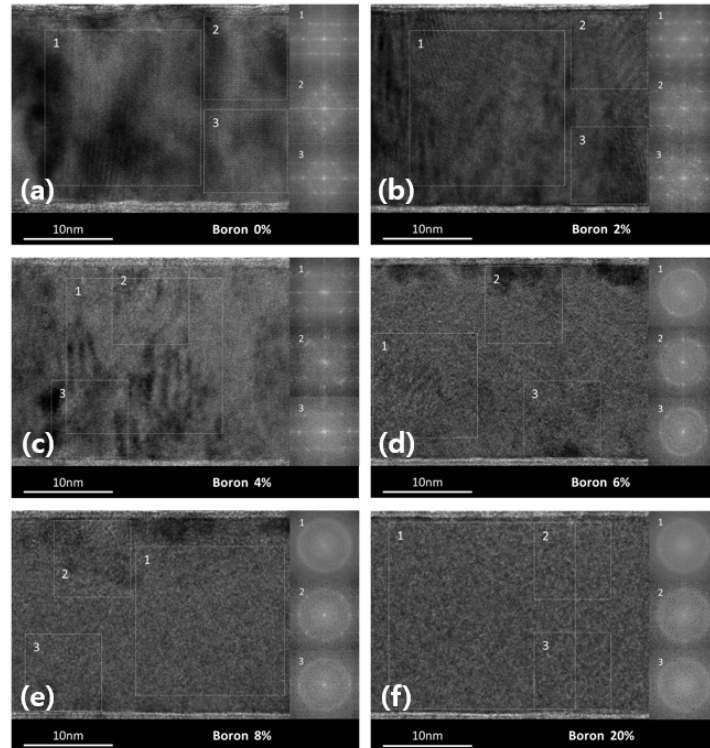


Fig. 3. Cross-sectional transmission electron microscopy (TEM) image and fast Fourier transform (FFT) images.

(a-g) is cross sectional TEM image. And each inset means results of FFT for each selected area of top and bottom interface, and middle of layer.

previous structural changes caused by boron concentration resulted in drastic property changes of CoFeB for the saturation magnetization (M_s), exchange stiffness (A_{ex}), and Gilbert damping constant (α). This work provides the criterion of crystallization of CoFeB and emphasize the effect of boron on both microstructure and properties.

Improved Spin-Orbit Torque Switching Efficiency by He⁺ Ion Irradiation

Suhyeok An^{1*}, Eunchong Baek, Jin-A Kim¹, Ki-Seung Lee^{2*}, Chun-Yeol You^{1†}

¹A Department of Emerging Materials Science, DGIST, Daegu, Korea

²Emerging Materials Science Research Center, DGIST, Daegu, Korea

*Correspondent to kslee@dgist.ac.kr and cyyou@dgist.ac.kr

The magnetic thin films with inversion symmetry breaking have been investigated because of its great potential for application of magnetic random access memory (MRAM) devices and scientific interests about spin-orbit coupling (SOC) phenomena. Especially because Heavy-metal (HM) / Ferromagnet (FM) / Oxide (MgO) structure has strong SOC at the HM/FM interface and inversion symmetry breaking system, resulting in strong perpendicular magnetic anisotropy (PMA) [1], spin-orbit torque (SOT) [2] and Dzyaloshinskii-Moriya interaction (DMI) [3,4]. Among them, the SOT driven magnetization switching is a perspective phenomenon because of its application to the spintronic devices. For more efficient SOT based spin devices, many researchers try to reduce critical switching current by HM layer modulation [5], interface modifying [6, 7], and ion irradiation [8, 9].

Here, we report that local magnetic properties are modulated by He⁺ ion irradiation in Pt/Co/MgO structure. The Pt(5)/Co(0.8)/MgO(2) structure is irradiated by He⁺ ion with the dose range from 0 to 30 ions/nm², then the reduction of switching current is shown about ~ 30% at dose amount of 30 ions/nm² under external magnetic field of 3 kOe. The reduction of switching current is related with effective PMA field and spin Hall angle (SHA), we analyze each phenomenon using generalized Sucksmith-Thompson method and harmonic Hall analysis, respectively. The result show the decrease of PMA field from 13.7 kOe to 8.5 kOe (~ 38%) and increase of SHA from 0.096 to 0.132 (~ 27%). And then, for understanding the reason of improvement of SHA, we conduct the resistivity measurement with temperature variation from 5 K to 225 K in 5 nm thickness single Platinum layer. The results show gradual increasing tendency in resistivity and decreasing tendency in residual-resistivity ratio (ρ_{300K}/ρ_{5K}) at higher dose amount. These imply that the He⁺ ion irradiation makes extra scattering sources in HM layer and result in increasement of resistivity and SHA.

References

- [1] Manchon, A. *et al.*, *J. Appl. Phys.* **103**, 07A912, (2008).
- [2] Miron, I. M. *et al.*, *Nature* **476**, 189–193 (2011)
- [3] Lee, J. M. *et al.*, *Nano Lett.* **16**, 62–67 (2015)
- [4] Cho, J *et al.*, *Nat. Comm.* **6**, 7635 (2015).
- [5] Lee J. W. *et al.*, *Phys Rev. B* **96**, 064405 (2017).
- [6] Kim Y. J. *et al.*, *Acta Mater.* **200**, 551-558 (2020)
- [7] Hasegawa K. *et al.*, *Phys. Rev. B* **98**, 020405 (2018)
- [8] Zhao X. *et al.*, *Appl. Phys. Lett.* **116**, 242401 (2020)
- [9] Dunne P. *et al.*, *Nano. Lett.* **20**, 7036-7042 (2020)

Static and time-resolved optical detection of magnetization vectors by spin Hall effect

Young-Gwan Choi^{1*} and Gyung-Min Choi^{1,2†}

¹Department of Energy Science, Sungkyunkwan University, Suwon 16419, Korea

²Center for Integrated Nanostructure Physics, Institute for Basic Science, Suwon 16419, Korea

*Corresponding authors

The charge-to-spin conversion phenomena driven by spin Hall effect (SHE) in nonmagnetic metal has been emphasized. To clarify the phenomena, electronic measurement techniques have been widely used with ferromagnetic metal(FM) layer, e.g. CoFeB thin film, to observe spin-transfer torque analysis, e.g. anomalous Hall measurement, planar Hall effect, and so on. However, with the FM film on the material, it is difficult to specify the physical origin of the spin-torque due to introduced other effects, e.g. Rashba interface states, anomalous spin-orbit torque in FM, and so on. Moreover, electronic measurement techniques usually observe static tilting angle of the magnetization vector of the FM film and is difficult to examine its detailed dynamic motion. Here, we introduce a measurement methodology for characterizing the spin polarization and its torque effects on a FM layer. Firstly, we observed magnetization vectors of a heavy metal(HM), Pt, without FM layer using magneto-optical Kerr effect (MOKE) with electrical bias. Second, we traced the precessional motion of the magnetization vector of HM/FM heterostructure by mediating time-resolved MOKE using femtosecond laser. We argue that this technique can pave the way of studying the current-driven spin-polarization and spin-orbit torque phenomena in static and time-domain regime.

Investigation of current-induced spin-orbit torques in $\text{Pt}_x\text{Mn}_{1-x}$ /ferromagnetic heterostructures

Pham Ngoc Luu Ly^{1*}, Kyun-Hun Ko¹ and Gyung-Min Choi^{1,2†}

¹Department of Energy Science, Sungkyunkwan University, Suwon 16419, Korea.

²IBS Center for Integrated Nanostructure Physics, Institute for Basic Science (IBS),
Sungkyunkwan University, Suwon 16419, Korea

The use of spin-orbit torque (SOT) to manipulate magnetization has shown great potential for the development of ultrafast and energy-efficient MRAM in recent years. In this work, we investigate the current-induced spin-orbit torque in $\text{Pt}_x\text{Mn}_{1-x}/\text{NiFe}$ heterostructure by varying the composition of PtMn alloy. We use the optical method based on the magneto-optical Kerr effect to detect the current-induced magnetization rotation both in-plane and out-of-plane directions. By analyzing quadratic MOKE and linear MOKE responses we extract damping-like and field-like components of spin-orbit torque. We also determine composition dependence spin Hall angle for all samples.

Direct Observation of Current-induced Spin Accumulation in InAs Two-dimensional Electron Gas (2DEG) Structure

Won-Bin Lee^{1*}, Seong-Been Kim^{2,3}, Kyung-Jin Lee¹, Kyoung-Whan Kim³,
Hyun-Cheol Koo^{2,3} and Gyung-Min Choi^{4,5}

¹Department of Physics, Korea Advanced Institute of Science and Technology, Daejeon 34141, South Korea

²KU-KIST Graduate School of Converging Science and Technology, Korea University, Seoul, 02841, South Korea

³Center for Spintronics, Korea Institute of Science and Technology, Seoul 02792, South Korea

⁴Department of Energy Science, Sungkyunkwan University, Suwon 16419, South Korea

⁵Center for Integrated Nanostructure Physics, Institute for Basic Science (IBS), Suwon 16419, South Korea

The momentum and spin of electrons are coupled by spin-orbit interaction and this coupling plays an important role in spintronics. The Rashba and spin Hall effects are two of the most representative phenomena due to the spin-orbit coupling (SOC) and conversion between charge and spin is possible by applying these effects. In this research, we investigated the spin-orbit coupling in InAs based two-dimensional electron gas (2DEG) quantum well structure directly by using the magneto-optical method. We applied a charge current into the InAs 2DEG sample, and directly observed current-induced spin accumulation in InAs 2DEG due to the spin-orbit coupling (SOC) by using the magneto-optic Kerr effect (MOKE). As a result, both in-plane spin accumulation throughout the channel by Rashba-Edelstein effect and out-of-plane spin accumulation by spin Hall effect at the edges of the channel were confirmed.

Reduced spin-orbit torque switching current by voltage-controlled magnetic easy-cone states

Jimin Jeong^{*}, Min-Gu Kang, Soogil Lee, Byong-Guk Park

Department of Materials Science and Engineering, KAIST, Daejeon 34141, Korea

Spin-orbit torque (SOT) generated by the spin Hall effect (SHE) and/or the Rashba Edelstein effect (REE) offers a fast and reliable switching of the perpendicular magnetization in spintronic devices such as magnetic random-access memories or spin logics [1]. To apply SOT technology to practical devices with low power consumption, it is necessary to reduce the switching current. For this, many studies have focused on enhancing the charge-to-spin conversion efficiency in heavy metal/ferromagnet structures or introducing the exotic materials such as topological insulators or Weyl semimetals that exhibit a large spin Hall angle [2].

In this work, we demonstrate that the SOT switching current is significantly reduced by modulating magnetic easy-cone states through voltage-controlled magnetic anisotropy (VCMA). The introduction of a thin Pt layer (0.2 nm) at CoFeB/MgO interface enhances VCMA effect and enables to effectively modulate the first- and second-order magnetic anisotropies of Ta/CoFeB/Pt/MgO structures by a gate voltage V_G ; when applying sequential negative voltage pulses, the first- (second-) order magnetic anisotropy gradually decreases (increases), modulating the easy-cone angle from 0 to 58 degree. This results in reduction of the SOT switching current by up to 50%. Furthermore, reversible and nonvolatile nature of the voltage-controlled easy-cone state allows the formation of multilevel states, which can be utilized in spintronic neuromorphic devices.

References

- [1] Adv. Mater. **32**, 1907148 (2020)
- [2] Nat. Mater. **17**, 808-813 (2018)

Unconventional angle dependence of magnetoresistance in GdO_x

Woon-Jae Won^{1*}, Jun-Ho Kang¹, Soogil Lee², Young-Hun Cho³,
Byong-Guk Park² and Kab-Jin Kim¹

¹Department of Physics, KAIST, Daejeon 34141, South Korea

²Department of Materials Science and Engineering, KAIST, Daejeon 34141, South Korea

³Center for Scientific Instrumentation, KBSI, Daejeon 34133, South Korea

Gadolinium (Gd) is an interesting rare-earth metal which exhibits fascinating electrical and magnetic properties. As the Gd is one of the crucial ingredients of ferrimagnet, its importance is rapidly growing with the emerging of new research field, named as ferrimagnetic spintronics [1,2]. One distinctive property of Gd is that it is very easily oxidized and forms an oxide compound, GdO_x . Recent study has shown that the oxidation and reduction of single Gd layer can be controlled by electric-field-driven oxygen ion migration [3]. However, oxidation dependence of magnetoresistance (MR) of GdO_x has not been investigated in a detailed way.

In this letter, we investigate the angle dependence of MR for the various oxidation levels of GdO_x . To this end, we prepared GdO_x microwire having various oxidation levels, and measured the resistance variation by rotating the magnetic field in xy, yz, zx planes. Here, we flow current along the wire longitudinal direction (x-axis). The angle dependent resistivity shows that $\rho(B_{\text{ext}} \parallel z) \gg \rho(B_{\text{ext}} \parallel x) > \rho(B_{\text{ext}} \parallel y)$, which is clearly different from the angle dependence of conventional anisotropic magneto resistance (AMR) or spin Hall magnetoresistance (SMR). This unique angle dependence is observed for various samples with different oxidation levels. We ascribe the underlying mechanism of unconventional angle dependence to the anomalous hall magnetoresistance (AHMR) [4], but further studies are required to elucidate the exact origin.

References

- [1] Kim, K. J. et al. Fast domain wall motion in the vicinity of the angular momentum compensation temperature of ferrimagnets. *Nature Materials* 16, 1187–1192 (2017)
- [2] Changsoo Kim, Soogil Lee, et.al. Distinct handedness of spin wave across the compensation temperatures of ferrimagnets. *Nature Materials* 19, 980–985 (2020)
- [3] Jun-Ho Kang, et.al. Control of electrical resistance and magnetoresistance by electric-field-driven oxygen ion migration in a single GdO_x wire. *NPG Asia Materials* 12, 44 (2020)
- [4] Yumeng Yang, Ziyang Luo, et. al. Anomalous Hall magnetoresistance in a ferromagnet. *Nature Communications* 9, 2255 (2018)

Multi-level States of GaMnAsP Single Layer Induced by Spin-orbit Torque

Kyung Jae Lee^{1*}, Seongjin Park¹, Phunvira Chongthanaphisut¹, Sanghoon Lee^{1†},
X. Liu², M. Dobrowolska² and J. K. Furdyna²

¹Physics Department, Korea University, Seoul 136-701, Korea

²Physics Department, University of Notre Dame, Notre Dame, IN 46556, USA

We have investigated spin-orbit torque (SOT) induced switching of a 25 nm GaMnAsP single layer with perpendicular magnetic anisotropy (PMA) grown by molecular beam epitaxy (MBE). We have fabricated Hall device along [100] crystal direction, in which Rashba-type and Dresselhaus-type spin-orbit induced (SOI) fields are perpendicular to each other. The SOT induced magnetization switching was carried out with a current density of $\sim 1.9 \times 10^6$ A/cm² under in-plane bias field of 500 Oe at 55 K. We have achieved a reproducible and tunable multi-level states of minor-loop by performing current scan ranging from 8.0×10^5 A/cm² to 1.9×10^6 A/cm² while monitoring Hall resistance. This multi-level states can also be produced by applying pulsed current with duration of 160 ms. The results suggest that the system can be used as a memristors for neuromorphic computing.

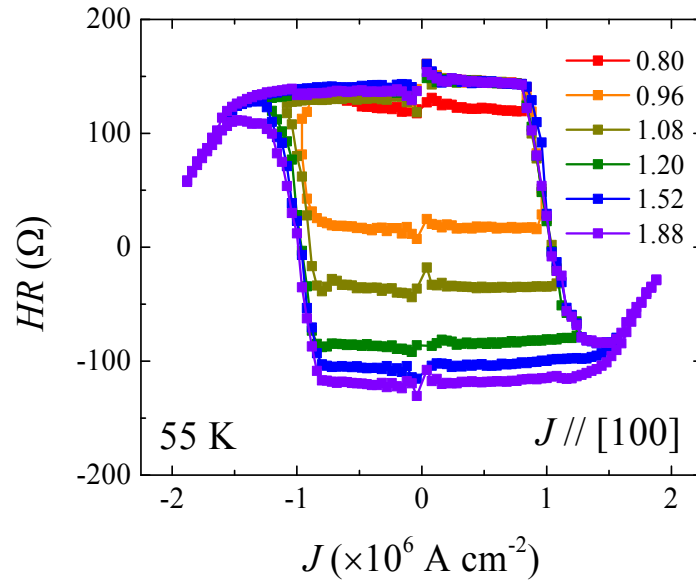


Fig. 1. Current scan minor loops obtained from a GaMnAsP single layer.

Ruderman-Kittel-Kasuya-Yosida-type interfacial Dzyaloshinskii-Moriya interaction in heavy metal/ferromagnet heterostructures

Taehyun Kim^{1*}, In Ho Cha¹, Yong Jin Kim¹, Gyu Won Kim¹, Andrey Stashkevich²,
Yves Roussigné², Mohamed Belmeguenai², Salim M. Chérif²,
Alexander S. Samardak^{3,4} and Young Keun Kim¹

¹Department of Materials Science and Engineering, Korea University, Seoul, Korea

²Laboratoire des Sciences des Procédés et des Matériaux, CNRS-UPR3407,
Université Sorbonne Paris Nord, Villetaneuse, France

³School of Natural Sciences, Far Eastern Federal University, Vladivostok, Russia

⁴National Research South Ural State University, Chelyabinsk, Russia

The interfacial phenomena have been recently revisited and experimentally illustrated because of its huge potential to explore novel magnetic behaviors such as Skyrmions, chiral domain wall dynamics, and spin-Hall effects [1,2]. Among various interfacial effects, interfacial Dzyaloshinskii-Moriya interaction (iDMI) is drawing attention [3]. Here, we have experimentally shown that iDMI can also be derived from FM/oxide interface by inserting MgO spacer layer between heavy metal and ferromagnetic metal.

We fabricated sample structure of Ta (3)/Pt (5)/MgO (t_{MgO})/CoFeSiB (0.9)/MgO (1.0)/Ta (2). The magnetically dead layer plot of t_{FM} vs. $M_s t_{\text{FM}}$ plot is used to calculate the effective saturation magnetization value $M_{s,\text{eff}}$ is obtained. Using Brillouine Light Scattering (BLS) spectroscopy, iDMI energy density is calculated. The most pronounced iDMI value ($D_{\text{eff}} = -0.70 \pm 0.06 \text{ mJ/m}^2$) occurred when there was no MgO spacer layer. As the t_{MgO} increases, iDMI energy density shows an oscillating-like behavior. To qualitatively understand the experimental results, a toy model based on RKKY exchange coupling was introduced. From the numerical simulation, we confirmed that the oscillation of the iDMI was the result of the RKKY-type interaction between itinerant electrons

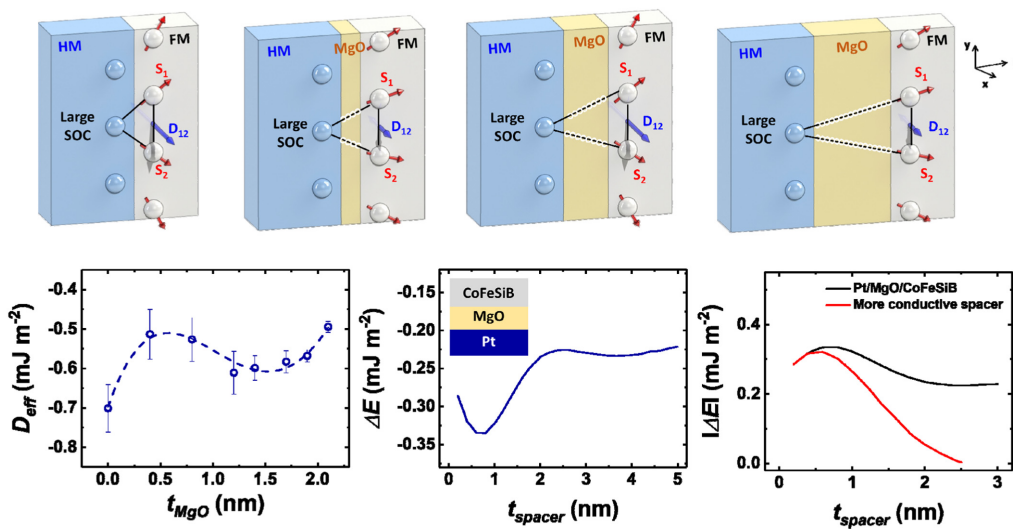


Fig. 1. Experimental and calculated iDMI energy density vs. t_{MgO}

through the spacer. Such behavior could be achieved with the help of reduction in MgO bandgap energy due to the oxygen deficiency. The structural analysis is conducted using X-ray Diffraction (XRD), Transmission Electron Microscope (TEM), and Secondary Ion Mass Spectroscopy (SIMS). Reduced MgO bandgap energy was confirmed using Reflective Electron Energy Loss Spectroscopy (REELS).

This study confirmed that the origin of the iDMI is an exchange mechanism linking the two ferromagnetic metal atoms via a spin-orbit coupling heavy metal atom and the RKKY-type interaction could be used to explain. Hence, the magnitude of iDMI could be modified through spacer layer thickness between heavy metal and ferromagnetic metal engineering.

References

- [1] A. Soumyanarayanan *et al.*, Nat. 539, 509 (2016).
- [2] S. Woo *et al.*, Nat. Mater. 15, 501 (2016).
- [3] J. Cho *et al.*, Nat. Commun. 6, 7635 (2015).

Current induced magnetization switching in GaMnAsP film with Perpendicular Magnetic Anisotropy

Seongjin Park¹, Kyung Jae Lee^{1*}, Phunvira Chongthanaphisut¹, Sanghoon Lee^{1†},
X. Liu², M. Dobrowolska² and J. K. Furdyna²

¹Physics Department, Korea University, Seoul 136-701, Korea

²Physics Department, University of Notre Dame, Notre Dame, IN 46556, USA

We have investigated spin-orbit torque (SOT) magnetization switching behavior of (Ga,Mn)(As,P) layer with perpendicular anisotropy. In order to study crystalline dependence of SOT magnetization switching, we have fabricated Hall devices along the $[1\bar{1}0]$ and the $[110]$ directions, in which the Rashba-type and Dresselhaus-type spin-orbit fields are parallel and antiparallel to each other. We have adapted Hall effect measurements to monitor magnetization reversal process of the film. The Hall resistance (HR) measured with in-plane and out-of-plane magnetic field revealed that the (Ga,Mn)(As,P) film has out-of-plane magnetic easy axis. The SOT switching experiments was performed by scanning amplitude of current under in-plane bias field. In this experiment, we have observed opposite switching chirality for the $[1\bar{1}0]$ and the $[110]$ directions, indicating opposite spin-orbit induced field for these two current directions. The results indicate that the Dresselhaus-type spin-orbit field is stronger than the Rashba-type field in a crystalline (Ga,Mn)(As,P) film.

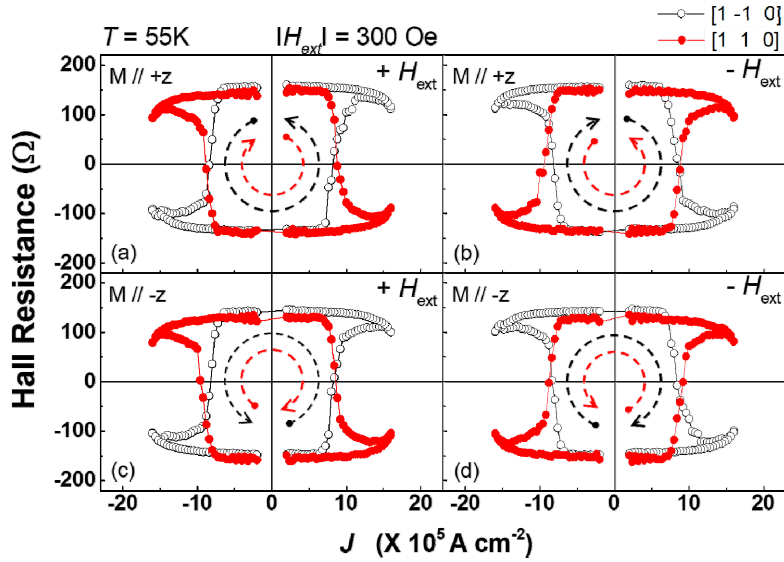


Fig. 1. (a). Current induced magnetization switching for the (Ga,Mn)(As,P) film. Hall resistance was measured as a function of current at 55 K for four initial conditions. Open and solid circles represent data obtained from the $[1\bar{1}0]$ and the $[110]$ measurements, respectively. Current scan sequences are shown as black and red dashed arrows, showing switching chirality for the $[1\bar{1}0]$ and $[110]$ direction, respectively.

Gigahertz frequency modulation of spin Hall oscillator via voltage controlled magnetic anisotropy engineering

Jong-Guk Choi^{1*}, Jaehyeon Park², Kab-Jin Kim² and Byong-Guk Park¹

¹Department of Materials and Science Engineering, KAIST, Daejeon 34141, Korea

²Department of Physics, KAIST, Daejeon 34141, Korea

Spin Hall nano-oscillators (SHNO), which activates the auto-oscillation motion of magnetization by spin current, is attracting attention as a neuromorphic device because it can easily interact with an external microwave signal through a synchronization process [1]. The SHNO as a neuromorphic device should be able to represent a wider range of frequencies in order to interact with signals of more diverse frequencies. However, the voltage-driven frequency modulation is still in the megahertz range, which is not sufficient to utilize SHNO as neuromorphic device.

Here, we demonstrate the voltage-driven frequency modulation of 2.1 GHz in a Pt/[Co/Ni]_n/AlO_x SHNO by a gate bias of up to 5V, which is 42 times larger than the previous high record [2]. A positive voltage increases the auto-oscillation frequency, and a negative voltage restores the frequency to its initial. Such large frequency modulation is found to originate from variation of perpendicular magnetic anisotropy field of 10⁻¹ T. Furthermore, It is possible to modulate frequency cumulatively using repetitive voltage pulses, suggesting that the proposed SHNO can act as synaptic device in neuromorphic computing. Our result will provide an important building block for spin-based low-power neuromorphic device applications.

References

- [1] Zahedinejad, M. et al, Two-dimensional mutually synchronized spin hall nano-oscillator arrays for neuromorphic computing, *Nat. nanotech.* **15**, 47 (2020)
- [2] Fulara, H. et al, Giant voltage-controlled modulation of spin Hall nano-oscillator damping, *Nat. Commun.* **11**, 4006 (2020).

Observation of Quantum-like Interference Effect in Graphene-based Devices with Random Co Clusters

Thi-Nga Do^{1,2*}, Sehee Lee³, Chanyong Hwang³, Tae Hee Kim^{1,2†}

¹IBS Center for Quantum Nanoscience, Ewha Womans University, Seoul, Korea

²Department of Physics, Ewha Womans University, Seoul, Korea

³Korea Research Institute of Standards and Science, Daejeon, Korea

The quantum correction to the conductivity in graphene has been taking numerous interests due to its unique electronic band structure as well as the chiral nature of its charge carriers.

In this work, we focused on demonstrating the interplay of graphene/Co interface for the observation of quantum-like interference effect in the graphene-based heterostructures. In order to clarify the role of interface effect, a sequence of devices as a function of Co thickness from 0 – 2.5nm sandwiched between large-area CVD graphene and 3.0nm-thick of Hall bar Pt has been prepared using *in-situ* shadow mask patterning technique by the UHV-MBE system. Surprisingly, the magnetoresistance (MR) results clearly indicated not only the co-existence of weak localization (WL) and weak antilocalization (WAL) effect at 77K but also a remarkable enhancement of both localization effects as decreasing the Co thickness. Interestingly, it is important to declare that we observed the highest upturn MR curvature in the sample with 0.5 Å at the large applied magnetic field, which could be elucidated by the random Co clusters act as the magnetic scattering centers. For microstructural characterization of the heterostructures, the careful analysis of interface properties was performed using the atomic force microscope (AFM).

Our results provide further insights into this phenomenon and highlight the aspect of interface engineering of 2D-material with other ferromagnetic materials to manipulate and develop highly effective spintronic devices with new functionalities.

Gate voltage control of spin Seebeck effect

Jeong-Mok Kim^{1*}, Mingu Kang¹, Cao-Van Phouc², Jong-Ryul Jeong² and Byong-Guk Park¹

¹Department of Materials and Science Engineering, KAIST, Daejeon 34141, Korea

²Department of Materials Science and Engineering, Chungnam National University, Daejeon 34134, Korea

Spin Seebeck effect [1], the transverse electrical current generation via injection of thermal spin current and inverse spin Hall effect in Ferromagnet/Non magnet metal bilayer, is receiving great attention because not only of its physical interest but also of its potential to be applicable in various heat sensing device. Gate voltage tuning of spin current (thermal spin current) [2] also has been actively studied which is enlarging the understanding of spin current generation mechanism and gives a degree of freedom as applicable spin phenomenon.

In this work, we report the gate voltage control of spin Seebeck effect. In the beginning, we experimentally demonstrate that the gate voltage effect can tune the spin thermoelectric voltage non-volitely in the W/CoFeB/AlO_x/ZrO₂ structure. **Figure 1** (a) shows the schematic of gate voltage modulation on spin thermoelectric signal in the W/CoFeB/AlO_x/ZrO₂/Ru structure. We measured the voltage in y-direction with the vertical temperature gradient induced by laser. Before the measurement, the gate voltage of 13 V is applied in 100 °C. Figure 1 (b) shows the gate voltage effect on spin thermoelectric voltage in W(4 nm)/CoFeB(2 nm)/AlO_x(2nm)/ZrO₂(40 nm)/Ru (20 nm) changing external magnetic field B_x , demonstrating the modulation ($\sim 10\mu\text{V}$) of spin thermoelectric signal by gate voltage with 13 V. As shown in the Figure 1 (c), by investigating the laser power dependence, we found that gate voltage effect is linearly increased with the laser power confirming that it is modulation of spin thermoelectric signal. In addition, we investigate the gate voltage effect

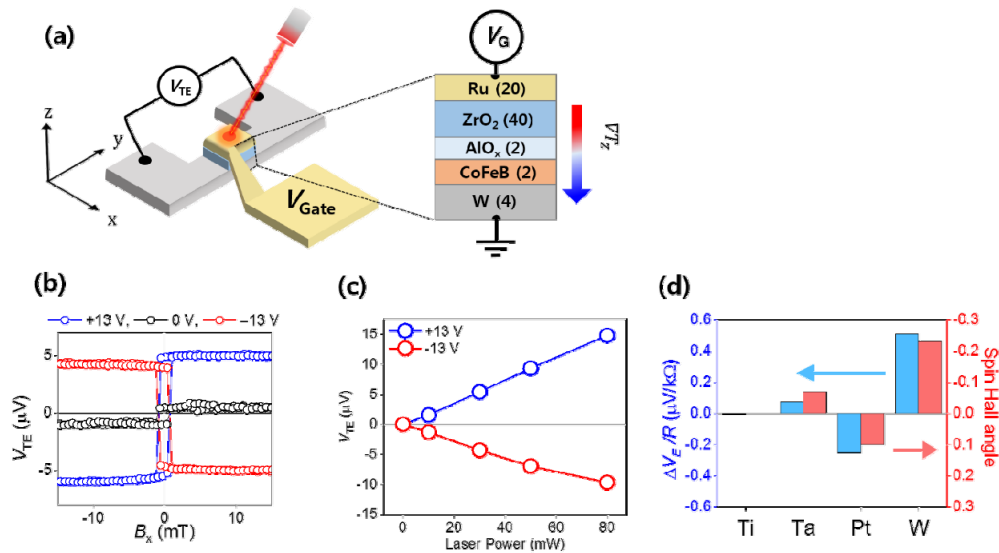


Figure 1. (a) Measurement schematic of gate voltage modulation on spin Seebeck effect in W(4 nm)/CoFeB(2 nm)/AlO_x(2nm)/ZrO₂(40 nm)/Ru(20 nm) structure. (b) Spin thermoelectric voltage after applying gate voltage 13 V with 30 mW laser. (c) Spin thermoelectric voltage after applying gate voltage ± 13 V with various laser power (0~100 mW). (d) Gate voltage effect on Spin thermoelectric signal ($\Delta V_E/R$, blue bar) in various NM (Ti, Ta, Pt, W) in NM(3 nm)/CoFeB(2 nm)/AlO_x(2nm)/ZrO₂(40 nm)/Ru(20 nm) structure and its spin Hall angle (Red bar).

on spin thermoelectric signal in metal which have various spin hall angle (Ti, Ta, Pt) as shown in the Figure 1 (d). We discovered that the gate voltage effect on spin thermoelectric signal (We define that ΔV_E is the difference of thermoelectric voltage in positive (+13 V) and negative (13 V) gate bias at 30 mW laser) has strong dependence with the spin Hall angle demonstrating that the gate voltage modulate the spin Seebeck effect. This results can pave the way toward the deeper understanding of spin Seebeck effect and realization of novel spin thermoelectric applications.

Method: The metal layers and AlO_x in $\text{NM/CoFeB/AlO}_x/\text{ZrO}_2$ multilayer structure were fabricated by magnetron sputtering with the base pressure under 3.0×10^{-8} Torr at room temperature and AlO_x is plasma oxidized. The ZrO_2 (gate insulator) is fabricated by Atomic layer deposition. The bar shaped structure of $15 \mu\text{m} \times 1 \text{mm}$ is patterned by photolithography and Ar ion milling. In order to apply gate voltage in the structure, Ru is sputtered on the sample with lift off method. The spin thermoelectric voltage was measured by nano-voltmeter with illuminating the laser beam of $5 \mu\text{m}$ diameter and 30 mW power inducing vertical temperature gradient. The thermoelectric voltage was measured after applying a gate voltage under the 100°C .

References

- [1] Uchida, K et al, Observation of longitudinal spin-Seebeck effect in magnetic insulators Phys. Lett. 97, 172505 (2010).
- [2] Jeon, K-R et al. Voltage tuning of thermal spin current in ferromagnetic tunnel contacts to semiconductors, Nat. Mater. 13, 360–366 (2014)

Control of magnetization compensation temperature in ferrimagnetic GdCo thin films by He⁺ irradiation

Jisu Kim^{1*}, Seyeop Jeong¹, Donghyeon Lee¹, Taekhyeon Lee², Suhyeok An³, Kab-Jin Kim²,
Ki-Seung Lee³, Chun-Yeol You³, Sanghoon Kim^{1†}

¹Department of Physics, University of Ulsan, Korea

²Department of Physics, Korea Advanced Institute of Science and Technology, Korea

³Department of Emerging Materials Science, Daegu Gyeongbuk Institute of Science & Technology

Ferrimagnet is a material whose magnetic moments are aligned in opposite directions like antiferromagnets with non-zero net moment. In a class of ferrimagnets composed of rare earth (RE)-transition metal (TM), the magnitude of each magnetic moment can be adjusted by changing the ratio of the RE-TM or the measurement temperature. Since the temperature dependence of the magnetization of each element is different, the magnetic moments cancel each other at the magnetization compensation temperature T_M .

In this study, He⁺ ions were accelerated with 20 keV energy to a 15-nm-thick Gd₃₆Co₆₄ film with perpendicular magnetic anisotropy. We observe that the T_M decreases after He⁺ irradiation. We also succeed in a local modulation of T_M using He⁺ ion beam. In addition, we will present that magnetic switching properties by current or external field can be modulated by the He⁺ irradiation.

References

- [1] Kab-Jin Kim et al., Fast domain wall motion in the vicinity of the angular momentum compensation temperature of ferrimagnets, *Nature Materials*, 16, 1187-1192, (2017)
- [2] Woo Seung Ham et al., Temperature dependence of spin-orbit effective fields in Pt/GdFeCo bilayers, *Appl.Phys.Lett.* 110, 242405, (2017)

Anomalous Hall effect in a quaternary compensated ferrimagnetic spin gapless semiconductor Heusler compound TiZrMnAl

T. Thuy Hoang^{1*}, Minkyu Park², Do Duc Cuong¹, S. H. Rhim¹ and S. C. Hong¹

¹Department of Physics and Energy Harvest-Storage Research Center, University of Ulsan

²Research Institute of Basic Sciences, University of Ulsan

(sonny@ulsan.ac.kr, schong@ulsan.ac.kr)

An intrinsic anomalous Hall conductivity (AHC) is predicted in the compensated ferrimagnetic half-metal inverse-Heusler Ti_2MnAl with AHC of $300 \Omega^{-1}\text{cm}^{-1}$ [1]. A spin gapless semiconductor(SGS)[2] magnetic material that has a finite band gap for one spin channel but a just closed (zero) gap for the other. Compensated ferrimagnetic SGSs can be promising solutions to achieve high AHC with no stray field. Recently, the quaternary Heusler compound TiZrMnAl (space group $F\bar{4}3m$) is predicted to be SGS with no magnetization, satisfying Slater-Pauling rule [3]. In this work, we investigate the AHC of TiZrMnAl compounds using VASP and the FLAPW method. Since Ti and Zr belong to the same group in the periodic table so to be equivalent in electronic properties, TiZrMnAl is stabilized in two phases of α -phase and β -phase which are distinguished by the octahedral environments, as shown in Fig. 1(a). We consider the two phases. Our results show that α -phase is energetically more stable by the energy difference of 0.34 eV/fu, compared to β -phase. The band structures obtained from calculations including spin-orbit interaction are presented in Fig. 1(b). One spin bands are denoted

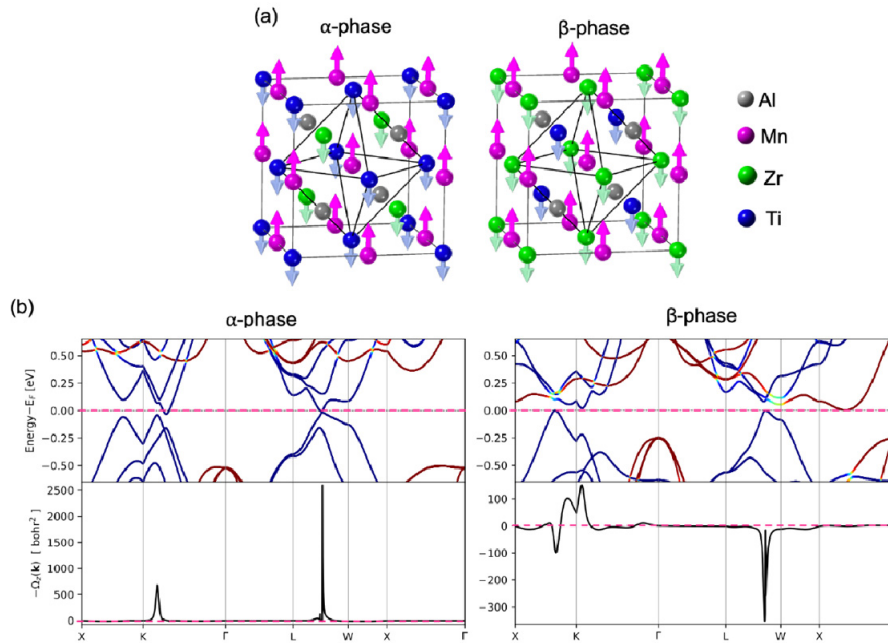


Fig. 1. (a) Octahedral environments of α - and β -phase and (b) band structures and Berry curvatures in α - and β -phase. E_F is set to zero.

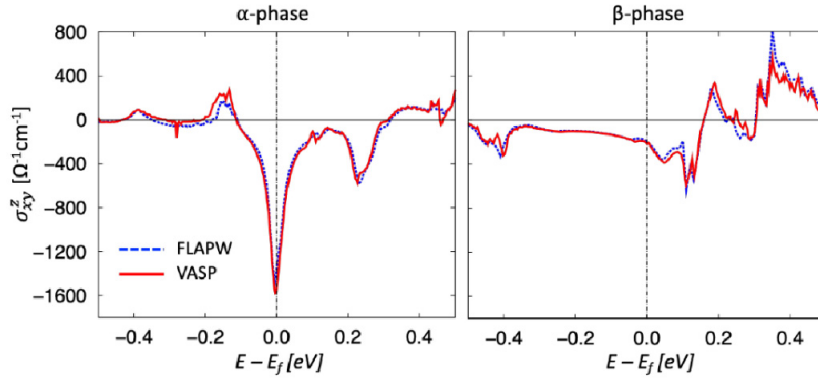


Fig. 2. Calculated AHC obtained from the FLAPW (dashed line) method and VASP (solid line).

in blue and the other ones done in red. TiZrMnAl in α -phase is clearly Type-I SGS; no gap in one spin channel and a gap in the other spin channel. However, it is quite interesting that TiZrMnAl in β -phase is a new type SGS which does not belong any types proposed previously[2]. The Mn local moment is compensated exactly by the anti-aligned Ti and Zr local moments, resulting in vanishing magnetization. TiZrMnAl in α -phase shows a significant AHC of $1470 \Omega^{-1}\text{cm}^{-1}$ while TiZrMnAl in β -phase does moderate AHC of $216 \Omega^{-1}\text{cm}^{-1}$. The large AHC of α -phase is originated from the large Berry curvature from the band touching point in one spin channel along the symmetry line $\overline{\text{LW}}$ (Fig 1. (c)). The calculated AHC are in a good agreement between VASP and the FLAPW method (Fig 2). We will discuss origin of the quite large AHC in α -phase with topology analysis by Wannier tight-binding models obtained from first-principles band structures.

References

- [1] W. Shi, L. Muechler, K. Manna, Y. Zhang, K. Koepernik, R. Car, J. van den Brink, C. Felser, and Y. Sun. Phys. Rev. B **97**, 060406(R) (2018)
- [2] X. L. Wang. Phys. Rev. Lett. **100**, 156404 (2008)
- [3] L. Hao, P. Cheng, R. Khenata, P. F. Liu, X. Wang, T. Yang. J. Magn. Magn. Mater. **508**, 166880 (2021)

Observation of spin-current transport in normal metal/Nb/ferromagnet tri-layers

Min Hyeok Lee^{1*}, Gyungchoon Go², Yong Jin Kim¹, In Ho Cha¹, Gyu Won Kim¹,
Taehyun Kim¹, Kyung-Jin Lee² and Young Keun Kim^{1†}

¹Department of Materials Science and Engineering, Korea University, Seoul 02481, Republic of Korea

²Department of Physics, Korea Advanced Institute of Science and Technology, Daejeon 34141, Republic of Korea

Spin-orbit torque (SOT) is drawing attention because it is applicable for the writing method of a brand-new memory device that is energy efficient and non-volatile. When electrical current is induced to normal metal (NM)/ferromagnet (FM) heterostructures, a transverse spin current is generated. An angular momentum transferred to magnetization by the generated spin current acts as a torque [1]. For the application of SOT to memory or logic devices, it is crucial to investigate the mechanisms of this new physical phenomenon. Many researchers had employed the experiment varying the NM thickness based on the NM/FM bi-layer structure to unveil the origin [2-4]. In this system, NM (or NM/FM interface) plays a single spin current source. However, to enhance the SOT efficiency, the experimental system has been improved to tri-layer structures containing more than one source [5, 6]. This study would like to discuss how the thickness dependence of SOT efficiency behaves in NM/Nb/FM tri-layer structures where either NM1/NM2 or NM/FM bilayer act as an additional spin current source. The SOT efficiency decreased as the Nb thickness (t_{Nb}) increased in Ta 3/Nb t_{Nb} /CoFeB 0.9 structure. This result suggested that the thicker Nb layer suppressed the spin current, which was generated from Ta (or Ta/Nb), from reaching the FM layer. However, in the Pt/Nb/CoFeB series in which Pt with a different SOC sign from Ta and Nb was employed, the behavior of SOT efficiency is different. When $t_{Nb} \leq 3$ nm, the device showed a positive signal but negative for $t_{Nb} > 3$ nm. The current-induced SOT switching also confirmed this sign reversal, which showed a well-designed experiment. These results provide a systematic understanding of the thickness-dependent SOT properties.

References

- [1] I. M. Miron *et al.*, Perpendicular switching of a single ferromagnetic layer induced by in-plane current injection, *Nature* 476 (2011) 189–193.
- [2] J. Kim *et al.*, Layer thickness dependence of the current-induced effective field vector in Ta|CoFeB|MgO, *Nat. Mater.* 12, 240-245 (2013).
- [3] I. M. Miron *et al.*, Current-driven spin torque induced by the Rashba effect in a ferromagnetic metal layer, *Nat. Mater.* 9, 230 (2010).
- [4] W. Zhang *et al.*, Role of transparency of platinum–ferromagnet interfaces in determining the intrinsic magnitude of the spin Hall effect, *Nat. Phys.* 11, 496-503 (2015).
- [5] Q. Ma *et al.*, Switching a Perpendicular Ferromagnetic Layer by Competing Spin Currents, *Phys. Rev. Lett.* 120, 117703 (2018).
- [6] S.-H. C. Baek *et al.*, Spin currents and spin-orbit torques in ferromagnetic trilayers, *Nat. Mater.* 17, 509-513 (2018)

A Spin-Orbit Torque efficiency in W/CoFeB heterostructures with W-Nb alloys insertion layers

Seok In Yoon^{*}, Min Hyeok Lee and Young Keun Kim[†]

Department of Materials Science and Engineering, Korea University, Seoul 02481, Republic of Korea

Magnetic random access memory (MRAM) is a non-volatile memory that maintains information even when the power is turned off, making it one of the superior candidates for the next generation memory devices. Recently, MRAM using spin-transfer torque (STT) as a writing mechanism has been commercialized. However, conventional STT mechanism has large operation energy and slow switching time. To solve the problem, spin-orbit torque (SOT), a newly coined writing mechanism, has been proposed as a solution [1]. The spin current generated by the spin Hall effect (SHE) and Rashba-Edelstein effect transfers the angular momentum to the magnetization and triggers the torque. Compared to the conventional STT, SOT provides rapid magnetization switching and enables low-energy operation. To develop MRAM device incorporating SOT, it is essential to investigate materials or their combinations with large SOT efficiency. A representative material of a large SOT efficiency is a β -W with an efficiency of 0.33 [2]. According to the recent theoretical calculation, an enhancement of the SOT efficiency can be achieved by using β -W and Ta alloys due to a modification of the energy band during the formation of the alloy [3]. To clarify the above-mentioned theoretically calculated result, we experimentally measured the SOT efficiency of W-Nb alloys. Nb is expected to show similar effect with Ta as Nb consists of same number of valence electrons. The structure of W 4/W_{1-x}Nb_x 2/CoFeB 0.9/MgO 1/Ta 2 (in nm) are deposited using ultra-high vacuum direct current and radio frequency sputtering system. By controlling sputtering power of W and Nb, the composition of W-Nb alloy is varied from 10% to 100%. Magnetic properties are measured by vibrating sample magnetometer (VSM). All of the as-deposited samples show the in-plane magnetic anisotropy (IMA). After 300°C annealing process, however, the samples exhibit pronounced perpendicular magnetic anisotropy (PMA) except for the samples with high Nb concentration (~80 at%). Samples with the PMA are patterned into a Hall bar device for the SOT efficiency measurement using harmonics Hall voltage measurement [4]. In the W-Nb alloy, the SOT efficiency initially decreases as the composition of Nb increases, but shows an increasing behavior as the composition of Nb is 50 at% or more. The trend of SOT efficiency follows the experimentally measured resistivity behavior of W-Nb alloy. To analyze the proportionality between the two physical parameters of SOT efficiency and resistivity, further structural analysis will be carried out.

References

- [1] I. M. Miron *et al.*, Perpendicular switching of a single ferromagnetic layer induced by in-plane current injection, *Nature* 476, 189–193 (2011).
- [2] C.-F. Pai *et al.*, Spin transfer torque devices utilizing the giant spin Hall effect of tungsten, *Applied Physical Letters* 101, 122404 (2012).
- [3] X. Sui *et al.*, Giant enhancement of the intrinsic spin Hall conductivity in β -tungsten via substitutional doping, *Physical Review B* 96, 241105(R) (2017).
- [4] K. Garello *et al.*, Symmetry and magnitude of spin-orbit torques in ferromagnetic heterostructures, *Nature Nanotechnology* 8, 587-593 (2013).

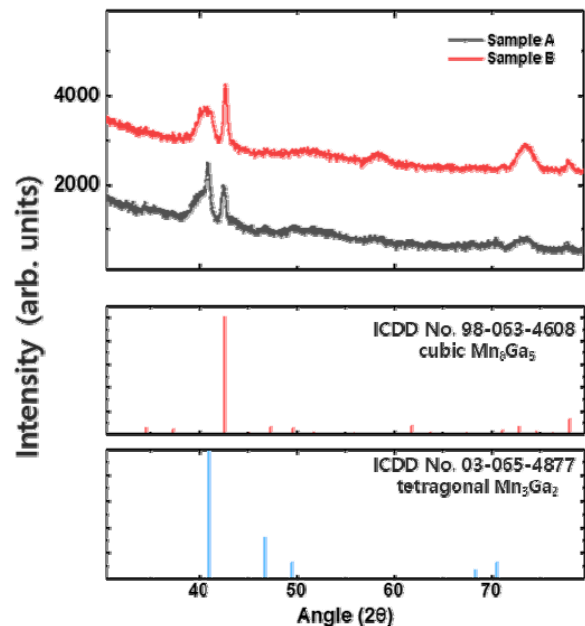
Analysis of magnetic and crystallographic properties of Mn-Ga thin films

Jeong Kyu Lee*, Gyu Won Kim, Taehyun Kim, Young Keun Kim

Department of Materials Science and Engineering, Korea University, Seoul 02481, Republic of Korea

Magnetic information can be stored and manipulated by using spin currents produced in magnetic heterostructures [1]. Antiferromagnets are a superior candidate in the field of spintronics because they possess several attractive properties such as fast switching speed, small stray fields, etc. Despite these advantages, being hard to read and write limits them from being used in spintronic devices. Alternatively, ferrimagnets which contain antiferromagnetic sublattices could be a possible candidate, as well. In this study, we aim to deposit the ferrimagnetic Mn-Ga thin films [2,3].

Thin films of varying compositions are grown on SiO₂ substrates by DC and RF magnetron co-sputtering at a temperature of 300°C. The composition of Mn is varied by controlling the deposition power. The film stacks are Si/SiO₂ substrate/W (5)/Mn_xGa_{1-x} (20)/Ta (3) with $x=60, 65$. These atomic compositions are selected to fabricate and confirm the crystallographic properties of the sputtered γ_1 (L1₀-MnGa) thin films. Magnetic properties are measured by vibrating-sample magnetometer (VSM). Microstructure of Mn-Ga alloy is measured using X-ray Diffraction (XRD). The samples are not fully magnetized with the applied magnetic field even at 19 kOe with no clear magnetically easy axis. The films exhibit x-ray diffraction (XRD) patterns corresponding to Mn-Ga alloys. As Mn concentration increase, the XRD peak of γ_1 (L1₀-MnGa) phase disappear which agrees well with the Mn-Ga binary phase diagram. SOT properties and quantitative elemental information of the samples are analyzed by harmonics Hall measurement and Auger electron spectroscopy, respectively. In summary, we were able to confirm the XRD patterns of co-sputtered γ_1 (L1₀-MnGa) phase Mn-Ga thin films.



References

- [1] I. M. Miron *et al.*, Nature 476(7359), 189-193 (2011)
- [2] K. Minakuchi *et al.*, J. Alloys Compd. 537, 332-337 (2012)
- [3] S. Mizukami *et al.*, Phys. Rev. B 85(1), 014416 (2012)

Electrical manipulation of exchange bias in IrMn/NiFe heterostructures

Jaimin Kang^{1*}, Jeongchun Ryu^{1†}, Jong-Guk Choi¹, Taekhyeon Lee², Jaehyeon Park², Soogil Lee¹, Kab-Jin Kim² and Byong-Guk Park^{1†}

¹Department of Materials Science and Engineering and KI for Nanocentury, KAIST, Daejeon 34141, Korea

²Department of Physics, KAIST, Daejeon 34141, Korea

Electrical manipulation of antiferromagnetic moment is a core technology of antiferromagnet-based spintronics with outstanding device characteristics including ultrafast operation and high-density integration in comparison to conventional ferromagnet-based devices [1]. Electrical manipulation of antiferromagnetic moments by electric current has been demonstrated in epitaxial antiferromagnets with broken inversion symmetry or antiferromagnet/heavy metal structures, in which spin-orbit torque (SOT) drives the antiferromagnetic domain wall [2].

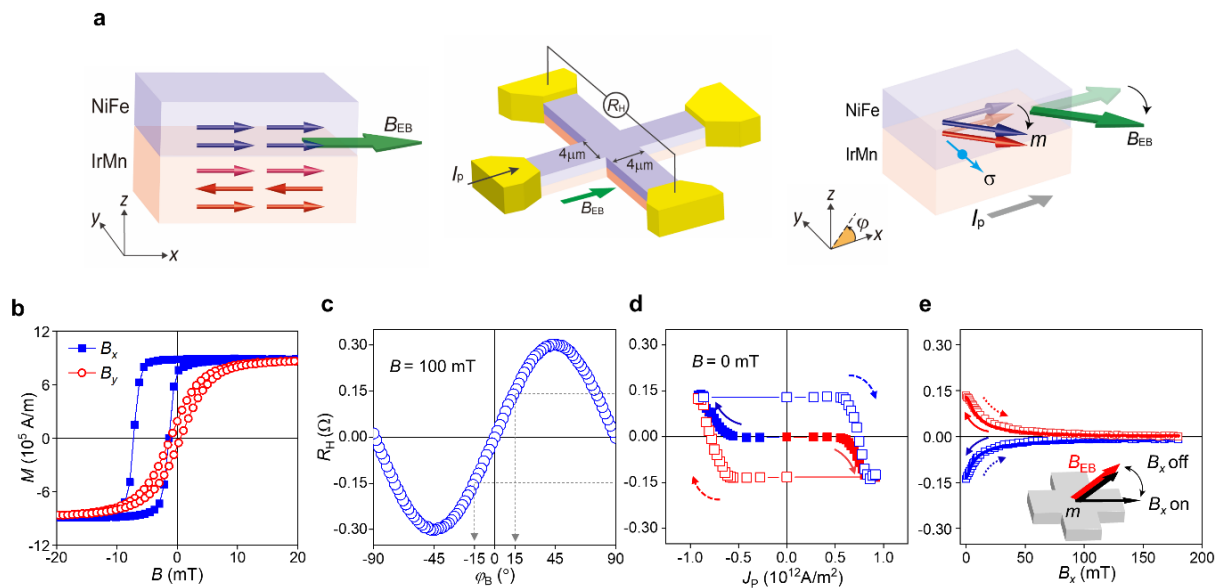


Figure 1. Current-induced manipulation of the exchange bias in IrMn/NiFe structure. **a**, Left: Exchange-biased

IrMn/NiFe structure, where the blue and red arrows represent magnetization (m) of NiFe and IrMn, respectively, and B_{EB} is the exchange bias field. Middle: The Hall bar device for electrical measurements. The

Hall resistance (R_H) is measured after applying an in-plane current pulse J_p . Right: Schematics of the current-induced exchange bias switching, where the magnetization direction of the IrMn/NiFe bilayer (ϕ_m) is modulated by the spin current with spin polarization (σ) arising from the IrMn. **b**, Hysteresis loop of IrMn (5 nm)/NiFe (4 nm) structure measured with magnetic fields along the x -axis (solid blue) and y -axis (open red).

c, R_H measured as a function of azimuthal angle under a magnetic field (ϕ_B) of 100 mT. **d**, The R_H vs J_p curves without the external magnetic field, where the arrows denote the sweeping direction of J_p . **e**, R_H as a

function of a magnetic field along x -axis (B_x). R_H is initially set to ± 0.14 by an J_p of $8.4 \times 10^{11} \text{ A/m}^2$, represented by the red and blue symbols. Open squares (lines) refer to increasing (decreasing) B_x . The inset illustrates the rotation and recovery of magnetization with respect to B_x .

Here, we report electrical manipulation of the exchange bias in IrMn/NiFe bilayers operating without a heavy metal. We show that the direction of the exchange bias is gradually modulated in ranges from -22 degrees to 22 degrees by in-plane current, which is independent of the NiFe thickness. This suggests that spin currents arising in the IrMn layer exert SOTs on uncompensated interfacial moments of antiferromagnets, subsequently rotating the antiferromagnetic moments coherently. In addition, the memristive characteristics are maintained in sub-micron devices, promoting nanoscale multi-level antiferromagnetic spintronic devices.

References

- [1] Jungwirth, T., Marti, X., Wadley, P. & Wunderlich, J. Antiferromagnetic spintronics. *Nat. Nanotechnol.* **11**, 231–241 (2016).
- [2] DuttaGupta, S. et al. Spin-orbit torque switching of an antiferromagnetic metallic heterostructure. *Nat. Commun.* **11**, 5715 (2020).

Thin-film study of molecular spin qubits using a surface-sensitive electron spin resonance spectrometer

Jisoo Yu^{1,2*}, Franklin H. Cho^{1,2}, Luciano Colazzo^{1,2}, Yejin Jeong^{1,2}, Juyoung Park^{1,2}, Junjie Liu³, Arzhang Ardavan³, Giovanni Boero⁴, Andreas J. Heinrich^{1,2}, Fabio Donati^{1,2*}

¹Department of Physics, Ewha Womans University

²Center for Quantum Nanoscience (QNS), Institute for Basic Science (IBS)

³The Clarendon Laboratory, Department of Physics, University of Oxford

⁴Laboratory for Microsystems, Ecole Polytechnique Fédérale de Lausanne (EPFL)

Electron spin resonance (ESR) spectroscopy is a powerful tool for establishing the quantum coherence of molecular spin qubits [1]. In order to determine their performance as quantum bits for quantum information processing, it is important to integrate them into solid-state substrates and characterize their interaction with the electrons of the substrate. However, this characterization requires tailored spectrometers with sufficient surface sensitivity.

Here, we utilize α , γ -bis(diphenylene)- β -phenylallyl (BDPA) and 2,2-diphenyl-1-picrylhydrazyl (DPPH) thin film as samples to characterize a home-built surface-sensitive ESR spectrometer. Both molecules are traditional standards in the ESR technique and have different characteristics on the surfaces [2], [3]. The spectrometer operates in the X band (10 GHz) in both continuous wave and pulsed mode in a wide range of temperature (2.5-300 K) and magnetic field (0-3.2 T). To maximize the microwave field in a 2D spin system, we developed a coplanar-type resonator, on whose surface we deposited the molecular films. We demonstrate a spin sensitivity of 10^{12} spins / G \cdot $\sqrt{\text{Hz}}$ in continuous wave mode at room temperature, allowing ESR measurements down to a single layer of molecular spins.

References

- [1] *Nat. Chem.* 11, 301 (2019).
- [2] *J. Phys. Chem. C* 116, 22857 (2012).
- [3] *Sur. Sci.* 700, 121676 (2020).

Demonstration of the current-driven Bloch line motion for novel magnetic memory operation

Jiseok Yang^{1*}, Kyoung-Woong Moon², Min Gyu Park¹, Soogil Lee¹,
Sanghoon Kim³, Mincheol Shin⁴ and Kab-Jin Kim¹

¹Department of Physics, Korea Advanced Institute of Science and Technology, Daejeon 34141, Republic of Korea

²Quantum Spin Team, Korea Research Institute of Standards and Science, Daejeon 34113, Republic of Korea

³Department of Physics, University of Ulsan, Ulsan 44610, Republic of Korea

⁴School of Electrical Engineering, Korea Advanced Institute of Science and Technology,
Daejeon 34141, Republic of Korea

Topological defects such as magnetic domain walls, vortices, and skyrmions have received significant attention because of their topological stability [1], which can be utilized for future memory devices. The magnetic Bloch line (BL), a winding spin structure that divides the domain wall, is also a topological defect, which has stable states with a nontrivial topological charge. Following the direct observation of the BL by MFM [2], the dynamic properties of the BL have also been investigated by electrical measurements backed up with micromagnetic simulations [3]. While the idea of using field-driven BL motion for memory device operations was proposed a long time ago [4], the current-driven BL motion, which is technologically more relevant, has not been considered as an operation mechanism for a BL memory.

In this presentation, we propose a BL racetrack memory that utilizes the current-driven motion of multiple BLs. Using micromagnetic simulations, we demonstrate that the writing and shifting of the BLs are possible using a spin-transfer-torque scheme. The writing efficiency and shifting velocity are found to be better than that of the domain wall-based racetrack memory. To emulate a more realistic situation, we examine the effect of random defects or edge roughness and find that the motion of the BL is robust against the sample imperfections. In addition to the simulation, we also experimentally verify the dynamics of the BL in Permalloy (Py) thin films. The field-driven and current-driven BL motions are successfully demonstrated in Py films, suggesting that the current-driven BL memory is experimentally achievable.

References

- [1] H.-J. Braun, *Adv. Phys.* **61**, 1 (2012)
- [2] J. Kim et al., *Appl. Phys. Lett.* **98**, 052510 (2011)
- [3] Y. Yoshimura et al., *Nat. Phys.* **12**, 157 (2016)
- [4] F. B. Humphrey et al., *IEEE Trans. Magn.* **21**, 1762 (1985)

Double Walker Breakdown of Ultrathin Magnetic Double Layers

Jaesung Yoon^{*}, Joon Moon, Kitae Kim, Seong-Hyub Lee, Sug-Bong Choe^{*}

Department of Physics and Astronomy, Seoul National University, Seoul, 08826, Republic of Korea

There are a lot of studies that have been proceeded about domain wall dynamics at magnetic thin films to make better magnetic memory devices. Particularly, many people largely focus on how to make the domain wall move effectively using perpendicular magnetic anisotropy (PMA), Dzyaloshinskii-Moriya interaction (DMI), spin-orbit coupling effect, etc. Since these phenomena are mostly generated at the interfaces adjacent to the magnetic layers, the magnetic multilayered structures which have multiple interfaces have drawn great attention.

For this study, we make magnetic double layers (Ta (5nm) / Pt (2.5nm) / Co (Xnm) / Pt (Ynm) / Co (Znm) / Pt (1.5nm)) using DC magnetron sputtering. And then, we measure the field-driven domain wall dynamics by means of magneto-optical Kerr effect (MOKE) microscope. In contrast to the magnetic single layer which shows single minimum conventionally, the magnetic double layers show double minima. The results are shown in Fig. 1. The micromagnetic simulation results reveal that each magnetic layer has different internal dipolar magnetic field and thus, the domain wall in each magnetic layer feels different magnetic field. Consequently, each layer has different Walker breakdown field for each domain wall, the domain wall velocity exhibits double minima with respect to in-plane field.

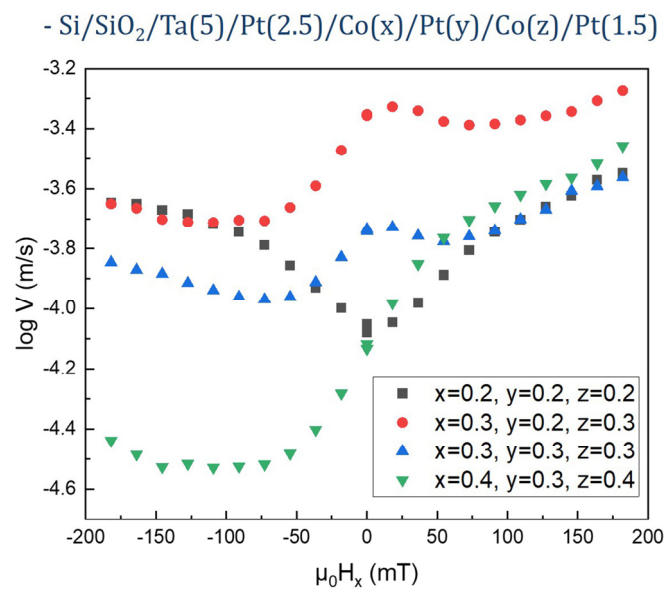


Fig. 1. The domain wall velocity plot for magnetic double layers with respect to in-plane field.
(fixed out-of-plane field)

A 3-dimensional control of exchange bias by spin orbit torque in Pt/Co/IrMn heterostructure

Eunchong Baek^{1*}, Suhyeok An¹, Woo-Yeong Kim², Ki-Seung Lee³ and Chun-Yeol You^{1†}

¹Department of Emerging Materials Science, DGIST, Daegu 42988, Korea

²Department of Materials Science and Engineering, Korea University, Seoul 02841, Korea

³Emerging Materials Science Research Center, DGIST, Daegu, Korea

Spin orbit torque (SOT) driven magnetization switching has opened up a new field of spintronics. It has been reported that SOT can switch a ferromagnet (FM) layer without the second ferromagnetic layer by spin current from the adjacent heavy metal (HM) layer^{1,2,3}. The injection of spin current by SOT can also switch the antiferromagnet (AFM) Neel vector^{4,5,6} which have been difficult to manipulate with other means such as a magnetic field. Furthermore, the exchange bias (EB) state in FM/AFM bilayer system was manipulated through SOT while the underlying mechanism is unrevealed yet^{7-8,9,10}. To understand how the SOT modulate EB state, related experiments are needed to provide the clues for the interfacial spin dynamics due to SOT, because the interfacial spin ordering at the interface will govern the EB state.

Here we observe SOT driven three-dimensional (3-D) control of the EB state in a Pt/Co/IrMn tri-layer. We control EB field directions with out-of-plane (OOP) and/or in-plane (IP) external magnetic fields with SOT. Similar to the field cooling methods, the magnetization of FM layer is imprinted into the EB field by SOT. Furthermore, manipulated in-plane EB field through SOT enables field-free switching of perpendicular magnetized FM without field-cooling. In order to support the experimental findings, we perform macro-spin simulations which suggest that the SOT induced EB manipulation is the result of SOT driven THz oscillation of interfacial AFM spins. In SOT induced EB manipulation, SOT has the similar role as heat in traditional field cooling, exciting the AFM spins to deviate from the local energy minimum state so that when the current is turned off, the EB is switched along the FM direction. Our work reveals the underlying mechanism of SOT driven EB manipulation and motivates to design novel spintronic devices.

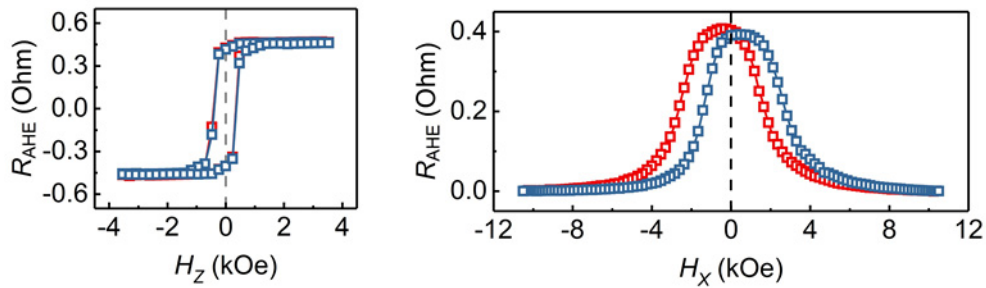


Fig. 1. Easy (H_z) and hard (H_x) axes Hall resistance R_{AHE} for writing magnetic field of +x (red), -x (blue) direction, respectively.

The trapezoidal shaped wire driven Domain wall dynamics under perpendicular magnetic anisotropy system

Dongryul Kim^{1*}, Woo-Yeong Kim², Suhyeok An¹, Eunchong Baek¹,
Ki-Seung Lee¹, Chun-Yeol You^{1†}

¹Department of Emerging Materials Science, Daegu Gyeongbuk Institute of Science and Technology, Korea

²Department of Materials Science and Engineering, Korea University, Seoul, Republic of Korea

*Corresponding author e-mail: cyyou@dgist.ac.kr

Dynamics of the Domain Wall (DW) has been actively investigated because of its possibility for future memory and logic devices. Up to recently, there are several suggestions for logic and memory devices which is based on DW dynamics including the racetrack memory, especially, Spin Torque Majority Gate (STMG) for logic devices which have logic state assigned by the configuration of magnetization.

Plenty of struggles have been tried to reduce the operation energy in the field of DW based devices. One of them is to modulate the geometry of the propagation line of DW. The energy decreases as the magnetic DW propagates to a narrow region of a trapezoidal shaped wire. In the point of view of the STMG operating principle, the transmit direction of logic state is not necessary to move reversibly. Then we can designate domain wall energy reduction direction as a flow direction of information. It means that STMG with a change structure take advantage of smaller operating energy.

To identify DW energy is affected by shape, we choose a Pt (5 nm)/Co (1.2 nm)/Pt (4 nm) heterostructure film that has a perpendicular magnetic anisotropy with the trapezoidal shaped wire, which is designed to be 30, 40 and 50 degrees. Here we experimentally confirmed that the finite effective field which push DW to the narrow wire region exists, and the effective field increases as the trapezoidal angle increases. Ultimately, if we find the optimal condition for the trapezoidal pattern size and angle to get large enough effective field, DW even can move spontaneously without the externally driving field or current.

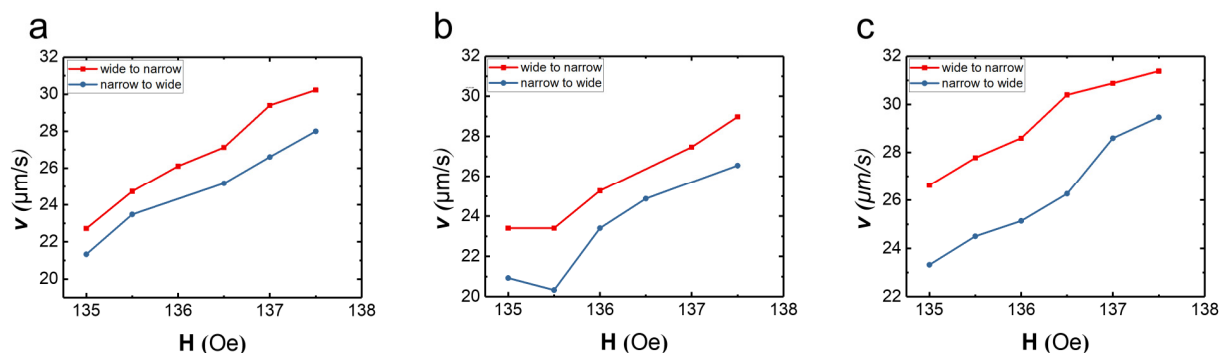


Fig. 1. Velocity difference between narrow regime and wide regime with different angle (a) 30, (b) 40, (c) 50 degrees

Scaling law of magnetic skyrmion motion in the creep regime

Moojune Song^{1*}, Mujin You¹, Seungmo Yang², Min Gyu Park¹, Kab-Jin Kim¹

¹Department of Physics, Korea Advanced Institute of Science and Technology (KAIST)

²Quantum Spin Team, Korea Research Institute of Standards and Science (KRISS)

Magnetic skyrmion은 위상학적 양자수(topological quantum number)를 갖는 자성 구조체이다. 이에 skyrmion은 위상학적으로 매우 중요할 뿐만 아니라, skyrmion이 전류에 의해 이동하는 속도가 빠르고 그 크기가 수십 nm 수준으로 작다는 점에서 새로운 메모리/로직 소자의 응용 측면에서 아주 중요하다. 그러한 skyrmion motion 연구의 중요성에도 불구하고 저전력 영역에 해당하는 skyrmion의 creep motion과 scaling law [1]에 대해서는 아직까지 충분한 연구가 이루어지지 않았다. Creep motion과 scaling law는 비단 자성 구조체의 움직임 뿐 아니라 고체 박막의 성장[2]이나 vortex dynamics[3], 다공성 매질에서의 유체 침습[4] 등 다양한 물리 현상에서 발견되는 보편적인 현상이다. 특히, 자구벽(magnetic domain wall)이 2차원 공간과 1차원 공간에서 creep motion을 할 때 속력-구동력 관계의 차이, 즉 차원간 특이성(interdimensional criticality)에 대한 연구[5]에서의 물리학적 발견이 그러했던 것처럼, skyrmion과 자구벽의 creep motion 거동을 비교하는 것은 물리학에서 상당히 중요한 문제이다.

이러한 skyrmion creep motion을 연구하기 위해, 우리 연구진은 W/CoFeB/Ta/MgO 시스템을 사용했다. 자기장 조절 방식[6]을 이용해 200 μm 의 넓은 폭을 갖는 2차원 공간에 지름 약 1 μm 의 skyrmionic bubble을 생성하고, W층에 전류를 흘려주어 이들이 SOT에 의해 움직일 수 있도록 하였다. Creep 영역의 skyrmion motion을 관측하기 위해 기존 연구보다 낮은 $7 \times 10^7 \text{ A/m}^2 \sim 1.6 \times 10^9 \text{ A/m}^2$ 수준의 전류 밀도를 걸어주었고, MOKE 현미경과 소프트웨어 기반 이미지 후처리 과정을 통해 약 650,000개 이상의 skyrmion을 추적한 결과 1 $\mu\text{m/s} \sim 150 \mu\text{m/s}$ 의 속력 범위에서 전류 밀도에 따른 skyrmion의 속력의 관계를 얻을 수 있었다. 이를 기존 자구벽의 creep motion 이론을 도입해 분석한 결과, skyrmion은 2차원 공간 자구벽의 scaling law를 따르지 않으며, 대신 1차원 공간 자구벽 운동에서 관측되었던 확률적 hopping 거동을 따른다는 것을 알 수 있었다. 이는 creep 영역에서 skyrmion 거동을 직접적으로 관측하고 통계적으로 분석한 첫 번째 연구 결과이다. 본 연구는 미지의 skyrmion 거동 특성을 밝혀냈다는 점에서 물리학적 의미가 있으며, 또한 skyrmion의 확률적 거동을 이용한 확률 컴퓨팅(probabilistic computing) 소자[7]의 개발에도 응용될 수 있다는 점에서 공학적 가치가 있다.

References

- [1] S. Lemerle *et al.*, *Phys. Rev. Lett.* **80**, 849 (1998)
- [2] J. Krim and G. palasantzas, *Int. J. Mod. Phys. B* **9**, 599 (1995)
- [3] G. Blatter *et al.*, *Rev. Mod. Phys.* **66**, 1125 (1994)
- [4] N. Martys *et al.*, *Phys. Rev. Lett.* **66**, 1058 (1991)
- [5] K. -J. Kim *et al.*, *Nature* **458**, 740 (2009)
- [6] K. -W. Moon *et al.*, *NPG Asia Mater.* **13**, 20 (2021)
- [7] J. Zazvorka *et al.*, *Nat. Nanotechnol.* **14**, 658 (2019)

Theoretical finding of robust dynamics of spin waves channeled in antiferromagnetic domain walls

Hyeon-Kyu Park^{*} and Sang-Koog Kim[†]

National Creative Research Initiative Center for Spin Dynamics and Spin-Wave Devices, Nanospinics Laboratory,
Research Institute of Advanced Materials, Department of Materials Science and Engineering,
Seoul National University, Seoul 151-744, South Korea

[†]Correspondence and requests for materials should be addressed to S.-K. K. (sangkoog@snu.ac.kr).

Antiferromagnets are one of novel magnetic materials composed of two or more sublattices being antiferromagnetically coupled. The Néel orders of antiferromagnets are controllable via optical switching [1-3], which enables facile formation of metastable magnetic textures such as domain walls and skyrmions. Furthermore, the dynamics of antiferromagnets have received a great attention due to their novel behaviors that differ from those of ferromagnets. For example, antiferromagnetic domain walls are known to be much faster than those of ferromagnetic counterparts, owing to their inter-atomic transfer of angular momentum [4-6]. Also, the absence of the skyrmion Hall effect in antiferromagnets enables unidirectional current-driven motion of antiferromagnetic skyrmions [7,8]. These features make antiferromagnets a promising alternative to ferromagnets in the field of spintronics.

Here, we theoretically calculated ultrafast propagations of spin waves channeled in antiferromagnetic Bloch-type domain walls based on a phenomenological theory developed by Hals *et al.* [9]. Our analytical derivation demonstrates that the dispersion relation of such channeled spin waves exhibits an extremely high group velocity of up to ~ 18.7 km/s without any forbidden band gap. Further, such electromagnetic-wave-like dispersion relation allows for dispersion-less and translational transmission of trains of low-frequency, long-wavelength digital signals in the channel. Our results [10] offer guidelines for the development of ultrafast information signal processing in nano-scale magnonic circuits composed of antiferromagnetic domain walls.

References

- [1] S. Loth, S. Baumann, C. P. Lutz, D. M. Eigler, and A. J. Heinrich, *Science* **335**, 6065 (2012).
- [2] P. Němec, M. Fiebig, T. Kampfrath, and A. V. Kimel, *Nat. Phys.* **14**, 229–241 (2018).
- [3] S. Manz, M. Matsubara, T. Lottermoser, J. Büchi, A. Iyama, T. Kimura, D. Meier, and M. Fiebig, *Nat. Photon.* **10**, 653–656 (2016).
- [4] T. Shiino, S.-H. Oh, P. M. Haney, S.-W. Lee, G. Go, B.-G. Park, and K.-J. Lee, *Phys. Rev. Lett.* **117**, 087203 (2016).
- [5] E. G. Tveten, A. Qaiumzadeh, and A. Brataas, *Phys. Rev. Lett.* **112**, 147204 (2014).
- [6] N. Thielemann-Kühn, D. Schick, N. Pontius, C. Trabant, R. Mitzner, K. Holldack, H. Zabel, A. Föhlisch, and C. Schüßler-Langeheine, *Phys. Rev. Lett.* **119**, 197202 (2017).
- [7] J. Barker and O. A. Tretiakov, *Phys. Rev. Lett.* **116**, 147203 (2016).
- [8] X. Zhang, Y. Zhou, and M. Ezawa, *Sci. Rep.* **6**, 24795 (2016).
- [9] K. M. D. Hals, Y. Tserkovnyak, and A. Brataas, *Phys. Rev. Lett.* **106**, 107206 (2011).
- [10] H.-K. Park and S.-K. Kim, *Phys. Rev. B* **103**, 214420 (2021).

Highly efficient heat-dissipation power driven by ferromagnetic resonance in superparamagnetic nanoparticles of ferrimagnetic $M\text{Fe}_2\text{O}_4$ ($M = \text{Fe}, \text{Mn}, \text{Ni}$)

Jae-Hyeok Lee, Yongsub Kim^{*} and Sang-Koog Kim[†]

National Creative Research Initiative Center for Spin Dynamics and Spin-Wave Devices, Nanospinics Laboratory,
Research Institute of Advanced Materials, Department of Materials Science and Engineering,
Seoul National University, Seoul 151-744, South Korea

We experimentally demonstrated that heat-dissipation power driven by ferromagnetic resonance (FMR) in superparamagnetic nanoparticles of ferrimagnetic $M\text{Fe}_2\text{O}_4$ ($M = \text{Fe}, \text{Mn}, \text{Ni}$) gives rise to highly localized incrementation of targeted temperatures. The power generated thereby is extremely high: two orders of magnitude higher than that of the conventional Néel-Brownian model. From micromagnetic simulation and analytical derivation, we found robust correlations between the temperature increment and the intrinsic material parameters of the damping constant as well as the saturation magnetizations of the nanoparticles' constituent materials. Furthermore, the magnetization-dissipation-driven temperature increments were reliably manipulated by extremely low strengths of applied AC magnetic fields under resonance field conditions. Our experimental results and theoretical formulations provide for a better understanding of the effect of FMR on the efficiency of heat generation as well as straightforward guidance for the design of advanced materials for control of highly localized incrementation of targeted temperatures using magnetic particles in, for example, magnetic hyperthermia bio-applications.

Split-gap orientation dependence of photon-magnon coupling strength in two inverted split ring resonators

Haechan Jeon^{1*}, Biswanath Bhoi¹, Bosung Kim¹, Loïc Millet^{1,2} and Sang-Koog Kim^{1†}

¹National Creative Research Initiative Center for Spin Dynamics and Spin-Wave Devices, Nanospinics Laboratory, Research Institute of Advanced Materials, Department of Materials Science and Engineering, Seoul National University, Seoul 151-744, South Korea

²Department of Applied Physics, INSA, 135 Avenue de Rangueil, F-31077 Toulouse, France

[†]Correspondence and requests for materials should be addressed to S.-K. K. (sangkoog@snu.ac.kr).

Photon-magnon coupling (PMC) has been studied to develop spintronics-based quantum information technology [1-4]. One of the most critical issues in the PMC studies is how to enhance the PMC strength that provides the wide bandwidth and high rate of information exchange. Therefore, understanding the resilience of PMC is a prerequisite for such applications. The fundamental dynamic characteristics of PMC have been studied including its abnormal anti-crossing effect[5], broadband coupling[6] and non-reciprocity[7].

In this study, we examined PMC strength variation with the relative orientation/position of split gaps in two inverted split ring resonators (ISRRs) in a hybrid system composed of two Inverted slit ring resonators (ISRRs) and a YIG film. The two ISRRs were patterned on a standard high-frequency laminate of copper/dielectric/copper substrate with following material parameters: relative dielectric constant, $\epsilon_r=10$; dissipation factor, 0.0012 at 10 GHz; dielectric height, 0.64 mm; thickness of copper cladding; 35 μ m. The YIG film was placed on top of the microstrip line just below the center of the multi photon resonators. Figure 1 shows the experimental setup for PMC measurements, where the input and output of the microstrip feeding line were connected to the ports of a calibrated vector network analyzer (VNA, Agilent PNA series E8362C). Then, transmittance coefficient of the S-parameters were measured to examine PMC as functions of the strength of DC magnetic fields and the frequency of ac current applied in the microstripline.

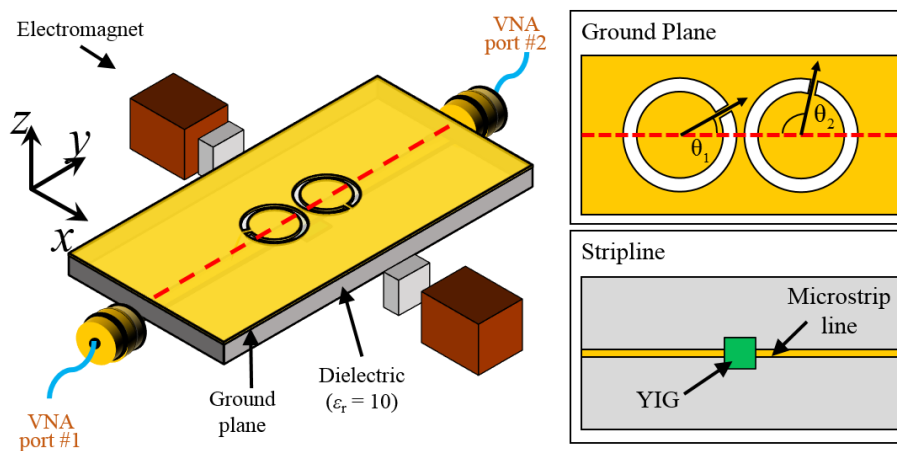


Figure 1. Schematic of hybrid sample

We observed contrasting dispersion spectra, e.g., normal/opposite anti-crossings for different relative orientations and positions of the split gaps between the two ISRRs. We also analytically derived PMC behaviors and its coupling strength between a photon's multiple resonance modes and the magnon mode, which are in good agreement with the experimental data. This robust hybrid system provides a more controllable way of PMC strength in a wide range of at room temperature. Furthermore, by extending this analytical model, we studied photon resonator arrays of either clockwise or counter-clockwise chirality in the planar structure. This work provides an additional degree of freedom to manipulate PMC through the chirality of multi-photon resonators.

References

- [1] A. Imamoglu, Phys. Rev. Lett., 102, 083602 (2009).
- [2] L. Bai, M. Harder, Y. P. Chen, X. Fan, J. Q. Xiao, and C.-M. Hu, Phys. Rev. Lett., 114, 227201 (2015).
- [3] R. Hisatomi, A. Osada, Y. Tabuchi, T. Ishikawa, A. Noguchi, R. Yamazaki, K. Usami, and Y. Nakamura, Phys. Rev. B, 93, 174427 (2016).
- [4] L. Kang, Q. Zhao, H. Zhao, and J. Zhou, Opt. Express., 16, 8825-69 (2008).
- [5] B. Bhoi, B. Kim, S. Jang, J. Kim, J. Yang, Y.-J. Cho, and S.-K. Kim, Phys. Rev. B 99, 134426 (2019)
- [6] B. Bhoi, S. Jang, B. Kim and S.-K. Kim. J. Appl. Phys. 129, 083904 (2021)
- [7] Y-P Wang, J. W. Rao, Y. Yang, et al and C.-M.Hu. PHYSICAL REVIEW LETTERS 123, 127202 (2019)
- [8] B. Bhoi, S.-K. Kim, Solid State Physics, Volume 70, 2019, Pages 1-77
- [9] B. Bhoi, B. Kim, J. Kim, Y-J Cho & S-K Kim, Scientific Reports **volume 7**, Article number: 11930 (2017)
- [10] B. Bhoi, B. Kim, Y. Kim, M-K. Kim, J-H. Lee, and S-K. Kim, Journal of Applied Physics **123**, 203902 (2018)
- [11] B. Kim, B. Bhoi, and S-K Kim, Journal of Applied Physics **126**, 163902 (2019)

Broadband photon-magnon coupling using multiple photon resonators

Seung-Hun Jang^{*}, Biswanath Bhoi, Bosung Kim and Sang-Koog Kim[†]

National Creative Research Initiative Center for Spin Dynamics and Spin-Wave Devices, Nanospinics Laboratory,
Research Institute of Advanced Materials, Department of Materials Science and Engineering,
Seoul National University, Seoul 151-744, Republic of Korea

[†]Correspondence and requests for materials should be addressed to S.-K. K. (sangkoog@snu.ac.kr).

We studied broadband characteristics of photon-magnon coupling (PMC) between an Yttrium Iron Garnet (YIG) film and arrays of inverted split-ring resonators (ISRRs) [1]. To achieve broadband photon-magnon interaction, we optimized the geometries of single ISRRs [2-5] and their array structures by conducting numerical simulations in order to vary the resonance frequency, bandwidth, and gain of PMC modes. With those optimal ISRRs arrays, we observed multiple anti-crossing dispersions between the photon and magnon modes from $|S_{21}|$ -versus-frequency measurements under different strengths of externally applied magnetic fields. It was found that the bandwidth of PMC increases up to an operating frequency range of ~ 2 GHz with increasing the number of ISRRs. On the basis of an electromagnetic classical model, we analytically derived coupling between photon-multi-modes and magnon modes in broad-range frequencies, which is in good agreement with the experimental data. This hybrid system provides a more reliable control not only of multiple-magnon-and-photon coupling in a wide range of operating frequencies but also the net coupling strength that is variable in a range of 30 to 90 MHz at room temperature. This experimental findings offer an optimized design of planar broadband photon-magnon devices.

References

- [1] B. Bhoi, S.-H. Jang, B. Kim, and S.-K. Kim, J. Appl. Phys., 129, 083904 (2021).
- [2] B. Bhoi, B. Kim, J. Kim, Y.-J. Cho and S.-K. Kim, Sci. Rep., 7, 11930 (2017).
- [3] B. Bhoi, B. Kim, S.-H. Jang, J. Kim, J. Yang and S.-K. Kim, Phys. Rev. B, 99, 134426 (2019).
- [4] B. Kim, B. Bhoi and S.-K. Kim, J. Appl. Phys., 126, 163902 (2019).
- [5] B. Bhoi and S.-K. Kim, Solid State Physics, vol. 70, Academic Press, pp. 1-77(Chapter one), (2019).

The change of interfacial magnetic properties depends on the stacking order in magnetic tri-layer systems

Jinyong Jung^{1*}, Jaehun Cho², Hyeok-Cheol Choi³, Kwang Hyun Lee²,
Chun-Yeol You^{1†}, Sug-Bong Choe³, June-Seo Kim²

¹Department of Emerging Materials Science, DGIST, Daegu 42988, Republic of Korea

²Division of Nanotechnology, Institute of Convergence, DGIST, Daegu 42988, Republic of Korea

³Department of Physics and Institute of Applied Physics, Seoul National University, Seoul, 08826, Republic of Korea

We have systematically investigated magnetic sandwich structures of the Pd/Co/Pt and Pt/Co/Pd by performing an inelastic light scattering method. Two examined individual multilayer structures are identical, but the stacking order is inverted each other. The surface magnetic anisotropy energy densities of the Pd/Co/Pt structures are dramatically decreased up to 34 % compared with the Pt/Co/Pd structures, while the interfacial Dzyaloshinskii-Moriya energy density is being kept. Surprisingly, the Pd/Co/Pt structures show a sustainable interfacial Dzyaloshinskii-Moriya energy density and an extremely suppressed surface magnetic anisotropy that the magnetic domain wall energy is almost zero. Finally, we have shown a small range of cobalt thickness on Pd/Co/Pt structures that the magnetic domain wall energy density becomes negative. This observation can open a new way to form magnetic skyrmion phases at room temperature with zero bias magnetic field.

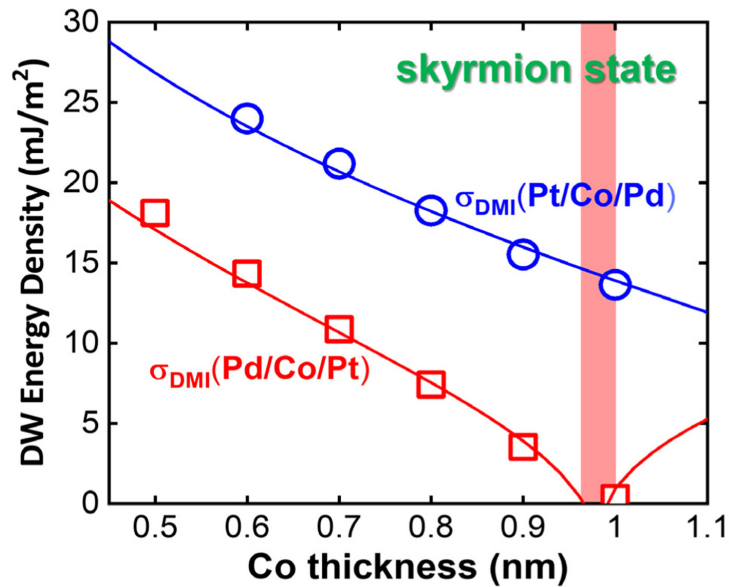


Fig. 1. The magnetic domain wall (DW) energy densities ($\sigma_{\text{DMI}} = \sigma_0 - \pi D$) as a function of Co thickness for Pt/Co/Pd and Pd/Co/Pt structures.

Conceptual design of time- and frequency-division demultiplexer: Coupled-gyration-propagation signal in arrays of vortex-state circular and chopped disks

Bosung Kim^{*}, Young-Jun Cho and Sang-Koog Kim[†]

National Creative Research Initiative Center for Spin Dynamics and Spin-Wave Devices, Nanospinics Laboratory, and
Research Institute of Advanced Materials, Department of Materials Science and Engineering,

Seoul National University, Seoul 151-744, South Korea

[†]Correspondence and requests for materials should be addressed to S.-K. K. (sangkoog@snu.ac.kr).

The function of multiplexing of information signals is the key to data transmission in telecommunication technologies and computer networks. As an alternative information carrier, collective excitations in spin textures with non-trivial topological charges such as vortex and skyrmion have been receiving a great attention owing to the novel wave characteristics of their coupled dynamic modes. Earlier studies have revealed that coupled gyration modes in arrays of either vortices [1-8] or skyrmions [9,10] can be used as information carriers with the advantage of relatively reliable control of their wave properties in micron- or nano-scale devices without Joule heating. Although the fundamentals of coupled modes and their potential application to information processing devices are reported, a new-concept demultiplexing operations based on coupled-gyration-mode signals have not been studied.

In this study, we explored, by micromagnetic numerical calculations, a robust control of coupled gyration modes propagating along specially designed vortex-state arrays by applying in-plane bias magnetic fields [11]. We also demonstrated conceptual operations of time- and frequency-division demultiplexers on the basis of the characteristic coupled modes of vortex gyrations in arrays composed of several disks of different combinations of circular and chopped shapes [11]. A specific arrangement of circular- and chopped-shape disks in vortex-state arrays and application of an in-plane static bias magnetic field in opposite directions allows for gyration-signal propagation with desired specific frequencies toward either longitudinal direction. This device concept offers an energy-efficient means of information processing without joule heating in cases where a low-damping magnetic material is used in micro-to-nanometer-scale magnonic circuits.

References

- [1] H. Jung, Y.-S. Yu, K.-S. Lee, M.-Y. Im, P. Fischer, L. Bocklage, A. Vogel, M. Bolte, G. Meier, and S.-K. Kim, *Appl. Phys. Lett.*, 97, 222502 (2010).
- [2] K.-S. Lee, H. Jung, D.-S. Han, and S.-K. Kim, *J. Appl. Phys.*, 110, 113903 (2011).
- [3] H. Jung, Y.-S. Choi, K.-S. Lee, D.-S. Han, Y.-S. Yu, M.-Y. Im, P. Fischer, and S.-K. Kim, *ACS Nano*, 6, 3712 (2012).
- [4] J.-H. Kim, K.-S. Lee, H. Jung, D.-S. Han, and S.-K. Kim, *Appl. Phys. Lett.*, 101, 092403 (2012).
- [5] D.-S. Han, A. Vogel, H. Jung, K.-S. Lee, M. Weigand, H. Stoll, G. Schütz, P. Fischer, G. Meier and S.-K. Kim, *Sci. Rep.*, 3, 2262 (2013).
- [6] D.-S. Han, H.-B. Jeong, and S.-K. Kim, *Appl. Phys. Lett.*, 103, 112406 (2013).

- [7] D.-S. Han, Y.-J. Cho, H.-B. Jung and S.-K. Kim, J. Appl. Phys., 117, 083910 (2015).
- [8] Y.-J. Cho and S.-K. Kim, AIP Advances, 9, 055028 (2019).
- [9] J. Kim, J. Yang, Y.-J. Cho, B. Kim, and S.-K. Kim, Sci. Rep., 7, 45185 (2017).
- [10] J. Kim, J. Yang, Y.-J. Cho, B. Kim, and S.-K. Kim, J. Appl. Phys., 123, 053903 (2018).
- [11] Y.-J. Cho, B. Kim, and S.-K. Kim, J. Appl. Phys., in press.

Effect of controlled stoichiometric vanadium oxide with respect to magnetic properties in Pt/Co/VO_x heterostructure

Kwonjin Park^{*}, Jae-Hyun Ha, Jinyong Jung, Jaehun Cho, Jung-Il Hong^{*}, Chun-Yeol You[†]
Department of Emerging Materials Science, DGIST, Republic of Korea

Beginning with the discovery of the interfacial exchange interaction between ferromagnet and antiferromagnet in oxidized cobalt nanoparticles, efforts have been made to understand the physical phenomena arising from the interface between various substances. Recently, a lot of theoretical and experimental studies have been conducted to find out how heavy metal or oxide adjacent to ferromagnet affects the magnetic properties of the system, but it has not been clearly understood. In our work, we investigated the effect of VO_x on the magnetic properties

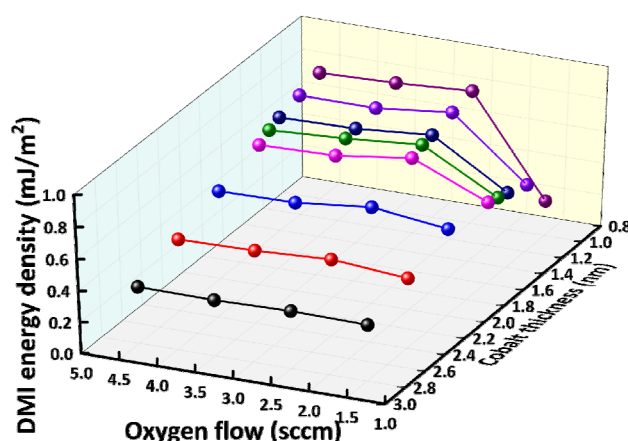


Figure 1. Trend of DMI with vanadium valence and thickness

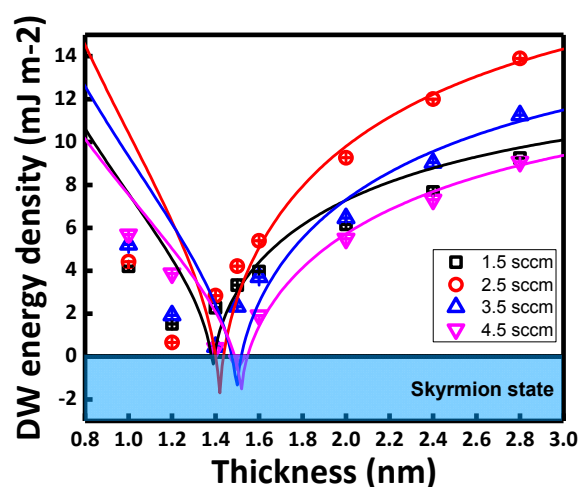


Figure 2. Variation of Skyrmion state with vanadium valence and thickness

of the VO_x/Co/Pt heterostructure by varying the ratio of mixed vanadium valences. From the results of BLS, it was confirmed that the VO_x thin film in which the exchange interactions of V⁴⁺ and V⁵⁺ were properly mixed influenced the surface anisotropy and saturation magnetization of their system. In addition, it causes peak shift in the spin wave frequency, which could be expressed as the corresponding interfacial DMI value. Such a change in magnetic properties implies that a globally effective g-factor may be considered. Our results are expected to provide a new interpretation for the effect of weak ferromagnetic oxide on interfacial DMI. Furthermore, we would like to propose that these experimental results could be considered in terms of operation of next-generation devices such as spintronics and Mottronics.

Keywords: vanadium oxide, mixed-valency, exchange interaction, magnetic anisotropy, spin wave frequency, Dzyaloshinskii-Moriya interaction

References

- [1] Geert Silversmit, *et al.*, Journal of Electron Spectroscopy and Related Phenomena. **135**, 167-175 (2004)
- [2] L. Krusin-Elbaum, *et al.*, Nat. **431**, 672-676 (2004).
- [3] E. Vavilova, *et al.*, Phys. Rev. B. **73**, 144417 (2006).
- [4] J. Cho, *et al.*, Nat. Commun. **6**, 8635 (2015).
- [5] Chun-Yeol You, N. -H. Kim, Current Appl. Phys. **15**, 298-301 (2015).
- [6] Moon, *et al.*, NPG Asia Materials. **13**, 20 (2021)

Coupling induced transparency and absorption in photon-magnon coupling

Biswanath Bhoi^{*}, Bosung Kim, Haechan Jeon and Sang-Koog Kim[†]

National Creative Research Initiative Center for Spin Dynamics and Spin-Wave Devices, Nanospinics Laboratory,
Research Institute of Advanced Materials, Department of Materials Science and Engineering,
Seoul National University, Seoul 151-744, South Korea

[†]Correspondence and requests for materials should be addressed to S.-K. K. (sangkoog@snu.ac.kr).

The prospect of a full control of electromagnetic waves has inspired intensive efforts on light-matter interactions in recent years. The two most interesting phenomena applicable to quantum information technology [1-3] are electromagnetically induced transparency (EIT) and absorption (EIA), arising from atomic coherences occurring in light-matter interaction. It is very difficult to construct a single system that exhibits both the phenomena simultaneously, due to the fact that conventional coupled systems often lack independent tenability and controllability of their eigenmodes. It is interesting to find a plausible method that would permit a single device where energy conversion or information transfer can be maximized through coupling-induced transparency (CIT) or absorption (CIA) [4-5].

In this regard, we fabricated a hybrid system composed of magnons (collective spin excitations) and microwave photons (electromagnetic excitations) in order to make them strongly couple with merits of flexibly tailored dispersion and damping rate [6-9]. Here we report on an experimental observation of the simultaneous occurrence of CIT and CIA in photon-magnon coupling (PMC) in a planar hybrid system that consists of a yttrium iron garnet (YIG) film and a multi-concentric inverted-split-ring resonator (ISRR). The observed CIT/CIA dispersions are ascribed to the multi-channel decay process through magnon-mediated interactions between the individual modes of concentric ISRR photon resonators. Furthermore, we achieved a substantial manipulation not only of CIT/CIA and coupling strength but also a reliable transition between different types of interactions by positioning differently the YIG film as well as varying the direction of bias dc magnetic fields. An analytical model adopting competition between the coherent and dissipative interactions is established to capture physical insights of magnon-mediated photon-photon interactions, which model precisely reproduces the experimental findings. This work provides promising guidance for designing effective, flexible, and controllable photon-magnonics devices that are highly demanded in the development of quantum technologies.

References

- [1] H. J. Kimble, *Nature*, 453, 1023 (2008).
- [2] Z. Xiang, S. Ashhab, J. You, and F. Nori, *Rev. Mod. Phys.*, 85, 623 (2013).
- [3] Z. Xu, S. Liu, S. Li, and X. Yin, *Phys. Rev. B* 99, 041104(R) (2019).
- [4] B. Bhoi and S.-K. Kim, *Solid State Physics*, vol. 70, Academic Press, pp. 1-77(Chapter one), (2019).
- [5] B. Bhoi and S.-K. Kim, *Solid State Physics*, vol. 71, Academic Press, pp. 39-71(Chapter two), (2020).
- [6] B. Bhoi, B. Kim, S.-H. Jang, J. Kim, J. Yang, Y.-J. Cho, and S.-K. Kim, *Phys. Rev. B* 99, 134426 (2019).
- [7] B. Bhoi, S.-H. Jang, B. Kim, and S.-K. Kim, *J. Appl. Phys.*, 129, 083904 (2021).
- [8] B. Bhoi, B. Kim, J. Kim, Y.-J. Cho and S.-K. Kim, *Sci. Rep.*, 7, 11930 (2017).
- [9] B. Kim, B. Bhoi and S.-K. Kim, *J. Appl. Phys.*, 126, 163902 (2019).

Magneto-Optical Kerr Measurement using Ultrafast Sagnac Interferometer

Yooleemi Shin and Ji-Wan Kim*

Department of Physics, Kunsan National University, Kunsan 54150, South Korea

*Email: hwoarang@kunsan.ac.kr

Since ultrafast Sagnac interferometer had been developed, the lattice displacement and differential reflectivity has been measured for non-magnetic metals [1]. In order to study the relation between spins and lattice in ultrafast timescale, it is necessary to measure the lattice displacement and demagnetization at the same time. Therefore, we modified ultrafast Sagnac interferometer to make it possible to obtain the lattice displacement $u(t)$, differential reflectivity $\Delta R(t)$, magneto-optical Kerr rotation $\Delta\theta_K(t)$, and Kerr ellipticity $\Delta\varepsilon_K(t)$ based on the Jones matrix approach [2]. Figure 1 shows (a) $u(t)$, (b) $\Delta R(t)$, (c) $\Delta\theta_K(t)/\theta_K$ and (d) $\Delta\varepsilon_K(t)/\varepsilon_K$ of ferromagnetic Co(20 nm)/sapphire measured by ultrafast Sagnac interferometer (solid circles) and time-resolved MOKE (solid lines) for comparison. It is found that their overall behaviors are fairly matched each other. Regarding the different relaxation of the precession between respective instruments, it is thought to be reasonable by the fact that the relaxation of the precession is sensitive to the pump intensity and the relative ratio of the pump and the probe spot sizes [3].

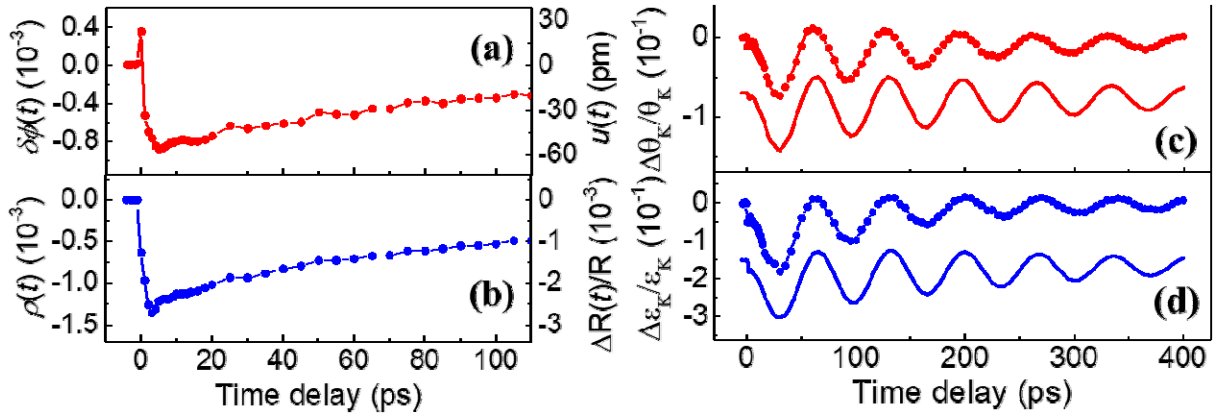


Fig. 1. (a) Lattice displacement $u(t)$, (b) differential reflectivity $\Delta R(t)$, (c) differential Kerr rotation $\Delta\theta_K(t)/\theta_K$ and (d) ellipticity $\Delta\varepsilon_K(t)/\varepsilon_K$ of Co(20 nm) measured by ultrafast Sagnac interferometer (solid circles) and time-resolved MOKE (solid lines).

References

- [1] D. H. Hurley and O. B. Wright, Opt. Lett. 24, 1305 (1999)
- [2] Yooleemi Shin and Ji-Wan Kim, Opt. Lett. (accepted)
- [3] V. Halté, J.-Y. Bigot, B. Palpant, M. Broyer, B. Prével, and A. Pérez, Appl. Phys. Lett. 75, 3799 (1999)

Dynamics of magnetic skyrmion bags induced by spin-transfer torques

Suyeong Jeong^{*}, Hee-Sung Han, Dae-Han Jung, Ganghwi Kim and Ki-Suk Lee

School of Materials Science and Engineering, Ulsan National Institute of Science and Technology,
Ulsan, Republic of Korea

Magnetic skyrmions are envisioned to be a good candidate for developing the next generation data processing/storage device due to their high stability [1] from the topological charge invariance [2]. In dynamic motions of skyrmions, the topological charge also plays a significant role: propagation direction of the skyrmions relative to the driving forces such as spin-transfer-torque (STT) or spin-orbit-torque (SOT) varies dramatically upon their topological charge, the skyrmion number. Under the STT or SOT, a skyrmion shows a diagonal motion not a parallel motion to the driving force direction, which is known as the skyrmion Hall effect. [3,4] and its direction depends on the sign of the skyrmion number. Recently, a skyrmionium with the skyrmion number of 0 is indicated to cancel out the skyrmion Hall effect by the combination of two skyrmions with opposite signs of skyrmion number [5]. Which reveals that the change in the skyrmion number of magnetic structures can lead to the variety of the skyrmion motions, which contributes to realizing multi-bit memory devices encoded by the skyrmion number. From this point of view, the concept of a skyrmion bag which contains multiple numbers of skyrmions in a larger skyrmion suggests that we can reconfigure the skyrmion number [6]. In this work, we report micromagnetic simulation results on various types of skyrmion bag dynamics under STT. We found that skyrmion bag dynamics varies dramatically depends on the net skyrmion number of skyrmion bags. We believe that our results can contribute to multi-bit information carriers based on skyrmion bags.

References

- [1] J. Sampaio, V. Cros, S. Rohart, A. Thiaville, and A. Fert, *Nat. Nanotechnol.* 8, 839–844 (2013).
- [2] N. Nagaosa and Y. Tokura, *Nat. Nanotechnol.* 8, 899(2013).
- [3] W. Jiang, X. Zhang, G. Yu, W. Zhang, X. Wang, M. B. Jungfleisch, J. E. Pearson, X. Cheng, O. Heinonen, and K. L. Wang et al., *Nat. Phys.* 13, 162 (2017).
- [4] K. Litzius, I. Lemesch, B. Krüger, P. Bassirian, L. Caretta, K. Richter, F. Büttner, K. Sato, O. A. Tretiakov, and J. Förster et al., *Nat. Phys.* 13, 170 (2017).
- [5] X. Zhang, J. Xia, Y. Zhou, D. Wang, X. Liu, W. Zhao, and M. Ezawa, *Phys. Rev. B* 94, 094420 (2016).
- [6] D. Foster, C. Kind, P.J. Ackerman, J.-S. B. Tai, M.R. Dennis, and I.I. Smalyukh, *Nat. Phys.* 15, 655–659 (2019).

Magnetic field tunability of a skyrmion diode

Dae-Han Jung^{*}, Hee-Sung Han, Ganghwi Kim, Suyeong Jeong and Ki-Suk Lee^{*}

Department of Materials Science and Engineering, Ulsan National Institute of Science and Technology,
Ulsan 44919, Republic of Korea

Magnetic skyrmions are topologically stable particle-like objects that are hailed as a potential technology for next-generation information storage and other processing applications. [1-5]. For device applications of magnetic skyrmions, it is essential to control the skyrmion motions by electrical means in geometrically confined boundaries. In this work, we show that a current-driven skyrmion motion can be unidirectionally controlled by forming an asymmetric shape of the device. Furthermore, we demonstrate tunability of the unidirectional motions in which the magnetic field can be used to switch on and off a circuit. A key working principle of the unidirectional motion and its tunability is investigated by micromagnetic numerical and analytical calculations. We believe that our results could provide guidelines to design skyrmion-based logic devices including a diode and a transistor element.

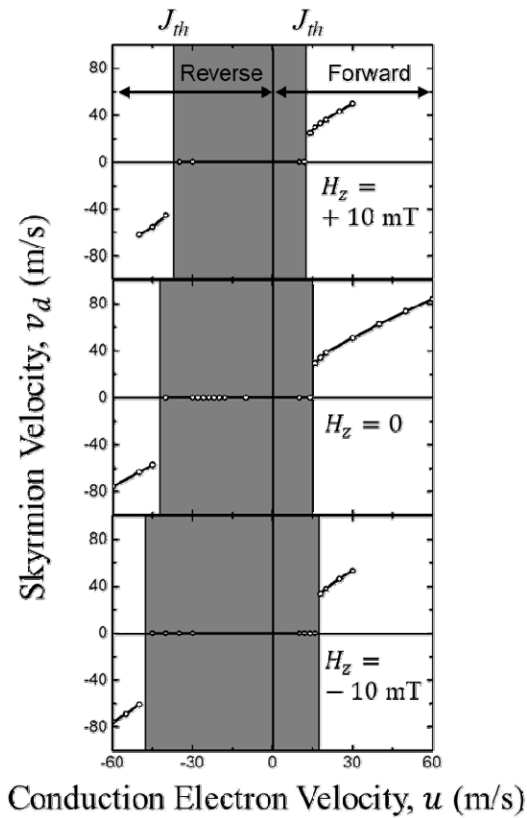


Figure 1. Field tunability of diode characteristics of skyrmion propagation

References

- [1] N. S. Kiselev, A. Bogdanov, R. Schäfer, and U. K. Röbber, *J. Phys. D* **44**, 392001 (2011).
- [2] A. Fert, V. Cros, and J. Sampaio, *Nat. Nanotechnol.* **8**, 152 (2013).
- [3] N. Nagaosa and Y. Tokura, *Nat. Nanotechnol.* **8**, 899–911 (2013).
- [4] J. Iwasaki, M. Mochizuki, and N. Nagaosa, *Nat. Nanotechnol.* **8**, 742–747 (2013).
- [5] R. Wiesendanger, *Nat. Rev. Mater.* **1**, 16044 (2016).

Symmetry-breakings for unidirectional skyrmion motions under spin-orbit and -transfer torques

Dae-Han Jung^{*}, Hee-Sung Han, Ganghwi Kim, Suyeong Jeong and Ki-Suk Lee^{*}

Department of Materials Science and Engineering, Ulsan National Institute of Science and Technology,
Ulsan 44919, Republic of Korea

Unidirectional control of magnetic skyrmion motions is an essential prerequisite for developing skyrmion-based spintronic devices. Here, we propose a method to achieve the unidirectional motions in a patterned nanowire with a symmetry-breaking by using spin-orbit torque (SOT) and spin-transfer torque (STT). We confirm the validity of the method by using micromagnetic simulation. The simulation results show that the direction of symmetry-breakings changes depending on the application of SOT and STT. We believe that this method can be used as a basic building block for skyrmion-based memory and logic devices with multiple operations.

Compositional development of M-type hexaferrite magnet without sintering additives

Jin-Young You¹, Ji-Hye Lee¹, Jun-Pyo Lim¹, Min-Ho Kim², Young-Min Kang^{1*}

¹Department of Materials Science and Engineering, Korea National University of Transportation, Chungju, 27469, Korea

²R&D Team, Union Materials Corp., Pohang, 37865, Korea

*Corresponding author email: ymkang@ut.ac.kr

We report a method for the development of ferrite magnet without sintering additive. Sintered M-type hexaferrites with chemical formula of $\text{Sr}_{0.3}\text{Ca}_{0.4}\text{La}_{0.3}\text{Fe}_{9.8}\text{Co}_{0.2-x}\text{Mn}_x\text{Si}_{0.135}\text{O}_{19-d}$ ($x = 0, 0.05, 0.1, 0.2$) and $\text{Sr}_{0.3}\text{Ca}_{0.4}\text{La}_{0.3}\text{Fe}_{9.8-y}\text{Co}_{0.2}\text{Mn}_y\text{Si}_{0.135}\text{O}_{19-d}$ ($y = 0.05, 0.1, 0.2$) have been prepared by conventional solid state reaction routes. High sintering density of more than 95% of the theoretical density is achieved in all hexaferrite samples when calcination is carried out at 1100 °C for 4 h, followed by sintering at 1230-1250 °C for 2 h without sintering additive input process. High saturation magnetization and coercivity can be achieved simultaneously at the $x = 0.05$ composition, where the Mn replaces part of the Co. The secondary phase Fe_2O_3 generated by the initial addition of SiO_2 is gradually reduced when the Fe contented is decreased in $\text{Sr}_{0.3}\text{Ca}_{0.4}\text{La}_{0.3}\text{Fe}_{9.8-z}\text{Co}_{0.15}\text{Mn}_{0.05}\text{Si}_{0.135}\text{O}_{19-d}$ samples and the single M-type hexaferrite phase can be confirmed from the sample of $\text{Sr}_{0.3}\text{Ca}_{0.4}\text{La}_{0.3}\text{Fe}_{8.3}\text{Co}_{0.15}\text{Mn}_{0.05}\text{Si}_{0.135}\text{O}_{19-d}$ ($z = 1.5$) which also exhibits optimized hard magnetic properties of saturation magnetization of 4581 G and coercivity of 4771 Oe. For the optimized composition, anisotropic sintered magnets have been fabricated and it showed excellent hard magnetic properties of remanent magnetic flux density of 4400 G and intrinsic coercivity of 4118 Oe, and maximum energy product of 4.72 M·G·Oe. This result is very promising because high magnet performances can be achieved by single batch process without inputting sintering additives during the process.

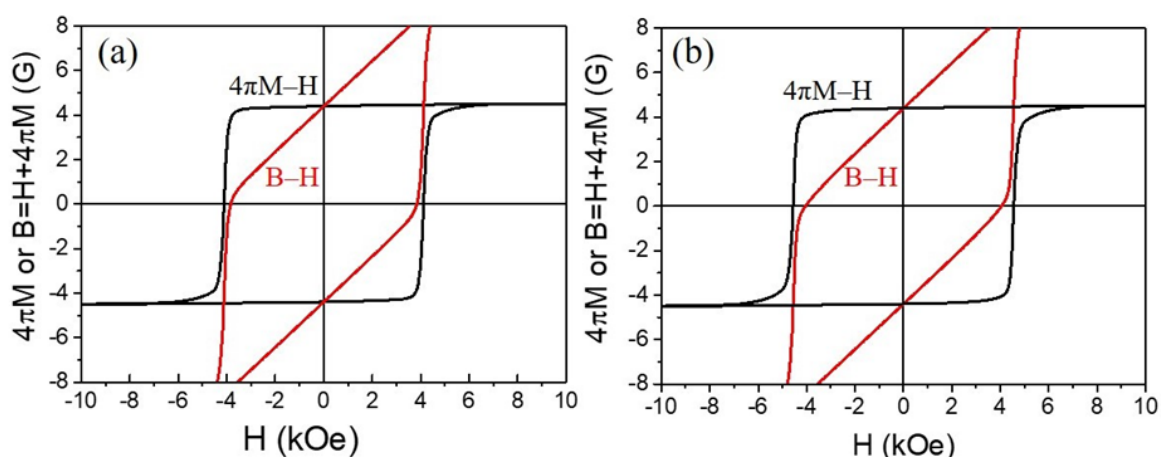


Fig. Magnetization curves ($4\pi M - H$ and $B-H$) of $\text{Sr}_{0.3}\text{Ca}_{0.4}\text{La}_{0.3}\text{Fe}_{9.8}\text{Co}_{0.15}\text{Mn}_{0.05}\text{Si}_{0.135}\text{O}_{19-d}$ (b) $\text{Sr}_{0.3}\text{Ca}_{0.4}\text{La}_{0.3}\text{Fe}_{9.8}\text{Co}_{0.2}\text{Si}_{0.135}\text{O}_{19-d}$ sintered anisotropic magnets sintered at 1230 °C.

HDDR 처리된 Nd-Fe-계 소결자석의 미세구조 변화가 자기적 특성에 미치는 영향

노태성^{1,2*}, 차희령¹, 김태훈¹, 김양도^{2†}, 이정구^{1†}

¹한국재료연구원, 자성재료연구실

²부산대학교, 재료공학과

Nd-Fe-B계 소결자석은 우수한 자기 특성으로 전기자동차 및 하이브리드 자동차의 구동모터에 핵심소재로 이용되고 있다. 그러나 내열특성이 취약한 Nd-Fe-B계 소결자석은 구동모터의 작동온도인 200℃에서 보자력이 급격하게 감소하는 문제점이 있다. 이와 같은 문제점을 해결하기 위해 자석에 Dy, Tb와 같은 중희토류를 첨가하여 보자력을 향상시키고 있지만, 중희토류 자원은 대부분 중국에서 생산되고 있어 수급 불안정 및 가격 문제가 지속적으로 발생하고 있는 실정이다. 중희토류를 첨가하지 않고 자석의 보자력을 향상시키기 위해서는 결정립 크기를 미세화하고, 비자성 물질로 균일하고 연속적인 입계상을 형성시키는 것이 필요하다. 특히, 자석의 표면영역은 산화, 반자장의 영향으로 내부영역에 비해 역자구가 쉽게 생성되기 때문에 표면영역의 미세조직을 적절히 제어하는 것이 중요하다. Nd-Fe-B계 자석의 결정립을 미세화하는 방법 중 하나로 hydrogenation-disproportion-desorption-recombination (HDDR) 공정법이 있다. HDDR 공정은 Nd-Fe-B계 합금의 조대한 결정립을 수소화 반응, 상분해, 수소방출 및 재결합 과정을 거쳐 Nd₂Fe₁₄B상의 단자구 크기인 300nm 수준으로 미세화가 가능한 기술이다. 또한, 공정조건을 적절히 제어하면 이방성 분말로 제조가 가능하다. 하지만 HDDR 공정의 경우 주로 분말 소재에 적용되어 왔고, 벌크 자석에서의 HDDR 거동에 관한 연구는 거의 보고되지 않았다.

본 연구에서는 Dy_{1.4}Nd_{21.8}Pr_{6.7}Fe_{bar}B_{0.9}M(Co, Al, Cu, Ga, Nb)_{2.0} (wt.%) 조성의 소결자석에 HDDR 처리하여 자석 표면에만 결정립이 미세화 된 자석을 제조하였으며, HDDR 공정온도 및 HD 반응시간에 따른 미세구조와 자기특성 변화를 조사하였다. HDDR 공정은 810~1000℃ 범위에서 실시하였으며, 공정 중 HD 반응 시간을 0.5~2h까지 변화하며 실험을 진행하였다. 실험결과, 수소화 반응 시, 초기 자석의 입계를 따라 수소가 확산되면서 결정립 표면부터 상분해가 일어났으며, 810℃와 920℃에서 0.5h동안 HD처리한 시료의 경우 각각 표면에서부터 약 200μm, 50μm 깊이까지 결정립이 미세화된 것을 확인하였다. 그러나 HDDR 공정 후, 표면 결정립이 미세화 되었음에도 불구하고 보자력이 오히려 감소하는 결과를 나타내었다. 이는 기존 소결자석 영역과 결정립 미세화가 일어난 영역 계면에서 비연속적이고 불균질한 입계상을 가지는 영역을 형성하였기 때문으로 판단되며, Kerr-microscopy를 통해 이러한 영역에서 자구가 쉽게 반전됨을 확인하였다. 상기 결과를 바탕으로 Nd-Fe-B계 소결자석의 HDDR공정에 의한 표면결정립 미세화 거동과 자기특성의 상관관계에 대해 논의하고자 한다.

Structure and magnetic properties of BaFe₁₂O₁₉ Nanoparticles

Jae-Young Choi^{1,2*}, Jeong-Min Lee¹, Youn-Kyung Baek¹, Jung-Goo Lee¹, Young Kuk Kim^{1†}

¹Korea Institute of Materials Science, Changwon, Republic of Korea 51508

²Pukyong National University, Busan, Republic of Korea 48513

We investigated evolution of structural and magnetic properties of BaFe₁₂O₁₉ (BaM) nanoparticles after prolonged annealing and the effects of residual Na ions are also discussed. The lattice contraction and enhanced population of oxygen vacancies were detected for extensively annealed BaM nanoparticles prepared with NaOH as a pH modifier during co-precipitation. Those changes in the lattice were attributed to the substitutional incorporation of smaller Na⁺ ions in the Ba²⁺ site in the lattice of BaM during prolonged sintering. Magnon scattering intensity from low temperature Raman spectra were reduced with prolonged annealing of the same specimen. The minimization of the magnon peak indicates the collapse of strong anti-ferromagnetic interaction between Fe³⁺ ions of bipyramidal sites and octahedral regions of BaM nanoparticles due to oxygen vacancies. The increase in saturation magnetization was detected for BaM nanoparticles after prolonged annealing, which was attributed to initiation of local ferromagnetic interactions induced by the local collapse of anti-ferromagnetic interactions due to increased number of oxygen vacancies.

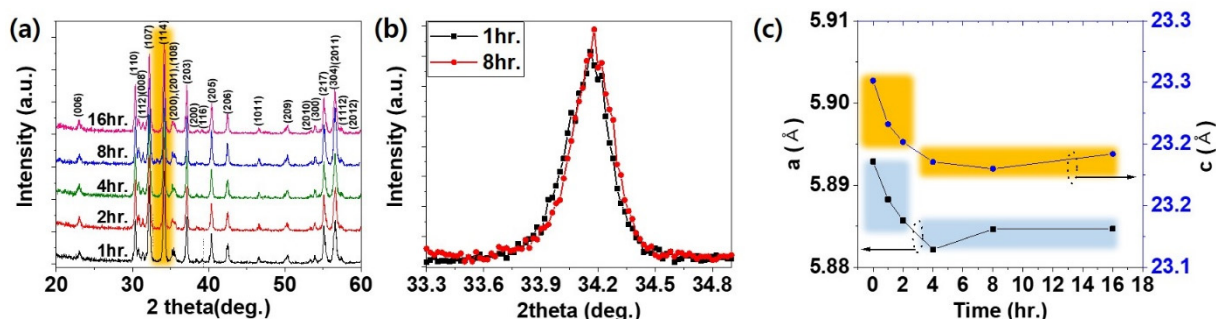


Fig. 1. (a) X-ray diffraction (XRD) of BaFe₁₂O₁₉ nanoparticles after annealing at 900°C for different duration time; (b) Enlarged XRD patterns denoting (114) plane for BaM nanoparticles; (c) The variation of lattice parameters as a function of annealing time. Lattice parameters at 0 hour denote that of as calcined BaM nanoparticles.

Na-La-Co계 M형 페라이트의 합성과 자기적 특성

손성우^{1,2*}, 김부안^{1†}, 권해웅^{1†}, 최재영³, 이정구³

¹부경대학교 재료공학과

²(주) 태평양금속 연구팀

³한국재료연구원 분말재료연구본부 자성재료연구실

Nd소결자석의 최대에너지적((BH)_{max})의 1/10 수준인 페라이트 소결자석은 주원료가 산화철로서 가격대비 성능이 우수하고 화학적으로 대단히 안정적인 장점을 가지고 있다. 이러한 이유로 현재 사용되고 있는 영구자석 중에서 중량으로는 가장 많은 생산량을 현재까지도 유지하고 있으며 각종 모터나 스피커 등의 다양한 분야에서 페라이트 소결자석이 사용되고 있다. 최근 희토류 가격이 수급 불안정이나 조달 리스크 등으로 다시 상승하는 경향을 보이고 있으며 Nd소결자석이 주로 사용되고 있던 산업용 모터나 전기자동차용 구동모터, 발전기 등에도 페라이트 소결자석의 적용이 검토되고 있다. 이미 Sr계, Sr 및 Fe의 일부를 각각 La, Co로 치환한 SrLaCo계, CaLaCo계의 페라이트 소결자석이 연구개발되어 상용화되어 있으나 최근 페라이트 소결자석의 수요가 증가하면서 기존의 페라이트 소결자석이 아닌 새로운 원소계의 페라이트 소결자석의 개발이 필요하다고 판단되었고 알칼리금속계 M형 페라이트 소결자석에 관해서 연구를 진행하였다. 이전 문헌에 따르면 알칼리금속-La의 조합에 의한 M형 페라이트 조성에 대해서 과거 연구된 적이 있으나 현재 양산되고 있는 고상반응법으로는 다결정체의 제작이 대체적으로 어려우며 주로 단결정체를 제작하여 자기적 특성을 평가하는 정도에 머물러 있고 기존 페라이트 소결자석을 대체할 수 있는 수준에는 미치지 못하고 있다. 본 연구에서는 고상반응법에 의하여 알칼리금속원소인 Na과 희토류원소인 La으로 조합한 NaLa계 페라이트 조성을 기준으로 Fe의 일부를 Co로 치환한 NaLaCo계 페라이트 시료의 몰 비 변경에 따른 상분석 및 자기적 특성을 조사하였고 Co를 치환하지 않은 NaLa계 페라이트 조성의 시료와 비교하였고 새로운 원소계의 페라이트 소결자석의 연구개발 가능성을 확인하였다.

Coercivity improvement in Nd-Cu infiltrated Nd-Fe-B hot-deformed magnets by controlling microstructure of initial HDDR powders

Jae-Gyeong Yoo^{1,2*}, Tae-Hoon Kim¹, Hee-Ryoung Cha¹, Yang-Do Kim^{2*}, Jung-Goo Lee^{1†}

¹Department of Magnetic Materials, Korea Institute of Materials Science,
797 Changwon-daero, Changwon 51508, Korea

²Department of Materials Science and Engineering, Pusan National University, 2, Busandaehak-ro 63beon-gil,
Geumjeong-gu, Busan 46241, Korea

Since the anisotropic Nd-Fe-B hot-deformed magnets are composed of much finer grains than commercial sintered magnets, the hot-deformed magnets have a great potential to obtain high coercivity and better temperature dependence of coercivity without using HRE elements. However, the hot-deformed magnets still have lower coercivity than that expected from their intrinsic properties. The low coercivity of the hot-deformed magnets is appeared to be due to the thin and non-uniform Nd-rich intergranular phase and high concentration of ferromagnetic Fe and Co in the Nd-rich intergranular phase. To obtain high coercivity of hot-deformed magnet, infiltration process using non-ferromagnetic material is necessary. However, the hot-deformed magnets produced from the melt-spun powders, a remarkable grain growth occurred during the infiltration above 700°C because the grains of initial melt-spun powder are too fine. Therefore, only low-melting point alloys such as Nd-Cu, Pr-Cu, or Nd-Al were used for infiltration. Such limitation in the process temperature for the infiltration leads to the significant reduction in remanence of the magnets because a large amount of paramagnetic diffusion source is required for high coercivity. Whereas, infiltration of Dy-compound as DyF₃, DyH_x, etc. could improve the coercivity even in a small amount, while minimizing the reduction in remanence. However, high processing

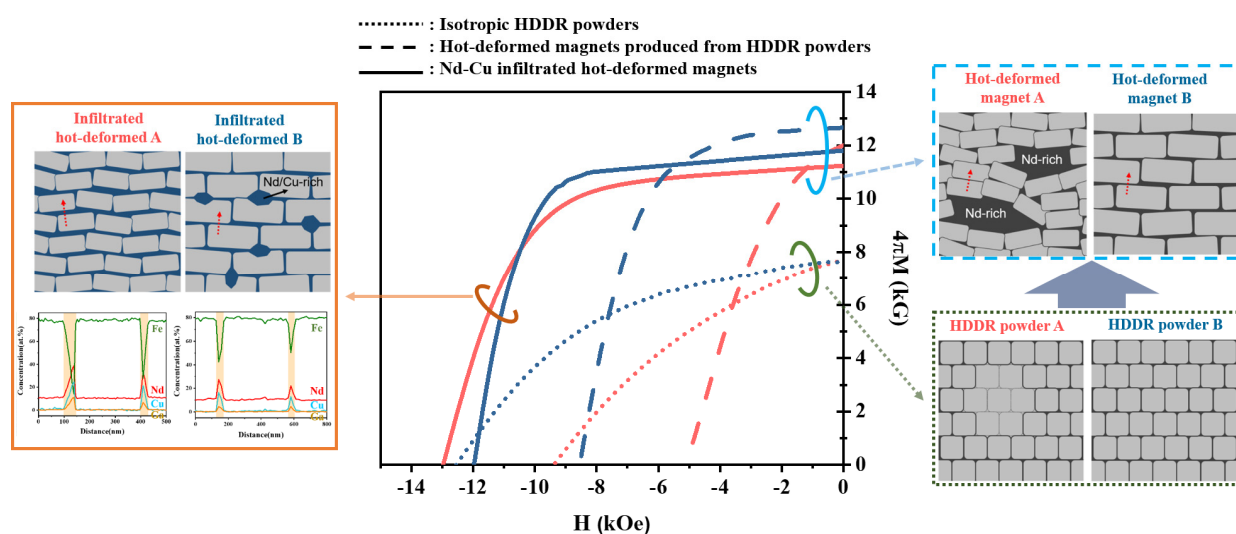


Fig. 1. magnetic and microstructural changes of initial isotropic HDDR powder A and B after hot-deformation and subsequent Nd-Cu infiltration processes.

temperature is required. Therefore, using the HDDR powders as an initial powders seems to have an advantage for infiltration at higher temperature because the average grain size of HDDR powders is bigger than that of melt-spun powders. In this approach, controlling the distribution of Nd-rich intergranular phases in the initial HDDR powders can be an important factor for achieving higher coercivity in the hot-deformed magnets by the infiltration because the intergranular phases in the HDDR powders are non-uniform and discontinuous. Thus, in this study, we comparatively investigated the magnetic and microstructural changes of two different HDDR powders with distinct microstructures of Nd-rich intergranular phases upon the hot-deformation and the Nd-Cu infiltration. To control the microstructure with distinct Nd-rich intergranular phase, A part of initial alloy was subjected to pre-annealing and the rest was un treated. Interestingly, the coercivity of hot-deformed magnets increased more rapidly after the infiltration process when the microstructure of intergranular phases in the initial HDDR powders was controlled to be non-uniform and discontinuous. A detailed influence of the microstructure of initial HDDR powders on the magnetic and microstructural properties of the Nd-Cu infiltrated hot-deformed magnets will be discussed, and a method to further increase the coercivity of the hot-deformed magnets by the infiltration process will be proposed based on the results.

Systematic process control for high performance MnBi magnets

Su Yeon Ahn^{1,2*}, Yang Yang^{1,3}, Jung Tae Lim¹, Jihoon Park¹, Jong-Woo Kim¹,
Soon Chul Hong², Chul-Jin Choi¹

¹Korea Institute of Materials Science (KIMS), Changwon

²Department of Physics, University of Ulsan

³School of Materials Science and Engineering, Pusan National University

In recent years, rare-earth-free permanent magnets have attracted considerable attention due to the concern over cost and supply crisis of rare-earth raw materials. Among the rare-earth-free permanent magnets, MnBi shows high magnetic crystalline anisotropy, high Curie temperature of 633 K and a noticeable positive temperature coefficient making it promising for possible industrial applications. For the future industrial applications, a detailed optimization process and mass synthetic process of qualified MnBi powder and bulk magnet should be established.

In this work, a systematic process control for *high performance* MnBi magnets has been investigated. A synthetic process of MnBi ingots via induction melting was tuned for high purity low-temperature phase (LTP) and mass production of MnBi powder. In addition, efficient particle size control and an inevitable post processes for homogeneity of LTP, microstructure, and finally, enhancement of magnetic property have been optimized. Meanwhile, the effect of Mg and Sb substitution on MnBi matrix has also been examined for enhancement of coercivity and higher energy products. A detailed optimization process and mass synthetic process of MnBi powder which has advantages for industrial applications will be presented in detail.

Effects of Sn Addition on the Microstructure and Magnetic Properties of MnBi Bulk Magnets

Yang Yang^{1,2*}, Jung Tae Lim¹, Jihoon Park¹, Hui-Dong Qian^{1,2},
Oi Lun Li², Jong-Woo Kim^{1*}, Chul-Jin Choi^{1†}

¹Korea Institute of Materials Science, Changwon 51508, Republic of Korea

²School of Materials Science and Engineering, Pusan National University, Busan 46241, Republic of Korea

Rare-earth free permanent magnets are current emerging issues of industry for the growing market demands. Among the rare-earth free permanent magnets, MnBi has attracted attention for large magnetocrystalline anisotropy constant ($K_1 \approx 1.6 \text{ MJ/m}^3$, at 300 K) [1] and unique positive temperature coefficient of coercivity (H_c) [2]. The low-temperature phase (LTP) of MnBi exhibits a saturation magnetization (M_s) of 80 emu/g, and the theoretical maximum energy product $(BH)_{\max}$ 17.7 MGOe at room temperature [3]. However, it is a challenge to fabricate MnBi bulk magnets while maintaining the superior magnetic properties of the powder, especially to prevent the reduction of H_c from powder to bulk. The effects of Sn adding on the microstructure and magnetic properties of MnBi bulk magnets have been systematically investigated. As known, the pure MnBi bulk magnets are challenging to reach high H_c in previous studies, and a few reference works have been reported about research on fabrication of high H_c MnBi bulks by adding the third element. It was found that the Sn-added MnBi bulk magnets show the increased H_c and the improved squareness, apparently related to restructuring the intergranular phase due to Sn element addition. The H_c of MnBi bulk magnet with 3 wt.% Sn reaches 11.6 kOe, which is 35 % higher than that of the pure MnBi magnet. In the sample of 1 wt.% Sn added MnBi bulk magnet, the H_c was elevated to 10.0 kOe, and the maximum energy product $(BH)_{\max}$ was recorded of 7.84 MGOe at room temperature. This makes Sn added MnBi bulk magnet a promising candidate for next-generation rare-earth-free bulk magnets.

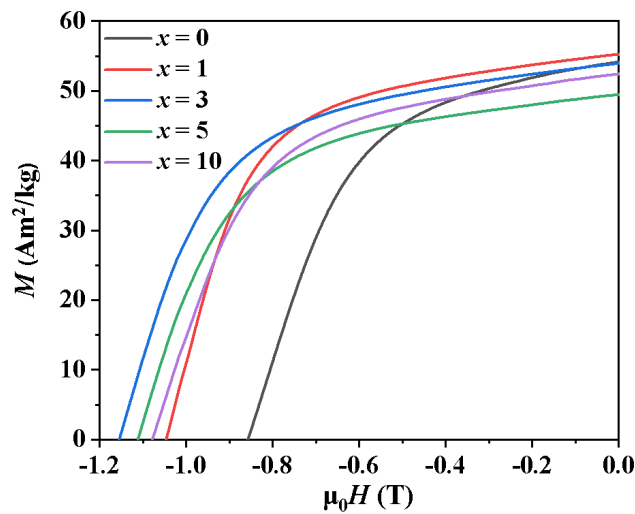


Fig. 1. Room temperature demagnetization curves of the MnBi bulk magnets added with Sn contents of (0, 1, 3, and 5 wt.%).

References

- [1] B.W. Roberts, Neutron diffraction study of the Structures and magnetic properties of Manganese Bismuthide, *Phys. Rev.* 104 (1956) 607-616.
- [2] J.B. Yang, K. Kamaraju, W.B. Yelon, W.J. James, Q. Cai, A. Bollero, Magnetic properties of the MnBi intermetallic compound, *Appl. Phys. Lett.* 79 (2001) 1846.
- [3] J. Park, Y.-K. Hong, J. Lee, W. Lee, S.-G. Kim, C.-J. Choi, Electronic structure and maximum energy product of MnBi. *Metals* 4 (2014) 455-464.

Influence of grain boundary diffusion process on grain alignment and magnetic properties of Nd lean Nd-Fe-B hot-deformed magnets

Ga-Yeong Kim^{1,2*}, Tae-Hoon Kim¹, Hee-Ryoung Cha¹, Yang-Do Kim^{2*} and Jung-Goo Lee^{1†}

¹Department of Magnetic Materials, Korea Institute of Materials Science, Changwon, Korea

²Department of Materials Science and Engineering, Pusan National University, Busan, Korea

Heavy rare earth elements such as Dy and Tb should be added for coercivity enhancement of Nd-Fe-B magnets. However, cost problem become more serious because the natural abundance of Dy and Tb comparing with Nd is lower than 10%. Therefore, many research was focused on modifying the microstructure to reduce the use of Heavy rare earth elements. On the other hand, Ce and La is the most abundant rare earth elements and constitute is more than 70% of the total rare earth element, and the price of Ce is about 10 times lower than Nd. Hence, it is a technologically interesting challenge to develop high-performance Nd-lean Nd-Fe-B magnets by substitution of Ce and La for Nd, which is also quite important from an industrial viewpoint. However, the magnetic properties of Nd-Fe-B magnets could be drastically deteriorated after replacing Nd with Ce and La due to inferior intrinsic magnetic properties of $\text{Ce}_2\text{Fe}_{14}\text{B}$ ($4\pi M = 11.7 \text{ kG}$, $H_a = 26 \text{ kOe}$) and $\text{La}_2\text{Fe}_{14}\text{B}$ ($4\pi M = 13.8 \text{ kG}$, $H_a = 20 \text{ kOe}$) compared to $\text{Nd}_2\text{Fe}_{14}\text{B}$ ($4\pi M = 16 \text{ kG}$, $H_a = 73 \text{ kOe}$). Melt-spinning technique has been employed to obtain ultrafine-grained magnetic powders which have high coercivity due to the ultrafine grains. The melt-spun powder, which has Isotropic nanocrystalline, is subjected to hot-deformation (hot-pressing and subsequent die-upset) process in order to induce grain alignment along the c-axis parallel to the pressing direction, increasing the $(BH)_{\text{max}}$. The mechanism of texture formation was well known that grains grew along the $[010]$ and $[100]$ axis into platelet shape and the $[001]$ axis of platelet grains were oriented parallel to the pressing direction by the interface-controlled solution-precipitation-creep process and grain boundary sliding during hot-deformation process. So, grain boundary characteristics could significantly affect the texture formation during hot-deformation process. In this study, effect of Nd-Cu infiltration of $(\text{Nd},\text{M})\text{-Fe-B}$ initial powder on hot-deformation behavior was investigated. Initial ribbons with the nominal compositions of $(\text{Nd}_{1-x}\text{M}_x)_{13.6}\text{Fe}_{\text{bal}}\text{B}_{5.6}\text{Ga}_{0.6}\text{Co}_{0.6}$ ($x=0$, $x=0.2/\text{M}=\text{Ce}$, $x=0.3/\text{M}=\text{Ce}$ and $x=0.3/\text{M}=\text{Ce}+\text{La}$, wt.%, named as ND, CE0.2, CE0.3 and CELA0.3, respectively) were prepared by a single-roller melt-spinning technique and then pulverized into powders. The melt-spun powders were then hot-pressed and subsequently die-upsetted. In our previous study, the grain boundary phase of ND magnet was quite uniformly distributed along grain boundaries. However, the grain boundary phase became unclear and the triple junction phase increased with Ce and La content. Especially, the grain boundary phase of CELA0.3 magnet was quite unclear in almost area, whereas a lot of big-sized triple junction phase was formed. The RE-rich phase acts as a lubricant promoting the grain boundary sliding to form c-axis textured anisotropic magnets during the hot deformation process. When the RE-rich phase is not evenly distributed across the grain boundaries, grain boundary sliding could be suppressed and the degree of alignment decreases. It was confirmed that the degree of alignment was decreased with increasing Ce and La content. However, the grain boundary diffusion process in initial powder was favorable to the improvement of alignment of $(\text{Nd},\text{M})\text{-Fe-B}$ hot-deformed magnets. Based upon these results, effect of grain boundary diffusion process of grain alignment and magnetic properties of Nd-lean Nd-Fe-B hot-deformed magnets will be discussed.

Phase transformation and magnetic properties of ThMn₁₂ structure Sm-Fe-Co-Ti-Si magnetic ribbons

Hui-Dong Qian^{1,2*}, Jung Tae Lim¹, Yang Yang^{1,2}, Jong-Woo Kim¹, Su Yeon Ahn¹, Hankuk Jeon¹, Tian Hong Zhou¹, Kyung Mox Cho², Jihoon Park^{1*}, Chul-Jin Choi^{1†}

¹Powder Materials Division, Korea Institute of Materials Science, Changwon,
Gyeongsangnam-do 51508, Republic of Korea

²School of Materials Science and Engineering, Pusan National University, Busan 46241, Republic of Korea

As early as the 1980s, Fe-rich compounds with a ferromagnetic tetragonal ThMn₁₂-type structure were known to be a promising hard magnetic material [1]. However, owing to the rapid development of Nd-Fe-B permanent magnets with large magnetic moments and strong anisotropies, ThMn₁₂-type Fe-rich compounds were not given enough attention at that time. Recently, ThMn₁₂-type Sm(Fe_{1-x}Co_x)₁₂ compound films with a saturation magnetization of 1.78 T, an anisotropy field of 12 T, and a Curie temperature of 586 °C, all of which are superior to those for Nd₂Fe₁₄B [2], were successfully produced. However, to stabilize the unstable ThMn₁₂ phase, partial Fe at 8i site must be substituted with a large amount of non-magnetic elements, such as Ti, V, Si, Al, Cr, or Mo. In addition, some researches on R(Fe, Si) compounds show the possibility that the R(Fe, Si) compounds could exhibit outstanding magnetic properties [3,4]. However, the phase transformation mechanisms of R(Fe, Si) compounds during the rapid solidification and heat treatment process still have not been clearly discussed in previous works. Therefore, in this work, the phase transformation mechanisms and magnetic properties were discussed to investigate the effect of Si addition in R(Fe, M) compounds.

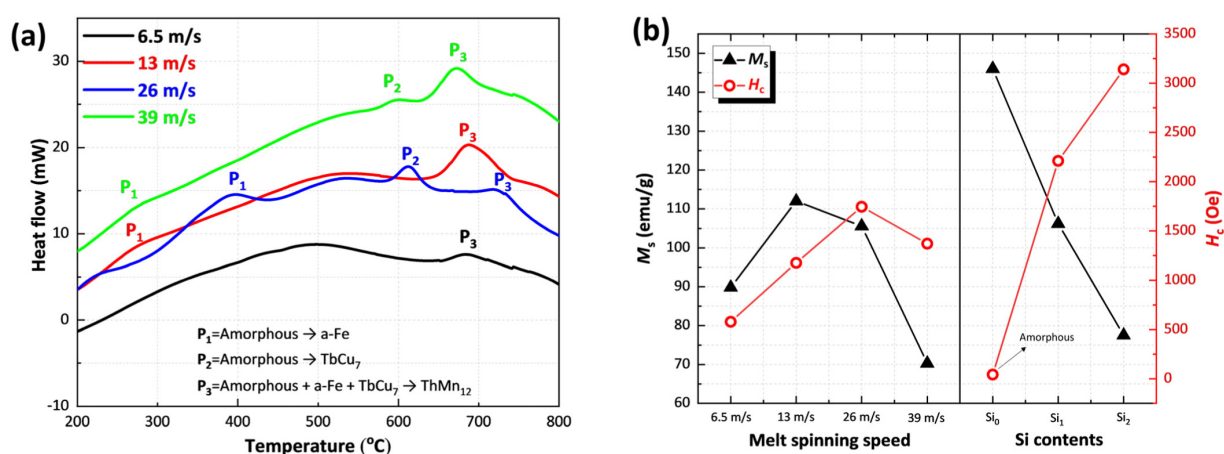


Fig. 1 (a) Differential Thermal Analysis of ground Sm(Fe_{0.8}Co_{0.2})₁₀Si₂ ribbons with different wheel speed; (b) Magnetic properties of Sm(Fe_{0.8}Co_{0.2})₁₀Si₂ and Sm(Fe_{0.8}Co_{0.2})₁₁Ti+Si_x ribbons.

Sm(Fe_{0.8}Co_{0.2})₁₀Si₂ and Sm(Fe_{0.8}Co_{0.2})₁₁Ti+Si_x ($x = 0, 0.5$, and 1) ribbons were successfully produced using a melt spinning method. In Fig. 1 (a), the phase transformation behavior from amorphous to ThMn₁₂ phase during heat treatment was systematically investigated by using the Differential Thermal Analysis. The three kinds of

phase transformations were indicated: 1) from the amorphous to α -Fe (P_1), 2) from the amorphous to TbCu₇ (P_2), and 3) from the amorphous + α -Fe + TbCu₇ to ThMn₁₂ (P_3). The magnetic properties of the Sm(Fe_{0.8}Co_{0.2})₁₀Si₂ ribbons with different melt spinning speed and the Sm(Fe_{0.8}Co_{0.2})₁₁Ti+Si_x ribbons with melt spinning speed of 39 m/s are shown in Fig. 1 (b). The maximum coercivity of the Sm(Fe_{0.8}Co_{0.2})₁₀Si₂ and Sm(Fe_{0.8}Co_{0.2})₁₁Ti+Si_x ribbons reach 1745 and 3140 Oe, respectively.

References

- [1] G.C. Hadjipanayis, A.M. Gabay, A.M. Schönhöbel, A. Martín-Cid, J.M. Barandiaran, D. Niarchos, *Engineering* **6** (2020) 141-147.
- [2] Y. Hirayama, Y.K. Takahashi, and S. Hirosawa, and K. Hono, Intrinsic hard magnetic properties of Sm(Fe_{1-x}Co_x)₁₂ compound with the ThMn₁₂ structure, *Scripta Mater.* **138** (2017) 62-65.
- [3] A.M. Gabay, N.N. Schegoleva, E.V. Belozerov, The structure and hard magnetic properties of rapid quenched (Sm,Zr)₁(Fe,Si)₁₂ alloys, *Phys. Met. Metallogr.* **94** (2002) 252-257.
- [4] J. Ding, M. Rosenberg, magnetic properties of melt spun and crystallized SmFe₁₀M₂, *J. Magn. Magn. Mater.* **83** (1990) 257-258.

Effect of Ti and V content on the magnetic properties of $\text{Sm}(\text{FeCo})_{12}$ -based magnets produced by melt-spinning method

Tianhong Zhou^{1,2*}, Hui-Dong Qian^{1,2}, Jihoon Park¹, Yong-Rae Cho², Chul-Jin Choi^{1†}

¹Powder Materials Division, Korea Institute of Materials Science, Changwon,
Gyeongsangnam-do 51508, Republic of Korea

²School of Materials Science and Engineering, Pusan National University, Busan 46241, Republic of Korea

Due to high Fe content, tetragonal SmFe_{12} -based magnets are expected to have a great performance in magnetization and energy density [1]. In order to stabilize their structure, additional elements, such as Ti, V, Nb, Mo, Ta, W, Al or Si, are necessarily substituted. Among these stabilizing elements, Ti is the most effective element that a small amount of Ti can stabilize the structure by replacing only a Fe atom at $8i$ site [2]. On the other hand, it is reported that V-doped SmFe_{12} -based magnets exhibited a larger value of coercivity than V-free magnets [3]. At the same time, the magnetization of the ThMn_{12} -type magnets can be enhanced by partially substituting Fe with Co at $8f$ site in tetragonal structure [4].

Therefore, in this work, we have studied the influence of Ti and V content in the $\text{Sm}(\text{Fe}_{0.8}\text{Co}_{0.2})_{12-2x}\text{Ti}_x\text{V}_x$ ($x = 0.5-1.0$) alloys. Amorphous ribbons were obtained using melt spinning process, and high density green bodies were produced by pressing the melt-spun ribbons under 12.5 GPa. The green bodies were heat treated at the temperature ranging from 700 to 850 °C. At the x from 0.6 to 1.0, we obtained high purity ThMn_{12} phase. It was found that the coercivity varies with increasing x contents as can be seen in Fig. 1, while the magnetization decreases due to increasing non-magnetic elements. The optimal x was found to be 0.6, and the corresponding remanent magnetization and maximum energy product were 80.6 emu/g and 7.29 MGOe, respectively. We have also studied the most suitable annealing temperature and Curie temperature for alloys of each component.

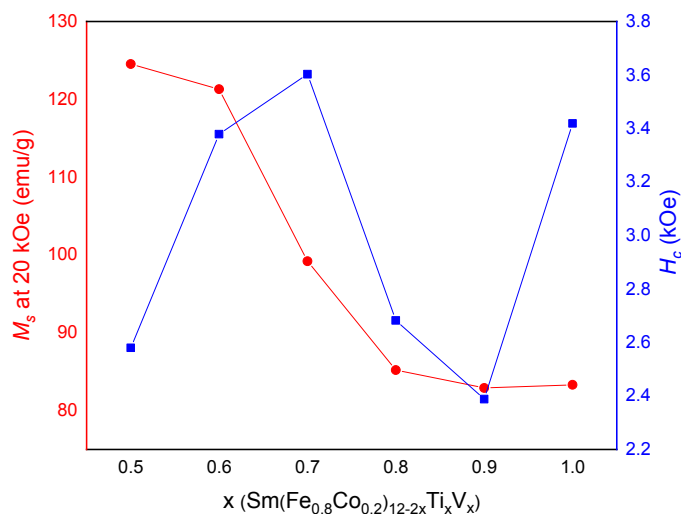


Fig 1. The saturation magnetization and coercivity of $\text{Sm}(\text{Fe}_{0.8}\text{Co}_{0.2})_{12-2x}\text{Ti}_x\text{V}_x$ ($x = 0.5-1.0$) at annealing temperature 800 °C

References

- [1] G.C. Hadjipanayis, A.M. Gabay, A.M. Schönhöbel, ThMn₁₂-Type Alloys for Permanent Magnets, Engineering, 6(2020) 141-147.
- [2] R. Coehoorn, Electronic structure and magnetism of transition-metal-stabilized YFe_{12-x} M_x intermetallic compounds, PHYSICAL REVIEW B, 15 June 1990-I.
- [3] Xin Tang, J. Li, A.K. Srinithi, Role of V on the coercivity of SmFe₁₂-based melt-spun ribbons revealed by machine learning and microstructure characterizations, Scripta Materialia, 200 (2021) 113925.
- [4] Chen Zhou, Frederick E. Pinkerton, J. F. Herbst, Magnetic properties of CeFe_{11-x}Co_xTi with ThMn₁₂ structure, Journal of Applied Physics, 115, 17C716 (2014)

Magnetic properties and microstructure evaluation of $(\text{Sm}_{0.9}\text{Zr}_{0.1})(\text{Fe}_{0.75}\text{Co}_{0.25})_{11.35}\text{Ti}_{0.65}$ particles with ThMn_{12} structure produced by reduction diffusion process

Hankuk Jeon^{1,2*}, JungTae Lim¹, Hui-Dong Qian¹, Jihoon Park¹,
Hyo-Jun Ahn² and Chul-Jin Choi¹

¹Korea Institute of Materials Science, Changwon, Gyeongsangnam-do 51508, Republic of Korea

²School of Materials Science and Engineering, Gyeongsang National University, Jinju,
Gyeongsangnam-do 52825, Republic of Korea

Permanent magnets are increasingly used in transportation technology and sustainable energy production for EVs, hybrid vehicles and wind turbines. High performance permanent magnets, such as Nd-based magnets, have problems with supply and high price. Therefore, developing rare-earth free or rare-earth lean permanent magnets is becoming an important task to solve the abovementioned issues. Herein, iron-rich rare-earth alloys with tetragonal ThMn_{12} structure, which can replace rare earth permanent magnets, is drawing attention due to its high saturation magnetization of 1.43 T, anisotropy field of 10.9 T, and Curie temperature of 800 K [1]. Although the magnetic properties of SmFe_{12} with ThMn_{12} structure have been already demonstrated, a number of studies to enhance coercivity are still underway. The coercivity increases as grain sizes approach to the single domain size. Therefore, in this work, we conducted experiments to obtain SmFe_{12} particles with single domain sized grains to acquire high coercivity through the reduction diffusion process.

In this experiment, Sm_2O_3 (Samarium Oxide), ZrO_2 (Zirconium Dioxide), Fe_2O_3 (Iron Oxide), Co, TiO_2 (Titanium Dioxide), Ca and CaO(Calcium Oxide) were used as starting materials. Sm_2O_3 and Ca were added in excess in consideration of vaporization, and CaO was added three times of the remaining substances excluding Ca. Here, Ca is used as a reducing agent, and CaO acts as a dispersant that alleviates the harmful effect on the coercivity caused by grain growth at the reduction temperature. The starting materials were homogeneously mixed using a ball milling process. The resulting mixture was heat treated in argon atmosphere. Then, it was washed in 9 steps using a detergent that dissolves unreacted Ca and remaining CaO, followed by drying in vacuum. We studied the magnetic properties and microstructure of the produced particles via VSM, XRD, and SEM. The magnetic properties of Sm-Zr-Fe-Co-Ti alloy has been enhanced by the fine particles by reduction diffusion process.

Reference

- [1] P. Tozman, H. Sepehri-Amin, Y. K. Takahashi, S. Hirose, K. Hono, *Acta Materialia*, 153, 354 (2018).

Melt-spinning 법을 이용한 Nd-Fe-B분말의 전열처리에 따른 열간 변형 영구자석의 입자거동 및 자기특성 변화

황진성*, 안종빈, 최판규

(주)디아이씨 신소재연구소

최근 열간 변형 소결법을 통해 Nd-Fe-B 소결 자석의 제조 및 관련 연구가 진행되고 있다. Melt-spinning 법으로 제조한 분말은 Cu wheel 직경, 회전 속도, 노즐 크기 등 다양한 변수로부터 결정립 크기가 결정되고, 이에 따른 결정립 크기는 불균일하다. 이를 개선하여 보자력과 잔류자화 값을 향상시키기 위해 650, 700, 750°C에서 전열처리 하여 분말의 결정립 성장 거동을 알아보았다. Melt-spinning 법을 통해 제조된 분말을 여러 온도에서 전열처리 공정을 거친 후 진공 상태에서 열간 가압 소결을 진행했다. 이후 이방성 Nd-Fe-B 자석을 얻기 위해 약 70%의 변형률로 열간 변형 공정을 진행했다. 전열처리 공정을 거친 열간 변형 영구자석의 미세 구조를 주사 전자 현미경(SEM)을 이용하여 관찰했으며, 자성 특성을 분석하였다.

열간 가압과 열간 변형은 일정한 압력 하에서 열을 가하기 때문에 성장할 수 있는 방향이 제한이 된다. 하지만 전열처리 같은 경우에는 열을 가하는 것은 동일하지만, 분말 상태에서 결정립 성장에 억제가 없이 A-plane, C-plane으로 골고루 성장이 일어난다. 외부 압력이 없는 전열처리 시 온도가 증가할수록 A, C-plane으로 결정립은 성장한다. 그러나 전열처리 온도 650°C에서는 C-plane에 비해 A-plane 성장이 두드러지게 먼저 일어났다. 그 이후 열간 가압과 열간 변형으로 외부 압력에 의해 결정립 성장이 억제되어 aspect ratio는 거의 동일하지만, 먼저 성장이 일어났던 A-plane 때문에 결론적으로 보자력이 감소하는 결과를 보였다. A-plane 성장이 많이 일어남을 확인했고 이로 인해 결정립의 형태가 달라져 보자력에 악영향을 끼침으로 사료된다. 결과적으로 결정립 크기, 결정립 형태와 결정립 배열의 변화는 Nd-Fe-B 영구자석의 보자력에 중요한 영향을 미치는 요인임을 확인했다.

머신 러닝 기반 High Br 54SH Grade 영구자석 입계확산 최적 공정 도출 연구

임현석^{1*}, 이철희¹, 나현민¹, 배석¹, 김동환²

¹LG이노텍

²성림첨단산업

새로운 연구 방법론인 머신 러닝 개발 기법을 활용하여 적은 실험 횟수로 영구 자석에 중희토 입계 확산을 통해 잔류 자기밀도 감소 최소화 및 보자력 증가를 극대화하여 높은 자기 특성을 도출하였을 뿐만 아니라 중희토 사용량을 최소화하여 세계최고 Br 특성을 갖는 54SH Grade 영구자석을 개발하였다. 개발된 영구자석을 이용하여 시뮬레이션 및 시제품 제작 검증 통해 모터 및 액추에이터에 적용 높은 변환 효율 및 사이즈 축소 결과를 확인 하였다.

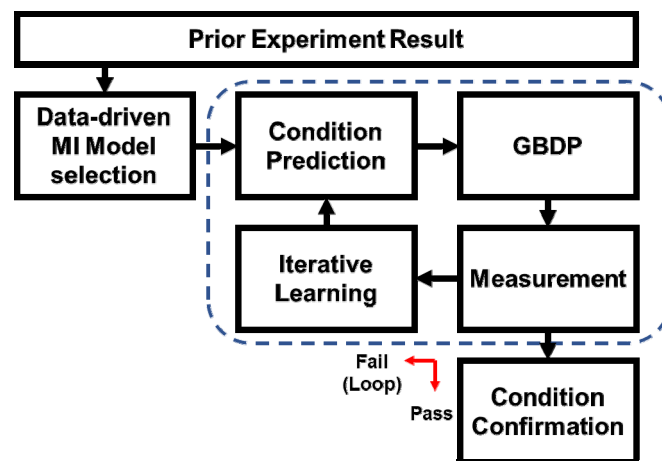


Fig. 1. 머신러닝을 이용한 영구자석 입계확산 공정 요약도

The effect of iron deficiency and additives of La-Co substituted Sr M-type hexaferrites on the Magnetic properties

Kanghyuk Lee^{*}, Junho Park, SungJoon Choi and Sang-Im Yoo[†]

Department of Material Science and Engineering, Research Institute of Advanced Materials (RIAM),
Seoul National University, Seoul, Korea

The Sr M-type hexaferrites ($\text{SrFe}_{12}\text{O}_{19}$) are one of the most widely used magnetic material due to their cost efficiency, strong uniaxial magnetic anisotropy along the c -axis, and excellent chemical stability. Recently, many studies have improved the intrinsic magnetic properties of M-type hexaferrites by substitution, such as saturation magnetization and crystalline anisotropy. Previous reports have been mainly focused on La^{3+} substitution for the Sr^{2+} site and Co^{2+} substitution for the Fe^{3+} sites of M-type hexaferrites. In addition, there is generally requires a non-stoichiometric of iron ratio between 10 and 12 on Ba M-type hexaferrites. While iron deficiency is known to be helpful for the grain growth and the structure formation of NiZn spinel ferrites. Particularly, $\text{SiO}_2\text{-CaO}$ is widely used by suppressing crystal growth and high sintering density through Liquid - Phase Sintering.

However, the effect of La-Co substitution and iron deficiency on magnetic properties of the Sr-La-Co M-type hexaferrites remains unexplored. In this study, therefore, we tried to investigate La-Co substituted Sr M-type hexaferrites $\text{Sr}_{1-x}\text{La}_x\text{Fe}_{12-x}\text{Co}_x\text{O}_{19}$, ($0 \leq x \leq 0.4$) and the effect of iron deficiency on the magnetic properties of $\text{Sr}_{1-x}\text{La}_x\text{Fe}_y\text{Co}_x\text{O}_{19-\delta}$ ($x = 0.15$, $10 \leq y \leq 12-x$) hexaferrites prepared by solid state reaction. The raw materials were ball-milled for 24 h with or without CaCO_3 and SiO_2 additive and calcined at 1280°C for 2 h in air. as-calcined powder was pressed into pellets and sintered at 1230°C for 1 h in air with SiO_2 and CaCO_3 additives. Samples were characterized by powder X-ray diffraction (XRD), vibrating sample magnetometer (VSM), and scanning electron microscope (SEM). In case of Iron deficient Sr-La-Co M-type hexaferrites, Powder XRD analyses revealed that M-type single phases were obtained with all Fe contents at sintering temperature. The saturation magnetization (M_s) of the Sr-La-Co M-type hexaferrite samples was around 72 emu/g. However, the coercivity (H_c) decreased with higher Fe content because the grain size was larger than the single domain size. The V_{cell} change due to substitution and iron deficiency seems to be inversely related to H_a obtained by magnetic hysteresis loops calculation. Detailed microstructures and magnetic properties will be presented for a discussion

This research was supported by Future Materials Discovery Program through the National Research Foundation of Korea (NRF) funded by the Ministry of Science and ICT (2016M3D1A1027835)

Keywords : Hexaferrite, magnetic property, iron deficiency, M-type hexaferrite

Synthesis and Characterization of SmFe₁₂-based compounds prepared by reaction-diffusion reaction

Kang-Hyuk Lee^{*}, SungJoon Cho and Sang-Im Yoo[†]

Department of Material Science and Engineering, Research Institute of Advanced Materials (RIAM),
Seoul National University, Seoul, Korea

The ThMn₁₂-type structure has attracted attention as permanent magnetic material due to the high anisotropy field, saturation magnetization (M_s), and Curie temperature (T_C). The Sm(Fe_{0.8}Co_{0.2})₁₁Ti (SFCT) materials have been intensively studied to synthesize high permanent magnets by controlling the doping element. In this study, we tried to investigate SFCT materials prepared by reaction-diffusion reaction. we prepared the SFCT precursor was prepared by a common co-precipitation method. The samarium nitrate hexahydrate, cobalt nitrate hexahydrate, titanium tetrachloride, and iron nitrate hexahydrate were dissolved in deionized water at 70 °C to form a homogeneous solution. The 3M KOH solution was slowly dropwise in the solution. Then the pH of the solution was adjusted slowly to pH 12 by adding dropwise ammonium hydroxide solution. The precipitates were collected by filtration. The precursors were heat-treated at 600 °C for 4h in H₂ gas. The hydrogen-reduced powders were mixed with calcium granules and pelletized. The pelletized samples were heated at 950 - 1050 °C for 1 h in Ar gas. Samples were characterized by using an x-ray diffractometer (XRD) with Cu-K α radiation source, a vibrating sample magnetometer (VSM), and scanning electron microscopy (SEM). The samples were obtained ThMn₁₂-type phase at 1050 °C for 1 h in Ar gas. The M_s and H_c values of Sm(Fe_{0.8}Co_{0.2})₁₁Ti samples were 95 emu/g and 1935 Oe. Detailed microstructures and magnetic properties will be presented for discussion.

This research was supported by Future Materials Discovery Program through the National Research Foundation of Korea (NRF) funded by the Ministry of Science and ICT (2016M3D1A1027835)

Keywords : SmFe₁₂-based compounds, ThMn₁₂-type, hard magnetic material

Enhancing magnetic and structural properties of chemically prepared Nd-Fe-B particles by reduction-diffusion method through optimization of heat treatments

Rambabu Kuchi^{1,2*}, Seunghyun Kim^{1,2,3}, Vitalii Galkin^{1,2,3}, Dongsoo Kim^{1,2†}

¹Korea Institute of Geoscience and Mineral Resources, Daejeon, South Korea

²Korea Institute of Materials Science, Changwon, South Korea

³Department of Materials Science and Engineering, Graduate School of Energy Science and Technology, Chungnam National University, Daejeon, South Korea

E Mail: rambabu.kuchi@kigam.re.kr, dskim69@kigam.re.kr

NdFeB magnets are widely used in advanced electric vehicles, electric motors for power generators, wind turbine generators, energy conversion systems and many other novel applications. However, the high energy density (BH_{max}) magnets are needed to utilise them. For this purpose, the NdFeB magnetic particles should prepare with higher magnetic properties which could mainly depends on the Nd₂Fe₁₄B phase purity, crystallinity and microstructure. To wards this direction, we report the cost effective and a facile chemical synthesis including spray drying and reduction-diffusion (RD) process with some modifications [1, 2]. Since the RD process has considerably affected the structural and magnetic properties of Nd-Fe-B particles so the optimization of heat treatments for RD is in high demand. Different heating rates (5, 10, 20, and 30°C/min) to reach annealing temperature (1000°C) of RD and keeping times for the RD process were used to prepare Nd-Fe-B particles. Among them, the sample prepared at 20°C/min heating rate (HR) with a 5 h RD time exhibited superior magnetic properties including the remanence (M_R) of 125 emu/g, saturation magnetization (M_S) of 140 emu/g, and (BH)_{max} of 10.66 MGOe. This was ascribed to the narrow particle size distribution, and phase purity with high crystallinity at optimized HR and RD time. Because the HR was controlling the particle nucleation and growth process and keeping time could ensure the completion of the RD process. This present modified RD process will also be useful to prepare other potential hard-magnetic particles.

Key words: NdFeB magnetic particles, heating rate, modified reduction diffusion, phase purity, shape uniformity

References

- [1] C.-Q. Chen, D. Kim, C. Choi, Influence of Ca amount on the synthesis of Nd₂Fe₁₄B particles in reduction –diffusion process, J. Magn. Magn. Mater. 355 (2014) 180–183.
- [3] Y. Wang, J. Ahn, D. Kim, W.J. Ren, W. Liu, Z.D. Zhang, C.J. Choi, Effect of washing process on the magnetic properties of Nd-Fe-B nanoparticles prepared by reduction-diffusion method, J. Magn. Magn. Mater. 439 (2017) 91–94.

Chemical synthesis of NdFeB particles with enhanced magnetic properties through planetary ball milling process of oxide powders

Seunghyun Kim^{1,2,3*}, Rambabu Kuchi^{1,2}, Vitalli Galkin^{1,2,4}, Dongsoo Kim^{1,2†}

¹Korea Institute of Geoscience and Mineral Resources, Daejeon, South Korea

²Korea Institute of Materials Science, Changwon, South Korea

³Department of Materials Science and Engineering, Chungnam National University, Daejeon, South Korea

⁴Graduate School of Energy Science and Technology, Chungnam National University, Daejeon, South Korea

E Mail : ks6615@kigam.re.kr, dskim69@kigam.re.kr

NdFeB based high energy density (BH_{max}) magnets are of enormous significance in various engineering applications include electric equipments, motors, generators, hard disc drives and electric vehicles. It has the high BH_{max} than other rare earth transition metal based magnets. The BH_{max} was strongly depends on the magnetic properties of NdFeB magnetic particles which are to be used to make the NdFeB magnets. The magnetic properties of NdFeB powder are determined from its phase purity, crystallinity and structure. These can be controlled in the powder synthesis process. In this work, we used spray drying and reduction diffusion methods for the production of Nd-Fe-B powders. In order to obtain excellent magnetic properties to the final powders, it is necessary to optimize the crystallinity and shape of the powder particles. Since the final NdFeB powders are obtained from their oxides so that the microstructure and phase purity of NdFeB oxides can effect them. The NdFeB oxides are formed from the heat treatment of spray dried powders and their properties has been controlled using planetary ball milling (PBM). The PBM of oxides were performed with different time intervals (1, 2 and 4 hrs) at 200 rpm in dry condition. The 1 hr PBM powders resulted fine particles and uniform shape (spherical shape) compared to 2 and 4hrs. The final particles prepared using PBM (1 h) showed enhanced magnetic properties include the coercivity of 3900 Oe, and remanent magnetization of 102 emu/g. It shows 21.9% higher coercivity compared to unmilled powder

Key words: NdFeB magnetic particles, planetary ball milling (PBM), shape, magnetic properties

Intrinsic Hard Magnetism and Thermal Stability of ThMn₁₂-Type Permanent Magnet: Density Functional Theory and Monte Carlo Simulation

Tumentsereg Ochirkhuyag^{1*}, Soon Cheol Hong^{2*} and Dorj Odkhuu^{1†}

¹Department of Physics, Incheon National University, Incheon 22012, South Korea

²Department of Physics, University of Ulsan, Ulsan, South Korea

E-mail: *schong@ulsan.ac.kr, †odkhuu@inu.ac.kr

Herein we propose a possible solution to realize an otherwise unstable ThMn₁₂-type SmFe₁₂ permanent magnet through systematic full-potential density functional theory and Monte Carlo simulations on ternary Sm–Fe–M compounds (M is a 3d or 3p metal substitute atom). Among the 11 metal elements (Ti–Ga and Al), only the simple metal Al, rather than the traditional transition metal substitute atoms, is predicted to be optimal; not only stabilizes the ThMn₁₂ structure with improved single-domain grain size but also promotes superior intrinsic magnetic properties at room temperature, including the uniaxial magnetocrystalline anisotropy (MA) up to 6.7 MJ·m⁻³, anisotropy field up to 16.4 T, and hardness parameter up to 3, to the state-of-the-art permanent magnet Nd₂Fe₁₄B. Numerical results of MA and MA-driven hard magnetic properties are described by the strong spin-orbit coupling and orbital angular momentum of the Sm 4*f*-electron orbitals. The other simple metal Ga, which is isoelectronic to Al, makes the present argument rather general, stabilizing the ThMn₁₂ phase while still preserving MA uniaxial.

Keywords: Permanent magnets, First-principle calculations, Monte-Carlo simulations, Uniaxial magnetic anisotropy

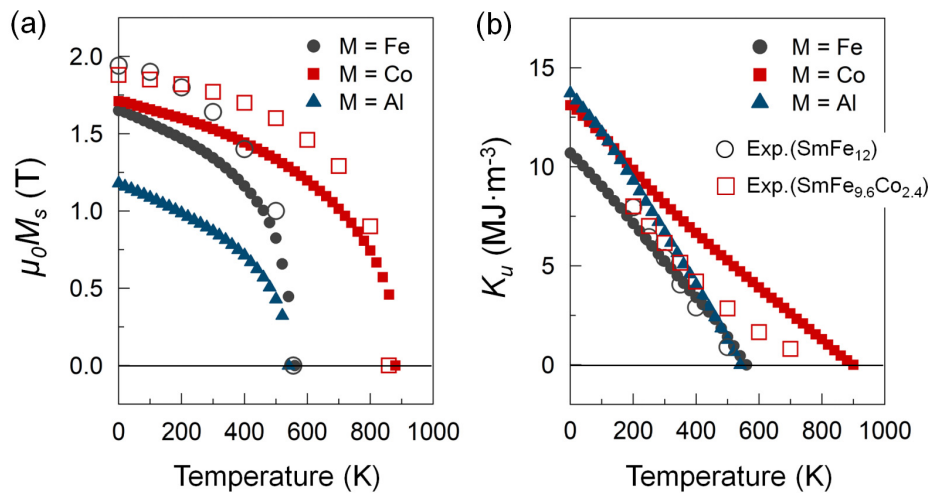


Fig 1. (a) Saturation magnetization $\mu_0 M_s$, and (b) uniaxial magnetocrystalline anisotropy K_u versus temperature of SmFe₁₀M₂ for M = Fe, Co, and Al. The open symbols denote the experimental data for SmFe₁₂ and SmFe_{9.6}Co_{2.4}, taken from Ref. [1].

This study was supported by the National Research Foundation of Korea (NRF) grant, funded by the Ministry of Science and ICT (2016M3D1A1027831 and 2020R1F1A1067589).

Reference

- [1] Y. Hirayama, Y.K. Takahashi, S. Hirosawa, and K. Hono, Intrinsic hard magnetic properties of Sm (Fe_{1-x}Co_x)₁₂ compound with the ThMn₁₂ structure, *Scr. Mater.* **138**, 62 (2017)

Micromagnetic Studies on the Enhancement of the Coercivity of B-doped $\text{Sm}(\text{Fe}_{0.8}\text{Co}_{0.2})_{12}$ Thin Film by Forming Amorphous Grain Boundary

Ganghwi Kim^{1*}, Dae-Han Jung¹, Suyeong Jeong¹, Namkyu Kim² and Ki-Suk Lee¹

¹School of Materials Science and Engineering, Ulsan National Institute of Science and Technology, Ulsan, Republic of Korea

²Powder Materials Division, Korea Institute of Materials Science, Changwon, Republic of Korea

SmFe_{12} -based compounds have been considered as a good candidate for a future permanent magnet without the critical elements such as Nd or Dy [1]. One of the most challenging issues to achieve a high-performance permanent magnet is that forming an appropriate grain boundary phase is suppressed in SmFe_{12} -based magnets [2,3]. Therefore, grain boundary effects to enhance magnetic properties such as remanence and coercivity rarely occur, and practical magnetic properties are assessed as relatively low. To overcome this, adding impurities can reinforce the performance of a permanent magnet by inducing the formation of the grain boundary phase. For example, Cu – Ga grain boundary infiltration [2] and co-sputtering of B [3] can cause the grain boundary phase formation. Especially, doping of B induces amorphous ferromagnetic grain boundary creation, which results in a significant improvement of coercivity and remanence [3]. Here, we report micromagnetic numerical simulation results about the grain boundary effect on the B-doped $\text{Sm}(\text{Fe}_{0.8}\text{Co}_{0.2})_{12}$ thin film. We employed a periodic boundary condition (PBC)-applied thin film of thickness 100 nm and located $\text{Sm}(\text{Fe}_{0.8}\text{Co}_{0.2})_{12}$ grains enveloped by the soft ferromagnetic grain boundary phase with relatively low saturation magnetization. Coercivity and remanence are calculated by hysteresis loops based on the steepest descent method [4]. We show that controlling the magnetic properties of the grain boundary phase or thickness of the grain boundary can influence coercivity and remanence. These boundary features adjust the exchange interaction among grain boundaries involved in domain wall pinning and domain nucleation. Our results could be used as a guideline to design the optimal grain boundary phase for high-performance permanent magnets.

References

- [1] Y. Hirayama, Y.K. Takahashi, S. Hirosawa, K. Hono, *Scripta Mater.*, **138** (2017), pp. 62–65
- [2] D. Ogawa, X.D. Xu, Y.K. Takahashi, T. Ohkubo, S. Hirosawa, K. Hono, *Scripta Mater.* **164** (2019) 140–144.
- [3] H. Sepehri-Amin, Y. Tamazawa, M. Kambayashi, G. Saito, Y.K. Takahashi, D. Ogawa, T. Ohkubo, S. Hirosawa, M. Doi, T. Shima, K. Hono, *Acta Materialia* **194** (2020) 337–342.
- [4] L. Exl, S. Bance, F. Reichel, T. Schrefl, H. P. Stimming, N. J. Mauser, *J. Appl. Phys.* **115**, 17D118 (2014)

First principles studies of new type of rare-earth free permanent magnet: $\text{Co}_3\text{Mn}_2\text{Al}$

Dorjsuren Tuvshin^{1*}, Tumentsereg Ochirkhuyag¹, Soon Cheol Hong^{2†} and Dorj Odkhuu^{1†}

¹Department of Physics, Incheon National University, Incheon 22012, South Korea

²Department of Physics, University of Ulsan, Ulsan 44610, South Korea

*schong@ulsan.ac.kr

†odkhuu@inu.ac.kr

Due to today's huge demand of many applications including motors of an electric vehicle, high-speed bullet trains, satellites and sustainability difficulty of the rare-earth (RE) elements, there have been intensive research interests recently centered at rare-earth free permanent magnetic materials and various methods to improve their uniaxial magnetic anisotropy (K_u) to at least half of the RE included magnets. MgZn_2 -type $\text{Co}_3\text{Mn}_2\text{X}$ alloys have recently received lots of attention due to their large saturation magnetization ($\mu_0 M_s$) of 1.7 T, Curie temperature of 820 K and K_u of 1.46 MJ/m^3 . In this study, we conduct systematic first-principles electronic structure calculations to further enhance the structural stability, $\mu_0 M_s$, and K_u by substitutional doping of other $3d$ transition metal elements on both Co and Mn-site. Furthermore, we reveal that K_u can even reach up to $2.11 \text{ MJ}\cdot\text{m}^{-3}$ without huge loss on $\mu_0 M_s$ and stability. These results demonstrate the feasibility of possible enhancements on the magnetic anisotropy and energy product of already potent magnet, making it best candidate of plugging the gap between RE and RE-free permanent magnetic materials.

This work is supported by Future Materials Discovery Program through the National Research Foundation of Korea (NRF) funded by the Ministry of Science and ICT (2016M3D1A1027831) and by the Korea Institute of Energy Technology Evaluation and Planning (KETEP) grant funded by the Korean government (MOTIE) (20192010106850, development of magnetic materials for IE4 class motor).

Electromagnetic wave absorption properties of M-type hexaferrite-perovskite manganese composites and bilayers

Jae-Hee Heo, Young-Min Kang*

Department of Materials Science and Engineering, Korea National University of Transportation,
Chungju, 27469, Republic of Korea

*Corresponding author email: ymkang@ut.ac.kr

We report on the electromagnetic (EM) wave absorption properties of $\text{SrFe}_{9.5}\text{Co}_{1.25}\text{Ti}_{1.25}\text{O}_{19}$ (SFCTO)- $\text{La}_{0.7}\text{Sr}_{0.3}\text{MnO}_3$ (LSMO) composites and bilayers. The powder samples of M-type Sr-hexaferrite, $\text{SrFe}_{12-2x}\text{Co}_x\text{Ti}_x\text{O}_{19}$ ($x = 1.25$) were synthesized by the solid-state reaction processes, and those of $\text{La}_{0.7}\text{Sr}_{0.3}\text{MnO}_3$ were prepared by the sol-gel method and calcination at 1200°C , respectively. XRD analysis revealed that the SFCTO and LSMO are single M-type hexaferrite and perovskite phases, respectively. The SFCTO is an insulating magnetic oxide and LSMO is a conductive magnetic oxide. The respective magnetic powders of SFCTO and LSMO were mixed with epoxy binder at a 9:1 wt% ratio, pressed into toroidal-shaped (inner and outer diameters of 3.04 and 7.00 mm, respectively) green compacts, and finally cured at 180°C for 1 h in air. The complex permittivity (ϵ' , ϵ'') and permeability (μ' , μ'') spectra (100 MHz–18 GHz) were measured on the toroidal SFCTO and LSMO samples, respectively, using a vector network analyzer (E5063A, Keysight) with an airline kit (85051BR03) and N1500A software (Keysight). The electromagnetic wave shielding effectiveness (SE) and reflection loss (RL) of the toroidal samples were also obtained from S-parameter measurements. The SE (S12) was measured using the two-port airline method and the RL (S11) was measured using a one-port Cu threaded hole socket.

Based on the measured ϵ' , ϵ'' and μ' , μ'' spectra of the two samples, the EM absorption properties were calculated and analyzed for the SFCTO (1-x) – LSMO(x) composites. The better EM absorption performances were obtained at the composites with $x = 0.4 - 0.6$, than single SFCTO ($x=0$) or LSMO ($x=1$). The SE and RL of SFCTO-LSMO bilayers were also measured. The RL spectra showed significantly different results depending on the stacking order of the two layers as shown in the below figure. The reasons for variation of the EM absorption properties in the SFCTO-LSMO composites and the bilayers will be discussed.

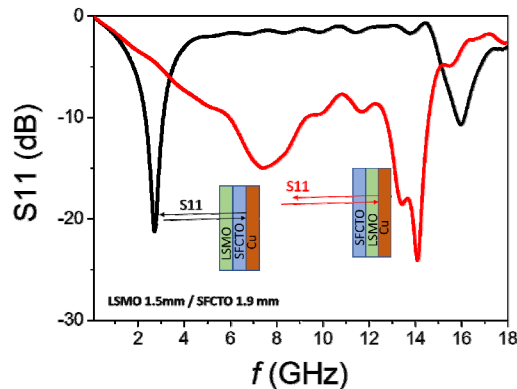


Fig. S11 (RL) spectra of the LSMO/SFCTO and SFCTO/LSMO bilayers measured using VNA with an airline kit and one-port Cu-end socket.

Electromagnetic wave absorption properties of multistacked hexaferrite-epoxy composites

Jae-Uk Kim, Young-Min Kang*

Department of Materials Science and Engineering, Korea National University of Transportation,
Chungju, 27469, Republic of Korea

*Corresponding author email: ymkang@ut.ac.kr

We report on electromagnetic wave (EM) absorption properties of multistacked hexaferrite-epoxy composites. Co-Ti substituted M-type hexaferrite powders, $\text{SrFe}_{12-2x}\text{Co}_x\text{Ti}_x\text{O}_{19}$ ($x=1.1, 1.2, 1.3$) were prepared by conventional solid-state reaction method. Each composition of powder was calcined at 1300°C for 2 hours in air. The calcined powders were ground into fine powders, mixed with 10 wt% of epoxy binder, pressed to form toroidal-shaped (inner and outer diameters of 3.04 and 7.00 mm, respectively) green compacts, and finally cured at 180°C in air for 20 min. The real and imaginary parts of permittivities (ϵ' , ϵ'') and permeabilities (μ' , μ'') were measured on the toroidal shaped composites using a vector network analyzer (VNA) with an airline kit in the frequency range from 0.1 to 18 GHz. RL spectra for the composites were calculated based on transmission line theory and measured ϵ' , ϵ'' , μ' , μ'' data. Also, the RL spectra were measured from S-parameter method using the VNA with airline kit and one-port Cu threaded hole socket.

The minimum RL value (RL_{\min}) < -20 dB could be obtained for the series of composites samples at the optimal thickness. The frequencies of RL_{\min} were 14 GHz, 10 GHz, and 6 GHz for $x = 1.1, 1.2$, and 1.3 samples, respectively. The RL spectra were also measured on the stacked three samples (A, B, C) with varying stacking orders as ABC, ACB, BAC, BCA, CAB, CBA. The RL spectra were slightly varied depending on the stacking order. However, it was very far from the sum of RL spectra in each sample. The measured RL spectra of the stacked samples were well fitted with calculated RL spectra at total thickness of three samples. Here, the RL calculation was based on volume-averaged ϵ' , ϵ'' , μ' , and μ'' values for each sample.

Electromagnetic microwave absorption properties of Mn-Ti substituted M-type Ba hexaferrite-epoxy composites

Su-Mi Lee, Min-Gu Kang, Young-Min Kang*

Department of Materials Science and Engineering, Korea National University of Transportation,
Chungju, 27469, Republic of Korea

*Corresponding author email: ymkang@ut.ac.kr

BaFe_{12-x}(Mn_{0.5}Ti_{0.5})_xO₁₉ (x=0, 3.5, 4.0, 4.5, 5.0, 5.5) hexaferrites samples were synthesized by solid state reaction at 1350 °C in air. XRD analysis revealed that single M-type hexaferrite phase was obtained for the samples with $0 \leq x \leq 4.5$ and insignificant amount of second phase formed for x = 5.0 and 5.5 samples. The calcined powders were ground to obtain fine powders and mixed with 10wt% of epoxy binder. The mixtures were pressed into disk and toroidal shaped green compacts, respectively, and cured at 180 °C for 1 h in air. *M-H* curves were measured using a *B-H* loop tracer on the disk samples. As the Mn-Ti substitution x increases, the saturation magnetization value (*M_s*) significantly decreased. The real and imaginary parts of permittivities (ϵ' , ϵ'') and permeabilities (μ' , μ'') were measured on the toroidal samples using a vector network analyzer (E5063A, Keysight) with an airline kit in the frequency range from 0.1 to 18 GHz. The μ'' spectra for the series of samples are presented in Fig. 1(a). Reflection losses (RLs) indicating the electromagnetic wave absorption performance were analyzed based on the ϵ' , ϵ'' , μ' , and μ'' spectra. The EM absorption area could be figured out in the RL maps plotted as a function of the sample thickness (*d*) and frequency (*f*) for the composite samples. The RL spectra at the optimal thickness are plotted at Fig.1 (b). The RL peak frequency gradually shifts to low frequency with increasing x. This can be attributed to the shift of μ'' peak frequency (Fig. 1(a)), which is caused by the decrease of magnetocrystalline anisotropy with increasing x. The decrease of RL peak intensity with increase of x is also due to decrease of μ'' peak height. It is demonstrated that the magnetic loss associated with μ'' is the dominating mechanism for EM absorption in GHz range and the increase of μ'' is very important for enhancing the EM performances in the hexaferrite based absorbers.

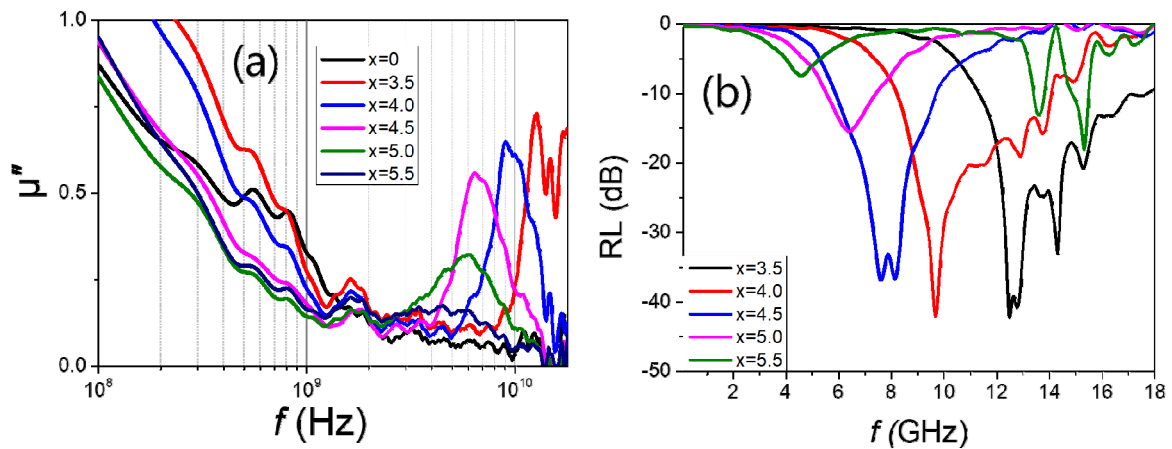


Fig. 1 Reflection loss (RL) spectra of BaFe_{12-x}(Mn_{0.5}Ti_{0.5})_xO₁₉ (x=0, 3.5, 4.0, 4.5, 5.0, 5.5)-epoxy (10wt%) composites

Coercive field variation of Co/Pt multilayer depending on Co thickness and annealing temperature

Seungha Yoon^{*}

Korea Institute of Industrial Technology, 6, Chemdangwagi-ro 208 gil, Buk-gu, Gwangju, South Korea

The magnetic films of perpendicular magnetic anisotropy have been widely used to current spintronic devices and the study of future applications. The Co/Pt multilayer is well known as a good perpendicular material for the devices using tunneling magnetoresistance (TMR), spin transfer torque(STT), and magneto-optic, when the Co and the Pt thickness are precisely controlled in a few nm scale.

In this study, we prepared [Co(*t* nm)/Pt(1.0 nm)]₃ multilayers to find the condition to have a good thermal stability. During the various process of the fabrication, the thermal stability is quite important to sustain the device working situation. The magnetic properties of the multilayers were characterized, when the Co thickness widely varied from 0.3 nm to 2.0 nm. The details of the coercive field depending on the Co thickness and the annealing temperature will be discussed.

Metal FDM 공정으로 제작된 등방성 미세조직의 17-4PH 스테인리스 강의 기계적 및 자성 특성 분석

Kwangsue Choi^{1,2*}, Seonghoon Yi¹, Hyo Yun Jung^{2†}

¹Department of Materials Science and Metallurgical Engineering, Kyungpook National University,
Daegu, Republic of Korea

²Korea Institute of Industrial Technology, Ulsan, Republic of Korea

Metal fusion deposition modeling (metal FDM) 공정은 금속 분말과 바인더가 포함된 필라멘트를 적층하고 소결하여 형상을 제작하는 금속 적층 제조 공정이다. 형상 제작의 자유도가 높아 다품종 산업 부품 제작에 경제적으로 장점이 있고 등방성 미세조직을 가져 이방성 미세조직을 가지는 powder bed fusion (PBF), direct energy deposition (DED)와 같은 금속 적층 공정 보다 등방성 특성의 자성 부품 제작에 적합하다. Metal FDM 공정으로 제작한 17-4PH는 소결 후 상대 밀도가 94 %로 나타났으며 인장 특성으로는 항복 강도 935.6 MPa, 인장 강도 1031.9 MPa 연신율 2.2 %이 측정되었다. 제조된 시험편의 연자성 특성으로는 VSM을 통하여 포화 자화를 측정하였고 BH-analyzer를 통하여 주파수에 따른 보자력, 투자율 그리고 철손 특성을 측정 하였다. 이러한 metal FDM 공정으로 제작된 17-4PH재료의 기계적 및 자기적 특성을 분석 함으로써 다양한 자성 특성의 산업 부품 제작 기초 데이터로 활용 할 수 있을 것으로 사료된다.

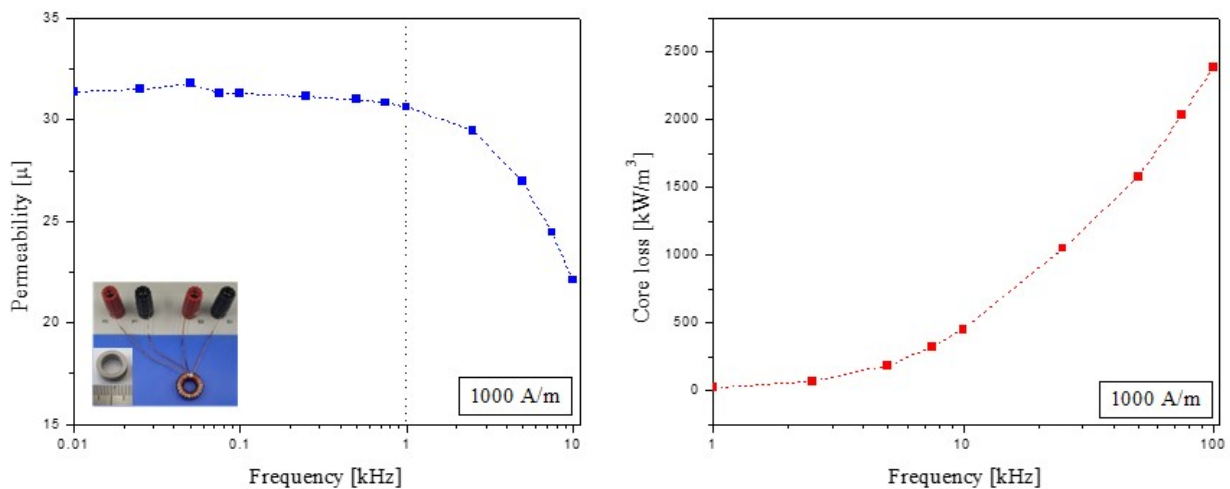


Figure. Magnetic properties of 17-4PH toroidal core which was manufactured by metal FDM

Comparison of structural, microstructure, and magnetic properties of nickel nanowires according to the shape of the magnetic field

Min Ji Shin^{1*}, Su Jeong Park², Akshay Kumar¹, Kavita Kumari³,
Seok Hwan Huh^{4*} and Bon Heun Koo^{2†}

¹School of Department of Materials Convergence and System Engineering, Changwon National University,
Changwon, Gyeongnam, 641-773, Republic of Korea

²School of Materials Science and Engineering, Changwon National University, Changwon,
Gyeongnam, 641-773, Republic of Korea

³Industrial Technology Research Institute, Changwon National University,
Changwon, Gyeongnam, 51140, Republic of Korea

⁴Department of Mechatronics Conversion Engineering, Changwon National University, Changwon,
Gyung-sangnam-do 51140, Republic of Korea

Recently, as the need for one-dimensional nanomaterials has rapidly increased, research on nanotechnology is actively conducted. Nanomaterials are generally not limited to the field of material engineering and are applied to various fields. Nanowires are currently regarded as one of the most efficient fields in nanotechnology. Although the diameter of the nanowire is very small, a few nanometers, it maintains a safe shape as a one-dimensional material. It overcomes the limitations of existing technologies by manufacturing materials with unique properties that were previously impossible. In this study, nickel, a soft magnetic material, was used to increase the magnetic flux density inside the material. This experiment was performed by a solution synthesis method and used $\text{NiCl}_2 \cdot 6\text{H}_2\text{O}$, NaOH , $\text{N}_2\text{H}_4 \cdot \text{H}_2\text{O}$, etc. The produced nickel nanowires were washed several times with ethanol and DI water and dried in a vacuum oven. The collected samples were analyzed using XRD, SEM, and PPMS equipment. Through the characteristic evaluation, it was possible to compare the samples collected when different types of magnetic fields were applied.

Keywords : Nickel, Nanowires, Shape of Magnetic Field, Characteristic Evaluation

Excellent absorption properties of Zn-substituted SrW-type hexaferrites in Ka-band for 5G application

Sungjoon Choi^{1*}, Seung-Young Park² and Sang-Im Yoo¹

¹Department of Materials Science and Engineering, and Research Institute of Advanced Materials,
Seoul National University, Seoul 151-744, Korea

²Spin Engineering Physics Team, Division of Scientific Instrumentation,
Korea Basic Science Institute, Daejeon 34133, Korea

The microwave absorption properties of Zn-substituted SrW-type hexaferrites ($\text{SrZn}_x\text{Fe}_{2-x}\text{Fe}_{16}\text{O}_{27}$; $\text{SrZn}_x\text{Fe}_{2-x}\text{W}$, where $x = 0.0, 0.25, 0.5, 1.0$, and 2.0) in Ka-band (26.5–40 GHz) were studied. The Zn^{2+} ion substitution for the Fe^{2+} ion is well known to increase both real and imaginary parts of permeability ($\mu_r = \mu' - j\mu''$) and permittivity ($\epsilon_r = \epsilon' - j\epsilon''$) [1-2]. The $\text{SrZn}_x\text{Fe}_{2-x}\text{W}$ ($x=0.0, 0.25, 0.5$, and 1.0) samples were annealed at the temperature region of 1000–1350 °C for 2 h in the PO_2 of 10^{-3} atm while the SrZn_2W was annealed in air to obtain single-phase.

In order to measure microwave absorption properties, hexaferrite-epoxy resin composites were fabricated with the filler volume fractions (V_f) of 30, 50, 70, and 90%. The real and imaginary parts of permittivity and permeability of $\text{SrZn}_x\text{Fe}_{2-x}\text{W}$ were measured by using a vector network analyzer (VNA, Agilent PNA N5525A) with a waveguide, and the reflection losses were calculated based on the transmission line theory [3]. The minimum reflection loss (RL_{\min}) of -68.4 dB at 28 GHz with the bandwidths of 2.48 GHz (26.50–28.98 GHz) below -20 dB, was achievable from a 0.64 mm-thick $\text{SrFe}_{1.75}\text{Zn}_{0.25}\text{W}$ ($x = 0.25$) composite, indicating that partially Zn-substituted SrW-type hexaferrites are strong candidates as microwave absorber appropriate for 5G applications. Detailed results will be presented for discussion.

References

- [1] J.H. You, S.I. Yoo, Improved magnetic properties of Zn-substituted strontium W-type hexaferrites, *Journal of Alloys and Compounds*, 763 (2018) 459-465.
- [2] R.S. Meena, S. Bhattacharya, R. Chatterjee, Complex permittivity, permeability and microwave absorbing properties of $(\text{Mn}_{2-x}\text{Zn}_x)\text{U}$ -type hexaferrite, *Journal of Magnetism and Magnetic Materials*, 322 (2010) 2908-2914.
- [3] E. Ni, AN UNCERTAINTY ANALYSIS FOR THE MEASUREMENT OF INTRINSIC-PROPERTIES OF MATERIALS BY THE COMBINED TRANSMISSION REFLECTION METHOD, *IEEE Transactions on Instrumentation and Measurement*, 41 (1992) 495-499.

Curvature-Induced symmetry breaking of Néel Caps in asymmetric ferromagnetic disk

Myeonghwan Kang^{1*}, Hee-Sung Han^{1,2}, Sooseok Lee¹, Young-Sang Yu², Soong-Geun Je³,
Hye-Jin Ok¹, Weilun Chao², Mi-Young Im² and Ki-Suk Lee^{1†}

¹Ulsan National Institute of Science and Technology, Korea

²Advanced Light Source, Lawrence Berkeley National Laboratory, USA

³Department of Physics, Chonnam National University, Korea

⁴Center for X X-ray Optics, Lawrence Berkeley National Laboratory, USA

In a nano-scaled ferromagnetic disk, a flux-closure magnetization configuration appears to minimize the magnetostatic energy such as demagnetization and exchange energies [1]. To reduce the total energy, the out-of-plane magnetization is allowed at the center of disk and it is called vortex core. This magnetic configuration has been studied in a two-dimensional (2D) structure. However, as increasing the thickness of the sample, to reduce the demagnetization energy along the thickness of the sample, the flux-closure domain structure has a complex 3D structure. In an asymmetric rectangular disk, the magnetization configuration in the circularity, polarity, and vortex core position. For example, asymmetric Bloch wall (ABW) with Néel cap is positioned between two shifted vortex cores. A rotating sense of an ABW, clockwise (CW) and counterclockwise (CCW) is an additional degree of freedom [2]: they are exactly same energy states. In this work, we report on the symmetry breaking of Néel caps according to curvature disk of permalloy disk by utilizing magnetic transmission soft X-ray microscopy (MTXM) and micromagnetic simulation. As increasing the curvature of permalloy disk, demagnetizing and exchange energy of Néel cap of clockwise (CW) direction is larger than that of Néel cap of counterclockwise (CCW). As decreasing the curvature of permalloy disk, the CW Néel cap is more stable than CCW Néel cap.

References

- [1] A. Hubert and R. Schäfer. Magnetic Domains. (Springer, Berlin, 1999)
- [2] F. Cheynis et al., Phys. Rev. Lett. **102**, 107201 (2009)
- [3] A. Masseboeuf et al., Phys. Rev. Lett. **104**, 127204 (2010)

Silane 첨가량에 따른 Fe-Ni 코어 효율 향상에 관한 연구

김예래*, 안지훈, 이민영, 이보화
 한국외국어대학교 물리학과, 산화물 연구센터
 bwlee@hufs.ac.kr

사용하는 전자기기의 수와 사용 범위가 늘어나면서, 내부 부품들 또한 고성능과 안정성을 갖춘 제품으로의 연구가 활발하게 진행되고 있다. 본 연구에서는 permalloy 계열의 Fe-Ni에 silane을 코팅하여 인덕턴스 및 투자율의 효율 향상을 목표로 하였으며, silane 첨가량에 따라 최적의 성능을 가질 수 있는 조건을 찾으려 하였다. Silane은 유기 실리콘 화합물(C-Si)을 포함하여 Si에 4개의 치환기가 있는 화합물을 의미한다. 이러한 silane의 한 종류인 APTES(3-Aminopropyl triethoxyethylane)는 아미노기를 가지며, 금속 산화물 표면과 유기 성분 사이의 계면에 -Si-O-Si-결합을 형성하는 실란화 과정을 일으킨다. 커플링제로 많이 사용되며 재료의 기계적 강도가 향상되며 표면을 정돈하는 효과가 있어, 기존 시료의 입자 표면 정돈의 효과로 투자율 향상에 도움을 줄 것으로 예상하였다.

Fe-Ni 인덕터 코어에 silane(APTES)의 코팅이 미치는 영향을 확인하였다. APTES 코팅은 mechanical stirrer를 사용하여 진행하였고, 코팅에 첨가되는 APTES양에 따른 인덕터 코어의 인덕턴스, 투자율, 코어손실 값을 impedance analyzer와 B-H analyzer를 사용하여 비교 및 분석하였다. 코팅되지 않은 Fe-Ni 인덕터 코어에 비해, 12g의 APTES가 코팅된 Fe-Ni 인덕터 코어는 1.5배 가량 높은 투자율을 가졌으며, 100MHz까지 안정적인 인덕턴스 값을 가졌다. 추가적으로 인덕터 성능을 결정하는 요소인 코어 손실 값의 폭은 상승하지 않았다. 이는 아미노기를 포함한 APTES의 입자 표면이 정돈되는 silane 코팅의 효과로, silane은 인덕터 코어의 투자율을 향상시켜 고효율 인덕터용 소재로 사용이 가능 할 것이다.

BiFeO₃의 전자기파 차폐가능한 주파수 이동에 관한 특성 연구

정우현^{1*}, 이민영¹, 김상우¹, 유성초², 이보화¹

¹한국의국어대학교 물리학과, 산화물 연구센터

²울산과학기술원 물리학과

일상생활에서 전자기기의 사용빈도가 많아지면서, 전자기기에서 발생하는 전자파 간섭으로 인한 오작동 및 인체유해의 문제가 대두되고 있다. 최근 차폐 성능이 우수한 물질들이 연구되고 있지만 다양한 장치, 용도에 따라 요구되는 주파수가 상이하다. 다양한 주파수 대역에서 발생하는 전자파를 선택적으로 차폐하기 위해, multiferroic BiFeO₃에 La의 도핑량에 따른 차폐가능한 주파수 대역을 연구하였다. Polycrystalline Bi_{1-x}La_xFeO₃ (BLFO) 샘플($x = 0 - 0.25$)은 Bi₂O₃, La₂O₃ 그리고 Fe₂O₃ 고순도 산화물을 전고체로 하여 고체반응법으로 합성하였다. 화학량론으로 혼합한 분말을 디스크 펠렛 형태로 제작하여 900 °C에서 12시간 동안 소결하였다. BLFO의 XRD 측정을 통해 rhombohedral에서 orthorhombic으로의 상전이를 확인하였고, VSM 측정을 통해 자기적 특성을 확인하였다. 마이크로파 흡수 특성을 변화시키기 위해 Bi에 La를 도핑한 결과로, La의 도핑량이 증가함에 따라 반사손실의 효과적인 공진주파수의 범위(≥ -10 dB)는 16 GHz에서 7 GHz까지로 조절 가능하였다. Reflection loss의 값은 16 GHz에서 약 -36 dB, 7 GHz에서 약 -34 dB으로 특정 주파수대역에서 99 % 이상의 차폐효과를 나타냈다.

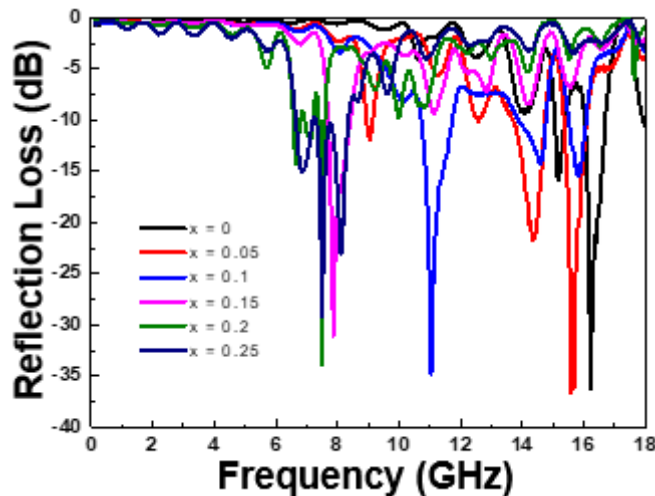


Fig 1. Reflection loss of Bi_{1-x}La_xFeO₃($x = 0 - 0.25$)

Enhanced microwave absorption properties of La-doping $\text{Ba}_3\text{Co}_2\text{Fe}_{24}\text{O}_{41}$ hexaferrite in the frequency range of 2-18 GHz

W.H. Jeong^{1*}, N. Tran^{2,3} and B.W. Lee¹

¹Department of Physics and Oxide Research Center, Hankuk University of Foreign Studies, Yongin 17035, Korea

²Institute of Research and Development, Duy Tan University, Da Nang, 550000, Viet Nam

³Faculty of Natural Sciences, Duy Tan University, Da Nang, 550000, Viet Nam

*E-mail: bwlee@hufs.ac.kr

We successfully prepared La doping $\text{Ba}_3\text{Co}_2\text{Fe}_{24}\text{O}_{41}$ ($\text{Ba}_{3-x}\text{La}_x\text{Co}_2\text{Fe}_{24}\text{O}_{41}$; $x = 0-0.5$) by conventional solid-state reaction method. La-doping significantly affected morphological, structural, and magnetic properties. Particle size and shape are changed by doping. The lattice parameters, a and c , decreased by doping, which could be attributed to the difference in ionic diameters of substitution element (La^{3+}) and host element (Ba^{2+}). The increase of saturation magnetization and coercivity could be originated from the enhancement of $\text{Fe}^{3+}\text{--O--Fe}^{2+}$ superexchange interaction and the increase of magnetocrystalline anisotropy, respectively. The La-doping also improved the microwave absorption performance in terms of reflection loss (RL) and effective absorption bandwidth. Significant improvement could be found in $x = 0.3$ and 0.5 samples. The minimum RL achieved for $x = 0.3$ sample with value nearly -50 dB. Extremely large effective bandwidth as 10 GHz also found in $x = 0.3$ sample. Besides $x = 0.3$, other samples also had shown pretty good microwave absorption performance, which proved that La-doping $\text{Ba}_3\text{Co}_2\text{Fe}_{24}\text{O}_{41}$ could be used for practical applications as promising microwave absorbers.

Keywords: Hexaferrite, $\text{Ba}_3\text{Co}_2\text{Fe}_{24}\text{O}_{41}$, La doping, Electromagnetic, Microwave absorption

Spin-wave multiplets excited in Sierpiński-like fractals

Gyuyoung Park* and Sang-Koog Kim

Korea National Creative Research Initiative Center for Spin Dynamics and Spin-Wave Devices, Nanospinics Laboratory, Research Institute of Advanced Materials, Department of Materials Science and Engineering, Seoul National University, Seoul 151-744, Republic of Korea

Sierpiński fractals have shown distinct novel behaviors in electronics [1, 2] and photonics [3, 4]. In this study, we designed aperiodic magnonic motifs of Sierpiński-like fractals through the superposition of scaled antidot-lattices. Spin-wave eigenmodes excited in the magnonic fractals were split according to a recursive sequence of $F_n = F_{n-1} + G_{n-1}$. The aperiodicity of total magnetic energy inside the motifs was found to result in those splits. When the aperiodicity of the magnonic crystal was decreased, the split modes became degenerated. The recursive evolution of multiplets is ascribed to the self-similarity inside the magnonic motifs, i.e, the same recursive sequence in the crystal geometry.

References

- [1] Veen, E. et al. *Phys. Rev. B* **93**, 115428 (2016).
- [2] Fremling, M. et al. *Phys. Rev. Research* **2**, 013044 (2020).
- [3] Nicola, F. et al. *ACS Photonics* **5**, 2418 (2018).
- [4] Yang, Z. et al. *Light: Science & Applications* **9**, 128 (2020).

NiCuZn-ferrite코팅에 따른 Fe-Si-Al의 자기적 특성 연구

김대유*, 안지훈, 박봉태, 우혁준, 이보화

한국외국어대학교 물리학과, 산화물 연구센터

bwlee@hufs.ac.kr

현재 스마트폰, 태블릿 PC 등 전자기기의 고성능화가 요구되고 있다. 본 연구는 전자기기의 고성능화의 구현을 위해 자성금속 분말인 Fe-Si-Al에 NiCuZn-ferrite을 코팅하고 이에 따른 자기적 특성 변화를 분석하여 전자기기 부품의 재료로 적용 가능한지 평가하였다. 공침법에 의해 제조된 $\text{Ni}_{0.2}\text{Zn}_{0.6}\text{Cu}_{0.2}\text{Fe}_2\text{O}_4$ 를 함량에 따라 Fe-Si-Al에 코팅하여 vibrating-sample magnetometer 측정을 통해 코팅된 분말의 포화자화, 보자력 등의 자기적 특성을 분석하였다.

해당 분말에 열경화성 바인더인 에폭시를 첨가, $\text{Ni}_{0.2}\text{Zn}_{0.6}\text{Cu}_{0.2}\text{Fe}_2\text{O}_4$ 첨가량 별 토로이달 형태로 시편을 제작하여, 화학적 공침법을 활용한 코팅방법으로 NiCuZn-ferrite가 Fe-Si-Al에 균일하게 코팅됨을 SEM/EDS 분석을 통하여 확인하였다. Impedance analyzer 와 B-H analyzer 분석을 통해 100kHz ~ 1MHz 대역의 자기적 특성 및 코어손실을 분석하여 NiCuZn-ferrite 함량의 변화에 따라 코팅 두께의 제어, 투자율 향상, 코어손실 감소 등의 자기적 특성이 향상됨을 확인하였다. 본 연구를 통해 NiCuZn-ferrite 코팅으로 포화자화, 투자율 향상, 코어손실 감소 등의 자기적 특성의 향상을 구현함으로써, NiCuZn-ferrite 코팅이 power inductor와 chip inductor 같은 전자기기 부품의 소재로의 적용이 가능함을 알 수 있었다.

FeCo@MnO₂ with a high microwave absorption and wide bandwidth using two-step method: Effect of MnO₂ layer thickness on magnetic/electromagnetic properties

Yeong Jun Park*, Jong Hwan Park, Su Jeong Suh, Byeong Sun Cho

Sungkyunkwan University, Department of Materials Science and Engineering, Suwon, Korea

Electromagnetic waves not only adversely affect the human body, but also cause interference between electromagnetic waves due to the development of wireless communication. Therefore, interest in an electromagnetic wave shielding has been increased to solve this problem. Especially, as 5G communication develops, the electromagnetic wave shielding material which can reduce the electromagnetic wave in a high-frequency area should be applied.

In this study, FeCo nanoparticles fabricated by a polyol process and an MnO₂ layer was coated on the surface to fabricate a high-frequency absorber, and the magnetic and electromagnetic properties were evaluated accordingly.

The average size of the synthesized FeCo was about 200 nm, and it was confirmed that the thickness of MnO₂ could be easily controlled by controlling the synthesis temperature and time. The optimum synthesis temperature was 60°C. In order to be used as an electromagnetic wave absorber in the high-frequency band, the initial permeability should be high and be over 1 in the high-frequency region. In the case of initial permeability, high saturation magnetization and low coercive force are required.

In this study, the magnetic and electromagnetic properties of FeCo depending on the thickness of MnO₂ were evaluated. The microstructure of the sample exhibiting the best electromagnetic properties was observed through TEM.

Effect of P addition on the Microstructure and Magnetic Properties of $\text{Fe}_{83.2}\text{Si}_{5.33-0.33x}\text{B}_{10.67-0.67x}\text{P}_x\text{Cu}_{0.8}$ Nanocrystalline Soft Magnetic Alloys

Hyun Ah Im^{1,2*}, Subong An^{1,2}, Kyoung-Hoon Bae¹, Sangsun Yang¹,
Jung Woo Lee² and Jae Won Jeong^{1†}

¹Metal Powder department, Korea Institute of Materials Science(KIMS),
797 Changwondae-ro Seongsan-gu, Changwon 51508, Korea

²Department of Materials Science and Engineering, Pusan National University, Pusan 46241, Republic of Korea

Soft magnetic materials require magnetic properties such as high permeability(μ), high saturation magnetic flux density(B_s), and low core loss. Si-Steel is widely used in terms of high Saturation flux density and cost reduction, but it is difficult to satisfy low coercivity (H_c) and low core loss. Therefore, it is inevitable to develop Fe-based nanocrystalline soft magnetic materials with high GFA and excellent soft magnetic properties. Nanocrystalline materials have the best soft magnetic properties when the crystal size is 10-15 nm. The purpose of this study is to minimize grain size and to enhance the soft magnetic properties. Cu(Immiscible elements) does not form a compound because it has no solid solubility with Fe. However, when a small amount is added to the Fe-based amorphous alloy, Cu atoms form clusters and act as a heterogeneous nucleation site of a-Fe site. P atoms distributed in amorphous residual matrix, which suppress grain growth, increasing the permeability and lowering the coercivity. Besides, according to previously studied **Makino et al.**, it was reported that the simultaneous addition of Cu and P resulted in a significant reduction in particle size to 10-20 nm. In this study, nanocrystalline ribbons with a composition of $\text{Fe}_{83.2}\text{Si}_{5.33-0.33x}\text{B}_{10.67-0.67x}\text{P}_x\text{Cu}_{0.8}$ ($x=1-4\text{at\%}$) have been fabricated by rapid-quenching melt spinning and thermal annealing. It has been demonstrated that the addition of small amount of P to the alloy improves glass forming ability, and increases resistance to undesirable $\text{Fe}_x(\text{B,P})$ crystallization. Among the alloys investigated in this work, $\text{Fe}_{83.2}\text{Si}_5\text{B}_{10}\text{P}_1\text{Cu}_{0.8}$ nanocrystalline ribbon annealed at 460 °C exhibits excellent soft-magnetic properties including low coercivity, low core loss, and high saturation magnetization. The uniform nanocrystallization in the $\text{Fe}_{83.2}\text{Si}_5\text{B}_{10}\text{P}_1\text{Cu}_{0.8}$ alloy has been also confirmed through high-resolution TEM analysis.

Keywords : soft magnetic materials. nanocrystalline, amorphous, magnetic properties, microstructures

Characteristics of crystalline and amorphous soft magnetic cores from Fe-based soft magnetic powders

Minwoo Lee^{*}, Yeonjoo Lee, Dohoon Kwon, Eunji Cha, Sungmin Kim, Daewon Jung, Hwijun Kim[†]
Korea Institute of Industrial Technology, Korea

Soft magnetic materials are used in powder generation, transfer, and convertor, and are extensively used in electric machines, power electronics, sensors, and electromagnetic interference shielding. Soft magnetic composites (SMCs) components are normally manufactured by modified powder metallurgy processes which are combined with new techniques, such as compaction, warm compaction, multi-step annealing followed by a heat treatment at relatively low temperature.

The recent increase in demand for high-efficiency electric motors, especially for electric vehicles (EVs) is finally starting to make a meaningful push into the global market, so the demand is growing in the global automotive industry. The properties of soft magnets depend on diverse manufacturing technologies and materials. The requirement for new soft magnetic materials in the field of the electric motors, high frequency power conversion parts and telecommunications has significantly caused the improvement of soft magnetic materials in Korea for the past decades. To meet the growing need for energy efficiency in power electronics and electric machines, we have been studying on a number of new soft magnetic composite cores with various structures like crystalline, amorphous and nanocrystalline. Compared to the currently most widely used crystalline SMCs, the amorphous SMCs exhibit more favorable properties, including high electrical resistivity, good saturation magnetization and low coercivity.

This presentation will introduce the results on frequency dependence of the soft magnetic cores manufactured from crystalline and amorphous powders by means of conventional powder metallurgy processes. While crystalline SMC cores show useful soft magnetic characteristics in low frequency range (~ 1000 Hz), amorphous SMCs cores exhibit valuable properties in high frequency ranges (~ 100 kHz). Furthermore, characteristics of SMC cores such as permeability, coercivity and core loss will be estimated in the various frequency ranges.

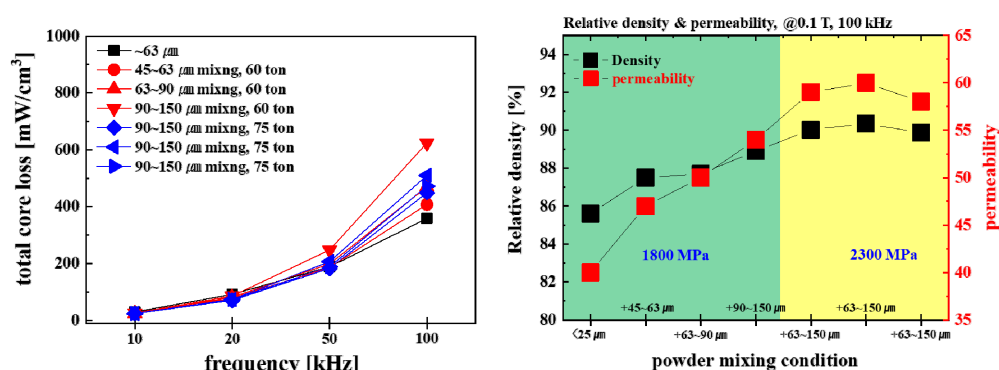


Fig. 1. Soft magnetic properties of FeSiCrBC amorphous SMC core

Keywords: Soft magnetic composites, Amorphous alloys, Nanocrystalline alloys, Soft magnetic properties, Powder metallurgy process, Soft magnetic core

졸-겔법으로 형성된 분말 표면 SiO_x 절연층이 연자성 복합체의 고온 열처리 후 자기적 특성에 미치는 영향

박종민^{1,2*}, 장민선¹, 구본욱¹, 김혜란¹, 권영태¹, 양상선¹, 이정우², 정재원¹

¹한국재료연구원 분말/세라믹연구본부 금속분말연구실

²부산대학교 재료공학부

1. 서론

우수한 자기 특성과 절연 코팅된 철 분말로 3차원 형상의 코어 제작이 가능한 연자성 복합체(SMC)는 고효율 특성 발현이 가능한 전자기 장치의 가능성을 보여준다 [1]. 대표적인 응용 분야로 모터가 있으며, 이러한 SMC의 이점은 현재 생산되고 있는 2차원 형태의 전기강판의 출력밀도 한계를 극복할 수 있을뿐더러 고투자율, 고포화자화, 낮은 철손 과 같은 필수적으로 만족되어야 할 요소도 갖추고 있어 크게 주목받고 있다.

SMC는 가용 주파수 대역이 확대됨에 따라 고주파수에서 발생하는 와전류 손실이 급증함으로 절연 물질을 연자성 분말 표면에 코팅하여 자기 특성을 향상시키는 연구가 진행되어오고 있다. 그러나 현재 널리 사용되고 있는 Fe@PO_4 같은 경우 650 °C 이상의 열처리에서 절연 특성의 저하로 이어진다. 특히, 고온에서 철손 증가 현상을 보이는 Fe@PO_4 코어의 단점은 현재 보완해야 하는 과제로 대두되고 있다.

이를 해결하고자 고온 열처리에서 절연 특성이 유지되는 코팅 물질의 개발이 필요하며, 더불어 우수한 금속 분말의 특성을 이용하여 와전류 손실을 최소화하기 위한 얇고 균일한 코팅층 형성 기술 개발이 중요한 과제로 떠오르고 있다 [2]. 본 연구에서는 650 °C 이상의 고온 열처리에서 절연성을 유지하면서 저철손 특성을 가지며, 자기 특성이 우수한 코어를 제작하는 것에 중점을 두어 진행하였다. 철손 감소와 열 저항성을 높이기 위해 졸겔 방법을 이용하여 Fe 분말 표면에 SiO_2 셀을 형성시킨 후 SMC를 제조하여 고온 열처리 실험 결과에 따른 철손 및 자기적 특성을 비교 분석하였다.

2. 실험 방법

본 연구에서는 와전류 손실을 줄이기 위해서, Fe 분말 표면에 SiO_2 코팅을 진행하였다. 평균 입도 200 μm 크기를 가지는 Fe 분말에 Tetraethyl orthosilicate (TEOS)를 혼합하여 교반 작업을 실시하였다. 이때 TEOS 농도는 0.01, 0.05, 0.1, 0.15, 0.2, 0.25 ml/g로 조절하였다. 절연 코팅층 형성에 중요한 요인이 되는 pH는 이온 측정기를 이용하여 측정하였으며, NH_4OH (Ammonia solution)를 이용하여 pH=11의 조건에서 실험이 진행되었다. 이후, 열처리 과정으로는 아르곤 분위기에서 박스 퍼니스를 이용하여 600, 700, 800 °C의 고온에서 각각 1시간씩 진행되었다. 다음으로 코어 성형은 Fe@SiO_2 분말을 이용하여 외경 25 mm-내경 15 mm-두께 3 mm 형상을 가지는 링 타입 코어를 랩 프레스하여 제작하였다. 이 때, 코어는 평균 95% 이상의 고밀도 특성을 나타내었다. 추가적으로 15 mm의 지름을 가지는 디스크 시편을 제작하여 고압에서의 절연 코팅층의 깨짐 현상을 확인하기 위해 미세구조 분석을 진행하였다. 분석 장비로는 X-ray diffraction (XRD)를 통해 조성 분석을 하였고, Scanning electron microscope (SEM)과 Energy dispersive X-ray spectrometer (EDS)를 통해 절연 코팅층의 두께와 샘플의 구성 원소를 확인하였다. 그리고 Vibrating-sample magnetometer (VSM)을 이용하여 포화자화, 보자력, 투자율을 포함하는 자성 특성 분석을 진행하였다. 마지막으로, AC BH analyzer (AC)와 DC BH loop tracer (DC)를 이용하여 0.05, 0.4, 1 kHz 영역 대에서의 철손 특성을 비교하였다.

3. 실험 결과

Fe@SiO₂ 분말의 조성분석을 위해 XRD를 측정한 결과 α -Fe의 피크인 45.01°, 65.55°, 83.06° 부근에서 확인되었고, SiO₂ 같은 경우 비정질이기 때문에 22.5° 부근에서 피크가 나타나지 않았다. VSM 결과로는 Fe의 포화 자화 값인 223.54 emu/g에서 비자성 물질인 SiO₂가 함유되어 3.15% 감소한 216.50 emu/g 값을 확인하였다. SEM와 EDS 결과를 통해 Fe 표면에 연속적으로 코팅된 평균 636.05 nm의 SiO₂를 확인하였다. 이를 바탕으로, 0.25 ml/g의 TEOS 농도를 가지는 샘플을 다수 제조하여 고온 열처리 실험을 진행하였다. 각각 600 °C, 700 °C, 800 °C에서 열처리된 코어에 AC, DC를 측정하여 비교한 결과 800 °C에서 Fe@PO₄ 코어는 0.4 kHz 조건에서 634.75% 이상 철손 증가율이 보이는데 반해 Fe@SiO₂는 현저히 낮은 34.47%의 철손 증가율이 보였다. 이어 DC 측정 결과 Fe@PO₄의 자속밀도는 0.551 T, 최대 투자율 202이 나온 반면 Fe@SiO₂의 자속밀도는 0.723 T, 최대 투자율 228이 나왔다. 이는 800 °C 열처리 시 Fe@SiO₂가 고온에서 더 우수한 성능을 가지고 있다고 볼 수 있다.

4. 결론

본 연구에서는 800 °C 고온에서도 절연성을 유지하는 SiO₂를 코팅하여 우수한 철손 특성을 발현하는 연자성 복합 분말 코어 제작을 목적으로 진행되었다. 먼저, TEOS 농도에 따라 SiO₂ 두께 최적화를 연구 진행하였다. 그 결과 0.25 ml/g의 농도 조건에서 가장 최적의 코팅을 확보하였으며, 더 나아가 고온 열처리 실험을 통해 800 °C에서 고온에서 취약한 PO₄가 코팅된 코어보다 더 우수한 철손 특성을 가지는 것을 확인하였다.

References

- [1] Liya Li et al., J. Alloys compd., **805**, 609-616 (2019).
- [2] Sounghun Lee et al., IEEE Trans. Power Syst., **53**, 1-4 (2017).

Effect of Ce/La addition on the soft magnetic properties in Fe-Si-B-P amorphous alloys

Young-Sin Choi^{1,2*}, Min-Woo Lee¹, Do-Hun Kwon¹, Eun-Ji Cha¹,
Jong-Ryoul Kim² and Hwi-Jun Kim^{1†}

¹Advanced Process and Materials R&D Group, Korea Institute of Industrial Technology, Incheon 21999, Korea

²Department of Materials Science and Chemical Engineering, Hanyang University, Ansan 15588, Korea

*khj@kitech.re.kr

Fe based amorphous alloys include metalloid elements in Fe matrix because they improve amorphous forming ability (AFA) leading to low coercivity and excellent core loss. However, Fe content is relatively decreased with increasing the content of metalloid elements, thereby lowering the saturation magnetic flux density. Several results have reported that the addition of Rare-earth (RE) metals can enhance magnetization in amorphous alloys.

In this study, the optimal addition amount of lanthanide elements such as Ce, La in Fe-Si-B-P amorphous alloys was investigated to increase the magnetization while maintaining the coercivity below 35 A/m. The large atomic radius of Ce and La causes lattice distortion and larger heat of mixing value of ΔH , which enhances AFA according to Miedema's model for atomic pairs. We estimated effect of Ce/La addition on the soft magnetic properties of Fe-based amorphous ribbons. The content of Ce and La additives changed from 0 to 2.5 at. % in $\text{Fe}_{81-(x+y)}(\text{SiBP})_{19}(\text{Ce}_x\text{La}_y)$ alloys. The magnetic and thermal properties of amorphous alloys were measured by vibrating sample magnetometer (VSM) and Differential scanning calorimetry (DSC), respectively. Also, amorphous forming ability was measured with changing ribbon thickness by varying the wheel speed during melt spinning process. Furthermore, the phase analysis was performed using X-ray diffraction (XRD) analysis.

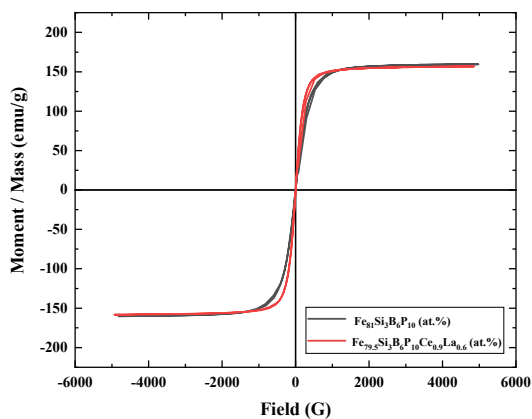


Fig. 1. The M-H curves of Fe-Si-B-P-RE ribbons in as-quenched states.

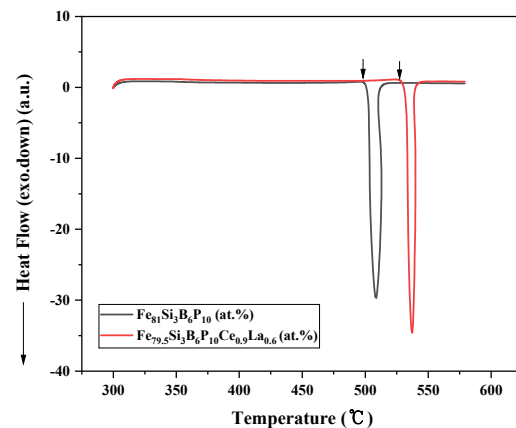


Fig. 2. The effect of RE on the onset crystallization of Fe-Si-B-P-RE amorphous alloys.

Keywords: Fe-based amorphous alloys, Metalloids, Rare earth, Soft magnetic properties, Amorphous forming ability

충진율에 따른 Ni-Zn 페라이트의 차폐특성 향상

김상우*, 이민영, 우혁준, 이보화

한국외국어대학교 물리학과, 산화물 연구센터

대표적인 차폐물질인 Ni-Zn 페라이트의 경우 소결 시편과 복합체 시편에서 차폐특성의 큰 차이를 보인다. 소결 시편의 경우 높은 밀도로 부피당 자화율이 높은 반면 폴리머와 혼합한 복합체는 폴리머 매트릭스로 인한 공극으로 차폐특성이 감소한다. 이러한 복합체는 보통 3.5 mm 이상의 두께에서 차폐특성을 나타내므로 경박단소를 요구하는 최신 전자기기에 적합하지 않다. 이 경우 2종이상의 나노분말을 첨가해 복합체의 충진율을 높이면 소결시편과 비슷한 특성을 나타낼 수 있다. 기본 분말은 고체반응법으로 합성한 $\text{Ni}_{0.5}\text{Zn}_{0.5}\text{Fe}_2\text{O}_4$ 를 사용했다. 충진율을 증가시키기 위한 나노분말은 공침법으로 합성한 NiFe_2O_4 를 사용했다. 차폐측정을 위한 복합체 시편은 모재와 나노분말의 비율이 10:0/ 8:2/ 6:4/ 4:6/ 2:8/ 0:10 인 토로이달 형태의 복합체로 제작하였다. 복합체의 밀도와 충진율은 밀도분석기에 의한 분석결과를 계산식에 대입하여 도출하였다. 복합체의 자성특성은 VSM으로 확인하였으며, SEM을 통해 분말크기 및 복합체의 단면을 관찰하였다. 전자파 차폐 특성은 VNA 네트워크 분석기를 통해 1-18GHz 주파수 영역에서의 반사 손실을 측정하였다.

Magnetic Properties as Fe/Co Ratio Variation in Fe-Co-V Alloy System

Hyunsol Son^{*}, Haein Choi-Yim[†]

Department of Physics, Sookmyung Women's University, Seoul 04310, Korea

Fe-Co-based alloy systems have remarkable soft magnetic properties, such as high saturation magnetization, high Curie temperature, low magnetocrystalline anisotropy, and low manufacturing cost. We add Vanadium to this FeCo alloy to make cold workable alloy without decreasing the soft magnetic properties. After all, our goal is to find the best composition of an alloy having the most fabulous soft magnetic properties. We investigated the Fe-based alloys of $\text{Fe}_{98-x}\text{Co}_x\text{V}_2$ prepared by the arc-melting system with high purity metals under a Ti-gettered Argon atmosphere. Then, we produced ribbons with 0.1-0.2mm thicknesses and 3-4mm widths with these samples using the melt spinning technique. After processing these ribbons, we analyzed the alloys' structural and magnetic properties. We verified the $\text{Fe}_{98-x}\text{Co}_x\text{V}_2$ alloy system as a typical BCC iron phase using X-ray diffraction (XRD). Also, we measured the magnetic properties of the ribbons by a vibrating sample magnetometer (VSM) and DC B-H loop tracer.

Thermal and Soft Magnetic Properties of Fe-Co-B-Si-Nb Amorphous Ribbons as Fe/Co Ratio Variation

Hyunsol Son^{*}, Haein Choi-Yim[†]

Department of Physics, Sookmyung Women's University, Seoul 04310, Korea

Fe-based amorphous alloy systems have attracted interest in the remarkable soft magnetic properties, high saturation magnetization, and low manufacturing cost. We added Niobium into the FeCo alloy system to improve glass-forming ability(GFA) without decreasing the soft magnetic properties such as high saturation magnetization and permeability with good thermal stability. We aimed to clarify the effect of the substitute Cobalt with iron and finally find a composition with the best soft magnetic and thermal properties. First, we investigated the alloys of $(\text{Fe}_x\text{Co}_{1-x})_{72}\text{B}_{19.2}\text{Si}_{4.8}\text{Nb}_4$ prepared by the arc-melting system with high purity metals under a Ti-gettered Argon atmosphere. Then, we produced rapidly solidified ribbons with 2-3mm widths and 20-30 μm thicknesses with these samples using the melt spinning technique. After processing these ribbons, we analyzed the alloy's structural, thermal, and magnetic properties. First, we verified $(\text{Co}_{1-x}\text{Fe}_x)_{72}\text{B}_{19.2}\text{Si}_{4.8}\text{Nb}_4$ alloy system as fully amorphous using X-ray diffraction (XRD). Then, the thermal properties, including crystallization temperature (T_x), were measured by differential scanning calorimetry (DSC). Lastly, we measured the magnetic properties of the amorphous ribbons by a vibrating sample magnetometer (VSM).

Understanding of magnetic cobalt spinel: A first-principles study

Inseo Kim^{1*}, Hyungwoo Lee¹, Ho-Hyun Nahm², Minseok Choi¹

¹Department of Physics, Inha University, Korea

²Graduate School of Nanoscience and Technology, Korea Advanced Institute of Science and Technology, Korea

Spinel compounds have been studied due to their unique and interesting magnetic property [1,2]. Two cobalt spinels, Co_3O_4 and Co_3S_4 have an antiferromagnetic ground state with the Néel temperature T_N of 40 K and 58 K, respectively. It has been believed that the exchange interactions between Co^{2+} lead to the magnetic property but those between Co^{3+} are negligible. In this work, we perform first-principles calculations to develop fundamental understanding of the magnetic property in the cobalt spinels. The magnetic properties of the antiferromagnetic Co_3O_4 and Co_3S_4 were investigated and compared using density functional theory with the Hubbard- U approach [3]. Then, the hidden magnetic phases of Co_3S_4 associated with Jahn-Teller-like distortion was explored [4].

References

- [1] J. Milam-Guerrero, A. J. Neer, and B. C. Melot, J. Solid State Chem. **274**, 1 (2019)
- [2] X. Yao, EPL **102.6**, 67013 (2013)
- [3] I. Kim, H. H. Nahm, and M. Choi, Curr. Appl. Phys. **22**, 65 (2021)
- [4] I. Kim, H. Lee, H. H. Nahm, and M. Choi, To be Submitted.

First-principles study of two dimensional magnetic oxides

Hyungwoo Lee^{*}, Minseok Choi

Department of Physics, Inha University, Korea

^{*}E-mail: minseok.choi@inha.ac.kr

Two-dimensional (2D) transition materials have been attracted attention since they are not only ideal platforms to investigate exotic physical phenomena but also are technically promising for applications. According to Mermin-Wagner theorem, long-range magnetic order is unstable in 2D system due to thermal fluctuation. However, magnetic anisotropy can remove this restriction and stabilize the long-range magnetic order in 2D system. In this talk, we present a first principle study of the magnetic ordering in 2D magnetic oxides. Spin-orbit coupling and the Hubbard- U scheme were employed. Several 2D magnetic configurations including 120° Néel configuration were considered, and stable crystal and electronic structure of the oxides were found at each magnetic configuration. In addition, strain effect on magnetic anisotropy was examined.

Strain effect on magnetic properties of atomically thin Fe_3GeTe_2

Gyeonghye Kim*, Qurat ul Ain, Soon Cheol Hong and S. H. Rhim

Department of Physics and Energy Harvest-Storage Research Center, University of Ulsan, Republic of Korea

According to the Mermin-Wagner theorem [1], no long-range order is possible in two-dimensional system. However, ferromagnetism in two-dimensional materials has been experimentally discovered. In particular, Fe_xGeTe_2 family ($x = 3, 4$, and 5) have relatively high Curie temperature larger than 130 K [2]. Here, we investigate strain dependent magnetic properties of monolayer Fe_3GeTe_2 (FGT) and bilayer using density-functional theory. In monolayer, Fe2 and Ge are on the same layer, which is sandwiched by Fe1 and Te layers. From this structure characteristics, Fe1 and Fe2, exhibit quite contrasting magnetic moments with 2.06 and $1.04\mu_B$, respectively. Under strain, magnetic moment of Fe1 change sensitively while Fe2 does not. Monolayer FGT prefer perpendicular magneto-crystalline anisotropy (MCA) for strain from -5 % to 5 %. Strain change the value of MCA energy, particularly compressive strain makes more change: from 4.72 to 0.85 meV/cell at strain of 0 and -5 %, respectively. Bilayer and bulk FGT energetically favor antiferromagnetic coupling without strain. However, with strain of 4.16 %, antiferromagnet to ferromagnet transition occurs in bilayer case.

References

- [1] N.D. Mermin and H. Wagner, Phys. Rev. Lett. **17**, 1133 (1966).
- [2] Zaiyao Fei et al., Nat. Mater. **17**, 778-782 (2018).

Spin Hall Conductivities of W-N Alloys

Quynh Anh T. Nguyen*, D. D. Cuong, S. C. Hong and Sonny H. Rhim

Department of Physics and Energy Harvest Storage Research Center,
University of Ulsan, Ulsan 44610, Republic of Korea

Motivated by recent reports on high spin Hall angle in W alloys [1-3], spin Hall conductivities (SHC) of W-N alloys are investigated theoretically using *ab initio* density functional calculations. Without N, SHC of α -W and β -W are -744 and 818 $\hbar/eS/cm$, respectively. Among various combinations, we focus on W_2N and WN. In particular, SHC of W_2N is enhanced 18.7 % over β -W. High SHC of W_2N is elucidated by large Berry curvature from $\frac{2}{3}FX$. On the other hand, in WN case, three structures, NaCl-type, hexagonal and NbO-type, are considered. SHC of NaCl- and hexagonal types are -619 and -696 $\hbar/eS/cm$, respectively, while NbO-type exhibits relatively low SHC of -194 $\hbar/eS/cm$. However, considering energetics, W_2N is more promising than WN, whose thermodynamic average is around -194 $\hbar/eS/cm$.

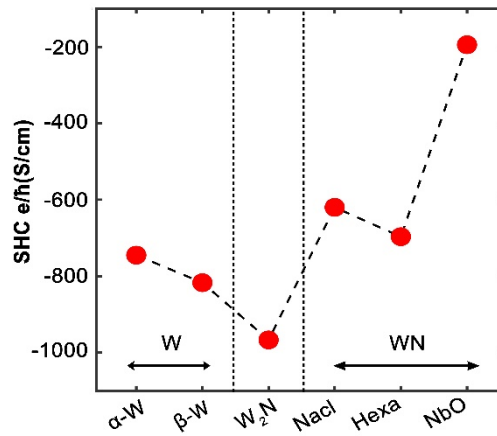


Fig. 1. Spin Hall conductivities of W-N alloys

References

- [1] K.-U. Demasius, T. Phung, W. Zhang, B. P. Hughes, S.-H. Yang, A. Kellock, W. Han, A. Pushp, and S. S. P. Parkin, Nat. Commun. **7**, 10644 (2016).
- [2] X. Sui, C. Wang, J. Kim, J. Wang, S. H. Rhim, and W. Duan, Phys. Rev. B **96**, 241105(R) (2017).
- [3] Y. J. Kim, M. H. Lee, G. W. Kim, T. Kim, I. H. Cha, Q. A. T. Nguyen, S. H. Rhim, and Y. K. Kim, Acta Mater. **200**, 551 (2020).

Anomalous Hall and Nernst Effect in Mn_3Al under Volume Change

Guihyun Han^{1*}, Minkyu Park², Soon Cheol Hong^{1,3} and S. H. Rhim^{1,3}

¹Department of Physics, University of Ulsan, Republic of Korea

²Research Institute of Basic Science, University of Ulsan, Republic of Korea

³Energy Harvest-Storage Research Center, University of Ulsan, Republic of Korea

Recent studies reported that anomalous Hall conductivity (AHC) can exist even without magnetization [1-3]. In this context, AHC of compensated ferrimagnet Mn_3Al with zero magnetization is investigated using *ab initio* calculations. Hydrostatic volume change was considered with fixed cubic structure retaining compensated magnetization. Volume change shifts bands near Fermi level thereby AHC reaches 1200 S/cm. Anomalous Nernst conductivity (ANC) is also calculated. ANC shows peaks in specific energy range, where van Hove singularity is also found, whose interplay is discussed.

References

- [1] Hua Chen, Qian Niu and A. H. MacDonald, Phys. Rev. Lett. **112**, 017205 (2014).
- [2] Yang Zhang, Yan Sun, Hao Yang, Jakub Zelezny', Stuart S. P. Parkin, Claudia Felser, and Binghai Yan, Phys. Rev. B **95**, 075128 (2017).
- [3] Libor Šmejkal, Rafael González-Hernández, T. Jungwirth, J. Sinova, Sci. Adv. **6** eaaz8809 (2020).

Anomalous Hall signatures of nonsymmorphic nodal lines in doped chromium chalcospinel CuCr_2Se_4

Subhasis Samanta¹, Gang Chen^{2,3} and Heung-Sik Kim^{1,4*}

¹Department of Physics, Kangwon National University, Chuncheon 24341, Korea

²Department of Physics and Center of Theoretical and Computational Physics,
The University of Hong Kong, Pokfulam Road, Hong Kong, China

³State Key Laboratory of Surface Physics and Department of Physics, Fudan University, Shanghai 200433, China

⁴Institute for Accelerator Science, Kangwon National University, Chuncheon 24341, Korea

Dissipationless transport has been a hallmark of topological phases of matters in condensed matter systems. Very often, dissipationless transport in quantum materials originates from band topology of electronic structures. An emerging phase of matter among the class of topological materials is nodal line semimetal, possessing symmetry-protected one-dimensional gapless lines at or close to the Fermi level in momentum space. Here, we study Cr-based ferromagnetic chalcospinel CuCr_2Se_4 via first principles calculations and *ab-initio* tight binding method to reveal true origin of large anomalous Hall signature upon electron doping, which was not well understood for more than a decade. We find that interplay between spin-orbit coupling and ferromagnetism of doubly degenerate nonsymmorphic nodal line at the zone boundary is responsible for previously observed distinct behavior of large anomalous Hall signature in the presence of electron doping. The splitting of nodal line via spin-orbit coupling produces a large Berry curvature, which leads to a sharp increase in anomalous Hall conductivity. The Hall response is largely tunable via switching of magnetization direction and varying doping concentration. The topological nature of anomalous Hall response makes CuCr_2Se_4 a promising candidate for realization of low power spintronics applications.

References

- [1] W.-L. Lee, S. Watauchi, V. L. Miller, R. J. Cava, and N. P. Ong, *Science* **303**, 1647 (2004).
- [2] W.-L. Lee, S. Watauchi, V. L. Miller, R. J. Cava, and N. P. Ong, *Phys. Rev. Lett.*, **93**, 226601 (2004).
- [3] Y. Yao, Y. Liang, D. Xiao, Q. Niu, S. Q. Shen, X. Dai, and Z. Fang, *Phys. Rev. B* **75**, 020401 (2007).

Symmetry Effects on Magnetocrystalline Anisotropy of hcp and fcc Cobalt: a First-principles Study

Thi H. Ho^{*}, Sonny H. Rhim and S. C. Hong

Department of Physics and Energy Harvest Storage Research Center,
University of Ulsan, Ulsan 44610, Republic of Korea

Density-functional theory calculations are performed to investigate symmetry effects on magnetocrystalline anisotropy (MCA) of Co. Both bulk and films in the hcp and fcc phases are considered. Within the framework of second-order perturbation theory^[1], MCA energy can be decomposed into spin channels, i.e., the spin-conserved $\uparrow\uparrow$ and $\downarrow\downarrow$, and the spin-flip $\uparrow\downarrow$ and $\downarrow\uparrow$ terms. Here, the first spin (\uparrow or \downarrow) symbol represents an occupied state, while the second spin (\uparrow or \downarrow) one does an unoccupied state. For example, $\uparrow\downarrow$ represents the coupling between an occupied \uparrow state and an unoccupied \downarrow state. The spin-channel decomposed MCAs of hcp and fcc Co in bulk are presented in Fig. 1. Generally, each spin channel contribution behaves in a quite similar way for both hcp and fcc Co. However, the net MCAs are quite different, 15.61 $\mu\text{eV}/\text{atom}$ of hcp Co and 0.53 $\mu\text{eV}/\text{atom}$ of fcc Co, whose reason should be revealed. In both hcp and fcc Co, the majority spin(\uparrow) bands are almost completely filled so that the negligible unoccupied \uparrow states cannot play a dominant role in determining a MCA energy. As a result, the spin channels of $\uparrow\uparrow$ and $\downarrow\uparrow$ contribute much smaller than those of $\downarrow\downarrow$ and $\uparrow\downarrow$, as shown in Fig. 1. The big difference between the MCAs of hcp and fcc Co comes mostly from the positive spin-flip $\uparrow\downarrow$ and the negative spin-conserved $\downarrow\downarrow$ terms. The negative spin-conserved $\downarrow\downarrow$ term of hcp Co is much smaller by 13.17 $\mu\text{eV}/\text{atom}$ in absolute value than that of fcc Co, while the positive spin-flip $\uparrow\downarrow$ term of hcp Co has higher MCA by 2.0 $\mu\text{eV}/\text{atom}$ than that of fcc Co, which results in the much stronger MCA of hcp Co than fcc Co.

In thin films, the surface effects are found to enhance MCA energies of both hcp and fcc Co. For the 9-ML films, the MCA energies of 253.04 and 207.64 μeV are obtained for hcp and fcc Co, respectively. Interestingly, the MCA energy of the fcc Co film is in the same order of magnitude as that of the hcp Co film. The reason is due to the dominant MCA contribution of the surface layers. The MCA values of surface layers are 171.8 and 188.7 $\mu\text{eV}/\text{atom}$ for the hcp and fcc Co, respectively.

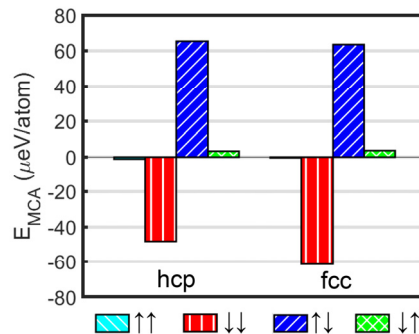


Fig. 1. The spin-channel decomposed MCA energies of bulk hcp and fcc Co.

Reference

- [1] D. S. Wang, R. Q. Wu, and A. J. Freeman, Phys. Rev. B **47**, 14932 (1993).

Role of Fe intercalation in bilayer MoS₂

Jin Jae Park^{*}, G. Hye Kim, Soon Cheol Hong and S. H. Rhim

Department of Physics, University of Ulsan, Ulsan 44610, South Korea

Recent years, there have been intensive and extensive studies on two-dimensional materials for intriguing physics as well as potential applications [1]. In particular, transition-metal dichalcogenides (TMDCs) have attracted in so-called valleytronics [2]. MoS₂ is a prototype of TMDCs, whose bulk phase has both inversion and time-reversal symmetry. Monolayer MoS₂, on the other hand, with broken inversion symmetry, has been explored in valleytronics, where the interplay between spin and valley plays an important role [3]. Fe intercalation into bilayer MoS₂ is investigated using *ab initio* calculations, which is a reciprocal counterpart of monolayer MoS₂, where Fe intercalation breaks time-reversal symmetry but retains inversion symmetry.

References

- [1] S. D. Sarma, S. Adam, E. H. Hwang, and E. Rossi *Rev. Mod. Phys.* **83**, 2 (2011).
- [2] J. R. Schaibley H. Yu, G. Clark, P. Rivera, J. S. Ross, K. L. Seyler, W. Yao, and X. Xu *Nat. Rev. Mater.* **1**, 16055 (2016).
- [3] D. Xiao D. Xiao, G.B Liu, W. Feng, X. Xu, and W. Yao *Phys. Rev. Lett.* **108**, 196802 (2012).

정방 왜곡에 따른 덩치 Mn_4C 의 스핀 구조 : 제일원리 계산

이준규*, 웬 티 꾸인 안, 호 후인 티, 임성현, 홍순철*

울산대학교 물리학과, 울산시 남구 대학로 93, 44610

최근 자기 화합물 Mn_4C 을 최초로 합성하는데 성공하였다는 보고가 있었다. XRD 실험을 통해 Mn_4C 은 격자 상수 $a = 3.868 \text{ \AA}$ 인 입방체 페로브스카이트 구조로 확인되었으며,[1] 또한 안정된 자기 구조는 그림 1의 (a)와 같은 준강자성체로 보고되었다.[1]

fcc Mn은 반강자성 상태가 안정적이고, Mn_4C 의 경우 준강자성 상태가 안정적이라고 보고된 바 있다. 이 때 Mn_4C 을 fcc Mn의 체심에 C이 결합된 화합물로 생각하면 흥미로운 점이 있다. fcc Mn의 체심에 C이 자리하게 됨으로 인해 Mn-Mn의 거리가 멀어지는 효과가 있고, C의 원자가 전자가 Mn-Mn 사이의 자성 결합에 영향을 미칠 수도 있을 것이다.

계산은 Vienna Ab-initio Simulation Package를 이용하여 수행하였다. 계산에 사용된 pseudopotential은 Projected augmented wave(PAW)로 생성하였고, 전자들 간의 교환상관 퍼텐셜은 Perdew-Burke-Ernzerhof에 의해 정립된 generalized gradient approximation(GGA-PBE)를 사용하였다. 자체 일관 계산에는 $14 \times 14 \times 14$ Monkhorst-Pack k-point 그물을 사용하였으며, 차단에너지는 500 eV을 주었다.

자체 일관 계산 결과 입방체 Mn_4C 의 안정된 격자 상수는 $a=3.784 \text{ \AA}$ 로 실험치 $a=3.868 \text{ \AA}$ 보다 0.084 \AA 만큼 작게 나타났고, 안정된 자기 구조는 Type-A와 같은 준강자성체로 실험결과와 일치했다. 이 때 Mn_{II} 는 X/Y/Z 모두 같은 자기 모멘트를 보였으며, Mn_{I} 와 Mn_{II} 의 자기 모멘트는 각각 $3.358 \mu_B$, $1.259 \mu_B$ 로 계산되어 총 자기모멘트는 $0.217 \mu_B/\text{unit-cell}$ 로 얻어졌다. 이 값은 실험치 $0.258 \mu_B/\text{unit-cell}$ 보다 $0.041 \mu_B/\text{unit-cell}$ 만큼 작았다.[1]

표 1. Type-A의 $c/a=1.00$, 격자상수는 $a = 3.784 \text{ \AA}$ 이고, Type-B의 $c/a=1.09$, 격자상수 $a = 3.69 \text{ \AA}$ 이다.

	Mn_{I} (μ_B)	$\text{Mn}_{\text{II}} - \text{X/Y}$ (μ_B)	$\text{Mn}_{\text{II}} - \text{Z}$ (μ_B)	Total ($\mu_B/\text{unit-cell}$)
Type-A	3.358	-1.259	-1.259	0.2173
Type-B	3.282	-1.575	0.031	0.3398

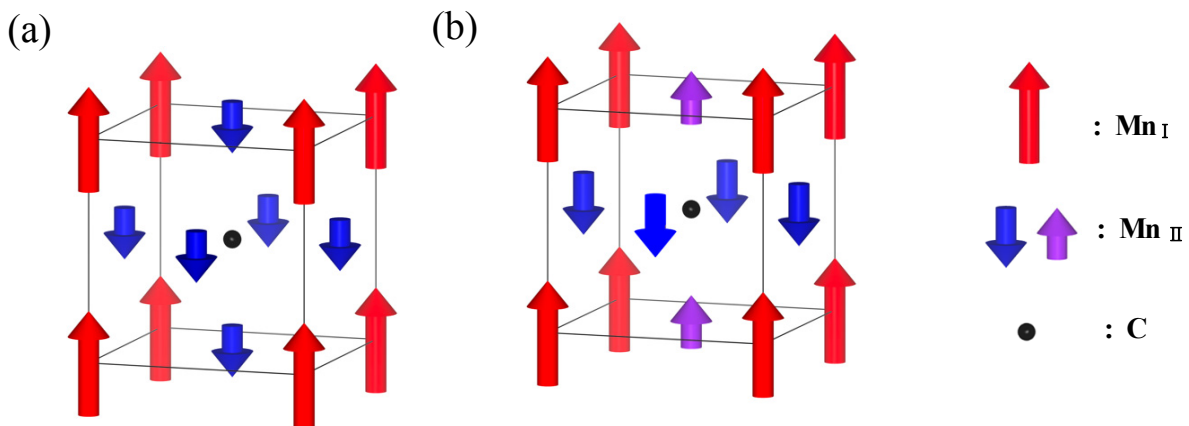


그림 1. Mn_4C 의 스핀 구조 (a) Type-A, (b) Type-B

앞선 계산을 통해 얻은 Mn_4C 의 안정된 상태에서의 부피를 이용하여 정방 왜곡 계산을 하였을 때 Type-A의 경우 $c/a=1.00$ 일 때가 가장 안정되었다. Type-B는 부피 변화를 주지 않았을 때 스핀 방향을 고정하는 것에 어려움이 있었고, 아직 가장 안정된 상태의 Type-B의 특성을 계산하지 못하였다. 따라서 c/a 를 고정한 뒤 부피 변화를 주며 특정 c/a 에서 안정된 Type-B를 계산하였다. 그 중 $c/a=1.09$ 에서, 안정된 격자 상수는 $a = 3.69 \text{ \AA}$ 로 나타났고, 이 때의 부피는 안정된 Mn_4C 보다 0.1% 컸으며 형상 에너지는 0.34 eV만큼 크게 계산되었다. 이 때 $\text{Mn}_{II}\text{-Z}$ 의 자기 모멘트가 $0.031 \mu_B$ 로 매우 작다.

References

- [1] Ping-Zhan Si, Hui-Dong Qian, Hong-Liang Ge, Jihoon Park, and Chul-jin Choi, Appl. Phys. Lett. **113**, 049903 (2018).
- [2] W. J. Takei, R. R. Heikes, and G. Shirane, Phys. Rev. **125**, 1893 (1962).

Tunable Two-channel Magnetotransport in SrRuO₃ Ultrathin Films Achieved by Controlling the Kinetics of Heterostructure Deposition

Eun Kyo Ko^{1,2*}, Han Gyeol Lee^{1,2†}, Sangmin Lee³, Junsik Mun³, Jinkwon Kim^{1,2},
Ji Hye Lee^{1,2}, Tae Heon Kim⁴, Jin-Seok Chung⁵, Suk Bum Chung^{6,7,8},
Miyong Kim³, Seo Hyung Chang^{9*} and Tae Won Noh^{1,2†}

¹Center for Correlated Electron Systems, Institute for Basic Science (IBS), Seoul 08826, Republic of Korea

²Department of Physics and Astronomy, Seoul National University, Seoul 08826, Republic of Korea

³Department of Materials Science and Engineering and Research Institute of Advanced Materials, Seoul National University, Seoul 08826, Republic of Korea

⁴Department of Physics and Energy Harvest-Storage Research Center (EHSRC), University of Ulsan, Ulsan 44610, Republic of Korea

⁵Department of Physics, Soongsil University, Seoul 06978, Republic of Korea

⁶Department of Physics, University of Seoul, Seoul 02504, Republic of Korea

⁷Natural Science Research Institute, University of Seoul, Seoul 02504, Republic of Korea

⁸School of Physics, Korea Institute for Advanced Study, Seoul 02455, Republic of Korea

⁹Department of Physics, Chung-Ang University, Seoul, 06974, Republic of Korea

[†]These authors contributed equally.

*cshyoung@gmail.com, and twnoh@snu.ac.kr

In the field of oxide heterostructure engineering, there have been extensive efforts to couple the various functionalities of each material. The Berry curvature-driven magnetotransport of SrRuO₃ ultrathin films is currently receiving a great deal of attention because it is extremely sensitive to extensive physical parameters. Although this is beneficial in terms of heterostructure engineering, it renders transport behavior vulnerable to nanoscale inhomogeneity, resulting in artifacts called “hump anomalies”. Here, we develop a method to tune the magnetotransport properties of SrRuO₃ ultrathin films capped by LaAlO₃ layers. We systematically controlled the kinetic process by varying the pressure during LaAlO₃ layer deposition and investigated the effects on nanoscale inhomogeneity in SrRuO₃ films. We found that the high-kinetic energy of the capping layer adatoms induces stoichiometric modification and nano-scale lattice deformation of the underlying SrRuO₃ layer. The control of kinetics provides us a way to modulate magnetization and the associated magnetotransport of the SrRuO₃ layer.

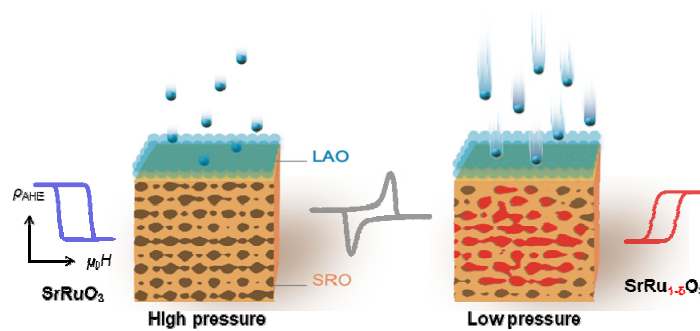


Fig. 1. By controlling kinetic process during the LaAlO₃ capping layer growth, inhomogeneous phase is induced in the underneath SrRuO₃ film. The control of kinetics provides us a way to modulate magnetization and the associated magnetotransport of the SrRuO₃ layer.

Anomalous Hall Effect in (1 1 1)-LaNiO₃ Thin Films with CaTiO₃ Capping Layer

Ji Hye Lee^{1,2*}, Hongjoon Kim^{1,2}, Jeong Rae Kim^{1,2}, Tae Won Noh^{1,2}

¹Center for Correlated Electron Systems (CCES), Institute of Basic Science (IBS), Korea

²Department of Physics and Astronomy, Seoul National University, Korea

Long-range magnetic order has been stabilized in thin films form although its bulk system does not show any magnetic order parameter in a few complex oxides. Among them, transition metal oxides (TMOs) have been massively investigated to explore various quantum phenomena such as high- T_c superconductivity, metal-insulator transition and multiferrocity (ferroelectric & ferromagnetism). One of TMOs, (111)-oriented grown rare-earth nickelate $R\text{NiO}_3$ (RNO) has been theoretically studied intensively. And recently, experimental demonstration of its polar metallic nature features has been successful in (111)-LaNiO₃ (LNO) thin films on LaAlO₃ (LAO) substrate thanks to the advance of thin-film growth technique [1]. However, the precise understanding of its long-range magnetic ground state and functionality of this materials are still lack.

In this study, we report the observation of ferromagnetism in ultrathin LNO films with dependency of sample thickness grown on (111)-LAO single crystal by pulsed laser deposition method. Structural properties was investigated through high resolution X-ray diffraction patterns in LNO thin films. And surface properties was characterized by atomic force microscopy. We also investigated the anomalous Hall effect (AHE) and magnetoresistance (MR) to figure out the origin of the ferromagnetic ground state in temperature-dependent transport measurement. Even by *in-situ* deposition of capping layer on top of the LNO surface, we explored Hall anomaly of LNO thin films by ferroelectric proximity effect. For this purpose, we deposited new perovskite CaTiO₃ (CTO) materials for ferroelectric top layer [2]. Our results may shed lights on using emergent functionality of magnetic oxides in spin-related device and realization of strongly correlated topological phase by modulating the order parameter of the system.

References

- [1] T. H. Kim *et al.* *Nature* **533**, 68 (2016).
- [2] J. R. Kim *et al.* *Nat. Commun.* **11**, 4944 (2020).

Investigation of ferromagnetic state of SrRuO₃ thin films by optical second harmonic generation

Chang Jae Roh^{1,2,3*}, Jeong Rae Kim^{1,2}, Jong Seok Lee³ and Tae Won Noh^{1,2}

¹Center for Correlated Electron Systems, Institute for Basic Science (IBS), Seoul 08826, Republic of Korea

²Department of Physics and Astronomy, Seoul National University (SNU), Seoul 08826, Republic of Korea

³Department of Physics and Photon Science, Gwangju Institute of Science and Technology (GIST),
Gwangju 61005, Republic of Korea

In these days, optical second harmonic generation (SHG) has been typically utilized to study not only crystallographic but also magnetic symmetry information of condensed matter systems. However, there is limitation to characterize ferromagnetic ordered state since generation of second harmonic wave is basically allowed to magnetic dipolar contribution. In this research, we investigate ferromagnetic phase of itinerant ferromagnet SrRuO₃ thin films. From monitored azimuth dependent second harmonic intensity at room temperature, bulk structural symmetries of SrRuO₃ thin films with thicknesses of 4, 10, 30, 50, 70, 90, and 250 nm are characterized as tetragonal for $t=4$ nm and orthorhombic for the thicker films ($10 \leq t$), respectively. As temperature decreases, the SHG intensity monotonically increases and largely enhanced below 160 K, which corresponds to the phase transition from paramagnetic to ferromagnetic phase without change of azimuth dependence. We analyze the monitored SHG results by considering electric quadrupole and magnetic dipole contributions, and discuss nonlinear optical probing of ferromagnetic state for condensed materials systems.

Non-BCS-type Superconductivity and its Correlation to Ferromagnetism in SrTiO₃/LaAlO₃/SrTiO₃ trilayer heterostructure

Yongsu Kwak^{1,2†}, Woojoo Han¹, Jinhee Kim¹, Jonghyun Song^{2*}

¹Korea Research Institute of Standards and Science, Daejeon 34113, Korea

²Department of Physics, Chungnam National University, Daejeon 34134, Korea

As a quest for two-dimensional conducting interface with exotic functionalities for future electronic devices, the perovskite heterointerface of LaAlO₃/SrTiO₃ (LAO/STO) has been intensively studied. For the LAO/STO heterostructure, the critical thickness of the LAO layer for metallic conduction is 4 unit cells (uc) according to the polar catastrophe scenario. However, we find that metallic conduction can also be induced at the LAO/STO interface with only 1 uc of LAO, as long as it is capped by 3 or more uc of STO. Consistent results are obtained from density functional theory calculations. For this STO/LAO/STO trilayer, we also confirmed a peculiar non-BCS-type superconductivity with a suppressed superconducting gap, which may imply a superconducting coupling distinct from previously reported BCS-type superconductivity in LAO/STO heterointerface. We also fabricated Josephson junction with STO/LAO/STO heterojunction and observed peculiar magnetoresistances which are attributed to the strong correlation between the superconductivity and ferromagnetism in the two-dimensional charge carriers at the hetero-interface. These observations suggest that the STO/LAO/STO trilayer can be another testing board to explore carrier conduction in two-dimensional electron systems for electronic device applications utilizing exotic functionalities.

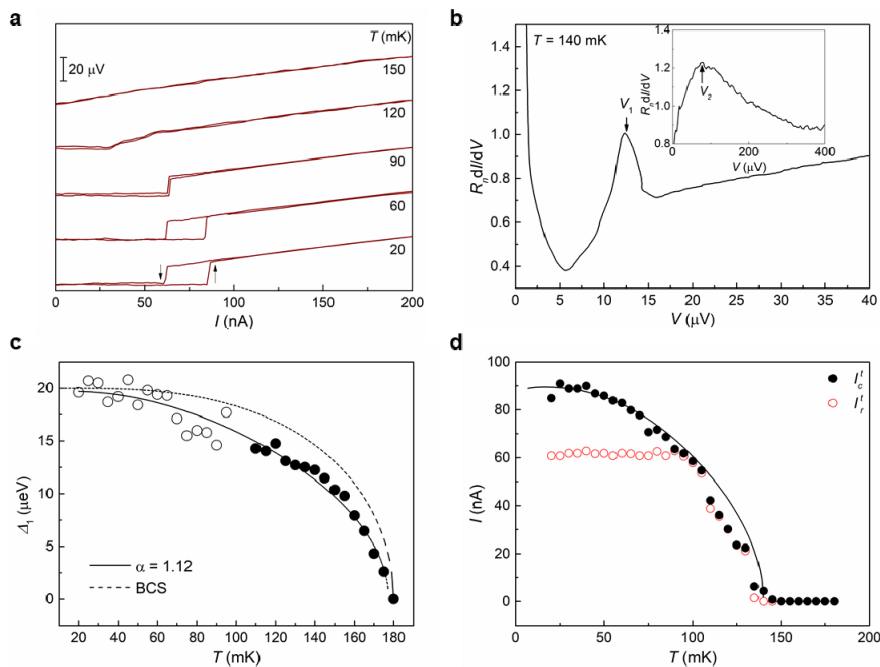


Fig. 1. Non-superconductivity of STO/LAO/STO trilayer system

Switching behaviors of NiFe nanorings on carbon nanotubes

Seungha Yoon^{*}

Korea Institute of Industrial Technology, 6 Cheomdangwagi-ro, Buk-gu, Gwangju, South Korea

Uniformly repeated sub-micron size ring patterns have been widely investigated for the future applications, such as magnetic random access memory, and magnetic logic devices. Because of the magnetic interaction between the ring patterns, the magnetic switching behaviors is one of key element to develop a dense devices.

The Ta(3 nm)/NiFe(20 nm)/Ta(1 nm) layers was deposited on top of the sub-micron size ring patterns consisting of carbon nanotubes, as a function of the ring size. An anodic aluminum oxide template was used for the formation of the ring arrays. The diameter of the rings was varied from 70 nm to 100 nm with a constant density of $\sim 1 \times 10^{10}$ [cm⁻²]. The details of the magnetization switching behaviors including magnetic dynamics of the nanorings in terms of the size and the magnetic field will be discussed.

Comparison of Coercivity and Ferromagnetic resonance frequency of Ferrites that Absorb Millimeter Waves

Gi-Ryeon Jo^{1,2*}, Min-Ji Pyo^{1,3}, Young-Guk Son², Youn-Kyoung Baek^{1†}

¹Powder & Ceramics Division, Korea Institute of Materials Science, Changwon, Korea

²School of Materials Science and Engineering, Pusan National University, Busan, Korea

³Department of Materials Science and Engineering, Pukyong National University, Busan, Korea

Ultra high frequency electromagnetic waves (30-300GHz) are expected to play an important role in next-generation high-speed wireless communications such as local area networks and radars for the distance between cars. However, currently materials that effectively restrain electromagnetic interference (EMI) in the region of millimeter waves almost do not exist. Magnetic materials are known as promising candidates for electromagnetic wave absorbers that due to ferromagnetic resonance. When a ferromagnet is irradiated with electromagnetic waves, electromagnetic wave absorption is observed due to the gyro magnetic effect.

The ferromagnetic resonance frequency (f_r) is proportional to the magnetocrystalline anisotropy field (H_a), which is expressed by $f_r = (\nu/2\pi)H_a$. When the sample consists of randomly oriented magnetic particles with a uniaxial magnetic anisotropy, the H_a value is proportional to the H_c value. According to the above equation, it is reasonable to assume that similar f_r can be shown in the magnetic materials with similar H_c . Thus, we have compared the ferromagnetic resonance frequency and magnetic properties of ferrites showing similar coercivities in this study

This study was supported by the Fundamental Research Program of the Korea Institute of Material Science (PNK7630)

Keywords: Strontium ferrite, Epsilon ferrite, Millimeter wave, EM absorber, Ferromagnetic resonance frequency

Single atomic spin sensing of magnetic interactions in a tunnel junction

Jinkyung Kim^{1,2*}, Won-jun Jang⁴, Thi Hong Bui^{1,2}, Deung-Jang Choi^{5,6,7}, Christoph Wolf^{1,3},
Fernando Delgado⁸, Yi Chen^{1,3}, Denis Krylov^{1,3}, Soonhyeong Lee^{1,3}, Sangwon Yoon^{1,3},
Christopher P. Lutz⁹, Andreas J. Heinrich^{1,2*} and Yujeong Bae^{1,2*}

¹Center for Quantum Nanoscience (QNS), Institute for Basic Science (IBS), Seoul 03760, South Korea

²Department of Physics, Ewha Womans University, Seoul 03760, South Korea

³Ewha Womans University, Seoul 03760, Republic of Korea

⁴Samsung Advanced Institute of Technology, Suwon 13595, South Korea

⁵Centro de Física de Materiales CFM/MPC (CSIC-UPV/EHU), 20018 San Sebastián, Spain

⁶Donostia International Physics Center (DIPC), 20018 Donostia-San Sebastian, Spain

⁷Ikerbasque, Basque Foundation for Science, 48013 Bilbao, Spain

⁸Instituto de estudios avanzados IUDEA, Departamento de Física, Universidad de La Laguna, 38203, Tenerife, Spain

⁹IBM Almaden Research Center, San Jose, CA 95120, USA

Single spins are widely regarded as a leading candidate for realizing next-generation quantum devices for sensing and quantum information processing. Detection and coherent control of single spins require to localize single spins and characterize its magnetic surroundings. Scanning tunneling microscopy in combination with electron spin resonance (ESR-STM) technique [1] enables a direct access to the quantum states of single magnetic atoms or molecules on surfaces. Using ESR-STM, we investigated spin resonance of hydrogenated Ti (TiH) atoms adsorbed on bridge binding site of MgO in a two-dimensional vector magnetic field. Here, the spin 1/2 TiH atom with no magnetic anisotropy was employed as a probe of magnetic environments at the tunnel junction. We found both ESR frequency and amplitude change as a function of the angle of vector magnetic fields. The resonance frequency varied by different vector magnetic fields indicates an anisotropy of the g-factor, resulting from the variation of angular momentum contributions due to the crystal fields. We developed a stereoscopic way to unravel the g-factor along the three principal axes. Moreover, ESR amplitude dependence on the direction of magnetic fields provides the further understanding of ESR mechanisms, which results from two factors, tunneling magnetoresistance (TMR) effect at the spin-polarized STM junction and the transverse magnetic field to drive ESR. Our results will enable to predict ESR active spin centers on different substrates as well as in other quantum-nanoscience platforms.

Reference

- [1] Susanne Baumann et al., Electron paramagnetic resonance of individual atoms on a surface, *Science*, 350, 6259, 417-420 (2015)

Home-built sub-Kelvin scanning tunneling microscope with electron spin resonance capability

Jiyeon Hwang^{1,2*}, Denis Krylov¹, Taehong Ahn^{1,2}, Lei Fang¹, Kyungju Noh^{1,2},
Andreas J. Heinrich^{1,2†} and Yujeong Bae^{1,2†}

¹Center for Quantum Nanoscience, Institute for Basic Science, Seoul, Korea

²Department of Physics, Ewha Womans University, Seoul, Korea

Scanning tunneling microscopy is a powerful tool to characterize the electronic and magnetic properties of atomic scale structures on a surface. Recent advances in increasing energy resolutions have been achieved functionalizing the STM tip by a well-characterized molecule [1,2] or integrating electron spin resonance with STM (ESR-STM) [3]. We present the design and performance of home-built STM with high frequency cabling, which is incorporated with a Joule-Thomson refrigerator and 2-axes vector magnets. Applying high frequency (microwave) electric fields to the STM junction through 50 Ohm coaxial cables causes significant loss of insertion power due to the impedance mismatch at the STM junction of ~ 1 GOhm, which limits the frequency range of applicable microwaves. To overcome this limitation, we introduced a microwave antenna and terminated the cable at 50 Ohm. Applying microwaves to the antenna rather than the STM tip allows us to reduce the formation of standing waves as well as to increase the transmission. Our work shows using the specially designed mechanical damper and optimizing the electrical noise levels provide the outstanding performance of STM for the single atom ESR experiment.

References

- [1] M. Ormaza et al., *Nano lett*, 17, 3, 1877-1882 (2017)
- [2] G. Czap et al., *Science*, **364**, 670-673 (2019)
- [3] S. Baumann et al., *Science*, **350**, 417-420 (2015)

Investigating the structural, magnetic and magnetocaloric properties in B-site Mo-doped $\text{La}_{1.4}\text{Ca}_{1.6}\text{Mn}_{2-x}\text{Mo}_x\text{O}_7$ ($0 \leq x \leq 0.3$) bilayer manganites

Akshay Kumar^{1*}, Kavita Kumari², Minji Shin¹, Seok Hwan Huh¹ and Bon Heun Koo^{1,2†}

¹School of Materials Science and Engineering, Changwon National University,
Changwon, Gyeongnam, 51140, Republic of Korea

²School of Materials Science and Engineering, Changwon National University,
Changwon, Gyeongnam, 51140, Republic of Korea

Magnetic refrigeration has attracted significant research interest because of having considerable advantages over the conventional gas compression refrigeration. Unlike the conventional gas compression refrigeration, the magnetic refrigeration is a green cooling technology which does not produce the harmful gases. In the present work, controlled substitution of molybdenum (Mo) in place of Manganese (Mn) was performed in $\text{La}_{1.4}\text{Ca}_{1.6}\text{Mn}_{2-x}\text{Mo}_x\text{O}_7$ ($x = 0.0, 0.1, 0.2$ and 0.3) to modify the magnetic and magnetocaloric behavior of the material. All samples were prepared through the conventional ceramic heating route. XRD profiles of the synthesized compounds revealed the tetragonal structure (I4/mmm) of bilayer Ruddlesden-Popper (R-P) Phase. However, some MoO_3 oxide and/or unidentified peaks in $x \geq 0.2$ doped samples emerged along with the R-P phase which suggest the dilution limit on B-Site doping for Mo. Temperature dependent magnetization measurements exhibit ferromagnetic to paramagnetic transitions above the respective transition temperature (T_C) of individual compounds. The parent compound displayed second order magnetic phase transition, while the first order transition was observed in the Mo-doped compositions. The maximum change in magnetic entropy (ΔS_M^{max}) values achieved for $x = 0.0, 0.1, 0.2$ and 0.3 samples are 2.98 J/kgK, 2.71 J/kgK, 2.64 J/kgK, 2.37 J/kgK respectively at 2.5 T applied field. Among the doped samples highest ΔS_M^{max} value was achieved for $x = 0.1$ sample. For the these compounds the relative cooling power (RCP) slightly increased to 102 J/kg for $x = 0.1$ sample compared to the parent compound 98 J/kg. RCP values decreased for high Mo-concentrations and reached a lowest value 68 J/kg for $x = 0.3$ sample. Sufficient structural analysis carried out here suggest that the tetragonal symmetry in the B-site doped bilayer manganites reduced to simple perovskite symmetry above the dilution limit ($x \geq 0.2$) thereby rigorously affecting the magnetic and magnetocaloric properties.

Keywords: magnetic refrigeration, Ruddlesden-Popper Phase, ferromagnetic, relative cooling power (RCP), magnetic entropy

Magnetic properties of LDH based low temperature synthesis of spinel oxide nanoparticle

Jun Han Lee^{1*}, Jaejung Song², Jae Won Jeong³, Seungho Cho² and Yoon Seok Oh¹

¹Department of Physics, Ulsan National Institute of Science and Technology (UNIST),
Ulsan 44919, Republic of Korea

²Department of Materials Science and Engineering, Ulsan National Institute of Science and Technology (UNIST),
Ulsan 44919, Republic of Korea

³Metal Powder Department, Korea Institute of Materials Science, 797 Changwondae-ro, Seongsan-gu,
Changwon 51508, Republic of Korea

The solid-state reaction method has been widely used for oxides synthesis because of its simplicity and effectiveness. However, it usually requires high synthesis temperature to induce the diffusion of atoms/ions during the reaction. Here, using layered double hydroxides (LDH) precursors, we synthesize the spinel oxide magnet NiFe_2O_4 . It is found that topotactic conversion from the LDH to the spinel structure enables to decrease the synthesis temperature. The oxides mixture is also used to synthesize the polycrystalline NiFe_2O_4 for comparison with the case of the LDH precursors. We characterize magnetic properties and morphology of our polycrystalline NiFe_2O_4 synthesized from the LDH precursors and the oxides mixture. In this presentation, we discuss and compare the physical properties of NiFe_2O_4 spinel oxides depending on the synthesis conditions.

Effect of reaction time on the structural, morphological and magnetic properties of Fe₃₀Co₇₀ nanoparticles

Kavita Kumari^{1*}, Akshay Kumar², MinJi Shin², Huh Seok Hwan³ and Bon Heun Koo^{1,2†}

¹Industrial Technology Research Institute, Changwon National University,
Changwon, Gyeongnam, 51140, Republic of Korea

²Department of Materials Convergence and System Engineering, Changwon National University,
Changwon, Gyeongnam, 51140, Republic of Korea

³Department of Mechatronics Conversion Engineering, Changwon National University,
Changwon, Gyeongnam, 51140, Republic of Korea

*Corresponding Author - bhkoo@changwon.ac.kr

The bimetallic nanoparticles as soft magnetic materials possess functional applications due to the low hysteresis losses, large saturation magnetization and high ferromagnetic character. Interestingly, these properties can be optimized in a number of ways. In this paper, the Fe₃₀Co₇₀ nanoparticles were prepared by reducing the precursors using sodium borohydride. The reaction time plays an important part in upgrading the properties of the material. The nanoparticles, prepared with the reaction times: 40min and 10min, were characterized using x-ray diffraction (XRD), low voltage field emission scanning electron microscopy (LV FESEM) and dc-magnetization. The effect of the reaction time was noticeably observed on the structural, morphological and magnetic properties of the nanoparticles. The XRD patterns confirm the formation of single-phase Fe₃₀Co₇₀ nanoparticles with crystallite size in nm range. The low crystallite size was observed for the low reaction time as determined using Scherrer's formula. The LV FESEM micrographs revealed the spherical shape morphology of the nanoparticles for 10 min reaction time. The nanoparticles were found to form chain-like structures with a reaction time of 40 min. The enhanced ferromagnetic character was observed with the high saturation magnetization at low reaction time. The enhanced reaction time has been found to hamper the magnetic properties of Fe₃₀Co₇₀ magnetic nanoparticles. Thus, the exquisite properties of Fe₃₀Co₇₀ nanoparticles were observed at a reaction time of 10 min, however, they were suppressed as the reaction time was increased to 40 mins.

Key words: Bimetallic Nanoparticles, X-ray diffraction, Low-voltage Field Emission Scanning Electron Microscopy.

Electron Spin Resonance of Atoms on a Surface

Yujeong Bae^{*}

¹Center for Quantum Nanoscience, Institute for Basic Science (IBS), Seoul 03760, Republic of Korea

²Ewha Womans University, Seoul 03760, Republic of Korea

^{*}Email: bae.yujeong@qns.science

Combining the spin-polarized scanning tunneling microscopy (STM) with electron spin resonance (ESR) [1] enables us to investigate spin states of single atoms and inter-atomic coupling with unprecedented spatial and energy resolution. Employing ESR-STM, we have characterized the magnetic dipolar [2], exchange [3,4], and even hyperfine interactions [5] of atoms on a surface. Such ESR experiments in STM have been performed measuring the ESR signals of atoms positioned directly under the tip. Beyond this single atom level, we present a new approach to control two electron spins simultaneously and independently. We found that it is possible to remotely control a spin, which is not directly under the tip, if we place a single-atom magnet next to it. This way to control the remote spin allowed us to control two spins in weakly coupled atoms. Our development widens the approaches to the multi-spin control in tailored spin structures on a surface.

References

- [1] Susanne Baumann et al., Science 350, 417 (2015).
- [2] Taeyoung Choi et al., Nat. Nanotechnol. 12, 420 (2017).
- [3] Kai Yang et al., Phys. Rev. Lett. 119, 227206 (2017).
- [4] Yujeong Bae et al., Sci. Adv. 4, eaau4159 (2018).
- [5] Philip Willke et al., Science 362, 336 (2018).

CoFe/MnIr 박막의 투자율 스펙트럼 분석

김동영*, 윤석수

안동대학교 물리학과

교환 바이어스 특성을 갖는 강자성/반강자성 박막은 HDD헤드 및 MRAM의 고정층으로 사용되고 있다. 강자성/반강자성 박막에서는 일방 이방성 에너지에 의한 교환 바이어스 특성과 함께 반강자성 재료의 두께에 따라 회전 이방성 에너지 특성, **training** 효과, 자기 점성 효과, 보자력 증가 현상 등 다양한 현상들이 나타나고 있다. 이러한 현상들은 강자성/반강자성 박막의 교환 결합 특성에 기인하며, 각각의 특성은 투자율 스펙트럼을 통하여 분석되고 있다. 본 연구에서는 다양한 현상들의 원인을 분석하기 위하여 CoFe/MnIr 박막의 저주파수 영역과 초고주파수 영역의 투자율 스펙트럼 측정 하였다. 저주파수 투자율은 자기저항 센서의 자체 자기장 측정법을 사용하였으며, 초고주파수 투자율은 마이크로파 투자율 측정 장치를 활용하였다. 저주파수에서 측정된 자기점성 효과는 강자성층을 따라 회전하는 반강자성층의 이환 특성과 초고주파수에서 반강자성층의 고정 특성을 연결시키는 매개 역할을 한다. 이러한 반강자성층의 이환 특성은 강자성/반강자성 박막에서 나타나는 다양한 현상들의 원인 규명에 활용될 수 있다.

Charge Trapping Memory Device Based on MoS₂ FET with CrPS₄

Minjeong Shin^{1*}, Mi Jung Lee¹, Chansoo Yoon, Gwangtak Oh¹, Woohyeon Ryu¹,
Sungmin Lee², Je-Geun Park², Bea Ho Park^{1*}

¹Affiliation A, Korea Division of Quantum Phase and Devices, Department of Physics,
Konkuk University, Seoul 05029

²Center for Quantum Materials & Department of Physics and Astronomy, Seoul National University, Seoul 08826

Atomically thin two-dimensional (2D) materials have emerged as promising candidates for flexible and transparent electronic applications [1, 2]. Here, we introduce non-volatile charge trapping memory devices, based on the 2D heterostructure field-effect transistor consisting of a few-layer MoS₂ channel and CrPS₄ charge-trapping gate stack. Clockwise hysteresis behaviors in transfer curves measured at room temperature show a strong dependence on the thickness of CrPS₄, which are attributed to charge trapping at trap sites in the CrPS₄ layers. Our heterostructure memory device with 75 nm-thick CrPS₄ layer exhibits both large memory windows up to 99.7 V and a high on/off current ratio (3×10^5) with good endurance during 625 cycles because of its excellent trapping ability of trap sites in the CrPS₄. Especially, the memory window size can be effectively tuned from 7.6 V to 99.7 V by changing the sweep range of gate voltage. Such high performances of the charge trapping memory device with a simple heterostructure provide a promising route towards next-generation memory devices utilizing 2D materials.

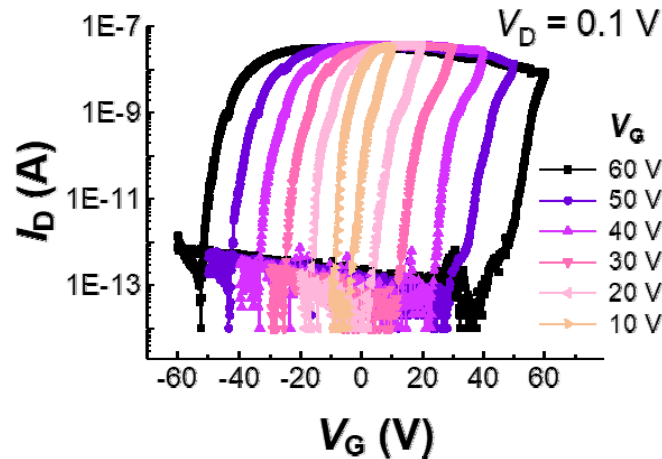


Fig. 1. Transfer characteristics of MoS₂ FET on bulk-like CrPS₄ with different sweeping range of V_G from 10 V to 60 V at $V_D = 0.1$ V.

Effect of Underlayer, CoFeB Composition and Annealing Temperature on Perpendicular Magnetic Anisotropy of CoFeB

Han Seok Ko*, Taehyun Kim, Jiyoung Lee, Young Keun Kim

Department of Materials Science and Engineering, Korea University, Seoul 02481, Republic of Korea

Recently, magnetic random access memory (MRAM) is getting attention as a next-generation memory device due to its high speed performance, low power consumption and long life span. Among several elements that consist of MRAM, magnetic tunnel junction (MTJ) structure is the most essential part as it directly governs writing and reading mechanism of MRAM. As MTJ with perpendicular magnetic anisotropy (PMA) have advantage of small switching current density over in-plane magnetic anisotropy MTJ, magnetic materials exhibiting perpendicular magnetic anisotropy (PMA) have attracted a lot of research interest [1]. Although previous studies presented several ferromagnetic material systems exhibiting PMA characteristics, including rare-earth transition-metal alloys, the MTJs with these alloys loss PMA after post-annealing process above 200°C [2]. Among the potential candidates, CoFeB/MgO is one of the most promising candidates with strong PMA even after 300°C post-deposition annealing process [3]. Here, we investigate the magnitude of PMA in underlayer/Co_xFe_{1-x}B/MgO structure by varying the materials of underlayer, composition of Co and Fe of CoFeB alloy and annealing temperature. Two different underlayers of W and Ta, which are known for their large spin-orbit coupling are used in this experiment [4]. Co₄₀Fe₄₀B₂₀ and Co₂₀Fe₆₀B₂₀ are used to compare their PMA characteristics. Co₄₀Fe₄₀B₂₀ is known to be advantageous over Co₂₀Fe₆₀B₂₀ as it requires small switching current density due to its small saturation magnetization (M_s) [5] and Co₂₀Fe₆₀B₂₀ is well known for its strong PMA [6]. Furthermore, 300°C and 400°C annealing temperatures were selected to examine each sample's thermal annealing stability since the temperature is maintained at 300°C-400°C during the back-end-of-line process. Microstructures of Ta and W were evaluated using X-ray diffraction (XRD). In the case of W underlayer, Co₄₀Fe₄₀B₂₀ exhibited PMA at 300°C and 400°C, while Co₂₀Fe₆₀B₂₀ exhibited PMA only at 400°C. In the case of Ta underlayer, Co₄₀Fe₄₀B₂₀ exhibited PMA at 300°C but it vanished at 400°C. The PMA characteristics of Co₂₀Fe₆₀B₂₀ with Ta underlayer was strong 300°C and weakened at 400°C. In addition, to investigate the effect of the annealing condition, 400°C annealing process was divided into three methods, direct 400°C annealing process, 300°C annealing followed by 400°C heat annealing, and 200°C annealing followed by 300°C annealing and then 400°C annealing. However, all these three processes showed the same result. From the experimental results, we have shown a rough guideline for selecting material combinations at different annealing temperatures with PMA.

References

- [1] M. Nakayama et al., Spin transfer switching in TbCoFe/CoFeB/MgO/CoFeB/TbCoFe magnetic tunnel junctions with perpendicular magnetic anisotropy J. Appl. Phys. 103, 07A710 (2008).
- [2] H. Ohmori et al., Perpendicular magnetic tunnel junction with tunneling magnetoresistance ratio of 64% using MgO (100) barrier layer prepared at room temperature.

- [3] S. Ikeda et al., A perpendicular-anisotropy CoFeB–MgO magnetic tunnel junction, *Nat. Mat.* 9, 721–724 (2010)
- [4] Y. Takeuchi et al., Spin-orbit torques in High-Resistivity-W/CoFeB/MgO, *Appl. Phys. Lett.* 112, 192408 (2018)
- [5] W. X. Wang et al., The perpendicular anisotropy of Co₄₀Fe₄₀B₂₀ sandwiched between Ta and MgO layers and its application in CoFeB/MgO/CoFeB tunnel junction., *Appl. Phys. Lett.* 99, 012502 (2011)
- [6] M. Yamanouchi et al., Dependence of magnetic anisotropy on MgO thickness and buffer layer in Co₂₀Fe₆₀B₂₀-MgO structure, *J. Appl. Phys.* 109, 07C712 (2011)

Stoner-Wohlfarth Model with Standard Deviation of Magnetic Easy Axis to Understand Magnetization Switching of Granular Films

Donghyeon Lee^{1*}, Donghyeon Han², Seyeop Jung¹, Nyunjong Lee¹,
Suzuki Ippei³, Takahashi Yukiko³, Sanghoon Kim^{1*}

¹Department of Physics, University of Ulsan, Korea

²Department of Physics, Korea Advanced Institute of Science and Technology, Korea

³National Institute for Materials Science (NIMS), Tsukuba 305-0047, Japan

A granular magnetic thin film is a well-known material system for achieving an ultra-high density recording media. Such nano-scale segregation of magnetic elements with excellent thermal stability can be made in the thin film. This material system typically consists of small grains in a few nanometers scale which is isolated by few nanometer-thick boundary. FePt-C is the most popular material for the hard disk drive industry. In general, L1₀-structured FePt grains surrounded by C are placed on an MgO layer. Grain size in the film varies in a range between 7 nm~20 nm. Magnetic easy axis of each grain is also deviated from the vertical direction to the plane.

In this presentation, we suggest the Stoner-Wohlfarth model with the standard deviation of the magnetic easy axis to understand the magnetization switching behavior of the FePt-C thin film. From our model, we can quantify a degree of deviation of the magnetic easy axis in the FePt-C granular film.

Magnetic difference with MoS₂ and Oxidized MoS₂ fabricated by Local chemical modification

DaYea Oh^{1*}, Duk Hyun Lee², Won Dong Kim², Woo Hyeon Ryu¹,
Gwang Taek Oh¹, Jong Wan Son¹, Bae Ho Park^{1*}

¹Department of Physics, Konkuk University, Seoul 05029, South Korea

²Quantum Technology Institute, Korea Research Institute of Standards and Science, Daejeon 34113, Korea

As the demand for nano scaled devices is increasing, Two dimensional (2D) materials have been theoretically and experimentally investigated in the last few decades. Among 2D materials, TMD(Transition Metal Dichalcogenide) materials which have layered structure shows extensively magnetic, electrical, and mechanical properties. Especially, hydrogenation of MoS₂ by high temperature and MoS₂ irradiated by proton shows unexpected ferromagnetic behavior which would lead to new spintronics devices.

In this works, we fabricate locally hydrogenated or oxidized MoS₂ using AFM lithography and confirm specific magnetic properties. Through Raman measurement, we identify that the pure MoS₂ surface modify hydrogenated or oxidized one under different lithographic condition. Also, Magnetic Force Microscopy (MFM) measurement support that hydrogenated or oxidized MoS₂ using AFM lithography shows novel magnetic properties comparing with pristine MoS₂. This result may attribute to the H or O atoms deposited on MoS₂ defect by AFM lithography.

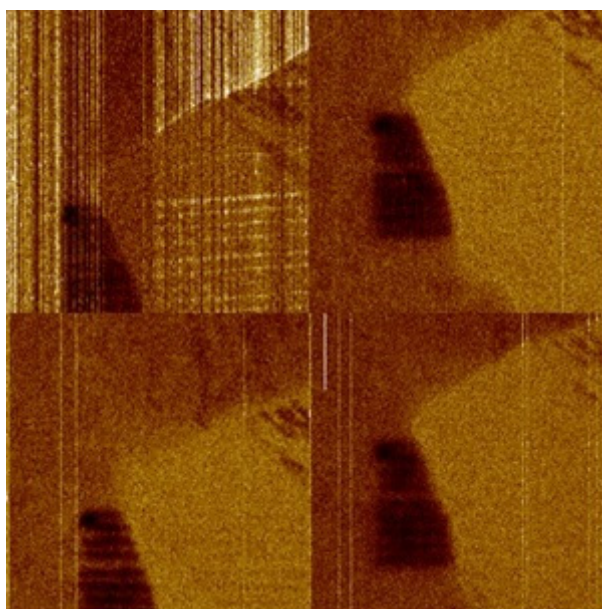


Fig. 1 MFM image of hydrogenated MoS₂ applied 1T of -1T

Manipulation of Magnetic Skyrmion by Localized Magnetic Field

Sooseok Lee^{1*}, Hee-Sung Han^{1,2}, Dae-Han Jung¹, Myeonghwan Kang¹,
Hye-Jin Ok¹, Namkyu Kim² and Ki-Suk Lee^{1†}

¹Department of Materials Science and Engineering, Ulsan National Institute of Science and Technology,
Ulsan 44919, Republic of Korea

²Center for X-ray Optics, Lawrence Berkeley National Laboratory, Berkeley, CA94720, USA

The magnetic skyrmions are particle-like swirling magnetic configurations characterized by topological numbers. They have been attracted much attention due to highly promising information carriers in spintronic device applications.[1-5] For practical applications, such information carriers must be written and deleted in a specific area of the magnetic thin film. In this presentation, we report experimental demonstrations of creating and removing skyrmions through a local magnetic field in the Pt/Co/Ta multi-layered film with perpendicular magnetic anisotropy (PMA). We utilized a highly localized stray field (H_{tip}) induced by magnetized tip of the magnetic force microscopy (MFM) for applying a local magnetic field [6]. As the tip-sample distance is decreases, H_{tip} becomes stronger and it reaches to the switching field of the PMA film, and the magnetization direction of the films can be switched locally and it induces creation of the magnetic skyrmions. Depending on the tip magnetization, the skyrmion polarization can be selectively reversed, as well as they can remain stably without an external magnetic field [7]. Furthermore, we demonstrated manipulation of a single skyrmion in confined geometry. We also investigated the stability of the magnetic skyrmions and compared it with that of the stripe domains. Our findings can provide a useful manipulation method for skyrmion based spintronic devices.

References

- [1] W. Kang *et al.*, *IEEE Electron Device Lett.*, **37**, 924–927 (2016)
- [2] G. Yu *et al.*, *Nano Lett.*, **17**, 261–268 (2017)
- [3] A. Fert, V. Cros, and J. Sampaio, **8**, 152–156 (2013)
- [4] R. Tomasello *et al.*, *Sci. Rep.*, **4**, 1–7 (2014)
- [5] S. L. Zhang *et al.*, *Nat. Commun.*, **9**, 2115 (2018)
- [6] A. Casiraghi *et al.*, *Commun. Phys.*, **2**, 1–9 (2019)
- [7] S. Lee *et al.*, *J. Magn.*, **25**, 458–462 (2020)

Stochastic Switching in Array of Co/Pt Nanodisks

Hee-Sung Han^{1,3*}, Sooseok Lee¹, Soong-Geun Je², Myeonghwan Kang¹, Hye-Jin Ok¹,
Namkyu Kim¹, Weilun Chao³, Mi-Young Im^{3*} and Ki-Suk Lee^{1†}

¹School of Materials Science and Engineering, Ulsan National Institute of Science and Technology,
Ulsan 44919, Republic of Korea

²Department of Physics, Chonnam National University, Gwangju 61186, Korea

³Center for X-ray Optics, Lawrence Berkeley National Laboratory, Berkeley, CA94720, USA

The stochastic switching characteristic of nanomagnets is the critical factor for realizing probabilistic computing based on the random fluctuation of magnetic state unit called probabilistic bit (p-bit). [1-4] A magnetic tunneling junction (MTJ) consisting of a patterned magnetic element is considered as a promising computing unit in the concept of artificial neurons and p-bits. [5,6] To realize computing nanodevices utilizing patterned magnetic units such as MTJ, extensive study on stochastic reversal of individual magnetic elements and their collective nature within arrays is essential. In this presentation, we show the stochastic behavior in the switching process of a perpendicularly magnetized Co/Pt disk within an array was directly observed utilizing full-field soft X-ray microscopy. [7] Within 50 repeated hysteretic cycles, we found the switching field for individual disks stochastically fluctuates and the stochasticity considerably depends on the disk size. We also observed that the trend of stochasticity can be changed with enlarging the disk radius due to multi-level switching in a disk. This work provides a comprehensive understanding of the intrinsic nature of the switching process in the Co/Pt disks within arrays and also paves the way for controlling the stochastic switching character for probabilistic computing.

References

- [1] Sethna, J. P.; Dahmen, K. A.; Myers, C. R. Crackling noise. *Nature*, 2001, **410**, 242–250.
- [2] Ryu, K.-S.; Akinaga, H.; Shin, S.-C. Tunable scaling behaviour observed in barkhausen criticality of a ferromagnetic film. *Nat. Phys.*, 2007, **3**, 547–550.
- [3] Devolder, T.; Chappert, C.; Katine, J. A.; Carey, M. J.; Ito, K. Distribution of the magnetization reversal duration in subnanosecond spin-transfer switching. *Phys. Rev. B*, 2007, **75**, 064402.
- [4] Petta, J. R.; Weissman, M. B.; Durin, G. Dependence of Barkhausen pattern reproducibility on hysteresis loop size. *Phys. Rev. E*, 1997, **56**, 2776.
- [5] Camsari, K. Y.; Faria, R.; Sutton, B. M.; Datta, S. Stochastic p-Bits for Invertible Logic. *Phys. Rev. X*, 2017, **7**, 031014.
- [6] Mizrahi, A.; Hirtzlin, T.; Fukushima, A.; Kubota, H.; Yuasa, S.; Grollier, J.; Querlioz, D. Neural-like computing with populations of superparamagnetic basis functions. *Nat. Comm.*, 2018, **9**, 1533.
- [7] Fischer, P.; Kim, D.-H.; Chao, W.L.; Liddle, J.A.; Anderson, E.H.; Attwood, D.T. Soft X-ray microscopy of nanomagnetism. *Materials Today*, 2006, **9**, 26–33

Optimization of spin Seebeck properties in YIG thin film by tuning the PVP concentration in MOD solution

Trinh Nguyen Thi, Phuoc Cao Van, Jong-Ryul Jeong^{*}

Department of Materials Science and Engineering, Graduate School of Energy Science and Technology,
Chungnam National University, Daejeon 34134, South Korea

In this study, we have investigated the dependence of the surface morphology and spin Seebeck effect (SSE) voltage on the poly[vinylpyrrolidone](PVP) concentration of polycrystalline $\text{Y}_3\text{Fe}_5\text{O}_{12}$ (YIG) ultrathin films on Silicon (Si) substrate synthesized by metal-organic decomposition (MOD) followed by the post annealing process. During the fabrication process, PVP concentration was systematically tuned from 0.5 to 2g meanwhile, all other conditions were fixed. By measuring the atomic microscope (AFM) and grazing incidence X-ray diffraction (GI-XRD), we realized the strong dependence of crystallinity and sample morphology on the PVP concentration. The 1g-PVP sample showed the smoothest surface with a root mean square (RMS) roughness of 0.2 nm. And it also has the best bulk uniformity which was exhibited through the shape and intensity of the XRD reflection peaks. This was further confirmed by scanning electron microscope (SEM) measurements of the cross-section of samples that presented uniform film without any pores. The SSE measurement was performed to obtain the output SSE voltage (VSSE) of all samples which is additionally patterned a Platinum (Pt) layer as a spin detection layer. Repeatedly, the 1g-PVP presented the highest performance which indicates the importance of the crystallinity as well as morphology to the spin-to-charge conversion efficiency of YIG films.

Keywords: $\text{Y}_3\text{Fe}_5\text{O}_{12}$ (YIG), poly[vinylpyrrolidone] (PVP), Spin Seebeck effect (SSE), metal-organic decomposition (MOD).

Majority gate logic using current-induced magnetic domain wall motion

San Ko^{1*}, Geun-Hee Lee¹, Byong-Guk Park² and Kab-Jin Kim¹

¹Department of Physics, KAIST, Daejeon 34141, Korea

²Department of Materials Science and Engineering, KAIST, Daejeon 34141, Korea

Existing computing technology is based on von Neumann architecture which is composed of memory unit for storing information and processing unit for performing logic operation. As the memory and processor are physically separated, data transfer between them consumes a substantial energy and time, which is known as von Neuman bottleneck. One way to overcome this bottleneck is to combine the memory and processor in a single space. This so-called processor in memory (PiM) technology will improve the performance of computer dramatically [1].

In this presentation, we propose a majority gate logic that utilizes the current-induced magnetic domain walls (DWs) motion, which can directly be connected to the DW-based racetrack memory [2,3,4] to build PiM. We use cross-wire geometry having four discrete branches, of which three branches are inputs and the other branch is output, and demonstrate that the cross-wire performs as majority gate by using micromagnetic simulations. The DWs created at the input branches are moved by current-induced spin orbit torque [5,6] and are congregated at the cross, from which the majority of the inputs are ejected to the output branches. This majority gates operates as AND, OR, NAND, NOR logic operations by properly selecting the inputs. In addition to the simulation, we also experimentally verify the DW-based majority gate in Co/Pt microwires. The current-driven DW motion and its logic operation is successfully demonstrated in Co/Pt cross-wire, suggesting that the majority gate is experimentally achievable.

References

- [1] H. S. Stone. IEEE Transactions on Computers, **C-19**, 73 (1970)
- [2] S. S. P. Parkin, US Patent 6834005 (2004)
- [3] S. S. P. Parkin *et al.* Science **320**, 190 (2008)
- [4] S. S. P. Parkin *et al.* Nature Nanotechnology **10**, 195-198 (2015)
- [5] S. Emori *et al.* Nature Materials **12**, 611-616 (2013)
- [6] K.S. Ryu *et al.* Nature Nanotechnology **8**, 527-533 (2013)

TMR sensor development for ultra-high frequency field applications

Seungha Yoon^{*}

Korea Institute of Industrial Technology, 6 Cheomdangwagi-ro, Buk-gu, Gwangju, South Korea

The high sensitivity of the magnetic sensors in the working field ranges could be the final goal to develop the magnetic sensors. However, the trade-off between the sensitivity and the working range limits its magnetic sensor for the various industrial applications. The working field range can be manipulated by the shape anisotropy of the element, different exchange couplings, and the magnetic material itself. The signal improvement has been well achieved by the Tunneling magnetoresistance (TMR) sensor, well known as a best magnetic sensor with the maximized output voltage depending on the magnetic field. In addition, the TMR sensor is now getting started to be utilized in various industrial items to exchange the old magnetic sensors.

So far most magnetic sensors have been focused on the static field or very low frequency field. And there are just a few studies on the future spintronic applications using ultra-high frequency magnetic fields, such as superconducting motors, magnetic bead for bio health, and magnetic resonance devices. In this study, the key issues for developing TMR sensors for measuring ultra-high frequency magnetic fields in terms of the structure of the TMR and the bridge circuits.

Individual and Collective Locomotion Control of Magnetic Microrobots Using a Single Electromagnet System

Seungchan Hwang¹, Armando Ramos Sebastian^{2*}, Minseo Goo¹,
Changho Yu², Sung Hoon Kim^{1,3†}

¹Department of Electronics Convergence Engineering, Wonkwang University, Korea

²Department of IT Convergence Mechatronics Engineering, Jeonbuk National University, Korea

³Wonkwang Institute of Materials Science and Technology, Wonkwang University, Korea

Locomotion of magnetic microrobots requires the use of several coils, ranging from a pair of coils for one-dimensional motion up to tens of coils for complete three-dimensional motion. This can result in voluminous, high-power consuming, and expensive electromagnetic systems that require complicated control algorithms. In this paper we present a novel single electromagnet system for two-dimensional locomotion of magnetic microrobots at a liquid surface. Taking advantage of the tendency of magnets to move toward the point of maximum magnetic field, we created a “trapping point” located at the axis of the electromagnet to confine a magnetic microrobot within it. To create the trapping point we balance the gravity, buoyancy, and magnetic forces acting on the magnetic robot to constrain the microrobot to the surface of the liquid at the position of the local point of maximum magnetic field. Then, the location of the trapping point along the fluid surface is changed through a set of rotations of the coil, by using a parallel robot. Due to the implementation of a trapping point, this new electromagnetic system can perform two-dimensional control of individual magnetic microrobots and swarms of magnetic microrobots. This results in a relatively smaller, cheaper, and lower-power system with simple controls that can achieve precise position control, even in open-loop systems. The improvements in efficiency make this approach suitable for a wide range of biomedical applications.

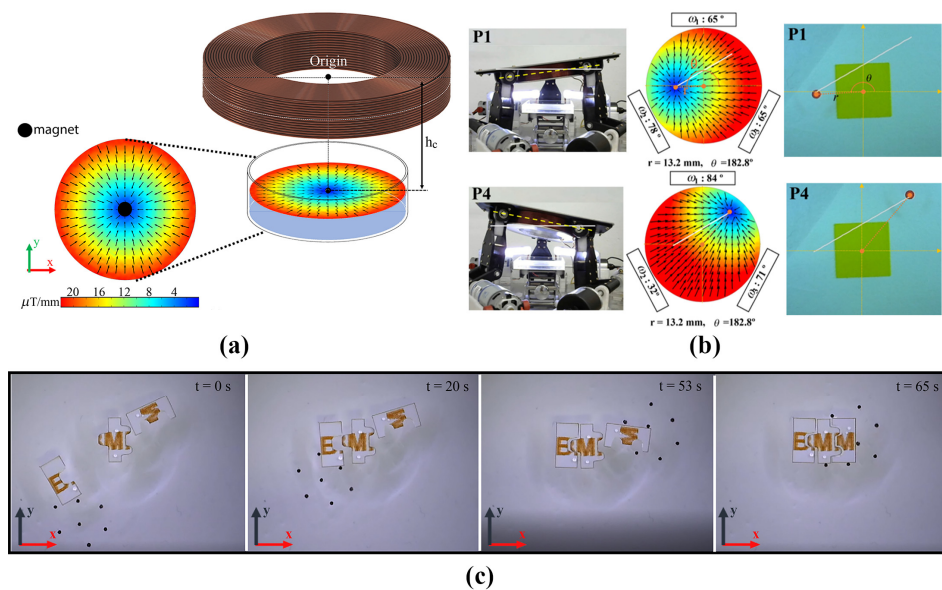


Fig. 1. (a) Trapping point mechanism. (b) Single microrobot locomotion control. (c) Magnetic swarm locomotion control.

Using Amorphous CoB Alloy as Transducer to Detect Acoustic Propagation and Heat Transport at Interface

Liu Jina^{*}, Gyung-Min Choi

Department of Energy Science, Sungkyunkwan University, Suwon 16419, Korea

Acoustic oscillation provides useful information regarding the interfacial coupling between metal transducer layers and substrate materials. The interfacial coupling can be significantly reduced by a mechanically soft layer between the transducer and substrate. However, preserving a thin, soft layer at the interface during fabrication is often challenging. In this study, we demonstrate that an amorphous CoB alloy on top of a sapphire substrate can substantially amplify acoustic oscillations. By analyzing the attenuation of acoustic oscillations, we show that a thin, soft layer with a thickness of $>2 \pm 1 \text{ \AA}$ exists at the interface. The intermediate layer at the interface is further verified by investigating heat transport. By analyzing the slow decrease of the temperature of the transducer layer, we determine a thermal conductance of $35 \pm 5 \text{ MW m}^{-2} \text{ K}^{-1}$ at the transducer/substrate interface. This low value supports the existence of a thin, soft layer at the interface. Our results demonstrate that an amorphous metal with B alloying effectively preserves the soft nature at the interface and detects the acoustic propagation and heat transport across it.

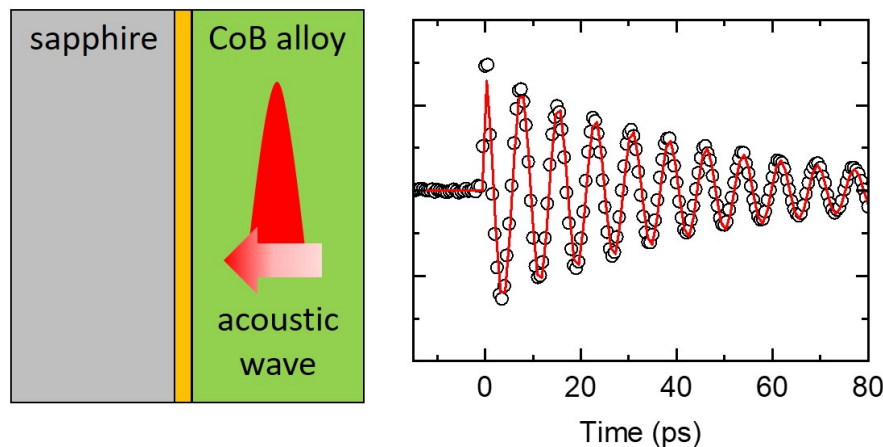


Fig. 1. Schematics for acoustic oscillation in CoB transducer

Modified torque magnetometry to determine magnetic anisotropy

Joonyoung Choi, In Hyuk Jo, Youn Jung Jo^{*}

Department of Physics, Kyungpook National University, Daegu 41566, Korea

We present a novel method for magnetic anisotropy measurement using membrane-type surface stress sensor (MSS). This sensor has a silicon membrane supported by four beams incorporating piezoresistive paths [1]. We modified the on-chip aluminum interconnect on the MSS to obtain more magnetic information of the material and used it for torque measurement. Angle-dependent torque measurement of magnetic materials were performed by rotating the device with respect to the applied magnetic field. Instead of one existing Wheatstone Bridge, we modified the on-chip aluminum interconnect to become two Wheatstone bridge circuits. These variations will allow simultaneous investigation of magnetic responses according to different crystallographic directions in a two-dimensional plane.

Reference

- [1] H. Takahashi et al., J. Phys. Soc. Jpn. 86, 063002 (2017).

Machine learning based Human Activity Recognition with mobile 3-axis magnetometers

Chunghee Nam*

Department of Electrical and Electronic Engineering, Hannam University, Daejeon 34430, Korea

Recently, human activity recognition (HAR) plays an important role in well-being life and context-aware IoT systems. HAR can be carried out in real-time by using sensory data collected from embedded sensor networks in mobile smart phones. Recent HAR investigations have shown that is solely based on 3-axis accelerometers, which is the most energy-efficient approach. In this presentation, I propose a simple approach for HAR process with built-in 3-axis magnetometers in a smart phone. Based on deep learning with convolutional neural network(CNN), I found 98% accuracy for 4 -classes (standing, sitting, jogging, and walking).

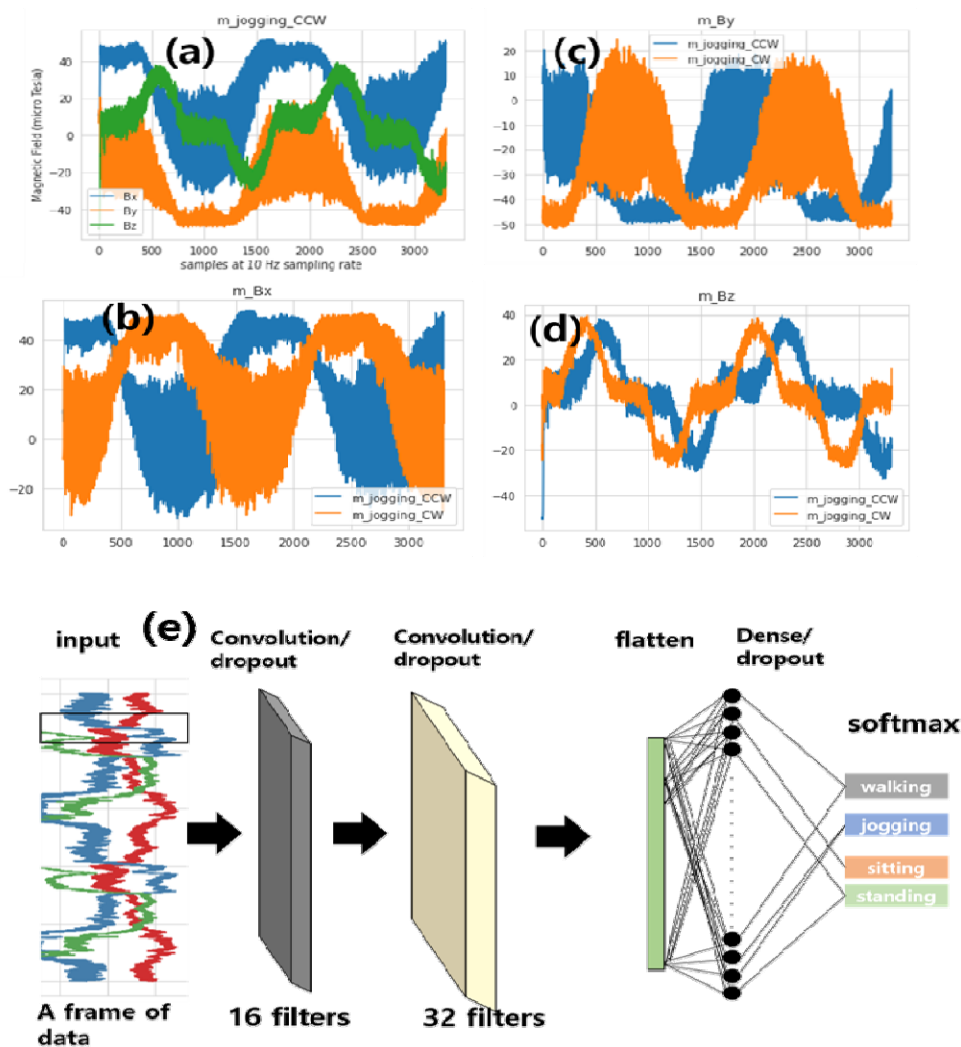


Fig. 1. (a)~(d) 3-axis magnetometer sensor data and (e) CNN network

A New Strategy of Finger Rehabilitation: Wireless Magnetic Actuation for Pinch motion

지동민^{1*}, 송원일¹, 김성훈^{1,2}

¹원광대학교 전자융합공학과

²원광재료과학기술연구소

뇌졸중을 겪고 있는 환자의 80% 이상은 운동 마비 증상을 겪는다. 또한 뇌졸중 환자 이외에도 관절이 약한 노약자들도 재활치료를 필요로 한다. 엄지와 검지를 사용하여 집는 운동은 물체를 정밀하게 잡고 고정하는데 중요하다. 따라서 엄지와 검지 재활은 손 재활 분야에서 매우 중요하다. 현재 개발되고 있는 재활 기기는 기계적 구조가 복잡하고, 와이어 등을 연결해 모터 동력을 전달하는 방식을 사용하고 있다. 따라서 모터 오작동 시 환자의 추가적인 부상을 발생시킬 수 있고, 환자의 손 상태에 따라 사용이 불가능한 단점이 있다. 본 연구에서는 재활 운동의 편의성을 고려하여 두 손가락 끝에 부착한 자석에 발생하는 자기력과 자기 돌림힘으로 구동되는 무선 재활기기를 개발하였다. 이 장치는 두 개의 자석을 연결하는 연결 조인트와 각 자석의 회전 조인트를 통해 자연스러운 꼬집는 동작을 구현한다. 제작된 장치는 최소한의 기계적 구조와 가벼운 재료를 사용해 57.2g의 가벼운 무게를 가지며, 손가락 끝 부분에 부착하는 간단한 착용 방식으로 환자의 손 상태에 따른 제약을 받지 않는다. 전자기 코일에서 교번 자기장을 발생시켜 반복적인 훈련을 수행할 수 있으며, 운동 강도와 속도를 선택해 사용할 수 있다. 3D 프린터와 인공 힘줄을 사용해 손가락 모델을 제작하고 개발된 재활 장치에 의해 발생하는 손가락 움직임을 관찰하고, 위치와 자기장의 세기에 따라 손가락 끝 부분에 발생하는 힘을 측정하였다. 다양한 실험과 자기 시뮬레이션을 통해 제안하는 무선 재활기기의 구동 방법 및 성능을 검증하였다. 본 연구에서 제안하는 재활기기는 기존의 로봇 메커니즘을 사용하는 방식과는 다르게 무선 구동, 가벼운 무게, 단순한 구조, 편리한 착용 방식으로 환자에게 뛰어난 편의성을 제공한다.

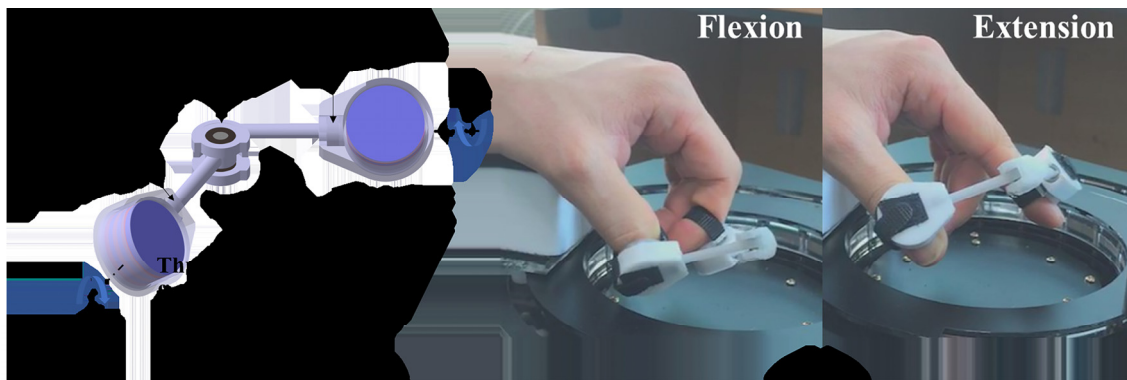


Fig. 1. Configuration of the proposed device

Optimization of Polycrystalline-YIG with a High Magnetization *via* the Correlation Between Mechanical Compression and Heat-Treatment in the Sol-Gel Synthesis

Hye-Jin Ok^{1*}, Min-Sun Jang², Inseon Oh¹, Jung-Woo Yoo¹ and Ki-Suk Lee¹

¹Department of Materials Science and Engineering, Ulsan National Institute of Science and Technology (UNIST), Ulsan 44919, Republic of Korea

²Metal Powder Department, Korea Institute of Materials Science (KIMS), Changwon 51508, Republic of Korea

Since Yttrium-iron-garnet ($\text{Y}_3\text{Fe}_5\text{O}_{12}$, YIG) discovered, it as a ferrimagnetic insulator can be applied in many fields such as spintronics and optoelectronic devices [1] because it has distinguished dynamic magnetic and optical properties [2-3]. Many studies were focused on the improvement of efficiency from applicated devices such as spin-thermoelectric by single crystal YIG of thin-film [4-5] due to its excellent magnetic properties. However, the thin-film type of single-crystal YIG had limitations of fabrication and handling. To achieve applicate easier, therefore, many researchers have been developed methods for polycrystalline-YIG characterized as single-crystal YIG.

In our previous studies, we suggested the sol-gel synthesis, which included a compression step to be able to obtain the perfectly crystalized polycrystalline-YIG with a high saturation magnetization (M_s) value, 75% similarity to theoretical value [6]. Among the various synthesis methods, a sol-gel is the most appropriate to implement high uniformity, purity, and fine quality oxide although a low-cost process [7]. In the polycrystalline-YIG, the microstructure morphology and magnetic characteristics by a phase transition are able to affect by various variables in the synthesis process. This study is an extension of the previous results, through an optimized sol-gel process, YIG was manufactured with 3-steps external process included fixed mechanical compression at 350 MPa for 5 minutes at room temperature, various conditions of calcination at 250, 450, 650, and 850 °C, and fixed condition of sintering at 1400 °C for 4 hours in the air. Moreover, the polycrystalline-YIG had implemented two types as powder and bulk, for investigation of the correlation of compression and heat treatment at various temperatures on the microstructure morphology and magnetic characteristics. Here, we might suggest the mechanical compression process plays an important role in increasing the density and obtaining improved magnetic characteristics. Surprisingly, a comparison of two polycrystalline-YIGs with and without mechanical compression in the same heat treatment showed an approximately 3 times increase in M_s values when mechanical compression was applied. More specifically, it has a high M_s of 32 emu/g and a low coercive field (H_c) of 24 Oe which means to become a perfect ferrimagnetic insulator of polycrystalline-YIG. In the case of powder type, particles that agglomerated and densified through additional sintering processes were observed improved M_s value. On the other hand, for bulk type YIG, even if the additional sintering process was performed does not significantly affect the particle morphology and magnetic properties due to unable to tune particles by the process of agglomeration and densification from already been formed. Also, at different temperatures of calcination, it was confirmed that the M_s can be changed by the sequence of mechanical compression and heat treatment. In general, in the case of mechanical compression after heat treatment, M_s was about 1.5 times higher even though it was the same type of powder. Consequently, we exhibit dramatically effect of the correlation

between mechanical compression and heat treatment for synthesizing polycrystalline-YIG of similar magnetic properties that is able to use instead of a single YIG. Our results guarantee that it is expected to be applied as a material with potential in spintronics applications.

References

- [1] K. Uchida, et al., Appl. Phys. Lett., **97**, 172505 (2010).
- [2] N.P. Simonenko, et al., Russ. J. Inorg. Chem., **61**, 843 (2016).
- [3] V. Cherepanov, et al., Phys. Rep., **229**, 81 (1993).
- [4] J. Lustikova, et al., J. Appl. Phys., **116**, 153902 (2014).
- [5] M. Akyol, et al., J. Magn. Magn. Mater., **493**, 165704 (2020).
- [6] M.S. Jang, et al., J. Alloys Comp., **711**, 693 (2017).
- [7] C. B. Carter, et al., Ceramic Materials science and engineering

Landau Level Tomography, Valley Chern Number, Nernst Effect in Moiré Superlattices

J. A. Crosse^{1,2} and Pilkyung Moon^{1,2,3*}

¹Arts and Sciences, New York University Shanghai, Shanghai, China

²NYU-ECNU Institute for Physics at NYU Shanghai, Shanghai, China

³Department of Physics, New York University, New York, USA

Incommensurately stacked two-dimensional atomic layers, which is known as moiré superlattices, provide unique opportunity to study many exotic phenomena such as Hofstadter's butterfly [1, 2], superconductivity and strongly correlated phase [3].

In this talk, we will first show the theoretical analysis of the Landau level tomography, obtained by a nanoscale on-tip scanning superconducting quantum interference device [SQUID-on-tip, Fig. 1(a)], of magic-angle twisted bilayer graphene. The results enabled us to map the local variation of the interlayer twist angle with precision better than 0.002° , and show that the correlated states are fragile with respect to the twist angle disorder [4].

We will also discuss the Landau level and Hofstadter spectrum of twisted double bilayer graphene, and show that two different arrangements, AB-AB and AB-BA, which differ in relative orientation but have very similar band structures in the absence of a magnetic field exhibit completely different energy spectrum [Fig. 1(b)] due to the difference between the valley Chern numbers [5].

Finally, we will discuss the magnetothermoelectric effects in graphene on hexagonal boron nitride, and show the magnetic-field induced valley splitting with an effective g-factor of about 130, which is attributed to the emergence of an orbital magnetic moment at the van Hove singularity [Fig. 1(c)] [6].

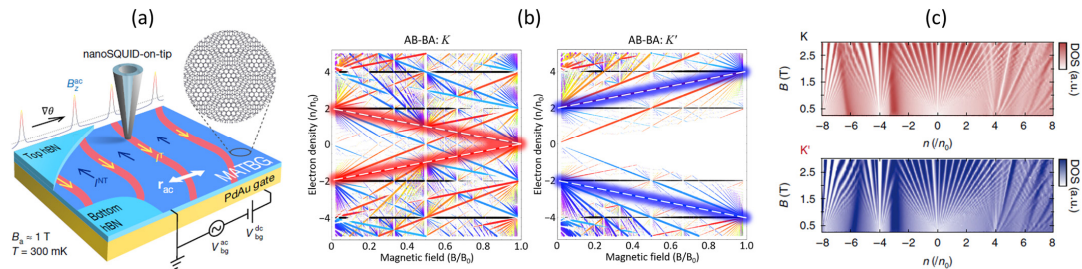


Fig. 1 (a) Experimental setup schematics of nano SQUID-on-tip over magic-angle twisted bilayer graphene.
 (b) Distinct Landau level gap structures of AB-AB and AB-BA twisted double bilayer graphene.
 (c) Density of states of graphene/hBN at different monolayer valleys.

References

- [1] Pilkyung Moon and Mikito Koshino, Phys. Rev. B 85, 195458 (2012).
- [2] C. R. Dean et al., Nature 497, 598 (2013); B. Hunt et al., Science 340, 1427 (2013).
- [3] Y. Cao et al., Nature 556, 44 (2018); Y. Cao et al., Nature 556, 80 (2018).
- [4] A. Uri et al., Nature 581, 47 (2020).
- [5] J. A. Crosse, N. Nakatsuji, M. Koshino, Pilkyung Moon, Phys. Rev. B 102, 035421 (2020).
- [6] R. Moriya et al., Nat. Commun. 11, 5380 (2020).

The effects of spin-Peierls distortion on thermoelectric properties: a first principle study of TiPO_4

Changhoon Lee^{1*}, Taesu Park², Ji Hoon Shim^{2,3}

¹Max Planck POSTECH Center for Complex Phase of Materials,
Pohang University of Science and Technology, Pohang, 37673

²Department of Chemistry, Pohang University of Science and Technology, Pohang, 37673, Korea

³Division of Advanced Materials Science, Pohang University of Science and Technology, Pohang, 37673, Korea

We investigated the effects of spin-Peierls distortion on thermoelectric properties by density functional theory calculations. The titanium(III) phosphate, TiPO_4 , which crystallize in the CrVO_4 structure type (space group Cmcm), shows low-dimensional magnetic properties and it undergoes a phase transitions towards a dimerized spin-Peierls state driven by the strong spin-exchange interactions. The spin-Peierls distortion increases a bandgap and generates peaks in the density of states at the conduction band minimum (CBM) and valence band maximum (VBM) which evolves strongly enhanced Seebeck coefficients. Consequently, a spin-Peierls distortion should be considered as an important factor to enhance the power factor (PF) of thermoelectric materials.

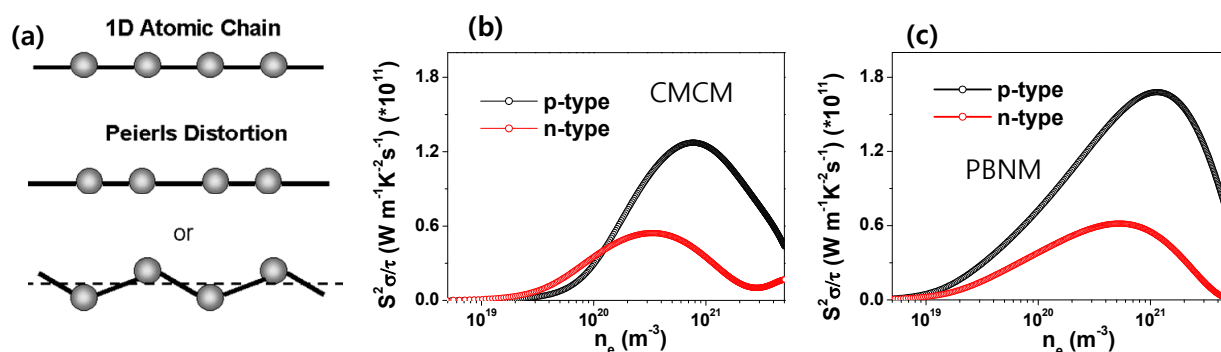


Fig. 1. (a) Schematic view of Spin Peierls distortion in one dimensional chain system. (b) the calculated PF for CMCM structure TiPO_4 , and (c) the calculated PF for PBNM structure TiPO_4 (Spin Peierls distortion)

희토류 자석합금의 균질화 및 HDDR 처리에 관한 연구

김상욱^{1*}, 김인호¹, 송창빈²

¹NATM(주) 기술연구소

²공주대학교 신소재공학부

최근 고성능 희토류 영구자석은 각종 가정용/산업용/국방용으로 사용되는 PC, 노트북 및 휴대용 스마트 통신기기, 발전기, 로봇, 의료기기 등 각종 전기·전자기기는 물론, “저탄소 녹색성장”을 기초로 하는 신성장 동력 산업으로 화두가 되고 있는 하이브리드 자동차(HEV), 전기자동차(EV), 풍력발전 등의 대표적/핵심적 부품소재로 그 수요가 급증하고 있을 뿐만 아니라, 그들 제품의 고효율화/소형화/경량화/고성능화 추세에 따라 보다 우수한 자기적 특성 향상 및 코스트 저감 등이 요구되고 있다. 그 일환으로 오래전부터 국내/외에서 자석합금의 제조법, 미세화기술, 배향/성형기술, 소결열처리, 코팅/착자, 고순도화 등 다양한 기초연구 및 기술개발이 활발하게 시도되어 왔다.

본 연구는 본 연구팀에 의해 수년전부터 새롭게 개발된 RSP냉각장치를 이용하여 Nd-Fe-B-X계 자석합금을 제조하였으며, 제조된 합금스트립의 HDDR처리전후의 미세조직 변화 및 자기적 특성을 주로 조사하였다.

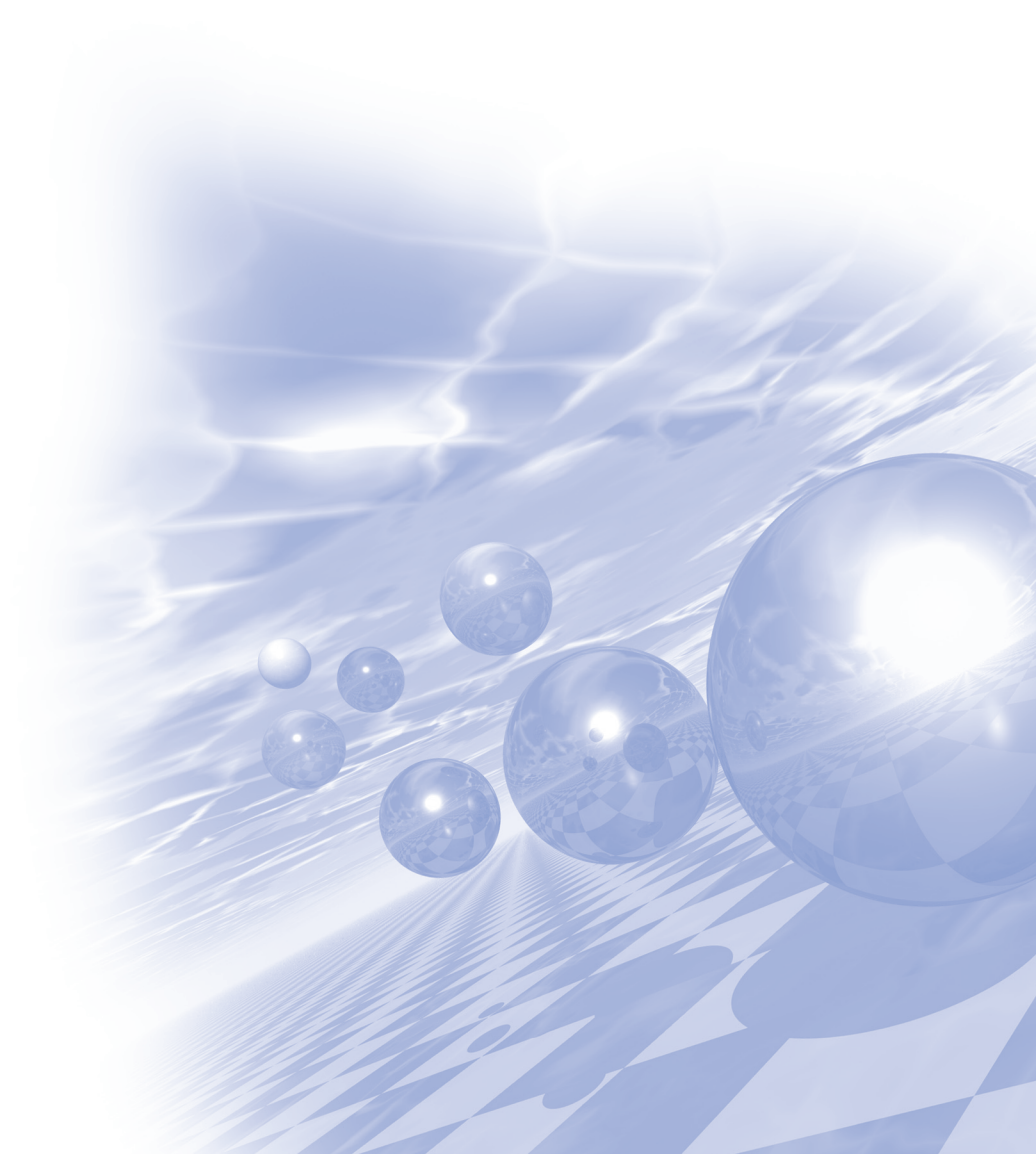
Keywords : 급속응고법(rapidly solidification process), 희토류 영구자석(rare-earth permanent magnet), 합금스트립(alloy strips), 미세편석(micro-segregation), HDDR(hydrogenation-disproportionation-desorption-recombination)



2021 KMS Summer Conference

Symposium 2

'Spintronics'



Antiferromagnetic Insulatronics: Spintronics without magnetic fields

Mathias Kläui^{1,2,3,*}

¹Institute of Physics, Johannes Gutenberg-University Mainz, 55128 Mainz, Germany

²Graduate School of Excellence Materials Science in Mainz, 55128 Mainz, Germany

³Centre for Quantum Spintronics, NTNU, 7034 Trondheim, Norway

*IEEE Magnetics Society Distinguished Lecturer

Klaeui@uni-mainz.de

While known for a long time, antiferromagnetically ordered systems have previously been considered, as expressed by Louis Néel in his Nobel Prize Lecture, to be “interesting but useless”. However, since antiferromagnets potentially promises faster operation, enhanced stability with respect to interfering magnetic fields and higher integration due to the absence of dipolar coupling, they could potentially become a game changer for new spintronic devices.

We recently realized switching in the metallic antiferromagnet Mn_2Au by intrinsic staggered spin-orbit torques [1,2] and characterize the switching properties by direct imaging. While switching by staggered intrinsic spin-orbit torques in metallic AFMs requires special structural asymmetry, interfacial non-staggered spin-orbit torques can switch multilayers of many insulating AFMs capped with heavy metal layers [3-5]. Furthermore electric fields can be used to generate strain to switch the AFM order parameter [6].

To read out the information, we demonstrate that we can obtain ultra-strong coupling from AFMs to ferromagnetic layers. This coupling leads to a perfect 1-to-1 imprinting of the AFM domain structure into the ferromagnet and read-out via established magnetoresistance effects (under review).

Finally, we study transport of spin in antiferromagnets. While typically spin transport lengthscales of a few nm have been reported for AFMs, for hematite, we find in a non-local geometry that spin transport of tens of micrometers is possible [7,8]. We detect a first harmonic signal, related to the spin conductance, that exhibits a maximum at the spin-flop reorientation, while the second harmonic signal, related to the Spin Seebeck conductance, is linear in the amplitude of the applied magnetic field [7]. The first signal is dependent on the direction of the Néel vector and the second one depends on the induced magnetic moment due to the field.

Recently we we also achieved transport in the easy plane phase [9], which allows us to obtain long distance spin transport in hematite even at room temperature [9,10]. This particular transport regime relies on the superposition of linearly polarized magnons to transport spin leading to a special field dependence of the transported spin polarization.

References

- [1] S. Bodnar et al., Nature Commun. **9**, 348 (2018)
- [2] S. Bodnar et al., Phys. Rev. B **99**, 140409(R) (2019)
- [3] L. Baldrati et al., Phys. Rev. Lett. **123**, 177201 (2019)
- [4] F. Schreiber et al., Appl. Phys. Lett. **117**, 082401 (2020); H. Meer et al., Nano Lett. **21**, 114 (2020)
- [5] L. Baldrati et al., Phys. Rev. Lett. **125**, 077201 (2020)

- [6] A. Barra et al., Appl. Phys. Lett. **118**, 172408 (2021)
- [7] R. Lebrun et al., Nature **561**, 222 (2018)
- [8] A. Ross et al., Nano Lett. **20**, 306 (2020)
- [9] R. Lebrun et al., Nature Commun. **11**, 6332 (2020)
- [10] A. Ross et al., Appl. Phys. Lett. **117**, 242405 (2020)

Electrical Spin Current Generation in Ferromagnets and Antiferromagnets

Vivek Amin^{1*}, Fei Xue^{2,3}, Paul Haney³, Mark Stiles³

¹Indiana University, Purdue University, Indianapolis

²University of Maryland, College Park

³National Institute of Standards and Technology, Gaithersburg

Electrical control of magnetic order has widespread applications for information and communications technology. One way to manipulate magnetic order in layered structures is to generate a spin current in a source layer that is absorbed by a nearby magnetic layer, causing a transfer of spin angular momentum or spin torque. Under an applied electric field, nonmagnetic, ferromagnetic, and antiferromagnetic materials all generate such spin currents. However, it is typically assumed that the spin torque occurs in a different layer than where the spin current was generated. For ferromagnetic and antiferromagnetic metals with appreciable spin-orbit coupling, conduction electrons can carry a substantial spin current flowing perpendicularly to the electric field with spin directions misaligned with the magnetic order parameter. In some cases, these symmetry-allowed spin currents can flow into the layer boundaries and exert substantial torques that can be measured through optical techniques such as MOKE. Thus, magnetic materials can be simultaneously the source and receiver of spin torques, suggesting a promising avenue to optimize electrical control of magnetic order.

In this talk, I discuss several mechanisms to electrically generate spin currents in ferromagnets, antiferromagnets, and magnetic interfaces. Each mechanism can have a different dependence on magnetization direction, crystal structure, and/or disorder. While measurements of spin torques at layer boundaries provide evidence of spin current generation, disentangling contributions from spin currents and from other sources remains an open challenge. We present both first principles and semiclassical transport calculations giving the strength and magnetization dependence of electrically generated spin currents in magnetic systems via intrinsic and/or extrinsic mechanisms. Shedding light on these mechanisms could help optimize electrical control of magnetic order with potential applications for information processing.

Two-dimensional magnetism and its spintronic device applications

Hyun Ho Kim^{*}

School of Materials Science and Engineering, Kumoh National Institute of Technology, Gumi, 39177, Korea

The family of two-dimensional (2D) materials has grown rapidly from semimetals and semiconductors to systems exhibiting collective electronic properties. In particular, several 2D magnetic compounds have been recently discovered. Experimental observations of the magnetic ground state in single atomic layers of such materials are not only important for fundamental interest, but also technologically relevant for next-generation spintronic devices. In this talk, I will present studies of atomically thin magnetic semiconductors CrX_3 ($X = \text{Cl}, \text{Br}, \text{and I}$) as well as their device applications. By sandwiching CrX_3 between few-layer graphene electrodes, we are able to fabricate high-quality van der Waals magnetic tunnel junctions and electrically probe the magnetic properties of the three materials. Moreover, we found that CrI_3 exhibits an extremely large tunnel magnetoresistance ($\sim 10^6\%$) as well as a robust memristive switching behavior that is tunable with magnetic field.

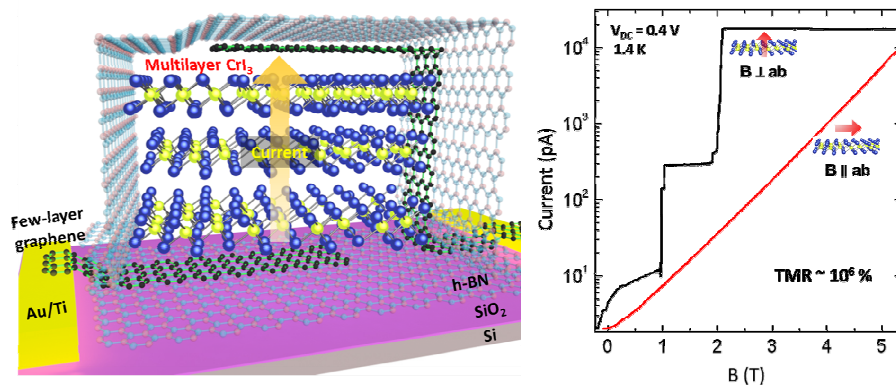


Fig. 1. Vertical van der Waals heterojunction device incorporating two-dimensional magnetic materials.

Out-of-plane spin polarization and antiferromagnetic spin Hall effect

Cheng Song^{1*}, Xianzhe Chen¹, Xiaofeng Zhou¹, Hyunsoo Yang², Feng Pan¹

¹Tsinghua University, China

²National University of Singapore, Singapore

The discovery of the spin Hall effect (SHE) enabled the efficient generation and manipulation of the spin current. The magnetic spin Hall effect provides a unique opportunity to control the spin current and relevant device performance with controllable magnetization. In this talk, we report the magnetic spin Hall effect both in non-collinear antiferromagnet Mn_3Pt and a collinear antiferromagnet Mn_2Au . We generate tiny out-of-plane polarized spin current (σ_z) when the charge current is applied along the axis perpendicular to the magnetic mirror plane of Mn_3Pt /permalloy bilayers, but robust when the current is parallel to the magnetic mirror plane in all of the Mn_3Pt films with different orientations. In Mn_2Au , the spin currents are generated at two spin sublattices with broken spatial symmetry, and the antiparallel antiferromagnetic moments play an important role. Therefore, we term the Néel vector-dependent spin Hall effect the ‘antiferromagnetic spin Hall effect’ (AFM-SHE). The out-of-plane spins from the antiferromagnetic spin Hall effect are favorable for the efficient switching of perpendicular magnetized devices, which is required for high-density applications. The antiferromagnetic spin Hall effect adds another twist to the atomic-level control of spin currents via the antiferromagnetic spin structure.

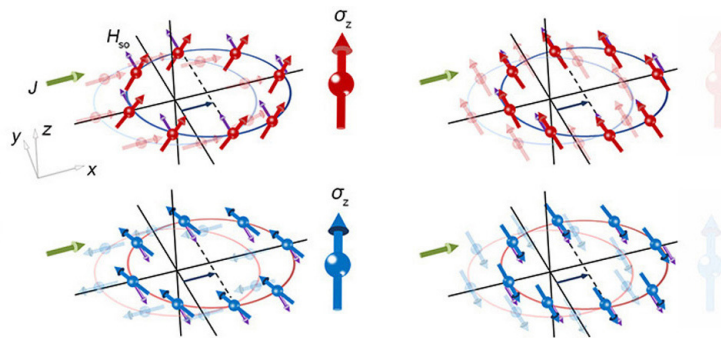


Fig. 1. Generation of σ_z via the AFM-SHE.

Electrical manipulation of non-collinear antiferromagnet

Shunsuke Fukami^{1,2,3,4,5*}

¹Research Institute of Electrical Communication, Tohoku University, Japan

²Center for Science and Innovation in Spintronics, Tohoku University, Japan

³Center for Spintronics Research Network, Tohoku University, Japan

⁴Center for Innovative Integrated Electronic Systems, Tohoku University, Japan

⁵WPI-Advanced Institute for Materials Research, Tohoku University, Japan

Electrical manipulation of magnetic materials has been of paramount interest in spintronics community for the last quarter century. Earlier studies focused on ferromagnetic materials and demonstrated magnetization switching, phase transition between ferromagnetism and para-magnetism, oscillation, resonance, and so on [1]. Among them, the spin-transfer torque induced magnetization switching has evolved into an essential ingredient in magnetoresistive random access memory technology, and other phenomena are also expected to be useful for new functional devices. In 2016, electrical manipulation of collinear antiferromagnet CuMnAs was demonstrated, where staggered spin-orbit torque was utilized [2]. Since the antiferromagnetic materials have been believed to have less chance of applications due to the difficulty to control the internal state, this study renewed the perception of spintronics research and opened a new paradigm, so-called antiferromagnetic spintronics. Besides, a very recent study [3] reported an electrical switching of non-collinear antiferromagnet, another type of antiferromagnets with chiral-spin structure exhibiting intriguing properties that was believed to be observed only in ferromagnets [4], where the observed phenomenon was explained by the same protocol with the spin-orbit torque induced switching of ferromagnetic materials [5,6]. So far, however, unique properties and functionalities of non-collinear antiferromagnet have not been unraveled.

Here I show a chiral-spin rotation in non-collinear antiferromagnet Mn₃Sn driven by the spin-orbit torque [7]; the phenomenon has no parallel in the research history of spintronics. We prepare cross-shaped Hall devices made of an epitaxial W/Ta/Mn₃Sn/Pt stack [8] and investigate the response of Hall resistance to the lateral current. We observe a characteristic fluctuation of the Hall resistance above a certain threshold, which can be consistently explained by considering persistent rotation of chiral-spin structure induced by the spin-orbit torque. We also find that the efficiency to manipulate the spin structure in this scheme is much higher than that in ferromagnet and collinear antiferromagnet.

The work has been carried out under a collaboration with Y. Takeuchi, Y. Yamane, J.-Y. Yoon, R. Itoh, S. DuttaGupta, B. Jinnai, S. Kanai, J. Ieda, and H. Ohno, and have been financially supported by JSPS Kakenhi 19H05622, 19J13405, and 20K22409 and RIEC Cooperative Research Projects.

References

- [1] A. Brataas, A. D. Kent, and H. Ohno, *Nat. Mater.* **11**, 372 (2012).
- [2] P. Wadley et al., *Science* **351**, 587 (2016).
- [3] H. Tsai et al., *Nature* **580**, 608 (2020).
- [4] S. Nakatsuji et al., *Nature* **527**, 212 (2015).

- [5] I. M. Miron et al., Nature **476**, 189 (2011).
- [6] L. Liu et al., Science **336**, 555 (2012).
- [7] Y. Takeuchi et al., Nat. Mater., 10.1038/s41563-021-01005-3 (2021).
- [8] J.-Y. Yoon et al., Appl. Phys. Express **13**, 013001 (2020).

Novel Spintronic Responses of Novel Materials: A Tale of Two Systems

Paul Haney^{1*}, Fei Xue^{1,2}, Duarte Pereira de Sousa³, Jian-Ping Wang³, Tony Low³

¹National Institute of Standards and Technology, Gaithersburg, Maryland 20899-6202, USA

²Institute for Research in Electronics and Applied Physics & Maryland Nanocenter,
University of Maryland, College Park, MD 20742

³Department of Electrical and Computer Engineering, University of Minnesota, Minneapolis, Minnesota 55455, USA

The discovery of new materials with unique magnetic ordering, crystal symmetries, and topological properties continues to stimulate the development of new spintronic devices. Spin-orbit coupling underlies many of the spintronic applications in materials, as it couples the electron spin with its real space motion and often plays a key role in determining the topological properties of a material's electronic structure. In this talk we'll describe the unique properties of two quite distinct materials systems: antiferromagnetic bilayer CrI_3 and magnetic tunnel junctions composed of one or more magnetic Weyl semimetals.

Bilayer CrI_3 is a two-dimensional Van der Waals material in which two ferromagnetic CrI_3 monolayers are coupled antiferromagnetically. We consider electron doped CrI_3 and theoretically study the current-induced torques present in this material. In the purely antiferromagnetic state, the two individually inversion symmetry-broken layers of CrI_3 form inversion partners, like the well-studied CuMnAs and MnAu . However, the exchange and anisotropy energies are similar in magnitude, unlike previously studied antiferromagnets in which the exchange energy is dominant. This difference leads to qualitatively different behaviors in this material. Using a combination of first-principles calculations of the spin-orbit torque and an analysis of the ensuing spin dynamics, we show that the deterministic electrical switching of the Néel vector is the result of dampinglike spin-orbit torque, which is staggered on the magnetic sublattices.

We then present results on magnetic tunnel junctions composed of one or more magnetic Weyl semimetal layers. For an asymmetric magnetic tunnel junction containing a conventional ferromagnet and a magnetic Weyl semimetal contact, we find unique features of the spin transfer torque. The Weyl semimetal hosts chiral bulk states and topologically protected Fermi arc surface states which we find govern the voltage behavior and efficiency of the spin transfer torque. We discuss the existence of a large field-like torque acting on the magnetic Weyl semimetal, whose efficiency can exceed the theoretical maximum of conventional magnetic tunnel junctions. This large field-like torque is derived from the Fermi arc spin texture and displays a counter-intuitive dependence on the Weyl nodes separation. We finally consider a magnetic tunnel junction composed of two Weyl semimetal contacts. For this system, we show that chirality-magnetization locking leads to a gigantic tunneling magnetoresistance ratio, an effect that does not rely on spin filtering by the tunnel barrier. Our results shed light on the new physics of multilayered spintronic devices comprising of magnetic Weyl semimetals, which might open doors for new energy efficient spintronic devices.

Electrically switching ferromagnets by spin orbit torques

Kaiyou Wang^{1,2*}

¹SKLSM, Institute of Semiconductors, CAS, Beijing, 100083, P. R. China

²Center for Excellence in Topological Quantum Computation and College of Materials Science & Opto-Electronic Technology, University of Chinese Academy of Science, Beijing 100049, P. R. China

*Email: kywang@semi.ac.cn

Electrically control the spin in solids is the core of spintronics. Generally, the spin-orbit torque switching controllably in above structures have to have the assistant of the external magnetic field. We investigated the spin Hall effect control the magnetization switching in heavy metal/ferromagnet multilayers and their applications [1,2].

Without external magnetic field, we realize the current-induced deterministic magnetization switching by applying spin current density and localized laser annealing, respectively [3,4]. We demonstrate different types of spin logic functions based on these devices [5,6]. In addition, we realized the adjustable electrical current-induced magnetization switching in a magnetic multilayer structure without external magnetic field utilizing interlayer exchange coupling and alloys [7,8]. We also investigated magnetic-field-free spin-orbit torque induced synaptic plasticity of a multi-state perpendicular ferromagnetic layer (FM1) in an antiferromagnetic interlayer exchange coupled Pt/FM1/Ta/FM2 structure [9].

References

- [1] Yi Cao, Guozhong Xiong, et al. *iScience* **23**, 101614 (2020).
- [2] Yucai Li, Kevin William Edmonds et al. *Advanced Quantum Technology*, **2**, 1800052 (2019).
- [3] Kaiming Cai, Meiyin Yang, Hailang Ju et al. *Nature Materials* **12**, 712 (2017).
- [4] Yi Cao, Yu Sheng et al. *Advanced Materials* **32**, 1907929 (2020).
- [5] Meiyin Yang, Yongcheng Deng et al. *IEEE Electron Device Letters* **40**, 1554 (2019).
- [6] Nan Zhang, Yi Cao et al. *Advanced Electronic Materials* **6**, 2000296 (2020).
- [7] Zelalem Abebe Bekele, et al. *Advanced Electronic Materials* **7**, 2000793 (2021).
- [8] Yu Sheng, Kevin W. Edmonds et al. *Advanced Electronic Materials* **4**, 1800224 (2018).
- [9] Yi Chao, Andrew W. Rushforth et al. *Advanced Functional Materials* **29**, 1808104 (2019).

Dynamics of orbital angular momentum in centrosymmetric systems

Seungyun Han¹, Kyoung-Wan Kim^{2*}, Hyun-Woo Lee¹

¹POSTECH, Korea

²KIST, Korea

Roles of orbital angular momentum have received a great attention in the spintronics community because of its large Hall effect in general contexts. However, detection of the orbital angular momentum transport is very challenging due to similarity of spin and orbital angular momenta. In this work, we reveal a fundamental difference between the orbital and spin angular momentum operators, in regard to the anticommutator algebra. The different algebraic properties result in oscillatory dynamics of orbital angular momentum, which is similar to the spin Hanle oscillation, but not requiring any symmetry breaking such as an external magnetic field. We identify a physical quantity named orbital torsion, which mediates the orbital Hanle oscillation. The relation between the orbital torsion and the orbital angular momentum is similar to that in the classical torsion pendulum (Fig. 1). Since the orbital torsion and related phenomena have no spin counterpart, the orbital torsion would be greatly helpful for experimental distinction of orbital angular momentum from spin angular momentum. We also propose several methods to detect the orbital torsion transport.

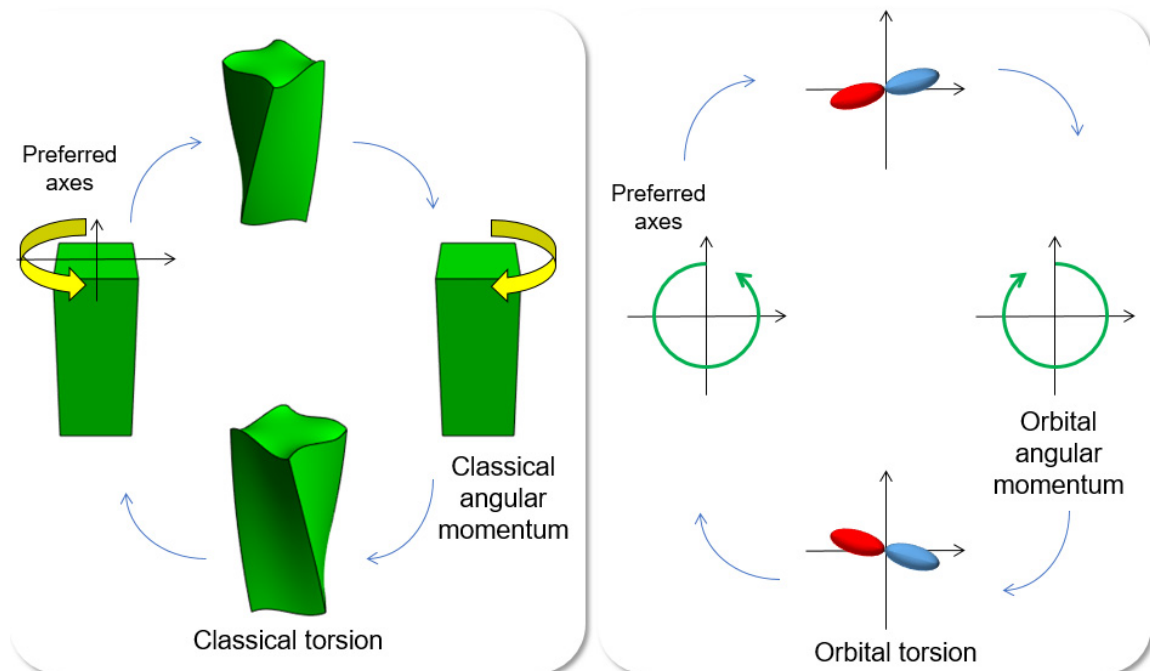


Fig. 1. Classical and orbital torsion dynamics

Direct Observation of Fe-Ge ordering in $\text{Fe}_{5-x}\text{GeTe}_2$ Crystals and Resultant Helimagnetism

Trinh Thi Ly¹, Jungmin Park^{2*}, Kyoo Kim³, Hyo-Bin Ahn⁴, Nyun Jong Lee¹, Kwangsu Kim^{1,5},
Tae-Eon Park⁵, Ganbat Duvjir¹, Nguyen Huu Lam¹, Kyuha Jang³, Chun-Yeol You⁶,
Younghun Jo², Se Kwon Kim⁷, Changgu Lee⁴, Sanghoon Kim¹, Jungdae Kim¹

¹Department of Physics and Energy Harvest Storage Research Center, University of Ulsan, Ulsan 44610, Korea

²Center for Scientific Instrumentation, Korea Basic Science Institute, Daejeon, 34133 Korea

³Korea Atomic Energy Research Institute, Daejeon 34057, Korea

⁴School of Mechanical Engineering, Sungkyunkwan University, Suwon 16419, Korea

⁵Center for Spintronics, Korea Institute of Science and Technology (KIST), Seoul, 02792, Korea

⁶Department of Emerging Materials Science, Daegu Gyeongbuk Institute of Science & Technology, Daegu 42988, Korea

⁷Department of Physics, Korea Advanced Institute of Science and Technology, Daejeon, 34141, Korea

The van der Waals (vdW) ferromagnet compared to conventional ferromagnetic materials provides a unique configuration of magnetic interactions due to its quasi two-dimensional (2D) nature. The pair-exchange interaction is mainly established within the 2D plane, while magnetic coupling between interlayers is weak. Therefore, the vdW ferromagnets are ideal for 2D spintronic devices that show various emergent spin-orbit coupled phenomena with time reversal and inversion symmetry breaking.

As a promising vdW ferromagnet, the Fe_nGeTe_2 family ($n = 3, 4, 5$) was proposed based on its high T_C (260 ~ 310 K) and large saturation magnetization. Recently, the unconventional magnetic properties of Fe_5GeTe_2 have been explained with magnetic anisotropy or/and spin reorientation by the Fe atoms in Fe_5GeTe_2 . However, the exact mechanism of such non-trivial magnetic behaviors is still unclear because it is also involved with the structural complexity in Fe_5GeTe_2 . Therefore, systematic study for finding the correlation between such non-trivial magnetic behaviors and the atomistic structure of Fe_5GeTe_2 is needed to realize room temperature spintronic devices with this new vdW ferromagnet.

In this study, we explore atomistic structures of an $\text{Fe}_{5-x}\text{GeTe}_2$ single crystal by low temperature scanning tunneling microscopy (STM) and its temperature dependent magnetic behaviors. Subset Fe layers in Fe_5GeTe_2 are expected to play a major role in magnetic ordering. STM topography reveals $\sqrt{3}\times\sqrt{3}$ superstructures on the cleavage surface of $\text{Fe}_{5-x}\text{GeTe}_2$, which are attributed to the ordering of Fe(1) layer. Intriguingly, observed $\sqrt{3}\times\sqrt{3}$ ordering of Fe(1)-Ge pair breaks the inversion symmetry, which is an important microscopic origin of the antisymmetric exchange interaction, known as Dzyaloshinskii-Moriya interaction (DMI). The temperature dependent magnetization of $\text{Fe}_{5-x}\text{GeTe}_2$ clearly shows commensurate-incommensurate transition, a typical helimagnetic behavior arising from the DMI, just below $T_C = 310$ K. We also confirm that spin reorientation behaviors are observed within the ranges of 120~260 K and 20~100 K due to competition between helimagnetism and other collinear properties. Our findings suggest that the Fe_5GeTe_2 crystal has helical magnetism with non-centrosymmetric ordering of Fe(1)-Ge pairs, which can be a source of topologically protected spin solitons to develop new types of topology-based spin devices.

Spin Rotation in Magnetic Metals

Xin Fan*

Department of Physics and Astronomy, University of Denver, Denver, Colorado, USA

The spin Hall effect in a nonmagnetic film enables spin/charge current conversion with a plethora of promising applications. In a conventional spin Hall effect, the charge current, spin current and spin polarization are all orthogonal to each other. This restriction can be a roadblock for practical applications, such as spin-orbit torques-based magnetic memories, where out-of-plane polarized spin current is preferred. A symmetry-breaking is necessary to lift such a restriction, which can be realized by the magnetization in magnetic materials. We show that the spin/charge conversion in typical magnetic metals exhibits an unusual symmetry as if the spins are rotated by the magnetization of the ferromagnetic metals, as shown in Figure 1. We refer to such effect as spin rotation. In this talk, I will be discussing experimental observations of the spin rotation effect in magnetic metals [1, 2], experimental techniques for studying this effect [3], as well as potential artefacts that should be taken into consideration when analyzing the results.

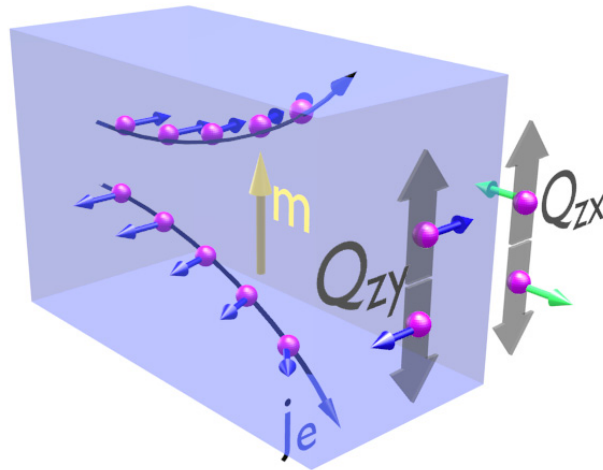


Fig. 1. Illustration of spin rotation in a magnetic metal

References

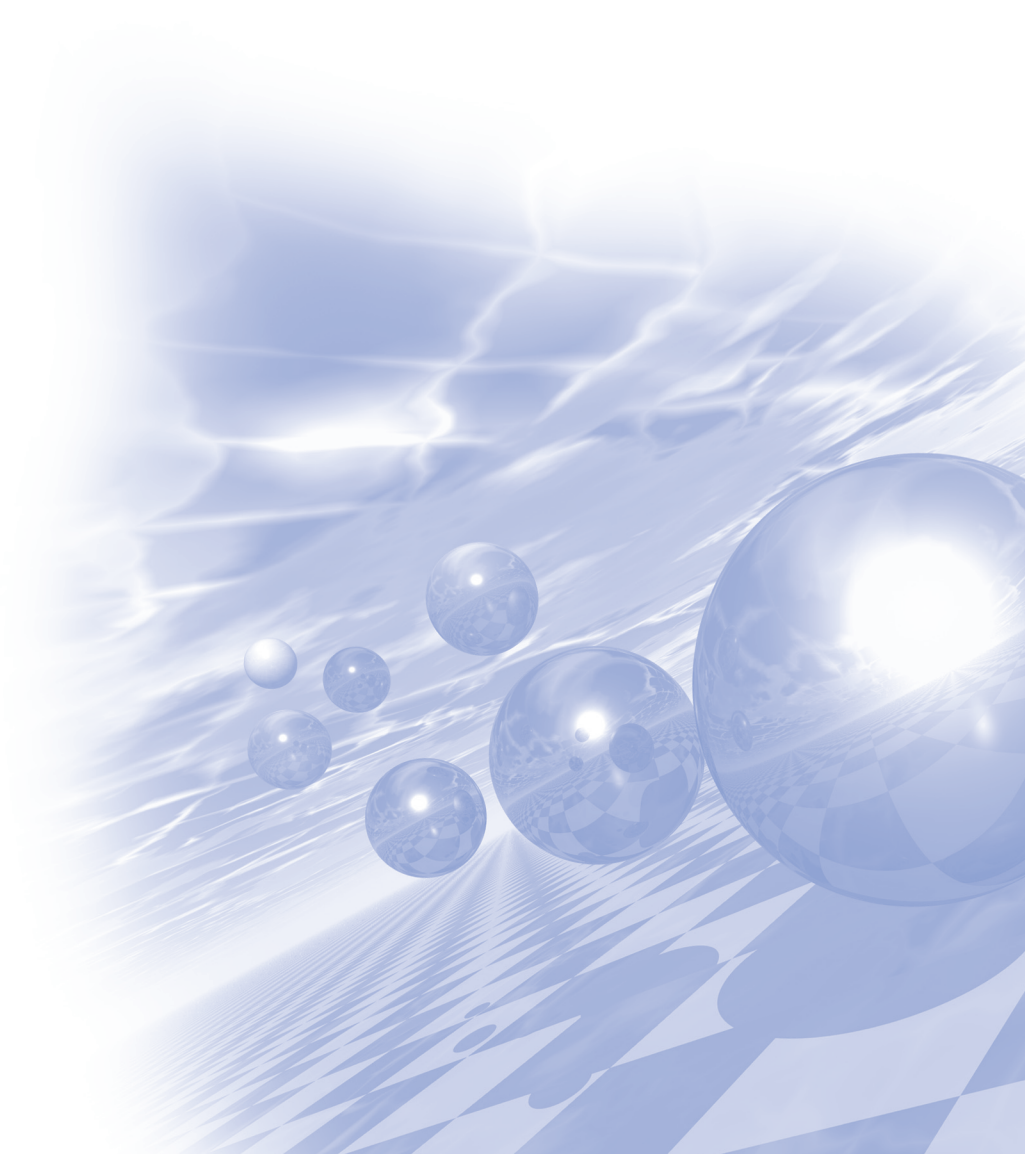
- [1] Humphries, A. M., Wang, T., *et al.*, Observation of spin-orbit effects with spin rotation symmetry, *Nature Communications*, 8, 911 (2017)
- [2] Aljuaid, W. S., Allen, S. R., Davidson, A., Fan, X., Free-layer-thickness-dependence of the spin galvanic effect with spin rotation symmetry, *Applied Physics Letters*, 113, 122401 (2018)
- [3] Wang, T., Lendinez, S., Jungfleisch, M. B., Kolodzey, J., Xiao, J. Q., Fan, X., Detection of spin-orbit torque with spin rotation symmetry, *Applied Physics Letters*, 116, 012404 (2020)



2021 KMS Summer Conference

Symposium 3

‘Permanent Magnetics’ &
‘Electro-Magnetic Energy Conversion’
공동세션



Nd가 저감된 영구자석 회전자와 자유형상 연자성분말 고정자를 활용한 로봇용 서보모터 개발에 관한 연구

양상선*, 김용진, 정재원, 권영태, 차희령, 김태훈, 이정구

한국재료연구원, 분말재료연구본부

우리나라 정부는 2050 탄소중립 달성을 2020년 선언하였으며, 이를 위한 미래 모빌리티용 구동부품의 효율을 향상시키기 위한 다양한 연구가 시도되고 있다. 로봇용 서보모터 역시 출력이 향상된 영구자석 회전자 개발과 전기강판 대비 형상자유도가 높은 분말SMC(soft magnet composite) 고정자를 사용하여 출력을 향상시키는 연구들이 수행되고 있다.

본 연구는 로봇용 서보모터에 적용하기 위한 회전자와 고정자 개발에 관한 연구로써, 최대에너지적을 향상시킬 수 있는 고가성비 영구자석소재의 개발과 투자율을 향상시키고 철손을 저감할 수 있는 고정자용 연자성소재의 개발을 수행하였다. 영구자석 소재의 경우, Nd-Fe-B계 소재와 동등한 최대에너지적을 보이면서 고가의 Nd를 약 30% Ce으로 대체할 수 있었다. 기존 Melt-spun 소재에서는 Ce치환량이 증가할수록 보자력 값의 저하와 함께 잔류자화 값이 감소되는 문제점이 있으나, 본 연구에서는 급냉공정의 도입을 통한 초기합금의 비정질상을 유지함으로써 Ce의 치환량이 약 30%임에도 열처리 이후에서까지 $CeFe_2$ 상 생성이 억제되고 다상구조(multi-maim phase)를 형성하여 약 41 MGOe의 최대에너지적을 갖는 NdCeFeB계 고가성비 영구자석 소재를 개발할 수 있었다. 연자성 소재의 경우, Fe-Si계 기반으로 B, P, C, Mo 등의 합금 원소가 투자율과 철손 값에 미치는 영향에 관한 연구가 수행되었다. 또한, 분말압축성형 공정을 사용하여 자유형상의 고정자 제조를 위해 Fe-Si-M계 칩(chip)과 순철 분말의 혼합비율에 따른 자기적 특성에 대한 연구가 수행되었다.

본 발표에서는 로봇용 서보모터에 적용하기위한 NdFeCeB계 고가성비 회전자용 영구자석 소재 개발과 형상자유도를 갖는 고정자용 Fe-Si계 기반의 분말 SMC 소재 개발 내용을 소개하고자 한다.

MR유체의 차량용 부품 적용사례 및 기술동향

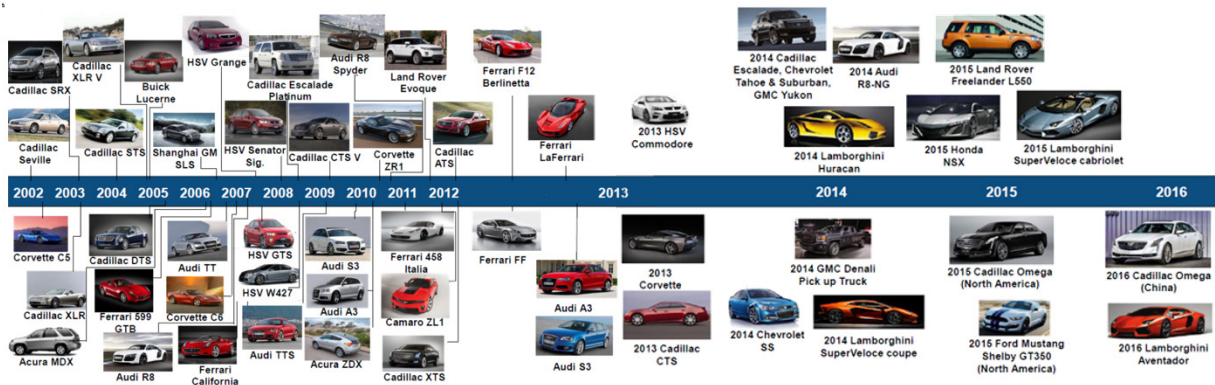
Eunjun Rhee*, Kyongho Kang

HYUNDAI ROTEM, Korea

MR유체란 실리콘 오일과 같은 절연성 유체에 수 μm 크기의 강자성 미립자를 분산시킨 것으로 외부에서 가해지는 자기장에 세기에 따라 유체의 겉보기 점도가 달라지는 스마트 유체의 일종이다. 고상 및 액상간 가역적 변화가 가능하며 응답성이 매우 빠르고 사용 온도범위가 넓으며 불순물 유입과 같은 오염에도 둔감한 성능변화를 나타내기 때문에 매우 광범위한 영역에서 적용되고 있다.

MR유체를 활용한 응용장치의 경우 단순한 구조로 소형제작 가능한 반면 강건하고 제품이 신뢰성이나 내구성이 우수하다. 특히 섭동부와 접촉면을 필요로 하지 않기 때문에 정밀도를 요하지 않아 기계가공에 많은 시간이나 비용을 들이지 않아도 되고 시스템 내부에 유입되는 먼지와 같은 오염물질에도 MR유체 시스템 성능에는 큰 영향이 없어 다양한 정밀 부품에 적용이 용이하다. 이 때문에 약 20여년 전 미국 LORD사에서 MR유체가 상용화되어 시판된 이후 자동차, 방산차량, 선박, 항공, 건설, 내진용 빌딩, 방산차량용 포사격 안정화를 위한 주퇴복좌시스템 등 폭 넓은 분야에서 다양한 형태로 활용되고 있다.

본 논문에서는 자동차 분야에서 활용되고 있는 MR유체 응용장치에 대해 소개하고자 한다. 앞서 언급한 바와 같이 미국 LORD사에서 MR유체의 최대 약점인 침전특성을 개선하면서 90년대 초반부터 고가의 승용차 중심으로 MR유체를 이용한 댐퍼를 적용하기 시작하였으며 최근에는 매년 4~6종의 신차종에 MR댐퍼가 적용되어 양산되고 있다. 차량용 속업소버 뿐만 아니라 브레이크, 클러치, 리타더, 엔진마운트, 시트용 댐퍼등에도 MR유체가 적용되어 MR유체 응용장치 시장은 나날이 커지고 있다. MR댐퍼를 차량에 처음 적용한 것은 미국 DELPHI사이며 LORD사의 MR유체를 사용하였다. 이들 두 회사는 양사간 상호 독점계약을 맺고 승용차용 MR댐퍼 개발하여 양산하고 있으며 전략적 중요성과 큰 부가 가치로 인해 미국을 제외한 다른 나라에는 기술이전을 제한하는 정책으로 인해 국내에서는 여러 연구기관이나 학교에서 관련 연구가 수행되고는 있었으나 양산이나 상용화 관련 사례는 거의 없었다. MR댐퍼는 캐딜락이나 아우디 카마로, 페라리 등과 같은 승용차에 적용되어 세계 여러 나라에서 시판되고 있었으나 높은 기술진입 장벽으로 인해 국내 자동차에서는 양산사례가 없었다. 그러던 중 2008년 현대로템이 방산분야에서 차륜형 장갑차용으로 MR댐퍼를 국산화 개발을 성공함으로써 새로운 전기를 맞기 시작하였다. 현대로템은 방산용 무인자율차량과 철도차량용 MR댐퍼를 잇달아 개발하였고 현대차 그룹의 기술교류를 통해 현대 상용차 및 승용차용 MR댐퍼를 개발하여 차량시험평가를 마무리하고 양산을 계획하고 있다.



희토자석 최근 시장 및 연구동향

김동환*

성림첨단산업(주) 연구소, 대구광역시 달서구 호림동 8

영구자석은 전류의 소비 없이 계속적으로 자기장을 발생시키는 소재로서 기존의 전자석 기능을 대체하면서 모터, 액츄에이터, 발전기 등 동력을 변환시키는 기기에서 에너지 절감 및 소형화에 기여하는 역할을 한다. 특별히, Nd-Fe-B계 자석은 영구자석 중 자기특성이 가장 우수하여 많은 모터 개발자의 주목을 받고 있는 실정인데, 2018년 기준 세계적으로 약 13 만톤의 자석이 생산되고 있고 매년 8.3%의 시장 신장율을 지속하면서 판매금액 기준으로 영구자석 중 가장 많이 사용되는 소재로 성장하고 있다.

하지만, 이들 Nd-Fe-B 자석에는 Nd, Pr의 경희토와 Dy, Tb의 중희토가 사용되고 있는데 2018년 기준 세계 희토 생산량의 약 70%가 중국에 편중되어 있고 중국의 희토 사용량도 지속적으로 증가하는 추세이므로 향후 중국으로부터 자석을 생산하기 위한 희토 조달이 용이하지 않는 상황이 발생할 가능성이 높다. 따라서 국내 친환경 자동차 등 희토자석을 사용하는 첨단분야의 안정적 생산을 지속하기 위해 산-학-연 및 정부가 공동으로 참여하는 희토자원 확보 대책이 필요하다.

본 발표에서는 고가이고 상대적으로 더욱 희귀한 중희토사용량을 최소화 하는 개발 현황과 희토자석을 생산하는 소결 및 가공공정에서 약 30%의 스크랩 혹은 슬러지가 발생하고 있고 희토원재료 확보 측면에서 이들 폐료를 합리적으로 처리하는 기술 확보가 필요한데, 이들 희토자석 생산 및 폐제품 회수로부터 발생하는 희토 자석 스크랩을 재사용하는 기술 현황과 향후 발전방안에 대해 제언을 하고자 한다.

References

- [1] M. Sagawa, S. Fujimura, N. Togawa, H. Yamamoto, Y. Matsuura, J. Appl. Phys. 1984, 55, 2083.
- [2] O. Gutfleisch, M.A. Willard, E. Brück, C.H. Chen, S.G. Sankar, and J.P. Liu, Adv. Mater. 2011, 23, 821-842.

스마트 절연 방법을 이용한 고온 초전도 전자석의 안정성 및 운전 특성 향상

김형욱*, 조영식, 김석환

한국전기연구원

초전도 기술은 높은 전류 밀도를 갖는 특성으로 인해 고자장을 필요로 하는 분야에 반드시 필요한 기술로써 인정받고 있다. 특히 초전도체 중 고온 초전도체(HTS)는 액체 질소 온도에서 초전도성을 유지함으로써 냉각 비용 측면에서 매우 큰 장점을 갖기 때문에 많은 초전도 응용 기술 연구자들이 고온 초전도 응용 기기를 상용화하기 위한 연구가 진행 중이다. 하지만 아직까지는 고온 초전도체를 이용한 응용 기기가 상용화된 사례가 드물다. 특히 고온 초전도 회전기기의 경우 세계적으로 상당한 비용으로 연구에 투자하였지만 모두 상용화로 이어지지 못하였다. 이유는 고온 초전도선의 구조적, 재료적 특성으로 인해 기계적, 전기적 안정성에 대한 신뢰성이 보장되지 못하였고 결국 영구 소손을 입었기 때문이다 [1]-[3].

본 논문은 고온 초전도 코일의 전기적 안정성 및 제어성을 확보할 수 있는 새로운 방법을 제안한다. 제안된 방법은 고온 초전도 코일의 턴 간에 스마트 절연(Smart insulation)체인 Metal-Insulator Transition (MIT) 특성을 갖는 물질인 산화바나듐(Vanadium oxide)을 코팅함으로써, 정상상태에서는 턴 간 저항이 절연체 수준으로 유지되어 충방전시의 지연 현상이 없고 과도 상태에서는 턴간 저항이 금속체 수준으로 낮아져 무절연 코일(no-insulation coil)과 같이 턴과 턴 사이로 전류가 건너 흘러 켄치가 일어나는 국부에 집중하여 일어나는 발열 현상을 완화시켜 코일이 영구되는 것을 방지해준다. 이 기술을 회전기에 적용할 경우 제어성과 전기적 안정성이 보장될 수 있다. 본 연구는 MIT 특성 및 제안된 방법의 타당성을 스마트 인슐레이션 코일 실험을 통하여 검증하였다.

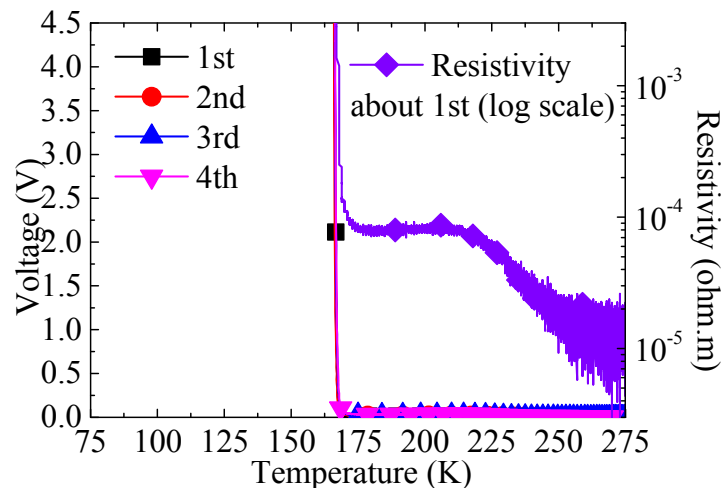


Fig. 1. Changes resistivity of vanadium oxide according to the temperature.

References

- [1] S. B. Kim, T. Kaneko, H. Kajikawa, J. H. Joo, J. M. Jo, Y. J. Han, and H. S. Jeong, "The transient stability of HTS coils with and without the insulation and with the insulation being replaced by brass

- tape,” *IEEE Trans. Appl. Supercond.*, vol. 23, no. 3, p. 7100204, Jun. 2013.
- [2] C. L. H. Thieme, K. J. Gagnon, J. Y. Coulter, H. Song, and J. Schwartz, “Stability of second-generation HTS pancake coils at 4.2 K for high heat flux applications,” *IEEE Trans. Appl. Supercond.*, vol. 19, no. 3, pp. 1626-1632, Jun. 2009.
- [3] H. W. Kim, J. Hur, S. W. Kim, D. W. Ha, R. K. Ko, J. P. Hong, J. H. Kim, H. Kim, J. H. Joo, S. B. Kim, and Y. S. Jo, “Electrical characteristic analysis according to contact resistance between turns of HTS coil,” *IEEE Trans. Appl. Supercond.*, vol. 26, no. 3, p. 4601504, Apr. 2016.

Development Status of Permanent magnets for Vehicle Motor

Hyungju Lee^{*}
Hyundai motor, Korea

As demand for motors in vehicles has soared, the development of materials applied to motors is also actively underway. Among them, the development of permanent magnets, which play the most important role in motor driving, is also actively underway. Permanent magnets in motors are materials that are directly related to the determination of motor performance/weight/size/cost, and require high performance/high efficiency/low cost.

In this presentation, I will introduce the types and characteristics of permanent magnets being applied to automotive motors, as well as discuss future development directions.

Electrical and Mechanical Characteristics Comparison of EV Traction Motor According to Electrical Steel Sheet

Young-Hoon Jung^{1*}, Jin-Cheol Park², Myung-Seop Lim²

¹R&D division, Hyundai Motor Company, Korea

²Department of Automotive Engineering, Hanyang University, Korea

Recently, since regulations for the vehicle using internal combustion engine (ICE) are enhanced, many motor companies have tried to convert to the electric vehicle (EV) from the ICE vehicle. The electric motor for EV traction should have high efficiency, high-speed and small size to improve the fuel economy. Due to the feature using the magnetic and reluctance torque simultaneously, the interior permanent magnet synchronous motor (IPMSM) using Nd permanent magnet (PM) is widely used for satisfying those characteristics. However, since the rare earth metal constituting Nd PM is produced in a limited area, there is a problem that the supply and price of Nd PM are unstable according to the international situation. For this reason, various motors are researched to replace the IPMSM using Nd PM, and the multilayer IPMSM using ferrite PM is one of those.

Due to the low residual induction of the ferrite PM, the multilayer IPMSM using ferrite PM has small magnetic torque and large reluctance torque. However, since the small magnetic torque adversely affects the high-speed operation region, the magnetic torque should increase as much as possible, and the usage of the ferrite PM should increase to do this. To reduce the high stress, the multilayer IPMSM using ferrite PM needs many bridges, which leads to deteriorating the electrical characteristics. In other words, the mechanical and electrical characteristics of the multilayer IPMSM using ferrite PM have a relationship with the trade-off.

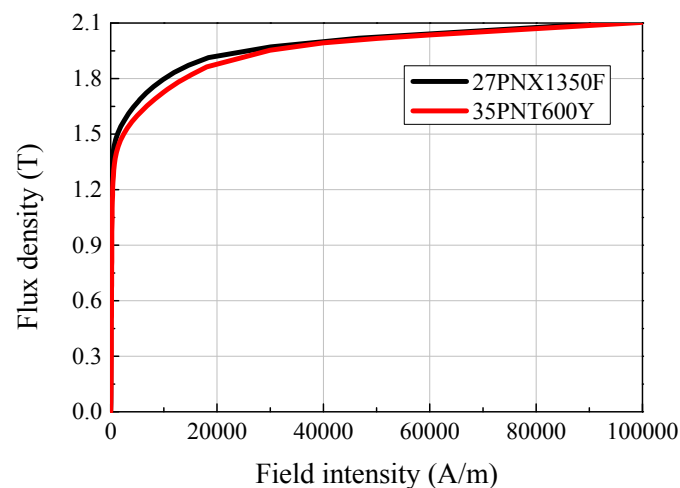


Fig. 1. BH curve of two electrical steel sheets

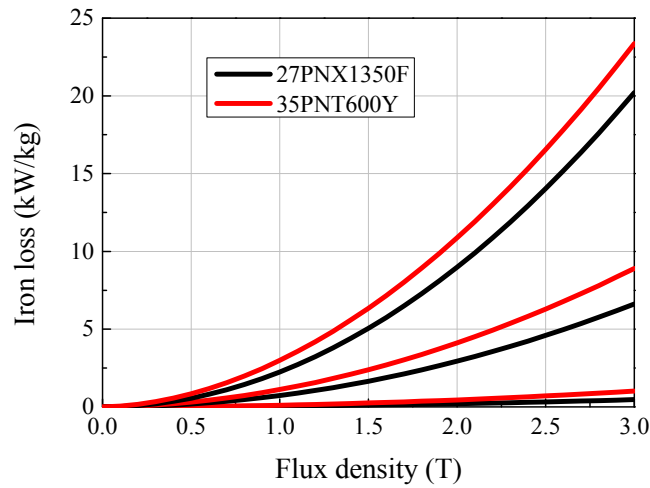


Fig. 2. Iron loss of two electrical steel sheets

Table 1. Mechanical characteristics of two electrical steel sheets

Item	Unit	27PNX1350F	35PNT600Y
Density	kg/m ³	7600	7600
Young's modulus	GPa	180	178
Poisson's ratio	-	0.3	0.3
Yield stress	MPa	420	620

In this paper, the electrical and mechanical characteristics of the multilayer IPMSM using ferrite PM designed for EV traction are compared according to the electrical steel sheet. Fig. 1 and 2 show the BH curve and iron loss data of the 27PNX1350F and 35PNT600Y, respectively, and Table 1 shows the mechanical characteristics of two electrical steel sheets. As shown in Fig. 1 and 2, the electrical characteristics of 27PNX1350F is better than 35PNT600Y. On the other hands, as shown in Table 1, the mechanical characteristics of 35PNT600Y is better than 27PNX1350F. To compare the characteristics according to the electrical steel sheet, the various electrical characteristics such as the efficiency, copper loss, and iron loss will be compared. Also, the mechanical characteristics such as the maximum stress and safety factor will be compared.

열간-변형 영구자석(hot deformed magnet) 기술 동향 및 연구방향

안종빈*, 황진성, 최판규

(주)디아이씨 신소재연구소, Dae-il Coporation

전기에너지 사용의 증가에 따라 모터, 발전기, 액츄에이터 등 각종 전동화부품의 수요가 지속적으로 증가하고 있고, 이에 따라 소형화, 경량화, 에너지절감을 위해 여러분야에서 다양한 연구가 수행되고 있다. 모터의 고출력, 고효율화하기 위해서 희토류 영구자석 사용량이 늘어가고 있다. 가장 많이 사용 되는 Nd-소결 영구자석(sintered Nd magnet)은 모터내부의 전자기 유도 교류 자기장에 의해 발생하는 와전류로부터 온도가 증가하게 되어 전체 효율이 감소시키는 주 원인으로 지적 된다. 열간변형 영구자석은 300-400nm 결정립크기의 nanocrystalline magnet이며 electrical resistivity가 150-300 $\mu\Omega\text{cm}$ 으로 Nd-소결 영구자석의 electrical resistivity가 140-180 $\mu\Omega\text{cm}$ 보다 2배 가까이 높기 때문에 고온환경에서 높은 보자력이 보장되고 모터 및 고속 발전기 사용에 적합하다. 열간변형 영구자석은 크게 hot pressing 공정과 hot deforming 공정을 통해 제작되어진다. Hot press 공정에서 자성분말을 full density에 가깝게 등방성 자석을 만들고, hot deformation 공정에서 소성가공을 통해 등방성상태의 자석을 성형압력방향으로 마그넷 스핀을 정렬시켜 이방성 벌크자석을 제조한다. 후방압출 또는 전방압출을 통해 마그넷의 형상과 자성특성 제어하는 연구가 되고 있고, 일본 다이도에서는 열간변형 공정을 통해 이방성 ring 자석을 제조하여 판매하고 있다.

자사에서는 melt spinning으로 제조된 NdFeB 나노상 결정립 분말의 고온소성변형 제어 기술을 연구중에 있으며, 개발 열간변형 영구자석을 160kW급 구동모터에 적용을 목표로 개발중에 있다.

Characteristics of Slotless Motor according to Electrical Steel and Bulk Core Materials

Ho-Young Lee^{1*}, Gi-Ju Lee¹, Jin-Yeong Shin¹, Seung-Young Yoon¹,
Myeong-Sik Jeong² and Soon-O Kwon¹

¹Safety System R&D Group, Kore Institute of Industrial Technology, Korea

²Mechanical Components and Materials R&D Group, Kore Institute of Industrial Technology, Korea

In recent years, as the electric vehicle market has grown, small actuators have been applied as automotive parts in a variety of ways. Consequently, low noises of actuators that were typically masked by the internal combustion engine's noise have begun to be noticed in electric vehicles, and as a result, regulations on vibratory noises of small motors are becoming increasingly strict.

This paper presents a magnetic circuit design to reduce the noise and production cost of motors that are used to operate automotive heating, ventilation, and air conditioning (HVAC) systems. The proposed motor has a slotless armature structure, which is advantageous in terms of reducing vibratory noise. Furthermore, the motor performance was analyzed according to the material, and based on this, a core suitable for mass production was selected and designed. Fig. 1 shows the structure of the slotless motor developed in this study, and Table 1 shows the major specifications. As core materials, 50PN1300, 50PN600, 35PN230, and bulk core were applied according to the grade of the electrical steel sheet, respectively. Because the target specifications were 500 rpm, a relatively low speed, and two poles, the power frequency was very low. Since the effect of iron loss is insignificant under these operating conditions, we also analyzed the motor performance for the bulk core and electrical steel sheet cases.

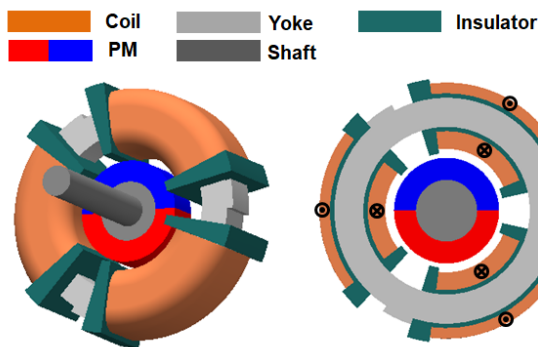


Fig. 1. Proposed slotless motor's structure

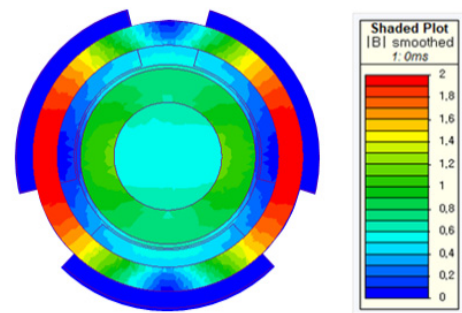


Fig. 2. Magnetic flux density distribution

Table. 1. Specifications of slotless motor

Pole number	Dimension				Yoke material			
	Stator diameter [mm]	Rotor diameter [mm]	Magnetic air-gap [mm]	Stack length [mm]				
2	20.05	16.45	1.725	4.5	50PN1300	50PN600	35PN230	SPCC

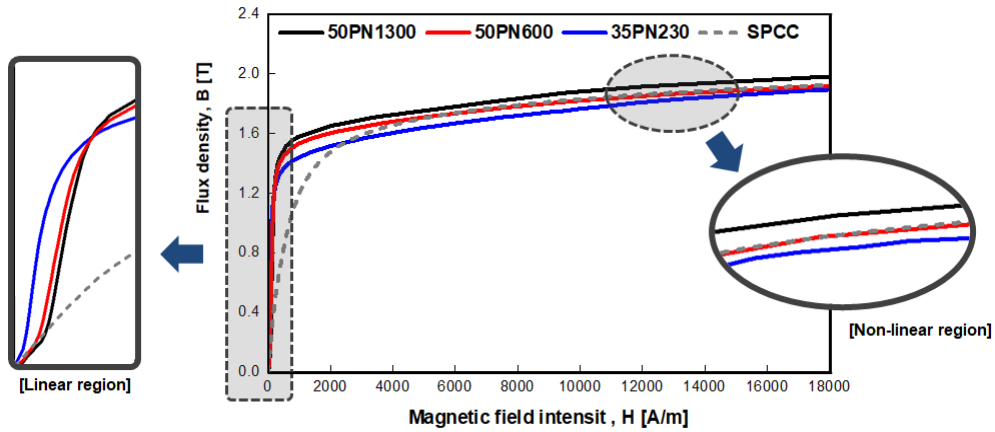


Fig. 3. BH curve of electrical steel sheets and bulk core

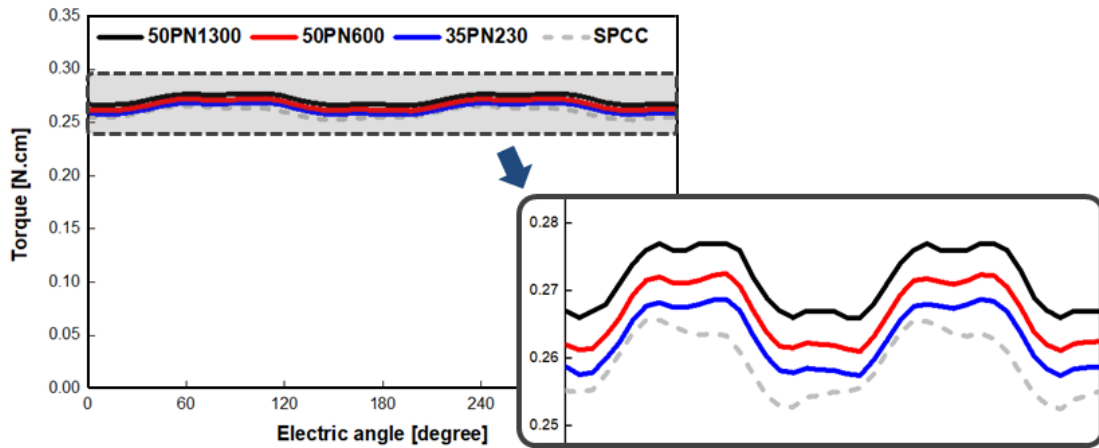


Fig. 4. Output torque comparison

The magnetic flux density of the armature core of the proposed model shows a slightly higher property, as shown in Fig. 2. Fig. 3 shows the B-H curve of the electrical steel sheets and the bulk core investigated in this study. Here, the low-grade electrical steel sheet shows a lower magnetic flux density at the operating point in the section before the magnetic saturation, compared to the high-grade electrical steel sheet. However, in the subsequent section, the magnetic flux density at the operating point is higher. As a result, the average torque of the model using the low-grade electrical steel sheet is about 3.5% higher than that of the model using the high-grade electrical steel sheet, as shown in Fig. 4. Furthermore, the model composed of the bulk core showed no notable performance degradation, and considering the production cost aspect, it would be an appropriate design.

Therefore, for applications in the low speed-high torque domain, it may be advantageous to apply a low-grade electrical steel sheet rather than a high-grade one in terms of motor performance and production costs. This study confirmed that the selection of the electrical steel sheet should be differentiated depending on the operating domain (speed-torque) of electric motors and demonstrated the importance of the electrical steel sheet selection.

Acknowledgment

This work was supported by Global Management Business (GMB) Korea grant funded by Korea government (MOTIE). (20014421, Development of 800v class high-efficiency electric compressor technology for indirect centralized heat management system based on hydrocarbon refrigerants)

Current Research and Challenges of Magnet Additive Manufacturing

Taeho Ha^{1*}, Joon Phil Choi¹, Hakseuon Lee²

¹Department of 3D printing, Korea Institute of Machinery & Materials, Daejeon 34103, Republic of Korea

²Department of 3D printing materials, Korea Institute of Material Science,
Changwon, Gyeongnam 51508, Republic of Korea

Magnets are the core components of motors that convert electrical energy into mechanical one. It plays a key role in the development next-generation products such as special medical devices, robots, and electric vehicles. The magnetic materials for the electric motor can be typically classified into soft and hard magnetic materials. A soft magnetic core is manufactured by overlapping two-dimensional electrical steel sheets, and a permanent magnet is formed using a mold. Recently, the motor components are required for high performance and small batch production. However, the conventional manufacturing method cannot achieve maximum performance due to design constraints. In addition, a mold is required even for small-volume production. Additive manufacturing (AM) is an attractive technology to directly fabricate net shape with increasing the design flexibility, which could offer the potential to produce new electric motors for low volume production in various industries. In this study, we would like to introduce the current status and challenges on additive manufacturing of magnetic material. The ISO/ASTM 52900-15 standard classifies additive manufacturing technology into seven processes: Material Jetting (MJ), Binder Jetting (BJ), Material Extrusion (ME), Vat Photopolymerization, Powder Bed Fusion (PBF), Directed Energy Deposition (DED). Among them, the present study will focus on the additive manufacturing of magnetic materials using PBF, BJ, and DED methods. In addition, we will present the research directions for the development of magnetic materials, processes, and equipment specialized for additive manufacturing of the Korea Institute of Machinery & Materials (KIMM) and Korea Institute of Materials Science (KIMS).

전기강판 포화도를 고려한 비대칭 형상을 적용 전동기 토크 특성 연구

윤명환*, 이기덕, 이정종

한국전자기술연구원 지능메카트로닉스 연구센터

매입자석형 동기전동기는 고토크밀도, 고효율, 그리고 넓은 운전 영역의 장점을 지니고 있다. 이런 장점들로 자동차, 군수 장비, 가전 제품 등 다양한 분야에 적용되고 있다. 하지만 매입자석형 동기전동기는 토크리플이 다른 타입의 전동기에 비해 큰 단점이 있다. 토크리플은 진동과 소음에 악영향을 주기 때문에 최소한으로 줄여야 한다. 토크 리플은 공극자속밀도가 정현적이지 못한 이유로 리플이 생길 수 있다. 형상 변화에 따라 자기저항이 변화하고 이에 따라 공극자속밀도를 조절할 수 있게 된다. 자기저항은 동일 기자력 기준 자속 경로의 길이에 비례하고 단면적과 투자율에 반비례한다. 이 논문에서는 투자율을 조절하여 자기저항이 변하고 공극자속밀도 특성이 바뀔 때 따른 토크 및 토크 리플 특성을 살펴본다. 그리고 반응표면법을 이용하여 토크리플을 저감할 수 있는 최적의 형상을 찾는다. 그림. 1은 이 논문에서 다루는 비대칭 형상의 예이다. 그림. 2는 반응표면법을 적용하기 위한 설계 변수를 나타낸다. 자석의 위치 및 자석의 회전각도에 따라 자석 중심 기준으로 보았을 때 철심의 면적이 좌우 서로 다르게 된다. 철심 면적을 줄이고 포화도를 높여 자기저항을 키워서 공극자속의 변화를 주는 것이다.

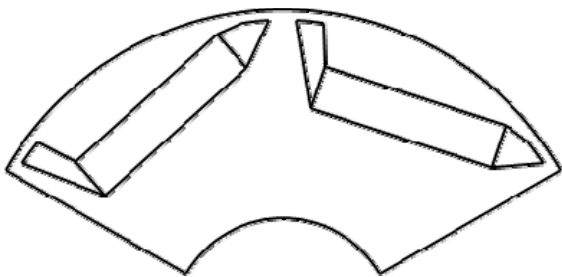


그림. 1. 비대칭 회전자 형상

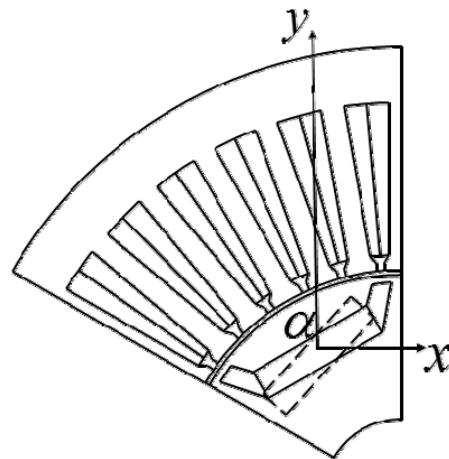


그림. 2. 반응표면법 설계 변수

Toward Development of Grain Boundary Diffusion Process for High-performance Nd-Fe-B Sintered Magnets

Tae-Hoon Kim^{*} and Jung-Goo Lee

Powder and Ceramics Division, Korea Institute of Materials Science (KIMS),
797 Changwondaero, Changwon-city, 51508, South Korea.

In this presentation, we propose a guideline on development of grain boundary diffusion (GBD) process for high-performance Nd-Fe-B sintered magnets based on recent analytical works revealing the microstructural characteristics of HRE (Heavy Rare-earth)-rich shells and Nd-rich grain boundary phases in grain boundary diffusion processed magnets. To understand the origin of the coercivity of 3.0 T that can be achieved only in the GBD processed Dy-alloyed magnets, Dy distribution in the course of the Dy-vapor GBD process applied to Dy-free and Dy-containing Nd-Fe-B sintered magnets have been comparatively investigated for two GBD process steps (GBD treatment step and subsequent annealing step) [1]. We have discovered a key microstructural contributor for the 3.0 T coercivity of the GBD processed Dy-alloyed magnets [1]. In addition, through a detailed microstructure observation on the Dy- or Tb- GBD processed magnets using the SEM and HAADF-STEM, the formation mechanisms of HRE-rich shells could be established from two perspectives: i) solid diffusion of HRE and ii) solidification of HRE-dissolved liquid [2, 3]. Based on these new findings, a method to further improve the coercivity of Dy-free Nd-Fe-B sintered magnets by the GBD process will be discussed.

References

- [1] Tae-Hoon Kim *et al.*, Acta Mater. **172**, 139(2019).
- [2] Tae-Hoon Kim *et al.*, Acta Mater. **93**, 95(2015).
- [3] Tae-Hoon Kim *et al.*, Scripta Mater. **178**, 433(2020).

코어 조립공차에 따른 로봇용 액추에이터 특성분석

박민로^{1*}, 박진철², 신선용², 이수경³, 임명섭²

¹Korea Institute of Robotics and Technology Convergence, Korea

²Hanyang University, Korea

³POSCO, Korea

최근 로봇 및 자동차를 포함한 다양한 분야에 전장화를 위한 영구자석 모터가 많이 이용 되고 있다. 그리고 모터의 성능을 향상시키고, 재료비를 저감하기 위해, 분할된 코어가 조립된 고정자를 적용하고 있다. 그러나 기존의 일반적인 고정자에 비교하여 분할코어를 적용하면 높은 점적률을 가져 고출력 고효율의 모터를 설계하기에 유리하지만, 분할된 코어를 조립해야하는 공정이 추가되게 된다. 따라서, 추가적인 공정으로 인해 고정자의 조립 공차를 발생시킨다는 단점이 있다. 이러한 조립 공차는 형상 치수와 성능의 예상치 못한 변동을 야기하게 된다. 따라서, 제작된 모터가 의도한 성능을 가지기 위해서는, 모터 설계 단계에서부터 조립 공차를 고려한 성능 예측과 설계 방법이 필요하다.

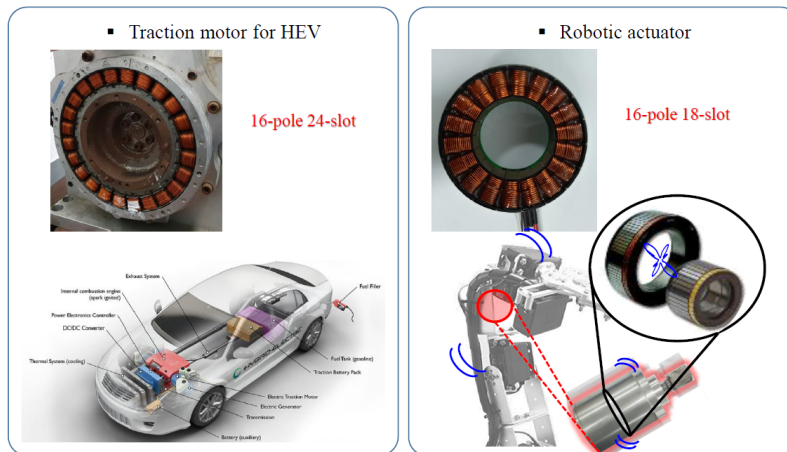


Fig. 1. Application of electric motor

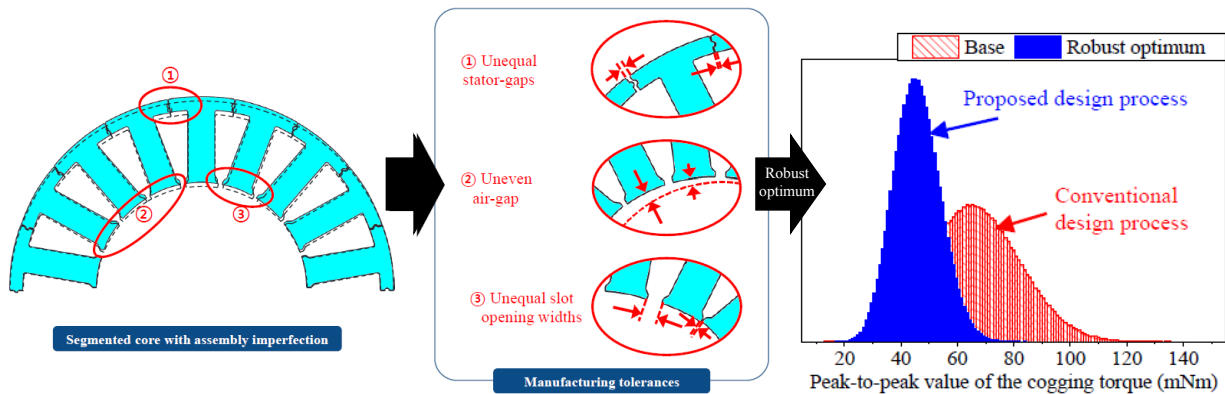


Fig. 2. Assembly imperfection of segmented core and robust design

본 논문은 분할코어의 조립 공차를 고려한 모터의 성능 분석과 이를 개선하기 위한 강건 설계 방법을 제안한다. 먼저, 제작된 모터의 형상 및 성능을 측정하여 분할코어의 조립 공차로 인한 성능의 변동을 확인한다. 그리고 분할 코어에서 발생하는 조립공차와 이로 인해 설계변수에 어떻게 영향을 미치는지 정의한다. 해당 설계 변수가 조립 공차와 같은 불확실성을 가질 때, 무부하 역기전력, 코깅토크 등과 같은 모터 성능에 미치는 영향을 분석한다.

다음으로, 불확실성을 가진 설계 변수를 고려하여 성능의 변동을 줄이기 위한 강건 설계를 수행한다. 정의된 불확실성 설계 변수를 반영한 분산 분석을 통하여 분할 코어의 조립 공차를 고려한 모터 성능의 강건성에 민감한 설계 변수를 선정한다. 선정된 설계 변수를 이용해 최적화 기법을 적용하여, 분할 코어 고정자의 조립 공차에 대한 모터 성능의 강건성을 최대화하기 위한 강건 최적 설계를 수행한다.

마지막으로, 기본 모델과 강건 설계안을 적용한 모델에 대해, 시뮬레이션 및 실험을 통해 강건 설계 안의 타당성과 성능 분석 방법을 검증한다.

Fabrication and Magnetic Properties of ThMn₁₂-type Sm(Fe_{0.8}Co_{0.2})₁₁Ti Bulk

Jihoon Park*, Hui-Dong Qian, Jung Tae Lim, Jong-Woo Kim and Chul-Jin Choi

Powder Materials Division, Korea Institute of Materials Science, Changwon,
Gyeongsangnam-do 51508, Republic of Korea

Iron-rich rare-earth (RE) alloys with tetragonal ThMn₁₂ structure have been extensively studied as a potential high performance permanent magnetic material due to its high saturation magnetization of 1.43 T, anisotropy field of 10.9 T and Curie temperature of 800 K [1]. However, its low intrinsic coercivity prohibits its use as a permanent magnetic material; the magnetization dramatically drops as the applied magnetic field reaches to zero in the hysteresis loop. In addition, phase decomposition and grain growth during sintering and high pressure compaction degrade the magnetic properties of bulk samples. Therefore, in this work, we have developed a new fabrication method to produce microstructure refined high density Sm(Fe_{0.8}Co_{0.2})Ti bulk magnet.

Amorphous Sm(Fe_{0.8}Co_{0.2})₁₁Ti ribbons were prepared by arc-melting raw material pieces and melt-spinning. The melt-spun ribbons were ground and pressed to produce green bodies, and the green bodies were annealed at various temperatures and times ranging from 750 to 850 °C and 10 to 30 min, followed by quenching. Here, the purity, density, and magnetic properties were controlled by optimizing pressing, annealing, and quenching conditions.

The fabricated high density Sm(Fe_{0.8}Co_{0.2})₁₁Ti bulk sample (7.72 g/cc) exhibits high purity ThMn₁₂ phase of higher than 97%. The saturation and remanent magnetizations are higher than the reported data, which results in greater maximum energy product (BH)_{max} of 12.22 MGOe than the reported 5 MGOe [2]. To the best of our knowledge, this (BH)_{max} is the highest value with composition of Sm(Fe-Co)Ti without any Zr, La, Ce, V, etc. doping. The details of the fabrication procedure, microstructure and magnetic properties will be discussed.

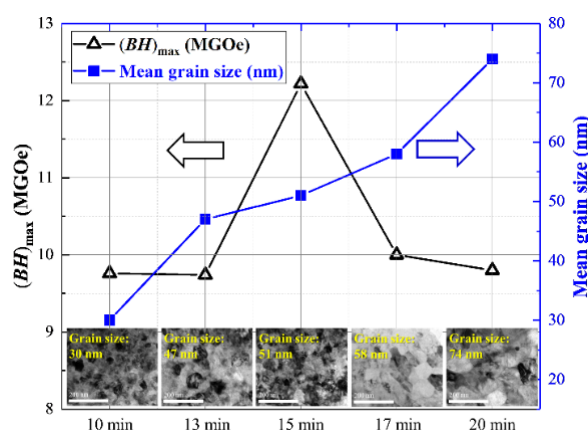


Fig. 1. Maximum energy products, (BH)_{max}, and corresponding mean grain sizes of the high density bulk magnets with increasing annealing time at 800 °C.

References

- [1] P. Tozman, H. Sepehri-Amin, Y. K. Takahashi, S. Hirose, K. Hono, *Acta Materialia*, 153, 354 (2018).
- [2] T. Saito, F. Watanabe, and D. Nishio-Hamane, *Journal of Alloys and Compounds* 773, 1018 (2019).

해석적 기법과 PSO알고리즘을 이용한 SPM 전동기의 초기설계 자동화 기법

Woo-Hyeon Kim^{1*}, Kyung-Hun Shin², Gang-Hyeon Jang¹, Hoon-Ki Lee¹, Jang-Young Choi¹

¹Chungnam National University

²Chonnam National University

영구자석형 전동기는 경량화 및 고효율화가 가능해 추진시스템 등 다양한 산업분야에 사용되고 있다. 그러나 그 설계법에 있어서는 기존에 설계된 전동기들의 경험적 데이터를 바탕으로 장하를 분배하는 장하분배법 혹은 설계 사양을 만족할 때까지 설계자가 반복적으로 설계하는 방법이 사용되고 있다. 이는 설계된 모델이 최적모델인지 판단할 수 없을 뿐 아니라, 경험적 데이터의 부재 시 초기설계 포인트의 선정이 어려운 단점이 있다. 이러한 문제를 해결하기 위해 최근 전동기의 초기설계 자동화 기법들이 제안되었다. 그러나 제안된 기법들은 동손만을 고려하였기 때문에 출력밀도와 효율을 고려한 설계에 적용되기 어렵다. 따라서 본 논문은 앞서 수행된 연구들을 기반으로, 해석적으로 철손과 와전류 손실을 도출하여 출력밀도와 효율을 고려한 초기설계 자동화 기법을 제안하고 직접 구동용 SPM전동기의 설계에 적용하여 그 타당성을 확인하였다. 본 논문에서 제안된 기법은 SPM의 자기장하를 결정하는 4개의 변수 극호비, 자석두께, 회전자 외경, 적층길이에 따라 고정자(자기장하)를 설계하는 design frame과 4개의 변수를 최적화하는 PSO알고리즘 그리고 Random search 알고리즘으로 구성된다. Fig.1. (a)는 제안된 기법의 플로우 차트를 나타낸다. 제안된 기법의 타당성을 확인하기 위해 직접 구동용 SPM전동기의 설계에 적용하였다. Fig.1. (b)는 Random search method를 통해 15000개의 디자인 후보군으로 도출한 파레토 프론트이며, 파레토 경계에서 효율과 출력밀도의 변화는 각각 3.6%, 600Kw/m³이다. 본 논문에서는 비교적 높은 출력밀도를 갖는 지점을 최적점으로 선정하였다.

제안된 기법의 최적모델 결과와 FEM을 통해 해석한 결과를 비교하였을 때, 역기전력 기본파 크기의 오차가 약 3% 발생하여 요구토크를 만족하기 위한 인가전류의 크기가 약 7 더 필요한 결과를 보인다. 이는 설계에 사용된 해석적 기법이 카터계수를 통해 대략적으로 슬롯 효과를 고려하였기 때문에 발생한 오차로 사료된다. 그러나 여러 디자인 포인트에 대한 효율적인 설계가 가능하기 때문에 초기설계 단계에서 유용하게 쓰일 수 있을 것으로 사료된다.

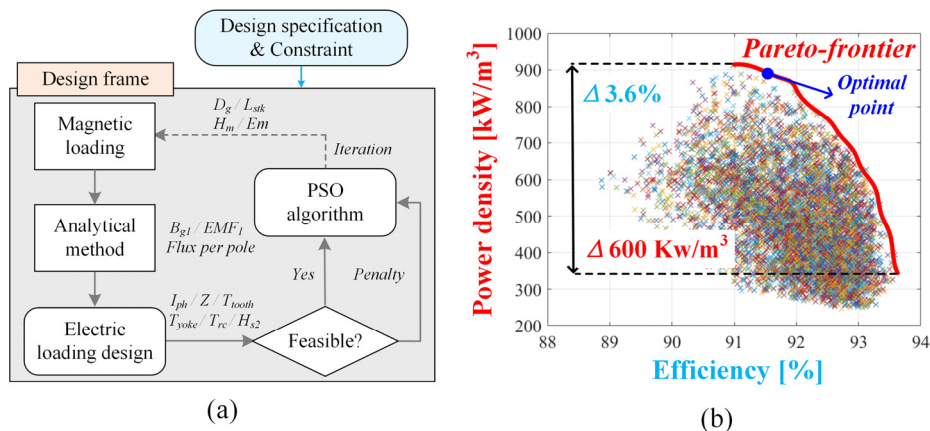


Fig. 1. (a) Proposed initial design automation frame
(b) Efficiency and power density pareto-front of 15000 design candidates

Grain Boundary Diffusion of La Based Low-melting Alloy to Nd-Fe-B Sintered Magnets

Ye Ryeong Jang^{1*}, Hyungju Lee², Jaeryung Lee², Hyun-Sook Lee^{1†} and Wooyoung Lee^{1†}

¹Department of Materials Science and Engineering, Yonsei University, Seoul 03722, Republic of Korea

²Department of Powder Materials Development, Hyundai Motor Company, Hwaseong 18280, Republic of Korea

The high-performance Nd-Fe-B magnets have been widely used in many different applications, such as motors, generators, actuators, hard disk drives, and communication devices, since their discovery in 1894. In order to improve the performance of Nd-Fe-B magnets, grain boundary diffusion process is carried out by using heavy rare-earth element (HRE) such as Dy or Tb. Many efforts have been made to prepare high-performance Dy/Tb

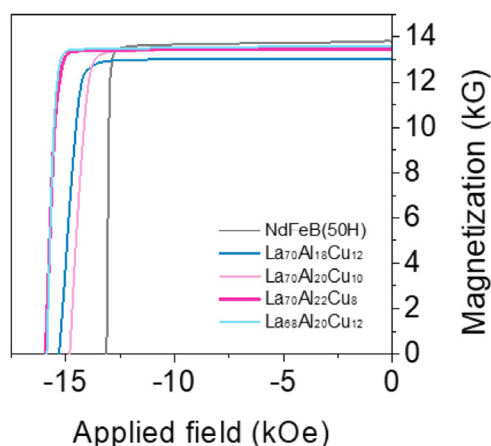


Fig. 1. Demagnetization curves for LaAlCu-GBDP magnets.

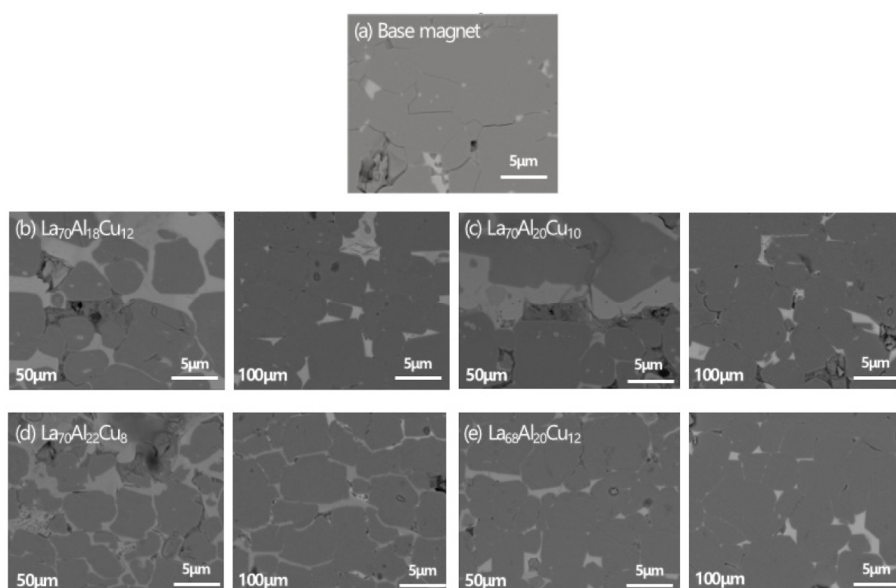


Fig. 2. BSE image for LaAlCu-GBDP magnets at a depth of 50μm and 100μm from the magnet surface.

diffused Nd-Fe-B sintered magnets. However, these heavy rare-earth elements (Dy, Tb) have a problem that prices and supply are unstable.

In this study, we have investigated the magnetic properties of Light rare-earth element (LRE) diffused Nd-Fe-B magnets. The alloys containing less expensive rare-earth element and low-melting metals work effectively as diffusion sources. Metals or compounds with low melting points can modify boundary structure by improving the wettability between intergranular phases and matrix phases. La based alloys effectively diffused along grain boundary phases and formed non-ferromagnetic phases, improving exchange decoupling and enhancing the coercivity. In order to analyze the microstructures, we use scanning electron microscopy. It is expected to provide solutions for cost reduction of GBDP and NdFeB magnets production by saving rare-earth resource.

해석적 방법을 이용한 영구자석 전동기의 특성 해석

이훈기*, 최장영†

충남대학교

영구자석 동기전동기는 속도 제어 등의 가변속 제어가 용이하고 에너지 밀도가 높은 희토류계 자석을 사용함으로써, 가전기기, 컴퓨터 주변기기 등 산업 전반에 필수적인 요소가 되고 있다. 영구자석 동기전동기에 대한 설계 및 특성에 대한 연구들이 활발히 진행되고 있다. 영구자석 동기전동기를 설계하거나 특성 해석을 수행할 경우 대표적으로 유한요소법과 해석적방법이 있다. 유한요소법의 경우 수치해석적인 방법 중에 하나로 해석 시 상용 툴을 이용하여 해석 수행을 할 수 있어 해석의 용이성이 높으나 사용되는 상용 툴 마다의 사용 방법을 익혀야 하고, 해석 모델의 형상이 복잡할수록 요소 분할이 어려워져 설계자의 경험에 의존하게 된다는 단점을 가지고 있다. 해석적 방법은 맥스웰 방정식을 이용한 전자계 특성을 해석하는 것으로 정확도가 높고 빠른 해석

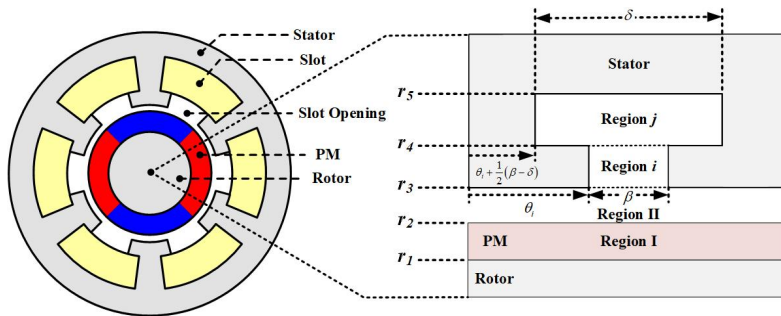


Fig. 1. 해석적 방법을 적용하기 위한 단순화 모델.

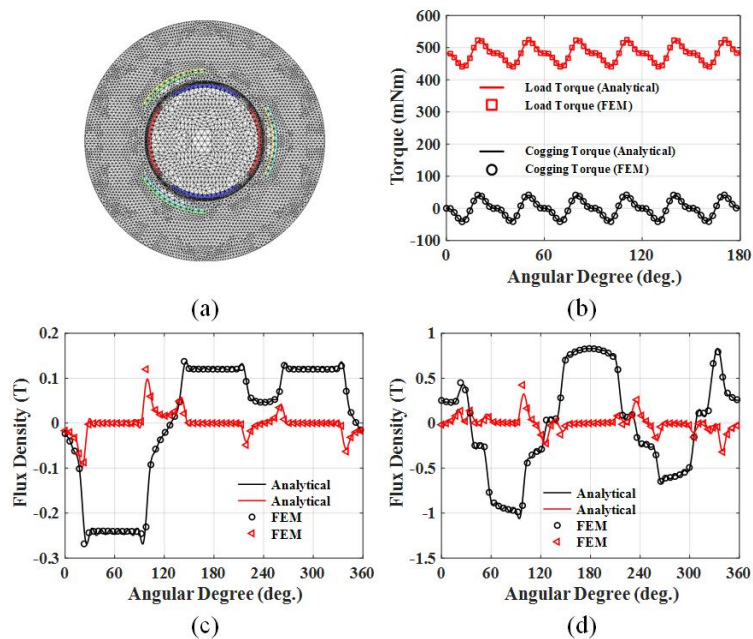


Fig. 2. 해석 결과: (a) 해석 모델의 요소 분할, (b) 전자기적 토크, (c) 전류에 의한 공극자속 밀도, (d) 부하시 공극자속 밀도.

이 가능하지만 이를 위해서는 푸리에 급수를 이용한 자화모델링의 정의, 맥스웰 방정식과 자기 벡터 포텐셜을 통해 도출되는 편미분 방정식을 기기의 형상에 맞는 다양한 경계조건을 고려하여 해를 도출하는 것이 선행되어야하며 자기포화현상을 고려할 수 없는 단점이 있다. 해석적 방법은 유한요소법과 비교했을 때 빠른 해석 시간의 장점이 있고 설계 파라미터에 직관적으로 특성 변화를 예측할 수 있기에 꾸준한 연구가 수행되고있다. 먼저 해석적 방법의 초기 연구는 슬롯리스 형태의 전기기기에 대한 많은 2 차원 해석 모델이 제안되었으며 대부분이 개방 회로 해석에 중점을 두었다. 철의 비투자율을 무한하다고 가정한다면, 슬롯리스 영구자석 기기는 매우 간단하며 단순한 영역에서 푸아송 및 라플라스 방정식을 계산하면 공극에서의 자기장을 예측 할 수 있다. 슬롯리스 영구자석 기기에 대한 또 다른 해석 방법은 해석 영역을 나누고 지배방정식으로부터 각 영역의 포텐셜을 계산하고 경계 조건을 이용하여 미정계수를 계산함으로써 해석적 방법의 연구가 활발히 진행되었다. 해석적 방법을 이용한 영구자석 기기의 해석 시 어려운 문제 중 하나는 고정자 측 슬롯의 존재로 인한 슬롯팅 효과를 고려하는 것이다. 영구자석 기기는 회전자와 고정자 사이 공극에서 자기장을 통한 에너지 변환이 발생하므로 정확한 공극 자계의 예측이 필수적이다. 고정자 및 회전자 슬롯의 존재는 공극 자계 분포를 왜곡시키며, 왜곡된 자계 분포는 전자기 특성에 큰 영향을 미친다. 그러므로 슬롯 현상을 고려하지 않고 영구자석 기기를 해석하게 된다면 전자기 특성에 대한 정확한 결과를 예측하기 어렵게 된다.

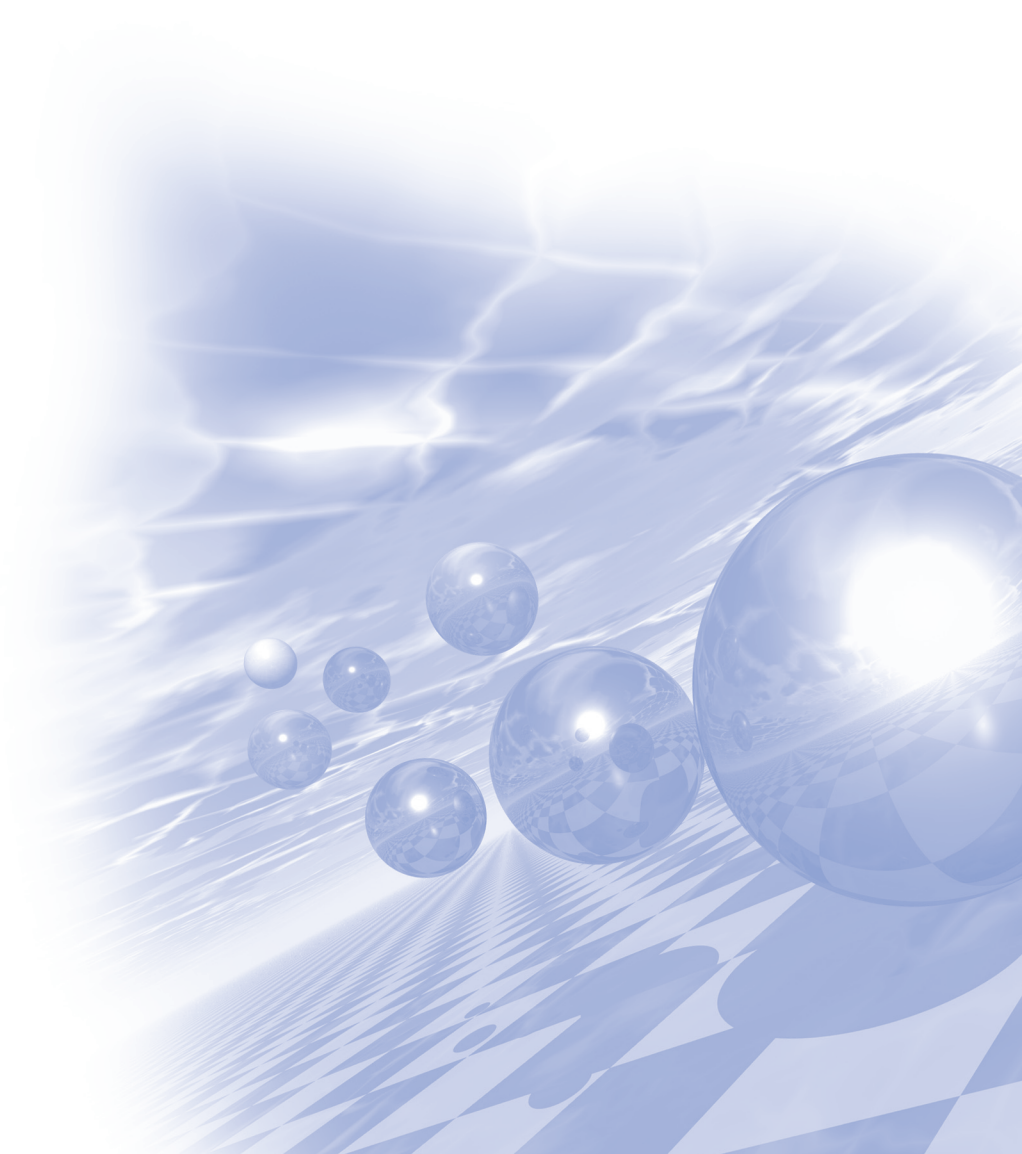
따라서 본 본문에서는 해석적 방법을 통해서 각 영역에 대한 지배방정식 도출하고, 영구자석 및 전류 모델링을 통해서 각 영역에서의 자계 특성을 해석하였다. 도출된 자속과 Maxwell Stress Tensor 를 이용하여 전자기적 토크를 유도하였다. 해석 결과는 유한요소 해석 결과와 비교함으로써 제시된 해석 방법의 타당성을 검증하였다.



2021 KMS Summer Conference

Symposium 4

'Quantum Magnetism'

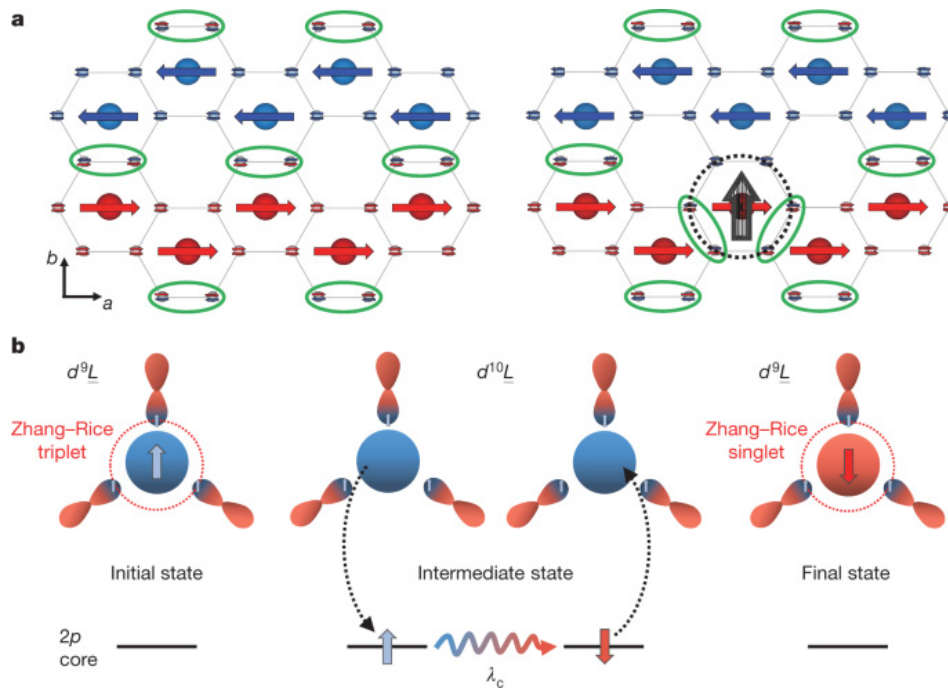


Quantum entangled magnetic exciton in magnetic van der Waals NiPS_3

Je-Geun Park^{*}

Department of Physics & Astronomy, Seoul National University, Korea

The subject of magnetism on two dimensions has been a long and rich history. With the recent discovery of a handful of magnetic van der Waals materials, the field has undergone a remarkable new revolution with many exciting breakthroughs [1,2]. Among those materials, NiPS_3 stands out for its unique XY-type Hamiltonian[3-5], which promises a possibility of study the Berezinskii–Kosterlitz–Thouless transition using real material. Another exciting recent observation is that NiPS_3 has intrinsically quantum entangled ground and excited states [6]. When probed by photons with energy higher than 1.5 eV, it produces a strong photoluminescence peak at low temperature with a remarkably narrow linewidth of 0.4 meV. It was also observed by optical absorption and RIXS (Resonant Inelastic X-ray Scattering) measurements.



References

- [1] Je-Geun Park, J. Phys. Condens. Matter 28, 301001 (2016)
- [2] Kenneth S. Burch, David Mandrus, and Je-Geun Park, Nature 563, 47 (2018)
- [3] C-T Kuo et al., Scientific Reports 6, 20904 (2016)
- [4] S. Kim et al., Phys. Rev. Lett. 120, 136402 (2018)
- [5] K. Kim et al., Nature Communications 10, 345 (2019)
- [6] S. Kang et al., Nature 583, 785 (2020)

Ferromagnetic spin waves of Cr-based van der Waals honeycomb materials

Jae-Ho Chung^{1*}, Lebing Chen² and Pengcheng Dai²

¹Department of Physics, Korea University, Republic of Korea

²Department of Physics and Astronomy, Rice University, U.S.A.

Recent discoveries of robust two-dimensional magnetism brought about a great research interest in van der Waals ferromagnets $\text{Cr}_2\text{Ge}_2\text{Te}_6$, CrI_3 and related compounds [1]. Experimental observations of their spin wave excitations are important because the underlying spin Hamiltonian can provide crucial information regarding the magnetic interactions governing the statics and dynamics of their long-range order. Given the ferromagnetic orderings on honeycomb lattices, their magnon bands are predicted to host the Dirac magnons which are the bosonic counterpart of Dirac fermions observed in the electronic band of graphene [2]. In this talk, we report the inelastic neutron scattering measurements of spin wave excitations in CrX_3 ($X = \text{Br}, \text{Cr}, \text{I}$). Their spin wave bands consist of two ferromagnon modes, which exhibit linear E - p dispersion relations at $Q_K = (1/3, 1/3)$. In CrI_3 at $T = 5$ K, we find that these two bands are separated by a ~ 2 meV gaps suggesting that its Dirac magnons are massive [3-4]. These results can be explained by considering a Heisenberg Hamiltonian with Dzyaloshinskii-Moriya interaction, thus providing experimental evidence that spin waves in CrI_3 can have robust topological properties [3]. We also applied the magnetic field within the honeycomb plane of CrI_3 and repeated the measurements of its spin wave excitations. The analysis of the field dependence rules out the recently proposed

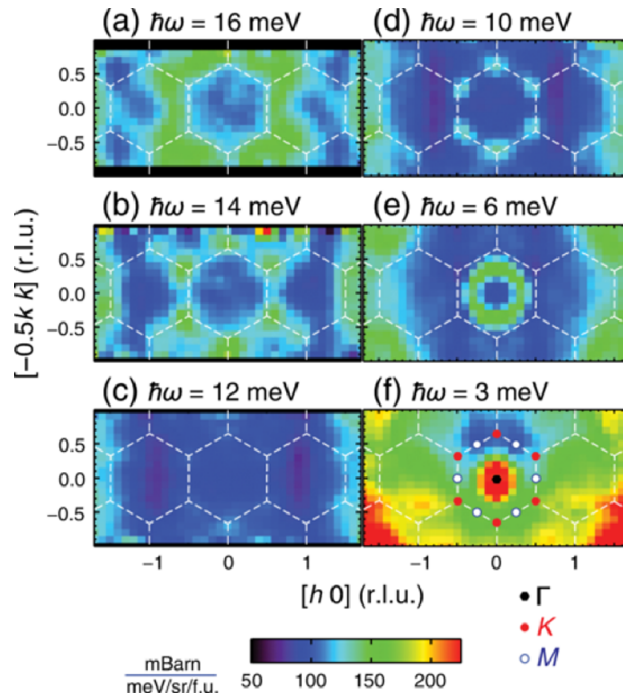


Fig. 1. Constant- E cuts of CrI_3 spin wave spectrum within the reciprocal planes parallel to honeycomb lattice. [3]

alternative gap opening mechanisms based on bond-dependent Kitaev exchanges [5]. In addition, we will also discuss the spin waves of CrBr_3 and CrCl_3 , respectively, where Dirac gap openings are not observed. [The work was supported by the National Research Foundation (NRF) of Korea (Grant no. 22020K1A3A7A09077712 and 020R1A5A1016518).]

References

- [1] C. Gong *et al.*, Nature 546, 265 (2017); B. Huang *et al.*, Nature 546, 270 (2017).
- [2] J. Fransson *et al.*, Phys. Rev. B **94**, 075401 (2016).
- [3] L. Chen *et al.*, Phys. Rev. X **8**, 041028 (2018); L. Chen, et al., Phys. Rev. B 101, 134418 (2020).
- [4] L. Chen *et al.*, submitted for review (2021).
- [5] I. Lee *et al.*, Phys. Rev. Lett. **124**, 017201 (2020).

Noncollinear magnetic order of a new magnetoelectric material determined by single-crystal neutron diffraction

Sungkyun Choi*

Center for Integrated Nanostructure Physics, Institute for Basic Science,
SungKyunKwan University, Suwon, Korea

In magnetoelectric materials, the magnetic structure can be controlled using an electric field, or, conversely, the electric polarisation can be controlled using a magnetic field. Developing these materials could lead to the next generation of energy-efficient devices.

One such candidate is $\text{Co}_4\text{Ta}_2\text{O}_9$ that belongs to a new family of magnetoelectric materials, $\text{A}_4\text{B}_2\text{O}_9$ (where $\text{A} = \text{Mn}, \text{Fe}, \text{Co}$ and $\text{B} = \text{Nb}, \text{Ta}$). Its magnetoelectric behaviour, however, is uncommon and not understood until now. Here we used single-crystal neutron diffraction combined with direction-dependent magnetic susceptibility measurement to accurately determine the magnetic order [1]: key information to explain its novel magnetoelectricity [2].

We found that, below 20.3 K, $\text{Co}_4\text{Ta}_2\text{O}_9$ exhibited unusual long-range antiferromagnetic order, where adjacent spins are pointing in opposite directions. The Co^{2+} ions form alternating the flat and buckled layers stacked along the vertical c-axis, with the magnetic moments lying in the horizontal plane. The buckled arrangement of magnetic ions can be a primary source of moments being aligned at a slight angle to one another, as shown in the figure below.

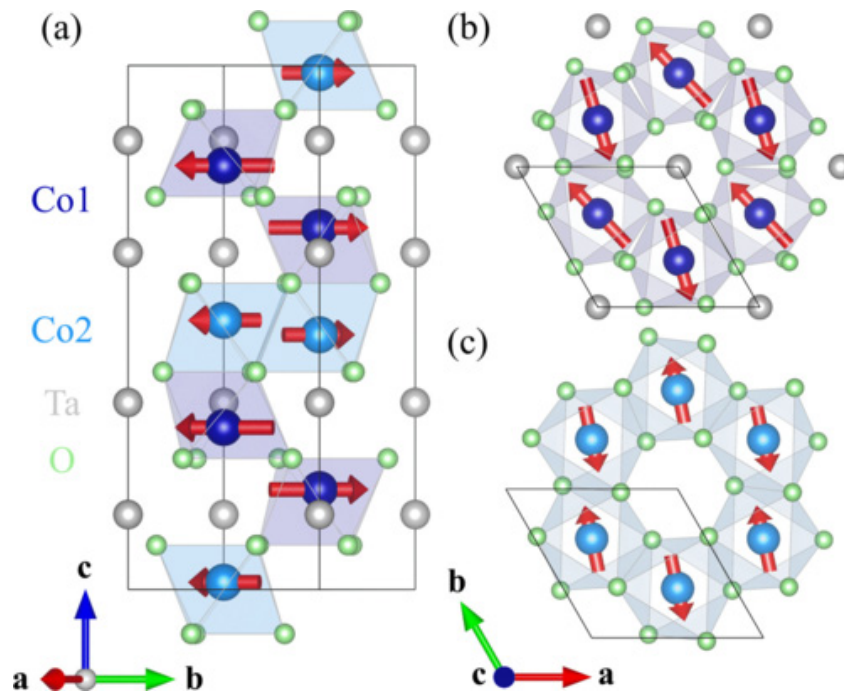


Fig. 1. The refined magnetic structure of $\text{Co}_4\text{Ta}_2\text{O}_9$ at 15 K

Surprisingly, this magnetic structure is different to that observed for $\text{Co}_4\text{Nb}_2\text{O}_9$, an isostructural and isoelectronic compound. Our result is unexpected, as it was thought that the magnetic behaviour of both compounds was due to the Co^{2+} ions, suggesting that nonmagnetic $\text{Ta}^{5+}/\text{Nb}^{5+}$ ions may also influence their novel magnetic property.

We further carried out symmetry analysis based on the determined magnetic order [1], which we were able to explain successfully why the peculiar magnetoelectricity is seen in $\text{Co}_4\text{Ta}_2\text{O}_9$ [2].

References

- [1] S. Choi et al, Physical Review B 102, 214404 (2020) (Editors' Suggestion).
- [2] Nara Lee et al, Scientific Reports 10, 12362 (2020).

Thermal Hall Transport in Spiral Magnet and Spin Liquid

Jung Hoon Han^{*}

Department of Physics, Sungkyunkwan University, Korea

I discuss recent observation of thermal Hall transport in a spiral magnet hosting the skyrmion lattice phase. The magnon thermal Hall effect caused by the magnons seeing the skyrmion as a source of emergent magnetic flux had long been predicted theoretically, but was not observed until recently [1]. The observed magnon thermal Hall effect (THE) finds convincing agreement with the model calculation which I will describe. In the second part of the talk, I discuss the observation of THE in a kagome spin liquid compound Cd-K [2]. A careful analysis of the data suggests dual origin of the transport coming both from phonons and some kind of spin excitations. A sketch of the theoretical idea behind such interpretation will be given.

References

- [1] M. Akazawa et al., arXiv:2102.06430 (2021).
- [2] M. Akazaka et al., Phys. Rev. X. **10**, 041059 (2020).

Deconfinement and hidden phases of U(1) quantum spin liquids

SungBin Lee*

Korea Advanced Institute of Science and Technology, Daejeon, 34141, Korea

Quantum spin liquids are one of the most intriguing phenomena with emergent gauge structures and fractionalized excitations. Here, we first revisit the mapping between spin-1/2 Hamiltonian and U(1) lattice gauge theory and discuss the rigorous argument for quantum deconfinement. Then we discuss how such emergent gauge fields and fractionalized particles can be controlled under the lattice strain effect and external magnetic field. In particular focusing on a U(1) quantum spin liquid, we argue possible frustration in gauge fields and large thermal Hall effect as a signal of such frustration. In addition, we develop a new formalism which leads a proper description of intermediate range in between deconfined quantum spin liquids and confined ordered phases. For a U(1) quantum spin liquid, particularly, we show it can give birth to abundant daughter phases such as a (charged-)Z₂ spin liquid and a super solid without need for fine-tuning of parameters. These results are of broad relevance to quantum spin liquids subject to a parton description and offer a new perspective for searching exotic hidden phases in quantum magnets.

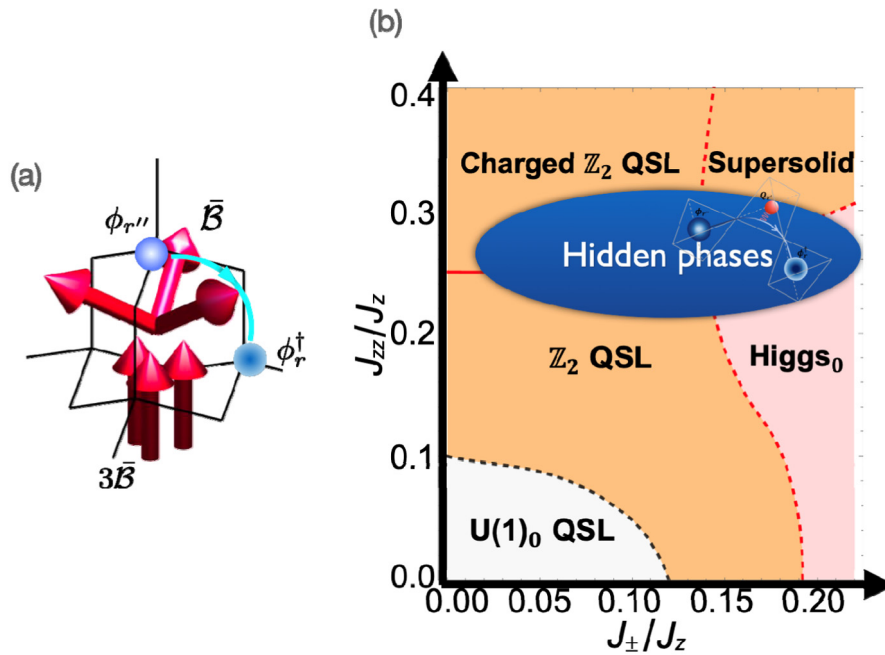


Fig. 1. (a) spinons in the background of staggered gauge fluxes
(b) Hidden phases due to gauge charge - spinon coupling

Composite Spin Construction of a Topological Order

Kyusung Hwang^{*}

School of Physics, Korea Institute for Advanced Study (KIAS), Korea

Topological orders are exotic but complex quantum states with massive entanglement and anyonic quasiparticles, lying beyond Landau paradigm. Exactly solvable models, if available, are of great importance as they enhance our understanding on esoteric structures of topological orders and anyons. Here we introduce a novel approach to build a Z_2 topological order on a particular type of lattices. Specifically, an exactly solved spin model is constructed on a honeycomb lattice by employing the newly discovered, composite spin representation. The model is shown to realize the toric code type Z_2 topological order. We provide an intuitive picture of our construction via an exact mapping to a quantum dimer model on a kagome lattice. We find this approach is applicable to any trivalent lattice. We discuss novel continuous topological transitions induced by additional interaction terms.

Field-angle anisotropy of magnetic excitation and specific heat in proximate Kitaev systems under an in-plane magnetic field

Beom Hyun Kim^{*}

Korea Institute for Advanced Study, Korea

The magnetic phase transition of proximate Kitaev system α -RuCl₃ under the magnetic field has recently drawn much attention because of putative intermediate spin liquid phase. The antiferromagnetic zigzag order of α -RuCl₃ is transferred into the polarized phase through the intermediate phase (IP) in the presence of the magnetic field. The non-Abelian spin liquid phase has been proposed as the IP because of observed half-integer plateau of thermal Hall conductivity and field-angle anisotropy of specific heat under the magnetic field.

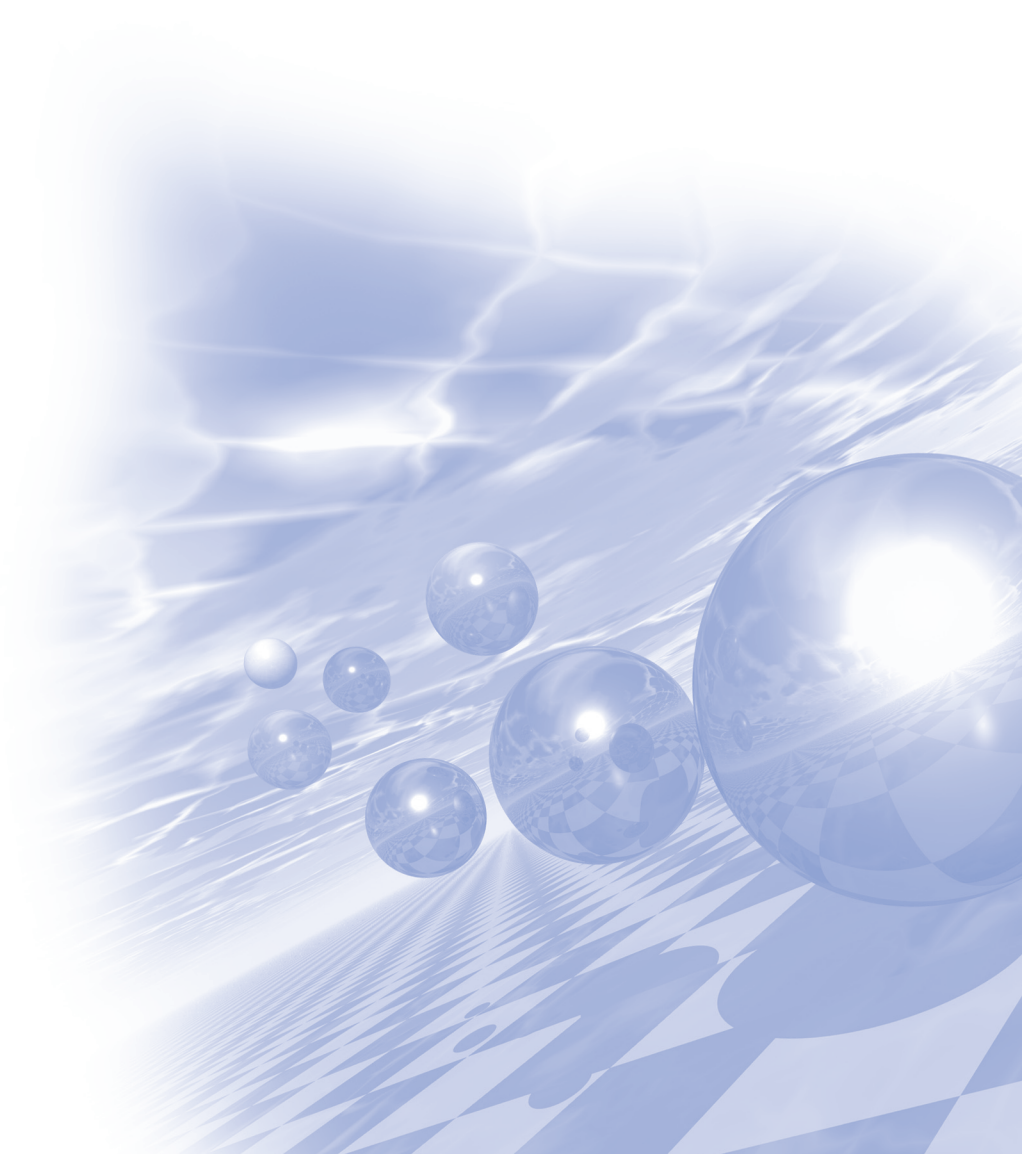
In this study, we investigated the field-angle anisotropy of magnetic excitation and specific heat in proximate Kitaev systems under an in-plane magnetic field. Using the exact diagonalization method and linear spin-wave theory, we demonstrated the magnetic specific heat in the polarized phase can show qualitatively the same field-angle behaviors as that in the non-Abelian spin liquid phase.



2021 KMS Summer Conference

Symposium 5

‘Magnetic Sensors and Micro-Devices’



자기 저항 신호를 이용한 저주파수 와전류 센서 개발 연구

김동영*, 윤석수

안동대학교 물리학과

침투 깊이(skin depth)에 의존하는 와전류(eddy current) 신호는 금속의 결함 검출, 두께 측정, 전기 전도도 측정 등 다양한 분야에 활용되고 있으며, 비파괴용 와전류 탐상 장치는 주로 코일이 사용되고 있다. 가스관과 같이 투자율이 높고, 두께가 두꺼운 강자성 금속 재료의 결함 검사 및 두께 측정은 침투 깊이가 우수한 저주파수 자기장이 요구된다. 저주파수 특성이 열악한 코일을 대체하기 위하여 자기저항(magnetoresistance, MR) 기반의 와전류 탐상 장치의 개발이 활발히 진행되고 있다. 본 연구에서는 자기저항(magnetoresistance, MR) 신호를 사용하여 SM20C 탄소강 강판의 와전류 신호를 측정하여 강판에 형성된 결함 및 두께 측정 성능을 분석하였다.

먼저, 코일과 자기 저항 신호를 사용하여 결함에 의해 유도된 와전류 신호를 측정하였다. 와전류 신호는 코일과 자기 저항 모두에서 결함의 깊이에 따라 증가하는 경향을 보였으나, 저주파수 결함 검출 성능은 코일보다 자기저항 신호가 매우 우수하였다. 한편, 자기저항 신호를 이용하여 저주파수에서 측정한 와전류 신호의 위상은 강판의 두께에 따라 선형적으로 증가하는 특성을 보였으며, 이는 강판의 두께 측정에 위상 변화가 유용하게 사용될 수 있다. 이렇듯 저주파수 특성이 우수한 자기 저항 신호는 강판 내부에 형성된 결함 검출 및 두께 측정을 위한 비파괴 검사용 와전류 센서로의 활용이 기대된다.

자기센서를 이용한 비파괴 결함탐상 및 인공지능을 이용한 결함 평가

박덕근^{1,3*}, 김재민¹, 서호건², 이진이⁴

¹한국원자력연구원, 재료안전기술개발부, 대전광역시, 대한민국

²한국원자력연구원, 인공지능응용연구실, 대전광역시, 대한민국

³주식회사 아이피트, 대전광역시, 대한민국

⁴조선대학교, 전자공학부, 광주광역시, 대한민국

배관의 손상을 탐지하기 위하여 펄스 와전류와 자기장 시각화하는 자기카메라를 통해 배관 결함을 비파괴적으로 평가하는 기술을 소개한다. 소형 배관의 내부에 홀센서 어레이를 이용한 자속밀도 측정을 통해 배관결함을 검출하였으며, 통계적 처리로 제거하기 어려운 노이즈 및 실험 상의 오차를 딥러닝 및 인공지능 기술을 도입하여 결함 검출 능력을 향상시켰다. 자속밀도분포 분석을 통한 비파괴 분석을 위해서는 배관 용접부의 기계적 특성값이 정적/시변 자속밀도 분포에 미치는 영향을 해석하는 것이 필요하다. 특히, 배관 용접부의 기계적 특성값에 따라 변화하는 전자기적 특성값에 대한 분석과 실험을 실시하고, 전자기적 특성값에 따라 변화하는 정적 자속밀도 분포와 시변 자속밀도 분포의 실험적 연구를 수행하였다. 이를 통해 용접부의 시험편 두께 변화, 균열, 자속밀도 분포와 시변 자속밀도 분포에 미치는 영향을 해석할 수 있다. 이 분석 결과를 토대로 균열, 결함 진전, 응력집중, 열화 등의 결함에서 발생하는 지표와 두께변화, 표면조도, 형상 등에서 발생하는 비결함 노이즈 신호를 구별하고, 이 둘을 정확히 평가하기 위한 전자계 인가방법을 해석하였다. 이 해석결과를 토대로 시험편에 인가하는 전류밀도 및 자속밀도의 크기와 주파수에 의한 결함-비결함 신호의 해상력을 파악하고자 하였다. 자기장 시각화 및 딥러닝을 통한 분석을 통해 결함의 분류 및 결함 형상의 시각화가 가능함을 확인하였다.

펄스 와전류를 이용한 비파괴 시험은 도체에 전류를 가할 때 발생하는 와전류의 변화량을 이용해 시험 대상을 분석하는 방법이다. 펄스 와전류 비파괴 검사는 배관의 외부 단열을 제거하지 않고 내부 결함을 검사할 수 있지만 비접촉식 비파괴 검사이므로 정확도 향상을 위해 많은 연구가 필요하다. 펄스 와전류 비파괴 검사 방법을 검증하기 위해 내부 계단 모양의 두께에 차이가 있도록 파이프 모양의 시험편을 측정 하였다. 시험편 소재의 합금 제조 공정의 특성상 소재의 불균일로 인한 측정 오차로 동일한 두께에서도 측정 값에 오차가 발생한 탓에 기존의 잘 알려진 통계적 신호 처리 방법으로는 실험 결과를 구별하기 어려웠고 분석하기도 어려웠다. 펄스 와전류 비파괴 시험을 개선하기 위해서는 측정 결과의 변화 인자 중 시험편의 두께 차이로 인한 변화량 추출 방법이 필요하다. SVM 을 통해 두께에 따른 측정 값의 변화량을 구별 할 수 있었으나, 측정 값 편차가 작은 시험편의 얇은 부분에서는 정확도가 떨어졌다. CNN 을 이용한 딥 러닝 알고리즘은 SVM 으로 변화량을 구별하기 어려운 구간에서도 변화량을 구별할 수 있었다.

자기장 카메라의 경우 측정을 원하는 부위에 접촉식 검사를 시행해야 하며 이면결함탐지는 어려운 대신 탐지 속도가 빠르며 신속한 검사가 가능한 데다 결함의 형상 판별에 강점이 있다. 펄스 와전류를 통한 검사의 경우 속도가 느리며 결함 형상 정보를 얻는 것이 어려우나 탐지면 직접 접촉 없이 검사가 가능하며, 이면 결함이나 보온재나 표면 보호재가 있음에도 결함 탐지가 가능하다는 장점이 있다. 상보적인 두 결함 검사 방식의 결합을 통하여 더욱 효율적이고 정확한 결함 탐지 방법이 가능할 것으로 기대된다.

3-축 자기장 gradiometer를 사용한 지하 매설물의 깊이와 크기의 추정

김은애^{1*}, 손대락¹, 류권상²

¹(주)센서피아

²한국표준과학연구원

지하에 매설된 철금속 물체를 탐지하는데 ElectroMetric Impedance(EMI), ElectroMagnetics Induction(EMI) 및 자기장 특성 방법을 사용하고 있다. EMI 방식은 주로 지하에 깊게 묻혀 있지 않은 물체를 탐지하는데 효과적이다. 땅속 깊이 있는 금속물체를 측정하는 데는 자기장을 측정하거나 자기장의 기울기(Magnetic gradiometer)를 측정하는 방법을 많이 사용하고 있다. 그러나 일반적으로 위치를 판단하고 있으며 탐지물체의 깊이나 크기를 측정하는데 많은 어려움이 있었다.

본 연구에서는 2개의 직각도가 보장되는 3-축의 자력계[1][2]를 동일 좌표축이 되고, 1-축을 수직 방향으로 일정거리에 두게 하여 피탐자물체의 의한 수직방향 자기장 gradiometer 성분과 수평방향의 자기장 gradiometer

성분을 측정하여 피탐지물체의 깊이와 물체의 magnetic moment 크기를 측정할 수 있는 방법을 고안하였다. Magnetic moment 크기는 피탐지물체의 질량에 비례하기 때문에 피탐지물체의 크기를 추정할 수 있다. 그림 1. 은 3-축 자력계 2개로 제작된 3-축 자기장 기울기 측정 자력계를 사용 지하 매설물의 거리와 크기를 추정하는 자력계의 구조이다. 수직 성분의 자기장 gradient 성분으로부터 구한 지하 매설물의 깊이 $r_z = \frac{l}{\sqrt[3]{\left(\frac{B_{1z}}{B_{2z}}\right)} - 1}$ 와 자기장의 수평

성분의 크기 $B_p = \sqrt{(B_x^2 + B_y^2)}$ 로부터 구한 지하매설물의 깊이 $r_p = \frac{l}{\sqrt[3]{\frac{B_{1p}}{B_{2p}}} - 1}$ 가 같아야 한다. 이 경우가

이론 적으로 잘 측정되었다는 것을 의미하며, 이 경우 수직 및 수평성분의 자기모멘트 m_z 및 m_p 로부터 자기모멘트의 크기 $m = \sqrt{m_z^2 + m_p^2}$ 을 구할 수 있고 이는 지하매설물의 크기에 비례하기 때문에 지하매설물의 깊이와 크기의 추정이 가능하여 진다.

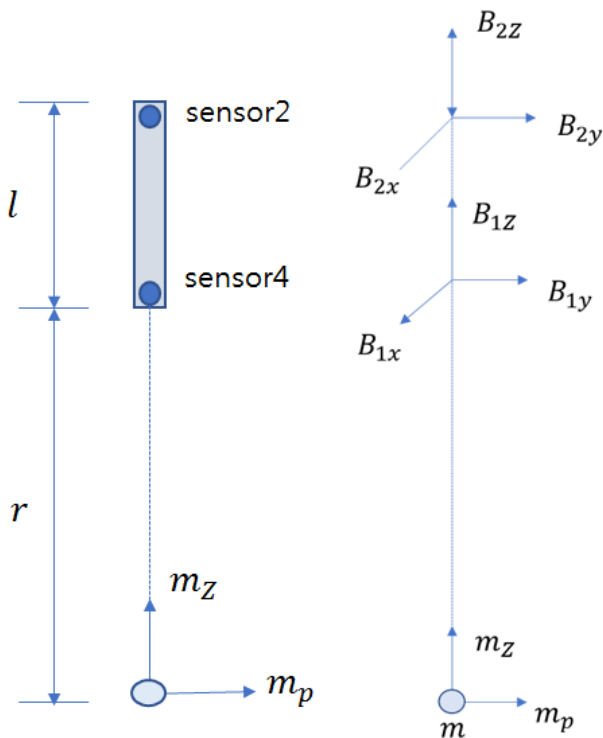


Fig. 1. Schematics of 3-axis magnetic field gradiometer.

References

- [1] 손대락, “피드백형 플럭스게이트 마그네토미터 제작”, 한국자기학회지, Vol.22, No.2, p.45-48(2012)
- [2] 손대락, “자기장크기 측정이 가능한 3-축 Flux-gate 마그네토미터 제작”, 한국자기학회지, Vol.29, No.5, p.171-176(2019)

Carbon fiber 및 Ag/AgCl 전극에 기반한 고감도 수중 전기장 센서

정현주*, 이상규, 배기웅, 양창섭

국방과학연구소 해양기술연구원

기뢰 및 항만감시체계는 표적으로부터 발생하는 자기장 신호를 주 탐지원으로 활용하고 있으나, 최근 탈자(deperming) 및 소자(degaussing) 기술 등 표적의 자기스텔스 기술이 나날이 발전함에 따라서 수중에서 자기 표적을 탐지하는 것이 점차 어려워지고 있다. 자기스텔스 표적을 탐지하기 위한 새로운 대안으로, 미국, 유럽 등 군사 선진국들은 수중 표적으로부터 발생하는 전기장 신호를 탐지하기 위한 전기장센서를 개발하여 자국 무기체계에 탑재하여 운용 중에 있다. 함정 선체는 해수에서 선체와 프로펠러간의 전위차로 인해 부식이 발생되고, 이로 인해 해수에서 부식 전류가 선체와 프로펠러 사이에 흐른다. 선체 부식을 방지하기 위해 함정은 ICCP 장비를 이용하여 선체 외부로 방식 전류를 강제적으로 인가한다. 선체 부식 전류와 ICCP 장비의 방식 전류에 의해 수중에는 전기장 신호가 발생된다. 이러한 신호는 함정 선체 폭에 해당하는 수십에서 수백~수천 $\mu\text{V}/\text{m}$ 의 크기를 가지지만 이를 감소시키기는 매우 어려우므로 수중 무기체계 입장에서는 좋은 탐지 신호원이 된다. 따라서 본 논문에서는 carbon fiber 및 Ag/AgCl 전극에 기반한 무기체계용 수중 전기장 센서에 대해서 기술하였다.

수중 전기장은 그림 1과 같이 해수 내 위치한 두 전극 사이의 전위 차(ΔV)와 두 전극 사이의 간격(L)으로부터 계산된다. 따라서 센서 전극 간격이 크면 클수록 센서의 감도와 잡음 대 신호비는 좋아지게 된다. 하지만 무기체계는 내부 공간상의 제약으로 센서 전극의 간격을 무한정 키울 수가 없고, 전극 간격이 크면 표적 탐지 시 공간 분해능이 나빠진다. 그러므로 센서 전극의 자체잡음을 줄임으로써 센서의 잡음 대 신호비를 증대시키는 것이 무기체계용 수중 전기장 센서에서는 매우 중요하다. 수중 전기장 센서의 전극 재질은 Ag/AgCl 혹은 carbon fiber소재가 주로 사용되고 있다. 잡음 준위는 1Hz에서 수 $\text{nV}/\sqrt{\text{Hz}}$ 이내 수준으로 큰 차이가 없지만 통상적으로 수 $\text{mHz}\sim 1\text{Hz}$ 대역의 극 저주파수 대역에서는 Ag/AgCl 전극의 잡음 수준이 탄소섬유 전극보다 우수한 것으로 알려져 있다.

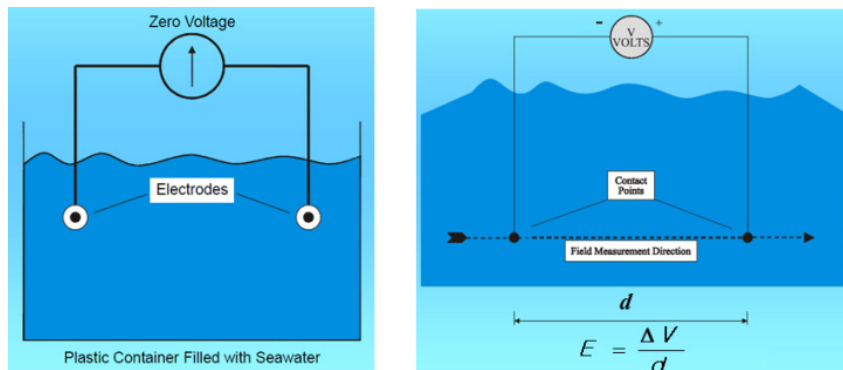


Fig. 1 Fundamental of underwater electric field sensor



Fig. 2. Ag/AgCl 전극 (Ultra PMES사)



Fig. 3. carbon fiber 전극(Polyamp사)

전기장 센서 전극에서 측정되는 신호는 매우 미약하므로 이를 증폭시키기 위한 저잡음 신호증폭기가 필요하다. 특히 관심주파수 대역이 수십 mHz의 극 저주파수 대역까지 포함되므로 신호 증폭기는 저주파수 대역에서 저잡음 특성을 가져야 한다. 이를 위하여 전기장 센서용 신호증폭기는 저 주파수 대역에서의 플리커 잡음(flicker or 1/f noise)을 줄이기 위한 초핑 방식의 신호 증폭 기술을 활용하고 있다. 초핑 증폭기는 그림 2와 같이 modulator/demodulator, transformer isolation, AC amplifier 등으로 구성되어 입력 신호 대역폭의 최소 10배 이상의 초핑 주파수로 수신된 전기장 신호를 변조한 후 증폭한다. 그림 2(b)에서 볼 수 있듯이 일반적인 신호 증폭기의 경우, 저주파수 대역에서의 입력 잡음이 크므로 고주파 대역으로 변조(modulation)된 신호는 증폭과정에서 증폭기의 잡음 특성에 큰 영향을 받지 않는다. 그림 3(c)와 같이 증폭된 신호는 복조(demodulation)를 통해서 원래의 전기장 신호 대역, 즉 저주파수 대역으로 복원이 되고 저주파수 대역의 잡음 신호는 고주파 대역 신호로 변조된다. 그림 2(d)와 같이 고주파 대역으로 변조된 잡음 신호는 Low Pass Filter를 통해서 제거된다[1].

수중 전기장 신호는 3축 방향에서 측정이 가능하다. 영국, 스웨덴 등에서 개발된 3축 수중 전기장 센서는 기본적으로 6개의 전극으로 구성되고, 센서 전극을 설치하기 위해 많은 공간이 필요하다. 따라서 공간적인 제약으로 6개의 전극을 설치하는 것이 어려운 무기체계의 경우, 아래 그림 3과 같이 소수의 인접한 전극사이의 전위차를 이용하여 4개 혹은 5개의 전극을 활용하여 3축 수중 전기장 센서를 구현할 수 있다. 이럴 경우 추가적인 신호 증폭기가 요구된다.

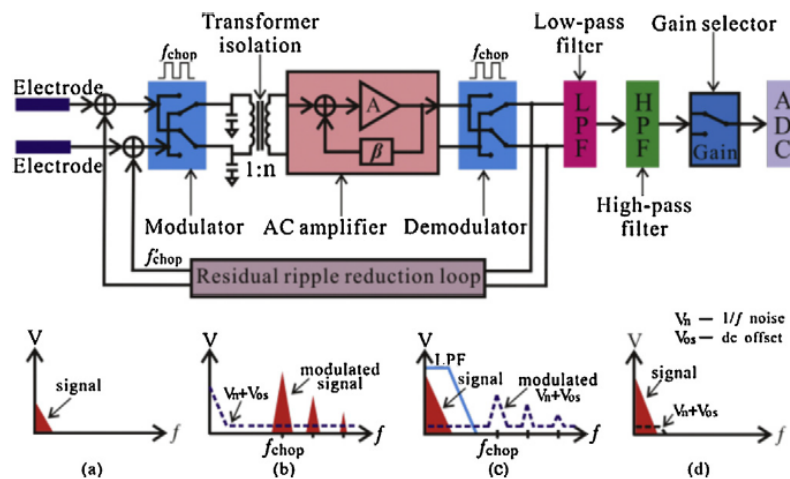


Fig 2. The basic principal of chopper signal amplifier[1]

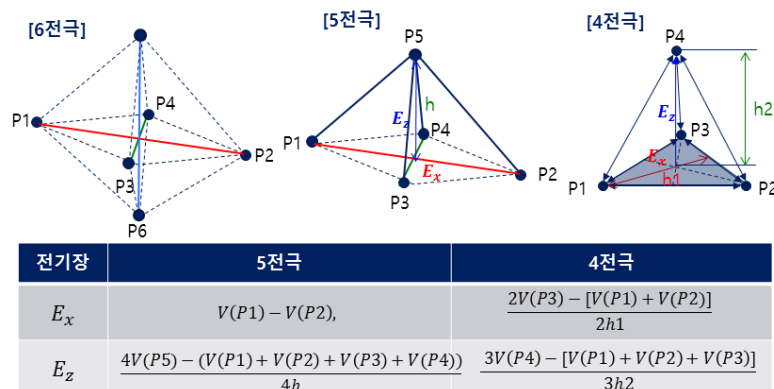


Fig. 3. Electric field calculation of 3-axis electric field sensor according to the electrode number

Reference

- [1] Z. Wang et al., Sensors and Actuators A, 213, pp. 70–78.

Study on the Possibility of Magnetic Field Communication for High-Sensitivity GMI Sensor

Jang-Yeol Kim*, Hyun Joon Lee, Jae-Ho Lee, Jung Hoon Oh and In-Kui Cho

Radio & Satellite Research Division, ETRI, Daejeon 34129, South Korea

Magnetic sensors play an increasing role in wireless sensor networks. Thus, studies have focused on the applicability of these sensors to wireless communication systems in underwater and underground environments [1]. In these environments, the conventional technique of using microwaves faces many challenges, including path loss, multi-path fading and signal propagation delays due to the presence of soil, rock and water, which are composed of various components [2-4]. Techniques that use the magnetic field can solve these issues. Specially, with a non-conventional medium, communication based on magnetic induction (MI) and the giant magnetoimpedance (GMI) are a good alternative when attempting to address the challenges of microwave-based communication. In order to communicate in extreme environments such as underwater and underground, a sensor capable of detecting a weak magnetic field is required, and a representative example is the GMI sensor. The GMI sensor has a high magnetic field-to-voltage conversion ratio to detect the weak magnetic field. In this paper, in order to experimentally verify the possibility of magnetic field communication using the GMI sensor, the GMI receiver was implemented using an off-diagonal GMI sensor as a receiving element, and the experimental results were analyzed. Here, the important characteristic of the GMI receiver for magnetic field communication is that it is equivalent to its own super-heterodyne radio topology, which performs typical amplitude modulation (AM) with respect to the external magnetic signal. In an off-diagonal GMI sensor, the output voltage spectrum shows that the external magnetic signal is up-converted when modulated with the carrier driving the sensor. Hence, the GMI sensor can be considered as identical to the combination of an antenna and an up-conversion mixer. Also, the voltage conversion ratio of the proposed off-diagonal GMI sensor achieved 194kV/T at an external alternating current (AC) frequency of 60kHz, showing the best performance. To verify the possibility of magnetic field communication for the proposed GMI receiver, a demonstration of OOK digital data transmission was conducted. When comparing transmitting and receiving waveforms, it was confirmed that the possibility of utilizing the GMI sensor as a receiver is apparent.

Acknowledgements: This work was supported by Institute of Information & communications Technology Planning & Evaluation (IITP) grant funded by the Korea government (MSIT) (No. 2019-0-00007, Magnetic Field Communication Technology Based on 10pT Class Magnetic Field for Middle and Long Range).

References

- [1] J.Y. Kim et al, "A novel experimental approach to the applicability of high-sensitivity giant magneto-impedance sensors in magnetic field communication", IEEE Access, vol. 8, pp. 193091-193101, 2020.
- [2] Z. Sun and J. F. Akyildiz, "Magnetic induction communications for wireless underground sensor networks", IEEE Trans. Antennas Propag., vol. 58, no. 7, pp. 2426-2435, July 2010.
- [3] S. Wang and Y. Shin, "Efficient routing protocol based on reinforcement learning for magnetic induction underwater sensor networks", IEEE Access, vol. 7, pp. 82027-82037, 2019.
- [4] Z. Sun and I. F. Akyildiz, "Underground wireless communication using magnetic induction", in Proc. IEEE Int. Conf. Commun., pp. 1-5, Jun. 2009.

Mechanism and manipulation of magnetic microrobot for medical applications

Sung Hoon Kim^{1,2*}

¹Department of Electronics Convergence Engineering, Wonkwang University 460 Iksandae-ro Iksan, Korea

²Wonkwang Institute of Material Science and Technology, Wonkwang University, 460 Iksandae-ro Iksan, Korea

Nanofibers are being widely applied in biomedicine, especially in tissue engineering given their porosity. We developed magnetic nanofibrous membranes aiming to devise new applications that use their thermal properties and mobility for actively targeted hyperthermia and microrobots. We fabricated Fe_3O_4 (iron oxide)/PAN (polyacrylonitrile) nanofibrous membranes and verified the properties of corresponding nanoparticles/fiber composites. Fe_3O_4 is a material with superparamagnetic properties under a critical size and can be controlled by a magnetic field and heated up by a high frequency alternating magnetic field. The Fe_3O_4 /PAN nanofibers in this study were prepared at concentration of 20, 25, and 30 wt% by dispersing Fe_3O_4 nanoparticles of 20 nm in a PAN solution. At a nanoparticle concentration of 30wt%, the magnetic membrane generated heat up to 49.9°C in a magnetic field of 15.57kA/m and a driving frequency of 205.9 kHz during 600 s. In addition, we investigated the performance for steering and active locomotion (robotic control) of a magnetic nanofibrous membrane with 3 mm in diameter by using magnetic force control. The ranges (0.08~.014 mT/mm) of fiend gradient provided an average movement speed of 2.15 mm/s with accurate steering. The robotic control ability of the proposed magnetic nanofibrous membrane seems promising for increasing the diversity of biomedical applications for magnetic nanofibers as microrobot.

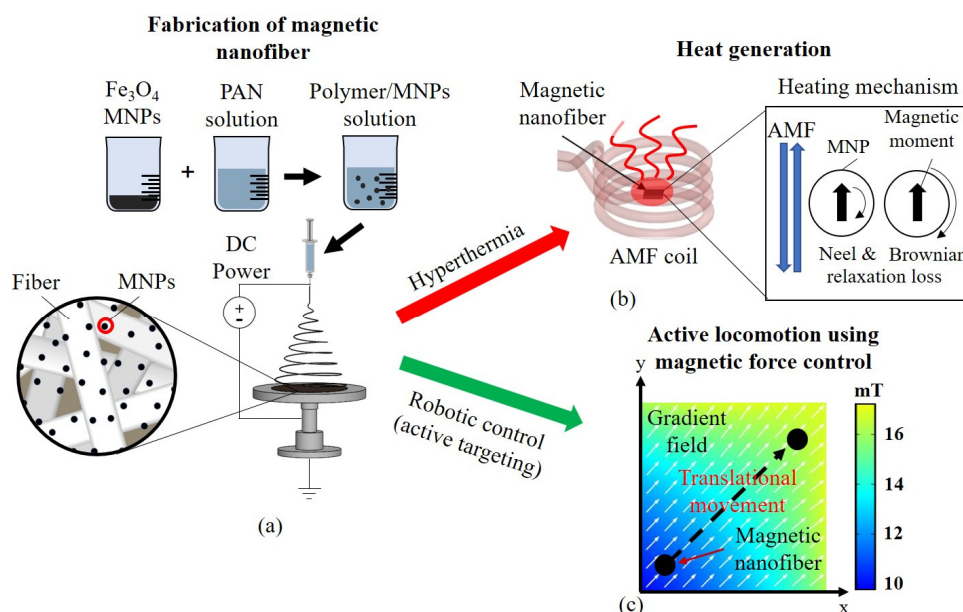


Fig 1. (a) Schematic diagram of electrospinning including nanoparticles. (b) Heating mechanism of developed magnetic nanofibrous membrane. (c) Principle of active locomotion using magnetic force.

친환경자동차(xEV)용 전류센서의 기술동향

박종민^{1*}, 황병봉¹, 이희성¹, 김대원¹, 조준호²

¹(주) 티엔씨 충남 아산시 둔포면 아산밸리로 304-29

²한국자동차연구원 충남 천안시 동남구 풍세면 풍세로 303

전기자동차의 수요 증가와 관련 기술의 발전은 친환경, 에너지 절약 등 사회적인 이슈에 부합할 뿐 아니라, 자동차 구동에 있어서 화석연료의 사용에서 전기에너지로 변화하게 되면서 기술적 패러다임을 변화시키는 것이다. 전기자동차의 구동이 전기에너지에 의해서 이루어지게 되므로, 전기자동차 내부 및 충전시스템에서의 전기에너지의 계측 및 관리는 에너지의 효율적인 사용은 물론 저탄소, 친환경에도 중요한 영향을 미칠 수 있다. 전기자동차에서 전기에너지 계측은 주로 전류 센서를 이용한 전류 측정으로 이루어지며, 에너지 저장 및 사용(배터리), 구동계(모터), 충전전 시스템을 포함한 다양한 목적으로 전류 센서가 사용되고 있다. 전류 센서의 성능은 전기자동차의 성능, 효율적 관리, 안정성, 에너지 절감에 직접적으로 연관되므로 전류 센서의 성능향상에 대한 요구도 전기자동차의 성능 발전과 고급화에 따라 증대되고 있다. 전류 센서는 크게 셉트 저항 타입, CT 타입, 자기 센서 타입으로 나눌 수 있다. 셉트 저항 타입 전류 센서는 필연적인 전력 소모와 과전류에 의한 불안정에 대한 문제가 있고, CT 타입의 전류센서는 원리상 직류 측정에 한계가 있다. 따라서, 자기 센서 타입의 전류 센서가 향후 전기자동차용 전류 센서의 핵심이 될 전망이다. 자기 센서 타입의 전류 센서의 성능 향상을 위해서 기존의 홀 센서이외에도 MR, GMR 등 자기 저항형 센서와 플렉스게이트 형 센서가 꾸준히 제안되고 있으며, 전류 센서의 사용 용도와 고급화에 대한 요구에 따라 고정밀화/고감도화가 시급하다. 본 강연에서는 전기자동차에 사용되고 있거나 사용이 예상되는 용도 및 시장 전망에 대해서 개괄한다. 또한 현시점에서의 전류센서의 성능을 바탕으로 기술적 전망을 전개하며, 전기자동차의 발전 전망에 부합하는 각종 전류센서의 향후 기술개발 방향을 제시하고자 한다.

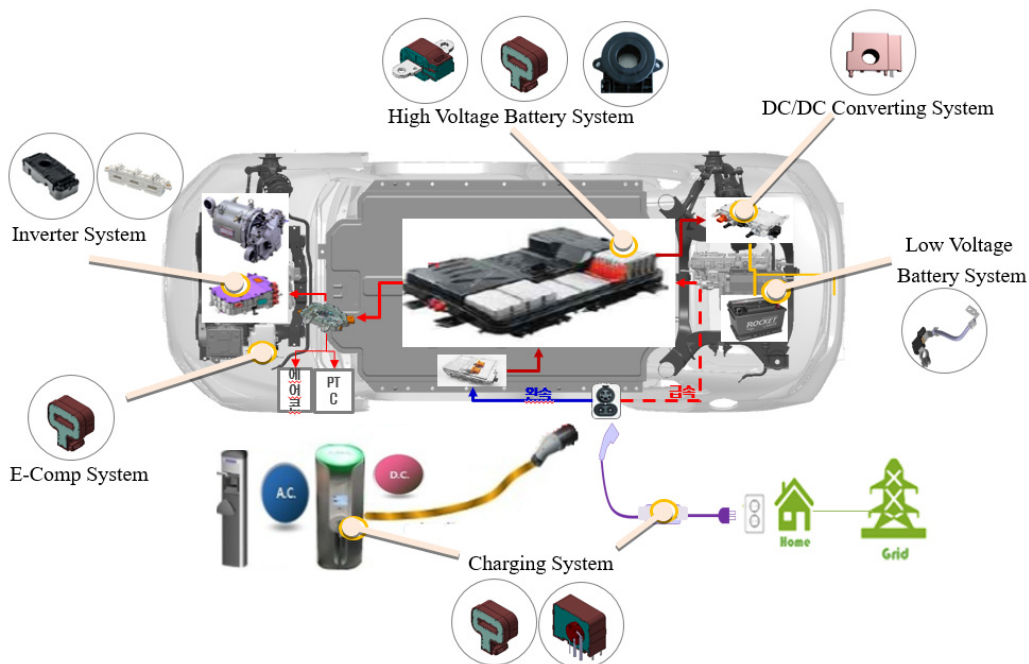


Fig. 친환경 자동차의 전류센서 적용현황

Development of pin-type magnetic sensing probe with PHR of the 10nT resolution targeting for highly integrated PCB analysis

Nam Young Lee^{1*}, Dal Ho Lee², Dae Sung Lee²

¹DNJTECH, 503, 65, Dongpyeon-ro 13beon-gil, Dongan-gu, Anyang-si, Gyeonggi-do, Korea

²Korea Electronics Technology Institute, 68, Yatap-dong, Bundang-gu, Seongnam-si, Gyeonggi-do, Korea

For characterization or failure analyses of electronic devices such as PCBs, the most common method is to measure the voltage waveform with an oscilloscope. Since there are many kinds of problems, however, that cannot be detected by the voltage waveform, several other methods such as x-ray transmission, infrared imaging or eddy current measurement have been applied for these analyses. But these kinds of methods also have limits to overall analyses because they are partially useful for finding some physical defects such as disconnection or short. Fundamentally, current waveform measurement during the operation of electronic devices should be analyzed, but commercially available current sensor has not yet been developed, especially for the applications on highly integrated PCB products with sub-mm fine pitch. In this project, we developed a high-sensitivity PHR magnetic sensor targeting for the application on highly-integrated PCBs. The developed magnetic sensor showed good enough features of an ultra-small size of below 100um, 10nT magnetic field resolution, 1mA current resolution, and 1MHz operating frequency, to be applied for the PCB analyses.

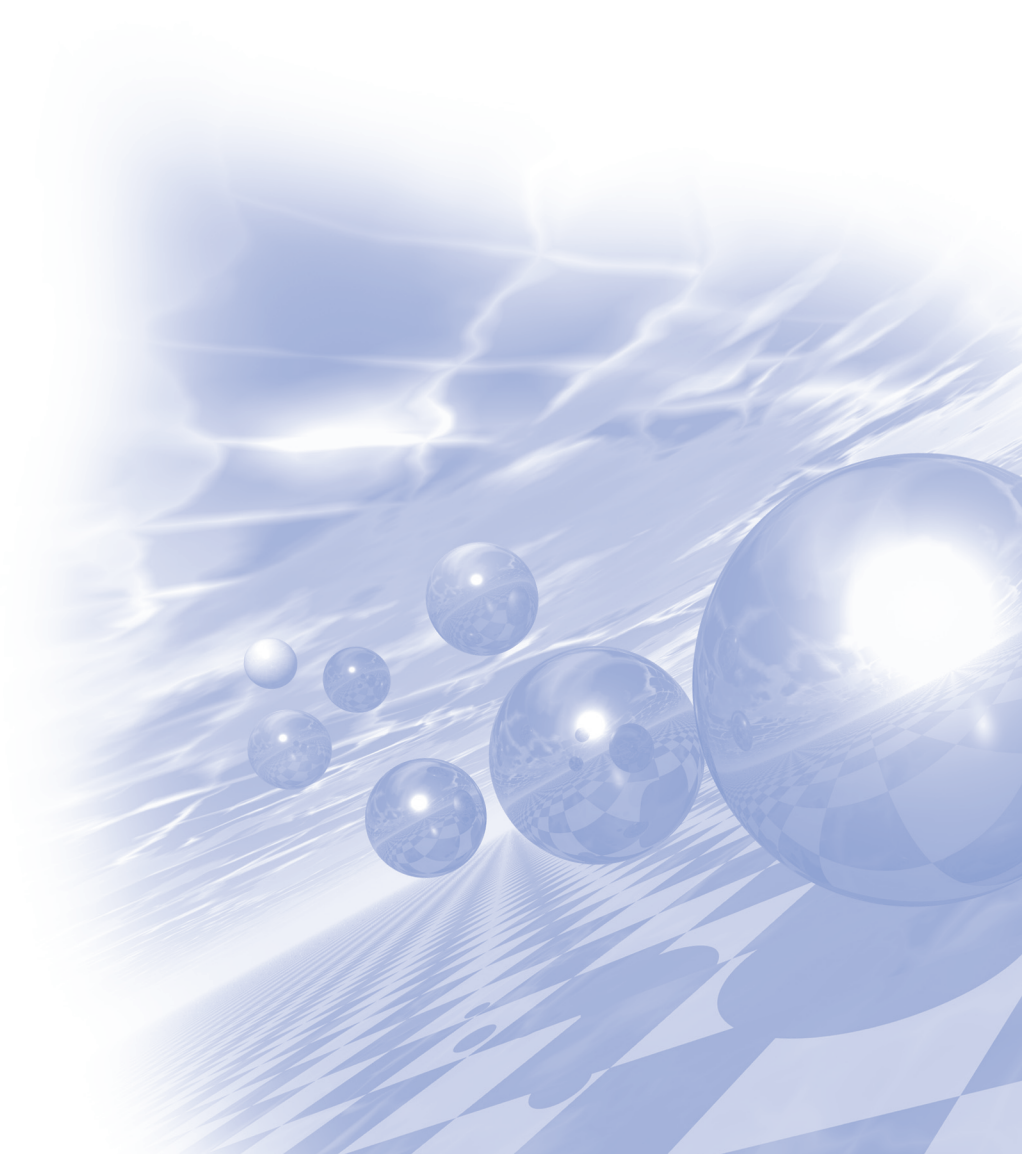
In this presentation, we will introduce the development process of the magnetic sensing probe and its characteristic results in detail, and show some proto-type image processing result of the current waveform generated in a test circuit, measured by the sensor. In future, we will develop the real-time image processing tool of the current waveform generated in any electronic device including EV by using this technology and expect that the tool will analyze the overall current map of the device and provide useful results for diagnosing its characteristics or failure analysis.



2021 KMS Summer Conference

Symposium 6

‘Magnetization Dynamics’



Observation of strong bulk spin-orbit torques in the van der Waals ferromagnet Fe_3GeTe_2

Franziska Martin¹, Kyujoon Lee^{1,2*}, Maurice Schmitt¹, Anna Liedtke¹, Aga Shahee¹,
Haakon Thømt Simensen³, Tanja Scholz⁴, Tom G. Saunderson¹, Dongwook Go⁵,
Martin Gradhand^{1,6}, Yuriy Mokrousov^{1,5}, Thibaud Denneulin⁷, András Kovács⁷,
Bettina Lotsch⁴, Arne Brataas³, Mathias Kläui^{1,3}

¹Institute of Physics, Johannes Gutenberg-University, 55099 Mainz, Germany

²Division of Display and Semiconductor Physics, Korea University, 30019 Sejong, Korea

³Centre for Quantum Spintronics, Department of Physics, Norwegian University of Science and Technology, 7491
Trondheim, Norway

⁴Max Planck Institute for solid state research, 70569 Stuttgart, Germany

⁵Peter Grünberg Institut and Institute for Advanced Simulation, Forschungszentrum Jülich and JARA,
52425 Jülich, Germany

⁶School of Physics, H H Wills Physics Laboratory, Tyndall Avenue, Bristol, BS8 1TL

⁷Ernst Ruska-Centre for Microscopy and Spectroscopy with Electrons and Peter Grünberg Institute,
Forschungszentrum Jülich, 52425 Jülich, Germany

The recent emergence of magnetic van der Waals materials allows for the investigation of current induced magnetization manipulation in two dimensional materials. Uniquely, Fe_3GeTe_2 has a crystalline structure that allows for the presence of bulk spin-orbit torques (SOTs), that we quantify in a Fe_3GeTe_2 flake. From the symmetry of the measured torques, we identify the current induced effective fields using harmonic analysis and find dominant bulk SOTs, which arise from the symmetry in the crystal structure. Our results show that Fe_3GeTe_2 uniquely can exhibit bulk SOTs in addition to the conventional interfacial SOTs enabling magnetization modification even in thick single layers without the need for complex multilayer engineering.

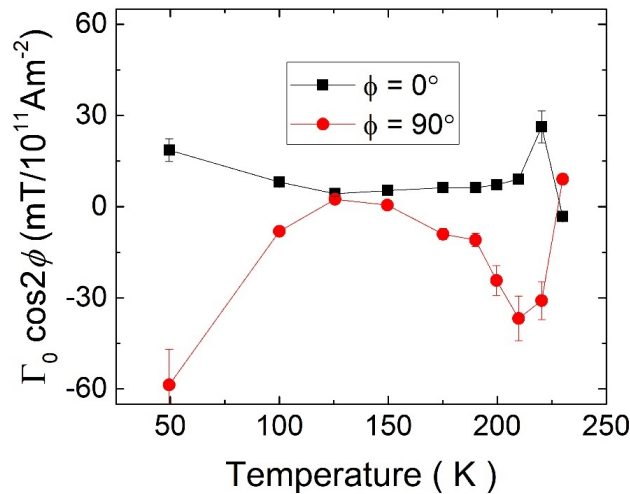


Fig. 1. Temperature dependence of bulk spin-orbit torque effective fields

Observation of Correlation Between Unidirectional Spin Hall and Magnon Magnetoresistances

Sanghoon Kim^{*}

Department of Physics, University of Ulsan, Ulsan, 44610, Korea

Magnons, quasi-particles from collective modes of spin excitations in a magnetic solid, have been one of the most intriguing and fundamental objects in the condensed matter physics. Such quanta of spin waves can result in exotic phenomena such as quantum Bose-Einstein condensation, spin pumping, spin Seebeck effect, and magnon-related transports. In addition to those important discoveries, various logic devices have been proposed for the future data technology because magnons can deliver information without Joule heating-induced power dissipation [1]. Here, i) energy-efficient generation, ii) long-range propagation, iii) clear detection are important issues for developing magnonic devices.

In this presentation, we suggest that magnetic thin films of epitaxially grown Cr/Fe bilayer with strong uniaxial magnetic anisotropy can have Ising-type exchange energy, resulting in an increase of magnon population via spin-flip process by spin current. In particular, the observed crystallographic dependence of magnon generation implies that the crystalline direction of current flow should be a considerable factor for the magnon generation.

Reference

- [1] A. V. Chumak, V. I. Vasyuchka, A. A. Serga & B. Hillebrands, Magnon spintronics. *Nat. Phys.* **11**, 453 (2015).

Current and Future Prospect of MRAM technology in Semiconductor Industry

Seung-heon Chris Baek^{*}

Center for Spintronics, Korea Institute of Science and Technology, Korea

Spintronic devices offer low power consumption, built-in memory, high scalability and reconfigurability, and could therefore provide an alternative to traditional semiconductor-based electronic devices. Today, a number of major semiconductor companies are developing STT-MRAM as a new type of non-volatile memory and some products are already appearing in the market by major foundries.

In this talk, I will give a brief introduction of what is going on in the industry regarding the development of MRAM, especially STT-MRAM. STT-MRAM technology shows the highest maturity among emerging memories. There are various applications and role of STT-MRAM in the semiconductor industry. We will go through current MRAM technology development, learn what makes MRAM such an attractive alternative to current semiconductor technology. Moreover, we will talk about the weakness and the challenge spintronic devices face. Finally we will talk about some new technologies for next generation MRAM.

References

- [1] Chung et al., IEDM Tech Digest 27.1, 2016
- [2] Aggarwal et al., IEDM Tech Digest 2.1, 2019
- [3] Alzate et al., IEDM Tech Digest 2.4, 2019
- [4] Han et al., IEDM Tech Digest 11.2, 2020
- [5] Naik et al., IEDM Tech Digest 11.3, 2020
- [6] Shih et al., IEDM Tech Digest 11.4, 2020
- [7] Baek et al., Semicon Korea STS S3, 2019
- [7] Baek et al., Nature Electronics 1 398-403, 2018

Photoinduced ultrafast magnetization dynamics in ferromagnetic thin films

Dong-Hyun Kim^{*}

Department of Physics, Chungbuk National University, Cheongju, Korea

Magnetization dynamics on ultrafast time scales has attracted much attention due to possible application for fast-operating spintronic devices. Nonequilibrium magnetization dynamics on femtosecond timescale is basically linked with fundamental entities such as spin, electron, and lattice in the solid. Recent findings on the photo-induced demagnetization behavior of ferromagnetic system will be introduced, where high flux photon pulses of femtosecond duration hit the sample with excitation of spin, electron, and lattice are followed. As an example of ultrafast magnetization dynamics, ultrafast magnetic cooling phenomenon under external magnetic fields will be introduced. Lastly, THz emission behavior involved with ultrafast spin dynamics will be also covered.

The interfacial Dzyaloshinskii-Moriya interaction in the heavy metal/Co/heavy metal sandwiched structure

Jaehun Cho*, June-Seo Kim

Division of Nanotechnology, Daegu Gyeongbuk Institute of Science and Technology (DGIST)

Recently, an additional exchange interaction, which is the so-called Dzyaloshinskii-Moriya interaction (DMI) at the interfaces between ferromagnets and heavy metals plays a crucial role in the formation of the non-collinear spin structure. The class of non-collinear magnetic structures is originated from the competition between the Heisenberg exchange and the DMI. The Brillouin scattering is useful equipment to investigate magnetic properties such as interfacial DMI, perpendicular magnetic anisotropy, and saturation magnetization.

In this study, we experimentally investigate the magnetic properties of a novel magnetic sandwich structure, which contains an interfacial DMI energy density. The systematic Brillouin light scattering measurement is performed for HM1/Co/HM2 structures to measure various magnetic parameters. Here, we choose Pt, Pd, W, Ta for the heavy metal layer. We will discuss the thickness dependent properties of interfacial DMI at the HM1/Co/HM2 sandwiched structures.

Quasi-Static Strain Effect on Ultrafast Magnetization Dynamics

Yooleemi Shin^{1,2}, Mircea Vomir³, Dong-Hyun Kim², Phuoc Cao Van⁴,
Jong-Ryul Jeong⁴ and Ji-Wan Kim^{1*}

¹Department of Physics, Kunsan National University, Kunsan 54150, South Korea

²Department of Physics, Chungbuk National University, Cheongju 28644, South Korea

³Université de Strasbourg, CNRS, Institut de Physique et Chimie des Matériaux de Strasbourg,
UMR 7504, Strasbourg 67034, France

⁴Department of Materials Science and Engineering, Chungnam National University, Daejeon 34134, South Korea

*Email: hwoarang@kunsan.ac.kr

The thermal lattice expansion by photo-excitation generates two types of strain, which are the well-known propagating strain pulse and the quasi-static strain (QSS) induced from long-lived thermal expansion of lattice within the penetration depth. The QSS has not been regarded despite its comparable amplitude to that of the propagating one. As one of principal reasons, we consider that QSS and thermal energy are inextricable in photo-induced experiments, therefore QSS effect, which is not familiar, might have been misled to be a temperature effect. The three-temperatures model, that we have used so far without a doubt, does not contain the information of strains that exist as long as thermal expansion does, but only consider the thermal effect, that is temperature profiles of sub-systems. This fact does not provide proper analyses and might hinder unveiling new physics in ultrafast phenomena. Here, we prove the existence of QSS using time-resolved magneto-optical Kerr effect and time-resolved Sagnac interferometer and demonstrate that QSS effect prevails over thermal effect in Co(25 nm)/sapphire and Ni (270 nm)/sapphire leading to the increase of spin precession frequency with the increase of the pump intensity. The intensity dependence of spin precession of two magnetostrictive materials are shown in Fig. 1(a) and 1(b), respectively.

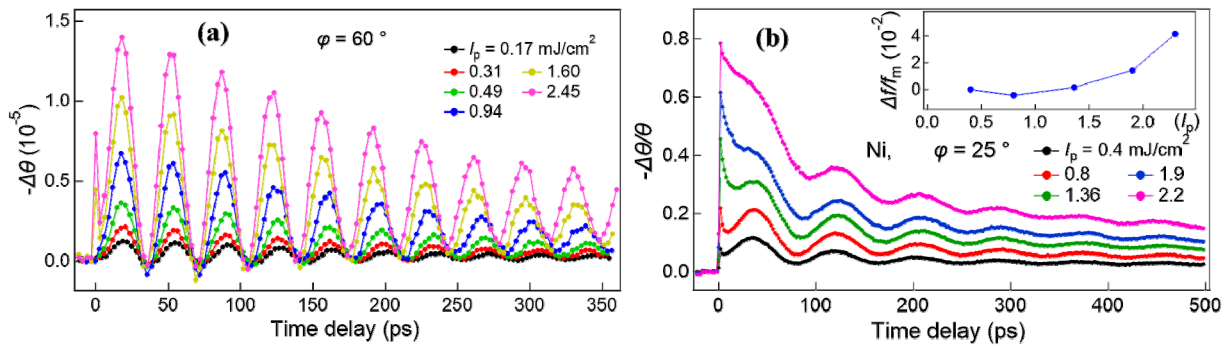


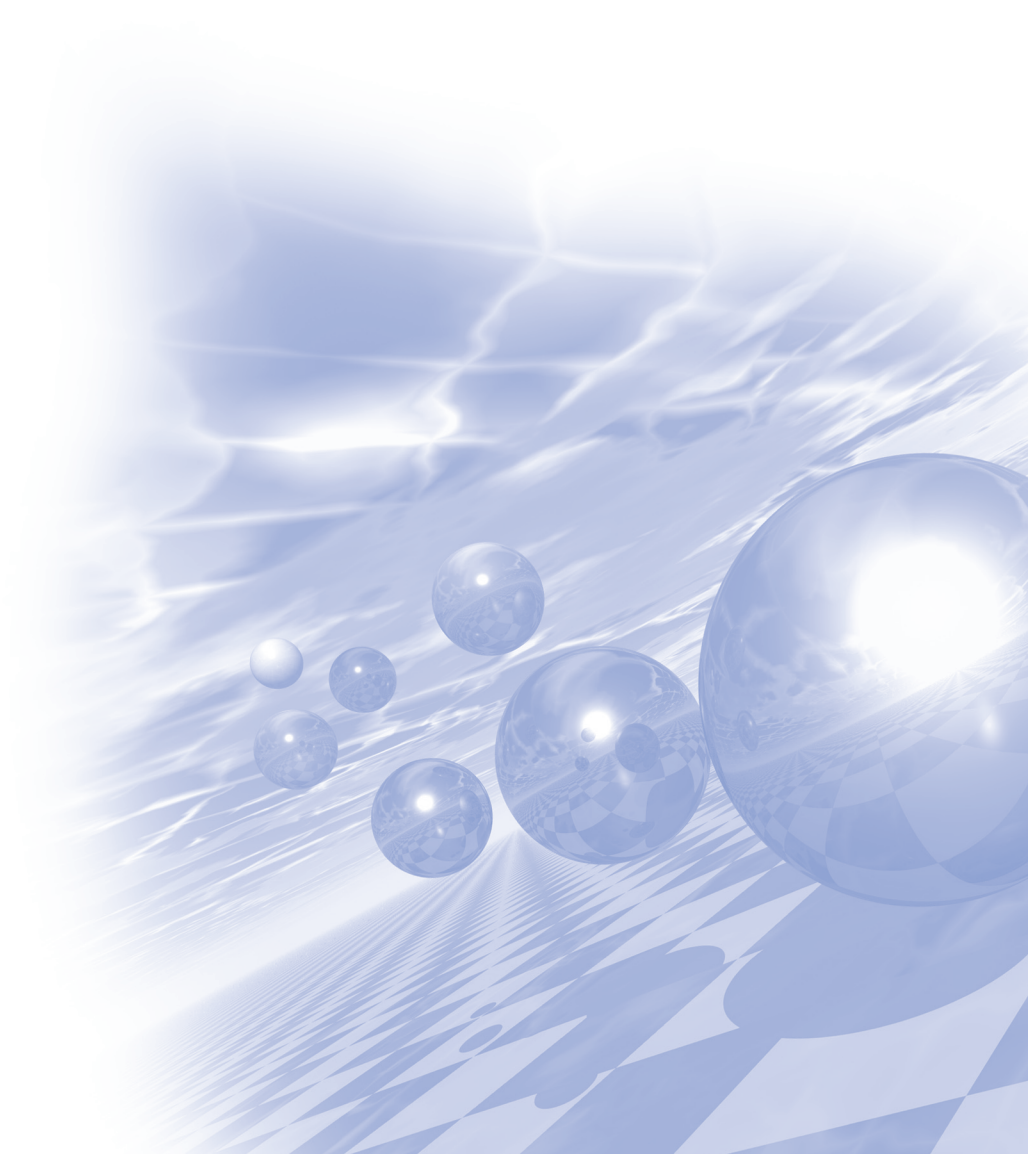
Fig. 1. Differential Kerr rotation of Co(25 nm)/sapphire (a) and Ni(270 nm)/sapphire (b) measured by ultrafast magneto-optical Kerr effect. The inset of (b) shows the inflection point of the spin precession frequency meaning that the thermal effect is dominant in a low pump intensity and the QSS effect becomes dominant in a high pump intensity.



2021 KMS Summer Conference

Symposium 7

'Mössbauer Magnetics'



Activation Study of Precipitated Iron-Based Catalysts for Fischer-Tropsch Synthesis using Mössbauer Spectroscopy

Dong Hyun Chun^{1,2*}

¹Carbon Conversion Research Laboratory, Korea Institute of Energy Research,
152 Gajeong-Ro, Yuseong-Gu, Daejeon 34129, Republic of Korea

²Advanced Energy and System Engineering, University of Science and Technology,
217 Gajeong-Ro, Yuseong-Gu, Daejeon 34113, Republic of Korea

Fischer-Tropsch synthesis (FTS) has been considered a promising way to convert low-value carbon-containing resources into high value-added products via syngas ($\text{CO} + \text{H}_2$). Precipitated iron-based catalysts are commercially viable catalysts for the FTS due to their high reproducibility in mass production as well as their high activity and low cost. In general, the as-prepared precipitated iron-based catalysts are composed of iron(III) oxides that are inactive for the FTS. Therefore, they should be subjected to a proper pre-activation treatment to change the as prepared catalysts into active phases for the FTS. Several oxide and carbide phases evolve in the precipitated iron-based catalysts during the pre-activation and subsequent FTS reaction. This is fairly different from other catalysts that remain in the metallic state during the reaction. This leads to difficulties in drawing active structure in the iron-based catalysts for FTS. Mössbauer spectroscopy has been known as a proven technique for detailed and quantitative analyses of multiple iron phases in the nanocrystalline iron-based catalysts. In this study, we report our recent understanding on the activation study of precipitated iron-based FTS catalysts. The crystallographic analyses by Mössbauer Spectroscopy revealed that the more the ϵ -carbide (Fe_2C) fraction, the longer the chain length of hydrocarbons.

철계코어셸 촉매가 적용된 연료전지용 막전극접합체의 촉매-이오노머 나노계면 제어를 위한 잉크 구조 연구

임성대*, 김성민, 박현욱, 우승희, 강윤식, 이은직, 박구곤, 박석희

연료전지연구실, 한국에너지기술연구원

고분자 전해질 연료전지는 친환경 고효율 에너지 변환 기술로서 수소차와 가정 및 건물의 발전시스템에 주로 적용되고 있다. 고분자 전해질 연료전지의 핵심 부품인 막전극접합체는 수소기체가 지나는 화학 에너지를 전기에너지로 변환하는 산소환원반응을 수행하면서 연료전지의 성능에 직접적인 영향을 준다. 막전극접합체는 수소이온 전도성 고분자막의 양면에 촉매층이 코팅된 구조를 지니며, 촉매층의 구조적 특성이 막전극접합체의 전기화학반응 속도를 결정하는 핵심 요인이 된다. 특히, 촉매층에서 촉매와 나노계면을 이루는 이오노머의 물리화학 특성이 산소환원 및 백금의 피독에 관여하면서 촉매층의 백금 이용률을 제어하는 주요 원인으로 보고되고 있다. 촉매/이오노머 나노계면구조를 제어하기 위하여 여러 방법들이 제안되고 있으며, 최근에는 촉매층 제조의 첫번째 과정인 잉크에 대한 관심이 이러한 관점에서 증가되고 있다. 현재, 잉크를 구성하는 주요 성분인 촉매, 이오노머, 용매간의 상호력 및 이러한 결과로 형성되는 잉크 구조에 대한 이해는 매우 낮은 상황이다.

본 연구에서는 철계 코어셸 촉매가 적용된 잉크 시스템에서 용매 특성에 따른 잉크 구조의 변화를 잉크의 분산 안정성 분석을 통하여 살펴보았다. 철계 코어셸 촉매는 우수한 산소환원반응 특성과 더불어 피스바우어 분광을 통한 나노 구조 분석이 가능한 장점으로 인하여 선정되었으며, 연료전지용 잉크에 일반적으로 사용되는 물과 노말프로필알코올의 혼합용매와 불소계 이오노머를 잉크 연구에 적용하였다. 혼합용매의 혼합 비율과 이오노머의 함량을 변수로 하여 제조된 잉크들의 분산 안정성은 원심력을 인가하며 잉크의 빛 투과도의 시간에 따른 변화를 측정하는 방식으로 분석되었다. 이를 통하여 시간에 따른 잉크 내 촉매 입자들의 뭉침 특성, 이오노머들의 존재형태 및 뭉침 특성 등을 살펴볼 수 있었다. 이를 통하여 잉크 내 촉매 입자와 이오노머, 이오노머와 용매, 용매와 촉매 입자 간의 상호력을 분석하고 이를 기반으로 최적 잉크 조성의 구조적 특성을 제안해 보고자 한다.

The Quantum Theory of Recoilless in Mössbauer Effect

Jong Woan Choi, Hyun Suk Kim, Jung Chul Sur*

Dept. of Semiconductor & Display Technology, Wonkwang Univ. Iksan, Korea

The Mössbauer effect was one of the last major discoveries in physics and the main concept is a process in which a nucleus emits or absorbs gamma rays without loss of energy to a nuclear recoil. The narrow resonance for nuclear gamma emission and absorption results from the momentum of recoil being delivered to a surrounding crystal lattice rather than to the emitting or absorbing nucleus alone and the depth of resonance is determined by the fraction of recoil-free emissions in the source and the resonant absorption cross section in the absorber. The recoil-free fraction of the source is defined to be the fraction of gamma rays that is emitted without recoil.

Solid-state physics tells us that lattice vibrations are quantized, coming only in packets called phonons. Particular theories provide different spectra of lattice vibrations.

The lattice vibrations of the Fe ion in Ba-ferrite was analyzed by Mössbauer spectra at different angles between the γ -ray direction and c-axis. The vibration on the 2b-site was more active compare to other direction and had very strong intensity in the Raman spectrum.

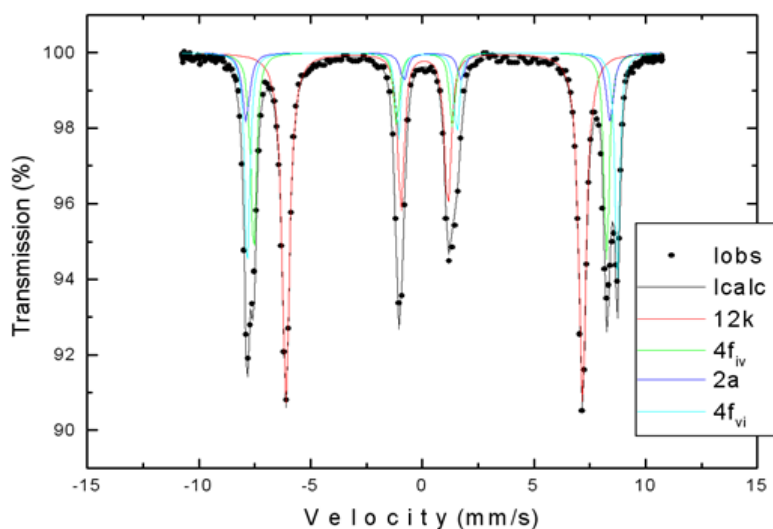


Fig. 1. A Mössbauer Spectrum in Ba-ferrite Single Crystal

The Mössbauer effect was one of the last major discoveries in physics and the main concept is a process in which a nucleus emits or absorbs gamma rays without loss of energy to a nuclear recoil. The narrow resonance for nuclear gamma emission and absorption results from the momentum of recoil being delivered to a surrounding crystal lattice rather than to the emitting or absorbing nucleus alone.

Study on cathode materials using Mössbauer spectroscopy

Hyunkyung Choi^{*} and Chul Sung Kim[†]

Department of Physics, Kookmin University, Seoul 02707, Korea

Various energy storage technologies have been commercialized and used domestically, and technology development is actively underway. The fastest-growing lithium-ion battery in the Energy Storage System is lightweight, has no memory effect, and easily maintains its charge capacity. It is widely used in portable electronic devices and electric vehicles because it can save energy without loss for a long time because of a low natural discharge. A lithium-ion battery is composed of a cathode material, an anode material, an electrolyte, and a separator. Lithium ions, which exist in an ionic state, generate electricity by moving from the cathode to the anode during charging and from the anode to the cathode during discharging. These cathode materials are a reactant participating in an actual electrochemical reaction, and they are required to have an energy density, an output characteristic, increased lifetime characteristics, and improved stability. Therefore, the lithium-ion activation capability of the cathode material determines the performance of the battery. In this presentation, the magnetic properties of iron-based cathode materials were analyzed using X-ray diffraction and Mössbauer spectroscopy. The Mössbauer spectroscopy allowed us to determine the valence states of iron in the crystal structures of cathode and also to unveil the presence of different iron-containing phases. In addition, we present the changes in the structure and iron oxidation state accompanied with lithium extraction and insertion in cathode materials, and study magnetic hyperfine interaction with temperature.

Introduction of Precise Nuclear Measurements and Geostandards

Gwang-Min Sun^{*}, Young Rang Uhm and Jaegi Lee

HANARO Utilization Division, Korea Atomic Energy Research Institute(KAERI), Daejeon, Rep.of Korea

^{*}E-mail: gmsun@kaeri.re.kr

Recently, as the use of analytical instruments increases, researches are actively conducted to improve the accuracy and precision of the analysis results. In particular, geostandards are used in many aspects such as deducting calibration curves in geochemical analysis and determining deviations by comparison with true values. In Korea, studies on the development and production of geostandards have been attempted with increasing demand for Korean geostandard materials, but subsequent work has not been carried out. Currently, research institutes that support the quantitative analysis are using geostandards from foreign research institute like USGS, NIST and GSJ etc. However, due to the disadvantage that it is expensive and difficult to obtain, it is necessary to develop a geostandards using Korean rocks. In this study, we selected three representative granite and obsidian samples and checked the feasibility of developments as a Korean geostandards. Moreover, in order to make a glass geostandard, natural glass rock is used for X-ray fluorescence analysis, Neutron Activation Analysis, and Mössbauer spectroscopy then we will examine the feasibility as a glass geostandards. Glass geostandards are essentially used to precision geochemical analyzers. Further, in order to overcome the limitation in the composition range of the geostandards, it is required to prepare a glass geostandards having a higher composition. In order to minimize the inhomogeneity from the microlites contained in the glassy rocks and the incomplete melting, we conducted the XRF and the Prompt gamma - ray Activation Analysis using the obsidians from Mt. Beakdu, Korea and the Kyushu, Japan, which are the main provinces of the obsidian artifacts excavated from the Korean Peninsula. And then we performed comparison with two analytical data from two different methods. The correlations of the major oxide contents show relative good coincidence between the PGAA and XRF bulk analytical data. Also, in mineralogical and geochemical studies on the Mt. Beakdu, Korea and the Kyushu, Japan, obsidians, the origination of the magma compositions and the crystallization as shown in analyses of Mössbauer spectra.

Proposals to extending Mössbauer study for the Korean cultural properties

Dong Hyeok Moon^{1*}, Eun Woo Lee^{1†}, Ji Hyeon Yoon¹, Young Rang Uhm², Chul Sung Kim³

¹Conservation Science Division, National Research Institute of Cultural Heritage (NRICH), Daejeon 34122, Korea

²HANARO Utilization Division, Korea Atomic Energy Research Institute (KAERI), Daejeon, 34057, Korea

³Department of Nano-electro Physics, Kookmin University, Seoul, 02707, Korea

(*uno23@korea.kr, +82-42-860-9064)

This study aimed to review on the Mössbauer studies for Korean cultural properties, and to make proposals for further advanced study by more various type of applications. In the case of overseas, Mössbauer spectroscopic studies on the components, manufacturing techniques, and characteristic factors of cultural properties is being actively performed. As a representative example, Lycurgus cup in ancient Rome, the red light emitting phenomenon of the blue body was observed by the surface plasmon effect of silver and gold nanoparticles, using the ¹⁹⁷Pt/Pt source and the gamma ray resonance effect. In addition, a comparative study was conducted on the chromaticity of Chinese Song Dynasty celadon and Korean Goryeo celadon by ⁵⁷Fe Mössbauer spectroscopic analysis using ⁵⁷Co/Rh. In the case of Korean cultural properties, iron mineral phase identification of natural raw materials such as Ulleungdo seokganju (natural red pigment) and obsidian (Neolithic tool), as well as the interpretation of coloring factors and formation process, have been studied by ⁵⁷Fe Mössbauer spectroscopy. Furthermore, research on the coloring pattern and manufacturing technique of the Goryeo celadon by oxidation state of trace iron ions in the silicate structure of glaze was conducted. Moreover, recently, it was applied to investigate the coloring effect and manufacturing technique depending on the composition and proportion of amorphous (low crystallinity nanoparticles) iron oxide, coated on the raw soil particles of pottery which fired in lower temperature than porcelain. As reviewed above, Mössbauer spectroscopy can provide newer and various information on the iron-containing cultural properties. Therefore, a further study using Mössbauer spectroscopy, is necessary to apply more various type of archaeological objects which containing iron component, such as earthen artifacts (sculptures, roof tiles, coffins, bricks and painted pigments, other than ceramic ware), glass, jewelry, and iron objects from the iron work archaeological site (iron ore, slag, iron furnace fragment, various iron wares or steel products). In addition, it is expected that it will be applicable to the investigation for national treasures and cultural assets exhibited in museums, which were impossible to collect samples, due to the recent development of the portable Mössbauer spectrometer by the Korea Atomic Energy Research Institute (KAERI). In consequence, it is expected that more innovative research will be possible for more diverse cultural properties, due to the application of Mössbauer spectroscopy and the improved analyzing system development.

Facile Synthesis of Fe@Pt Core-Shell Nanoparticles and Their Electrocatalytic Activity for Oxygen Reduction Reaction

Hyun-Uk Park^{1†}, Eunjik Lee^{1*}, Jeongyun Jang¹, Min Ho Seo², Gu-Gon Park^{1†}

¹Fuel Cell Laboratory, Korea Institute of Energy Research (KIER),
152 Gajeong-ro, Yuseong-gu, Daejeon, 34129, Korea

²Fuel Cell Research & Demonstration Center, Future Energy Research Division, Korea Institute of Energy Research (KIER), 20-41 Sinjaesaengeneogi-ro, Haseo-myeon, Buan-gun, Jeollabuk-do, 56332, Korea

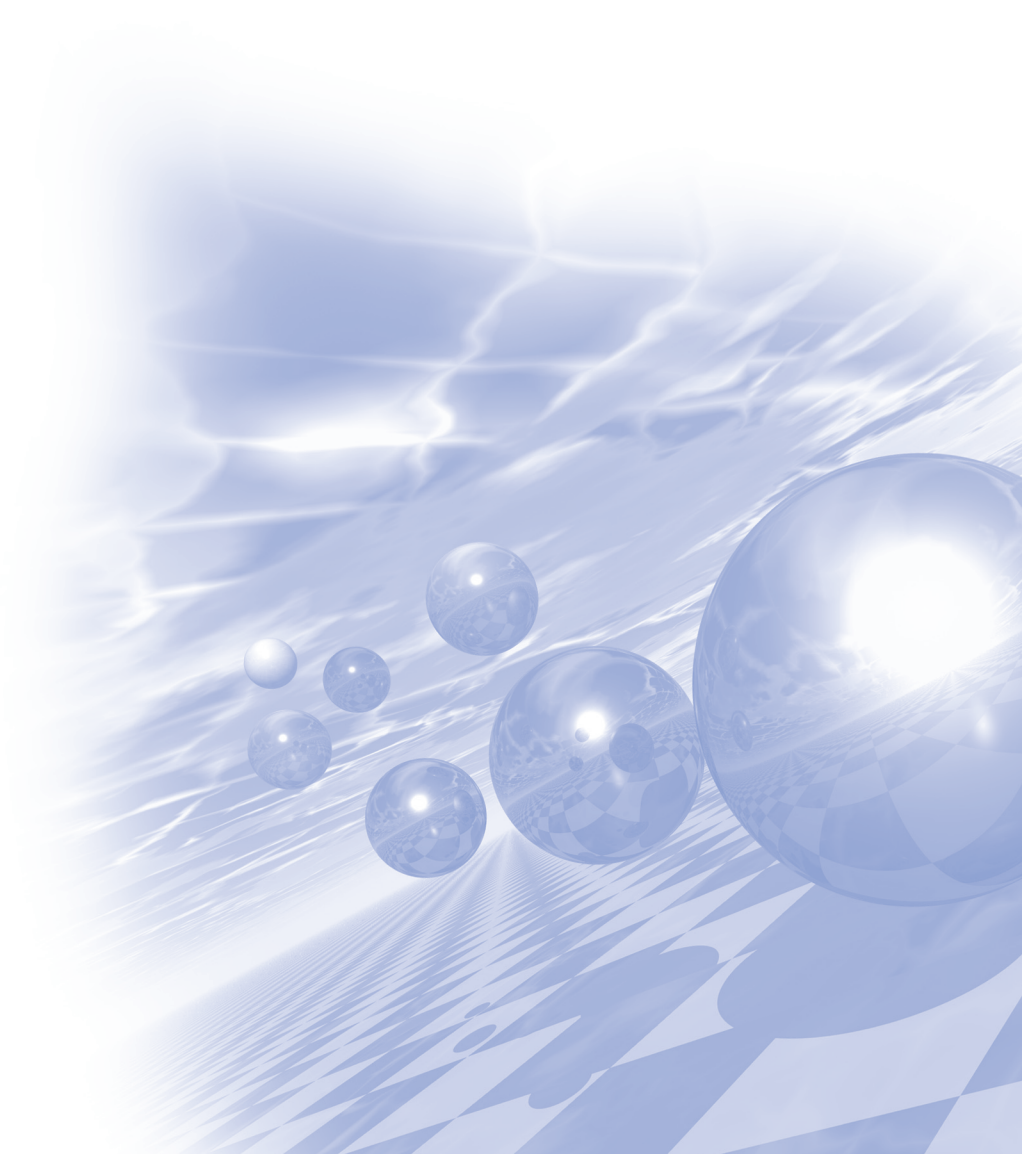
In this work, we propose a method to easily control the size of the core-shell nanoparticles (NPs) by controlling the pressure of the inert gas during the heat treatment process. As synthesized Fe@Pt/C catalysts were conducted heat treatment with varied pressure control (1, 40, 80 bar) under inert atmosphere. The average size of the metal NPs was distributed in the range of about 3 to 5 nm, and the particle size was clearly reduced in inverse proportion to the pressure. By scanning transmission electron microscopy (STEM) analysis, we also confirmed that the catalysts show clear M core-Pt shell structure. We also confirmed that the NPs retained the core-shell structure even after heat treatment at all pressure conditions and were successfully applied to the oxygen reduction reaction (ORR) electrocatalysts, confirming that the mass activity was higher than commercial Pt/C (HiSPEC4000) catalyst. Theoretical calculations show the correlation between the size of metal NPs and external pressure. Herein, we introduce a novel particle size control method and our unique synthetic approach can be a promising way to obtain intermetallic structure NPs with controlled particle size.



2021 KMS Summer Conference

Symposium 8

'Theory and Computational Magnetism'



Anomalous exciton and magneto-electric effect in a layered antiferromagnet

Young-Woo Son^{*}

Korea Institute for Advanced Study, Seoul 02455, Korea

In this talk, I will present my recent theoretical and computational works on anomalous optical excitations in a layered antiferromagnet, NiPS_3 [1]. It is shown that a spin-orbit-entangled exciton state is responsible for anomalously sharp photoluminescence (PL) and its temperature dependence. The new exciton forms through a transition from a Zhang–Rice triplet to a Zhang–Rice singlet on antiferromagnetic background. Using computational spectroscopic results, anomalous resonant inelastic X-ray scattering and optical absorption at the energy associated with the sharp PL can be explained well. I will discuss a possible emergent multiferroic behavior or interplay between dipolar interaction and magnetism that may support coherent many excitonic excitation. If time allowed, I will also present our newly developed efficient first-principles computational method [2,3] that can compute electronic, magnetic and phononic properties of solids as accurate as the GW approximation with a computational load comparable to conventional local or semilocal functional calculations.

References

- [1] S. Kang *et al.*, Nature **583**, 785 (2020).
- [2] S. Lee and Y.-W. Son, Phys. Rev. Research **2**, 043410 (2020).
- [3] W. Yang, S.-H. Jhi, S. Lee and Y.-W. Son, arXiv:2106.07201 (2021).

Anomalous Hall effect in compensated collinear ferrimagnet: Symmetry analysis in Mn_3Al

Minkyu Park^{1*}, Guihyun Han², S. H. Rhim²

¹Research Institute of Basic Sciences, University of Ulsan, 93, Daehak-ro, Nam-gu, Ulsan 44610, Republic of Korea

²Department of Physics, University of Ulsan, 93, Daehak-ro, Nam-gu, Ulsan 44610, Republic of Korea

It has long been believed that anomalous Hall effects (AHE) can only be observed in ferromagnets. However, any magnetic material can exhibit AHE because the time-reversal symmetry is broken by a magnetic order. Moreover, the symmetry imposes constraints on anomalous Hall conductivity $\sigma_{\alpha\beta}$. In this work, we investigate the compensated ferrimagnet Mn_3Al based on the symmetry. The symmetry analysis shows that only σ_{xy} can be nontrivial and first-principles calculations confirm $\sigma_{xy} = -320 (\Omega\text{cm})^{-1}$. The nature of Berry curvature responsible for the intrinsic origin of AHE is further identified along high-symmetry lines using group theory: a lifted degeneracy at L and a level repulsion along $\frac{1}{2}KT$.

Terahertz field-induced phase transition via nonlinear phonon interaction

Dongbin Shin*, Angel Rubio

Max Planck Institute for the Structure and Dynamics of Matter, 22761 Hamburg, Germany

Light-matter interaction has been attracted attention in the field of condensed matter physics and optics from the last century. Recent studies revealed that applying terahertz (THz) field on the material can lead the enhancement of material property or induce the phase transition. For example, high temperature superconductivity ($\sim 100\text{K}$) is experimentally observed by illuminating the THz-field on the K_3C_{60} from its lower superconducting critical temperature ($\sim 30\text{K}$) at the ambient condition. In our work, we investigated the THz field-induced phase transition based on the first principle calculation. At first, we show the microscopic details of THz field-induced ferroelectric phase transition in SrTiO_3 , which is demonstrated in the recent experiment. In second, we suggest the THz field-induced Weyl points in the trivial semimetal HgTe . Especially, we revealed that the nonlinear phonon interaction is the main mechanism of these THz field-induced phase transition. Our studies highlight that THz field can be a great tool for manipulating material properties.

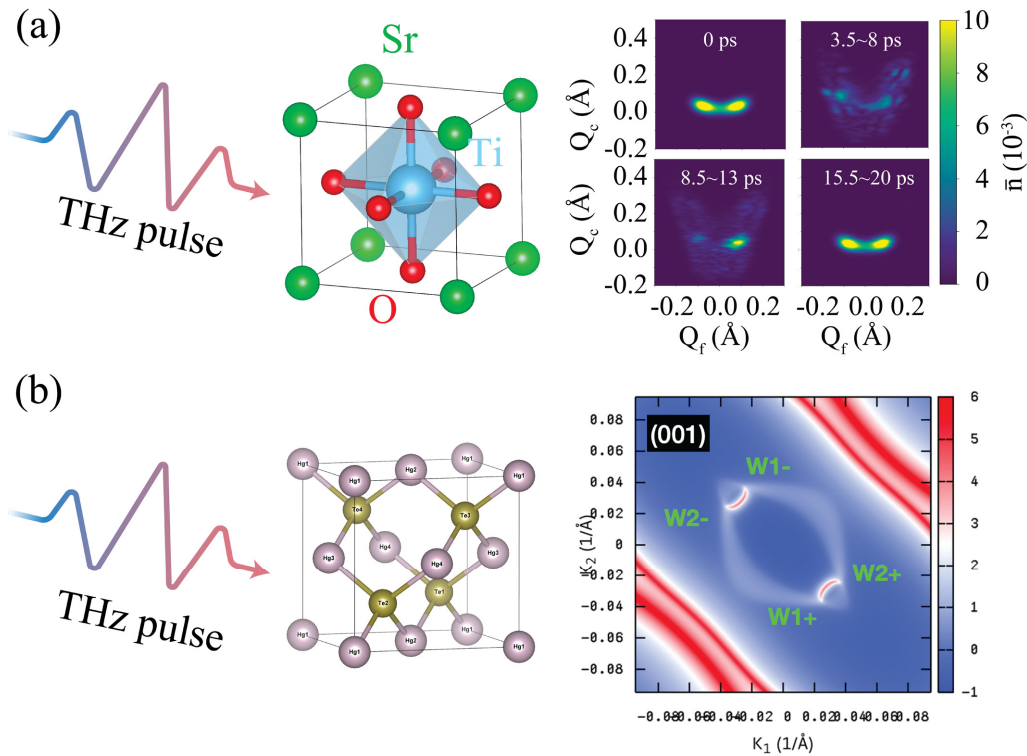


Fig. 1. (a) THz field-induced ferroelectric transition in SrTiO_3 . (b) THz field-induced Weyl points in HgTe .

All-optical fast control of band topology by exploiting the correlation between Berry curvature and magnetic anisotropy

Bumseop Kim, Mahmut Sait Okyay, Noejung Park*

Department of Physics, Ulsan National Institute of Science and Technology, Ulsan, 689-798 Korea

The effect of light pulse on magnetic materials have attracted broad interest in the perspective of laser-induced demagnetization and ultrafast controls of spin [1-3]. Here we focus on the fact that, beyond such passive roles, appropriately selected light conditions can result in more active effect in terms of magnetization density and magnetization direction. We selected a few examples of two-dimensional ferromagnetic insulators, and performed real-time time-dependent density functional theory by implementing the external light field in terms of vector potential. We find that asymmetric single-cycle light pulses can rotate the anisotropic local magnetization direction smoothly as shown in Fig 1. We discuss the effect of this optical reorientation of local moment, in the context of Mermin-Wagner's theorem, on the long-range order of two-dimensional magnet. Our first-principles computations of real materials expect that this optical control of magnetization direction can adjust the Berry curvature distribution over the Brillouin zone, which eventually can switch the topological nature of quantum anomalous Hall state of ferromagnetic insulators.

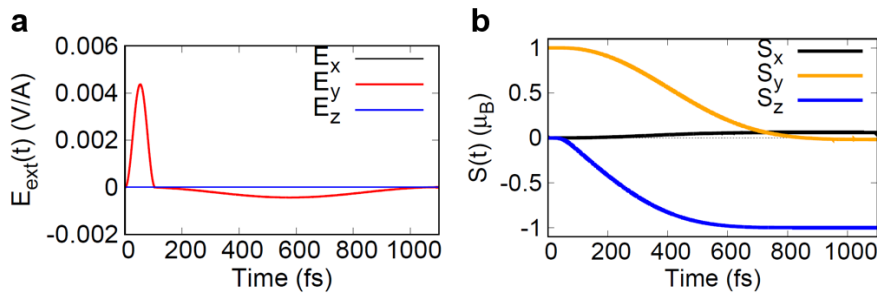


Fig. 1. (a) Asymmetric single-cycle light pulse.

(b) spin dynamics of a model system of the two-dimensional anisotropic ferromagnet.

References

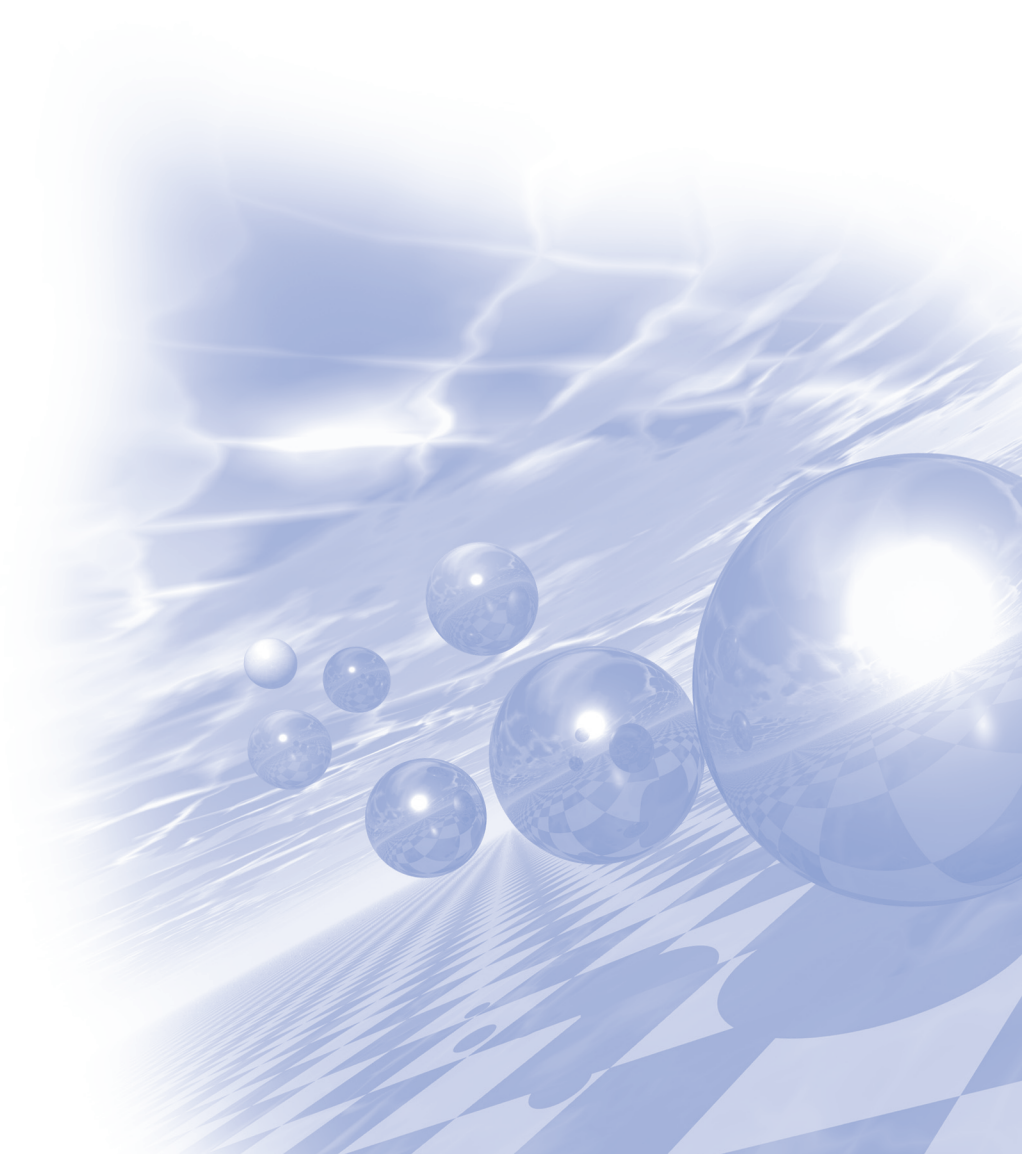
- [1] C. D. Stanciu, et al. Phys. Rev. Lett. **99**, 047601 (2007)
- [2] A. V. Kimel, et al. Nat. Phys. **5**, 727-731 (2009)
- [3] F. Siegrist, et al. Nature **571**, 240-244 (2019)



2021 KMS Summer Conference

Symposium 9

'Low Dimensional Magnetism'



Controlling the Magnetic Properties of the Van der Waals Ferromagnet Fe_3GeTe_2

Hyejin Ryu^{1*}, Se Young Park^{2,3}, Dong Seob Kim¹, Yu Liu⁴, Jinwoong Hwang^{5,6},
Younghak Kim⁷, Wondong Kim⁸, Jae-Young Kim⁹, Cedomir Petrovic⁴, Choongyu Hwang⁶,
Sung-Kwan Mo⁵, Hyung-jun Kim¹, Byoung-Chul Min¹, Hyun Cheol Koo¹, Joonyeon Chang¹,
Chaun Jang¹ and Jun Woo Choi¹

¹Center for Spintronics, Korea Institute of Science and Technology (KIST), Seoul 02792, Korea

²Center for Correlated Electron Systems, Institute for Basic Science (IBS), Seoul 08826, Korea

³Department of Physics and Astronomy, Seoul National University (SNU), Seoul 08826, Korea

⁴Condensed Matter Physics and Materials Science Department, Brookhaven National Laboratory,
Upton, New York 11973, United States

⁵Advanced Light Source, Lawrence Berkeley National Laboratory, Berkeley, CA 94720, USA

⁶Department of Physics, Pusan National University, Busan 46241, Korea

⁷Pohang Accelerator Laboratory, Pohang University of Science and Technology, Pohang 37673, Korea

⁸Quantum Technology Institute, Korea Research Institute of Standards and Science (KRISS), Daejeon 34113, Korea

⁹Center for Artificial Low Dimensional Electronic Systems, Institute for Basic Science (IBS), Pohang 37673, Korea

Identifying material parameters that affect magnetic properties of ferromagnets is key to optimize materials better suited for spintronics applications. Here, we propose an effective hole doping method to modulate the magnetic anisotropy of a van der Waals ferromagnet, and explore the physical origin of this effect. Experimental measurements of the doping and thickness dependent magnetic properties of thin $\text{Fe}_{3-x}\text{GeTe}_2$ show a significant suppression of the magnetic anisotropy with hole doping. From the measured and calculated doping dependent electronic structure, we find that the energy gain by the spin-orbit induced band splitting is reduced by the chemical potential shift associated with hole doping, which in turn reduce the magnetic anisotropy energy. The identified mechanism provides an understanding of the doping induced modulation of magnetic properties in Fe_3GeTe_2 thin films.

Engineering ferromagnetic lines in graphene by local functionalization using AFM lithography

Bae Ho Park^{1*}, Ik-Su Byun¹, Danil W. Boukhvalov², Duk Hyun Lee³, Wondong Kim³,
Jaeyoon Baik⁴, Hyun-Joon Shin⁴ and Young-Woo Son²

¹Division of Quantum Phases & Devices, Department of Physics, Konkuk University, Seoul 05029, Korea

²School of Computational Sciences, Korea Institute for Advanced Study, Seoul 02455, Korea

³Interdisciplinary Material Measurement Institute, Korea Research Institute of Standards and Science, Daejeon 34113, Korea

⁴Pohang Accelerator Laboratory, Pohang 37673, Korea

Monolayer graphene with sp^2 -carbon-atom network is a promising platform for next-generation spintronic devices due to its high carrier mobility and long spin relaxation length. For implementation of practical and high-density graphene-based spintronic devices, we need to define nanoscale areas with ferromagnetic properties on graphene. Up to now, conventional ferromagnetic metal electrodes accompanied by barrier insulators have been used for injection and detection of polarized spins in graphene-based spintronic devices. If graphene-based materials show ferromagnetic behaviors, they will become ideal candidates for spin injectors and detectors, because they structurally, chemically, and electrically match well with pristine graphene. In this presentation, I will report on local magnetic characteristics of nanoscale graphene oxidized and hydrogenated by atomic force microscope (AFM) lithography without conventional sources of surface contamination and chemical agents. By using AFM lithography, we can selectively control functional groups and their coverages on the nanoscale at the surface of graphene. By performing magnetic force microscope (MFM) measurement, we can clearly distinguish local magnetic signal of selectively oxidized or hydrogenated graphene from that of surrounding pristine graphene which does not produce ferromagnetic signal. The nanoscale oxidized and hydrogenated graphene show experimental evidences for room-temperature ferromagnetism. From x-ray magnetic circular dichroism photoemission electron microscope (XMCD-PEEM) measurement, we also identified remarkable asymmetry in carbon K edge XMCD spectra, which strongly indicates that the observed ferromagnetic order in functionalized graphene layers is intrinsic.

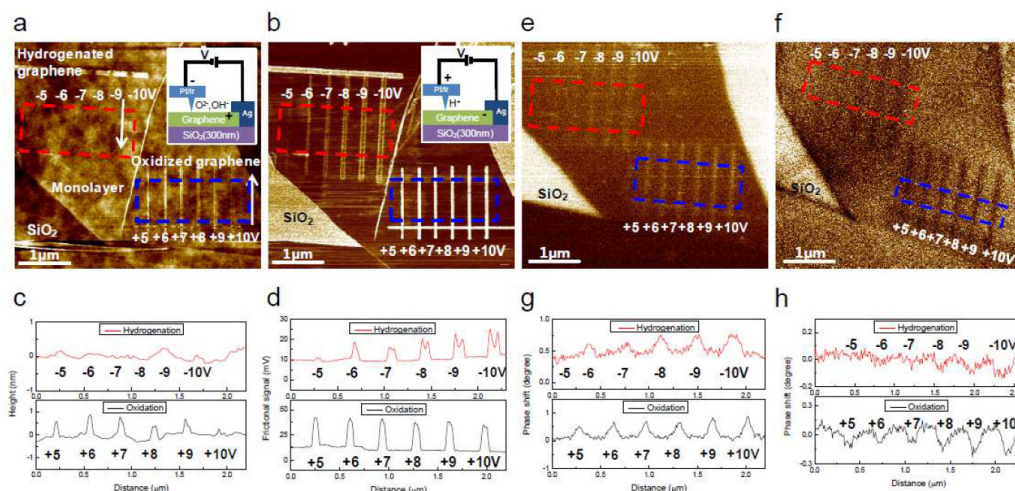


Fig. 1. AFM and MFM characterization of the oxidized and hydrogenated graphene lines on monolayer graphene

Exchange bias effect in van der Waals magnetic materials

Jun Woo Choi^{1*}, Hyung Keun Gweon¹, Hee Young Kwon¹, Kyoung-Whan Kim¹,
Zi Qiang Qiu², Hyejin Ryu¹, Chaun Jang¹

¹Center for Spintronics, Korea Institute of Science and Technology, Seoul 02792, Korea

²Department of Physics, University of California, Berkeley CA 94720, USA

The discovery of intrinsic magnetism in thin exfoliated van der Waals (vdW) magnetic materials has led to extensive investigation on its fundamental material properties and potential device applications. The layered structures, well-defined interfaces, and weak interlayer coupling of vdW magnets suggest that these are ideal material systems to study two-dimensional (2D) magnetic properties. Despite the promise on providing unique opportunities to study 2D magnetic phenomena, there has been a lack of reports on properties unique to vdW magnets that truly distinguish them from ultrathin epitaxial magnetic films (e.g. Co, Ni, Fe), the historical material-of-choice for investigating low-dimensional magnetism.

In this work, we report a magnetic characteristic unique to vdW magnetic materials. We thereby provide very strong evidence that magnetic properties of vdW magnetic materials could be fundamentally different from conventional magnetic materials. An exchange bias effect is observed in a naturally oxidized vdW ferromagnet Fe_3GeTe_2 , owing to the emergence of antiferromagnetic ordering in the surface oxide layer [1]. Surprisingly, the magnitude and thickness dependence of the exchange bias effect is considerably different from those expected in conventional magnetic thin films. Using macro-spin and analytical calculations based on textbook energy equations, we find that these observations are the consequence of the weak interlayer magnetic exchange interaction (J_{inter}) inherent to vdW magnets. Our “weak J_{inter} model” proposes a new exchange bias mechanism exclusive to vdW magnets, demonstrating unique magnetic energetics of these materials [1].

Reference

- [1] H. K. Gweon et al., *Nano Lett.* 21, 1672-1678 (2021).

Robust quantum oscillation of Dirac fermions in a single-defect resonant transistor

Heejun Yang^{*}

Department of Physics, Korea Advanced Institute of Science and Technology (KAIST), Daejeon 34141, Korea

Correspondence to: h.yang@kaist.ac.kr (H. Yang)

While the massless Dirac fermions produce large energy gaps between Landau levels (LLs), exploiting the quantum Hall effect at room temperature requires large magnetic fields to overcome the energy level broadening by charge inhomogeneities in the device. In this talk, I will demonstrate the robust quantum oscillations of Dirac fermions in a single-defect resonant transistor, which is based on local tunneling between lattice-orientation-aligned graphene layers. A point defect in the h-BN, selected by the orientation-tuned graphene layers, probes local LLs in its proximity at room temperature and low magnetic field (2 Tesla) by minimizing the energy broadening of the LLs by charge inhomogeneity.

Dirac Fluid Tesla Valves in Graphene

Young Duck Kim^{*}

Department of Physics, Kyung Hee University, Seoul 02447, South Korea

^{*}ydk@khu.ac.kr

The strongly interacting charge carrier movement in the solid can be described by hydrodynamic transport such as Fermi liquid in metal or Dirac fluid in graphene. In this system, the charged particles such as electron and hole's interaction get dominant scattering source in the transport. Recently, many experimental results about the hydrodynamic phenomenon in graphene were reported by various studies. In graphene, through the reduced screening effect near charge neutrality point or Dirac point, the collective charge carriers flow like a liquid by significantly enhanced electron-electron scattering. Although many studies reveal various aspects of the hydrodynamic charge flow, the on-set conditions according to scattering length relations and influence in charge flow by geometry are still elusive. Here we demonstrate the hydrodynamic transport in graphene and non-reciprocal current flow in Tesla valve geometry near Dirac point.

Ferroelectricity-driven angular momentum textures: from spins and orbitals to Berry curvatures

Hosub Jin^{*}

Department of Physics, Ulsan National Institute of Science and Technology, Ulsan 44919, Korea

In symmetry-broken crystalline solids, pole structures of angular momentum textures such as spin and orbital angular momentum, and Berry curvature (BC) can emerge, which have been utilized as a versatile tool for various electronic applications. For example, the monopole component of the BC is induced by the time-reversal symmetry breaking, and the BC dipole arises from a lack of inversion symmetry, leading to the anomalous Hall and nonlinear Hall effects, respectively. In this talk, we show that the ferroelectricity can couple to unique spin, orbital and BC distribution, which indeed offers charge- and spin-controllable photocurrents. We also verify the fundamental relation between the ferroelectricity and the dipole component of the angular momentum and BC textures. The ferroelectricity can be a useful and fundamental tool to control the various pseudo-vector textures and the corresponding nonlinear optoelectronic responses.

Rashba effects on the transport properties of low-dimensional systems

Jung-Woo Yoo^{*}

Department of Materials Science and Engineering, Ulsan National Institute of Science and Technology, Korea

Systems having inherent structural asymmetry retain the Rashba-type spin-orbit interaction, which ties spin and momentum of electrons in the band structure leading to coupled spin and charge transport. This coupled spin-charge transports have been evidenced in various experimental platforms and could be utilized for various electronics. In this talk, I will present Rashba effects on the transport properties of low-dimensional systems, such as LAO/STO interface and PtSe₂. The broken inversion symmetry in these systems can induce intriguing transport properties. When the time-reversal symmetry is further broken, the system could exhibit directional propagation of itinerant electrons, i.e. the rightward and leftward currents differ from each other. In addition, the Rashba spin-orbit interaction can be further tuned by applying gate bias, so does the nonreciprocal charge transport [1].

Reference

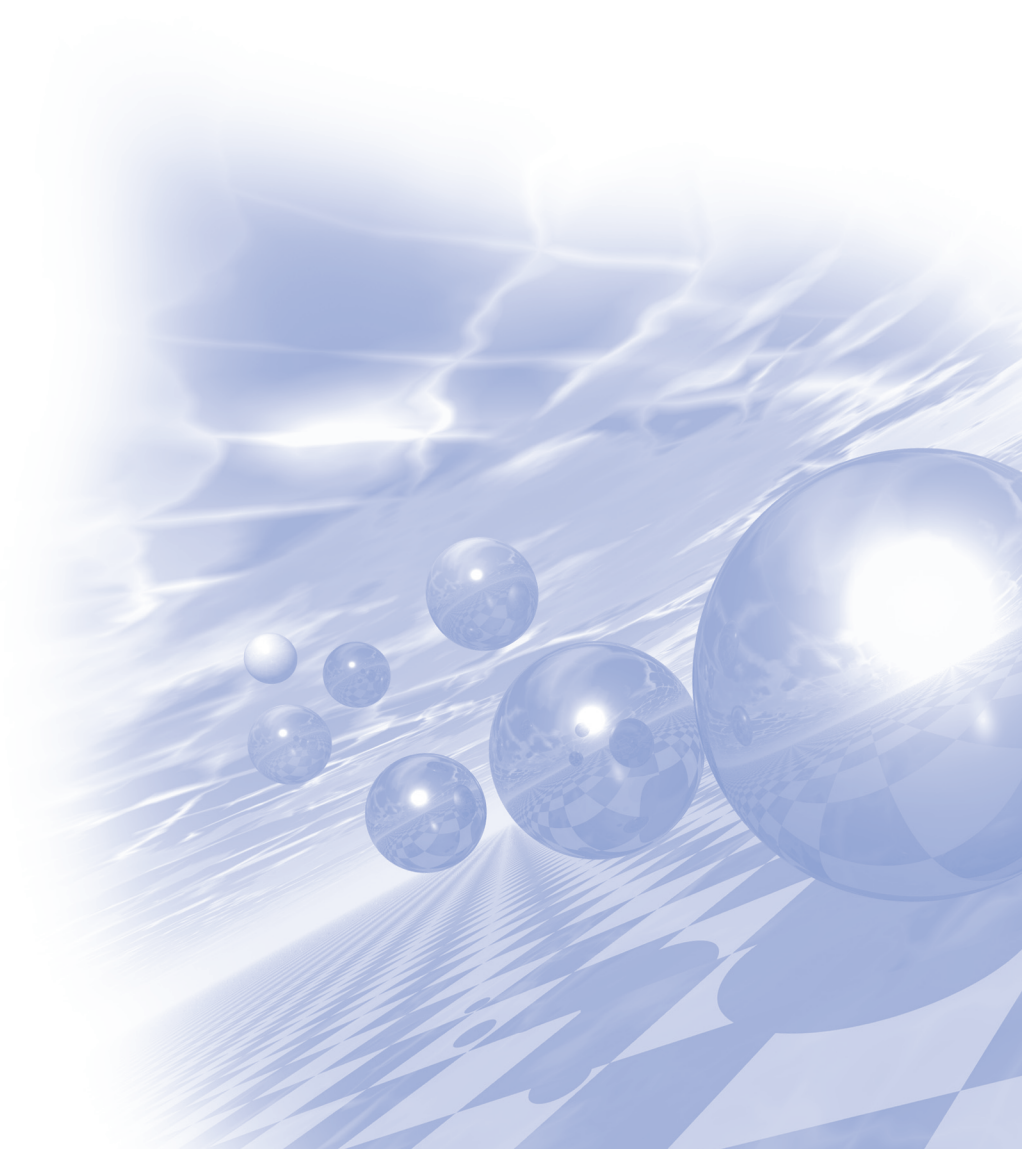
- [1] Gate-tunable giant nonreciprocal charge transport in noncentrosymmetric oxide interfaces, Nat. Comm. **10**, 1-8 (2019)



2021 KMS Summer Conference

Session 1

‘신진과학자 콜로키움’



Spin wave non-reciprocity in spin superfluids

Gyungchoon Go and Se Kwon Kim*

Department of Physics, KAIST, Daejeon 34141, Republic of Korea

In a chiral magnet, it has been predicted that a spin-wave propagating along a particular direction and its opposite direction can propagate with different velocity. This novel phenomena, called magnetochiral nonreciprocity, allows efficient magnetic logic device applications such as spin wave diode [1]. For the spin wave nonreciprocity, the chirality of the magnetic material such as chiral exchange interaction (or chiral spin structure) is crucial [2,3]. Here we theoretically demonstrate that the spin wave nonreciprocity can occur in the easy-plane magnet with U(1) symmetry which is known to be the spin superfluid state. We show that the chiral spin structure is manipulated by the electric current flowing in metallic contact and possibly induces the nonreciprocity of the spin waves. We also discuss that the non-reciprocal thermal transport driven by the magnon in the spin superfluid [4].

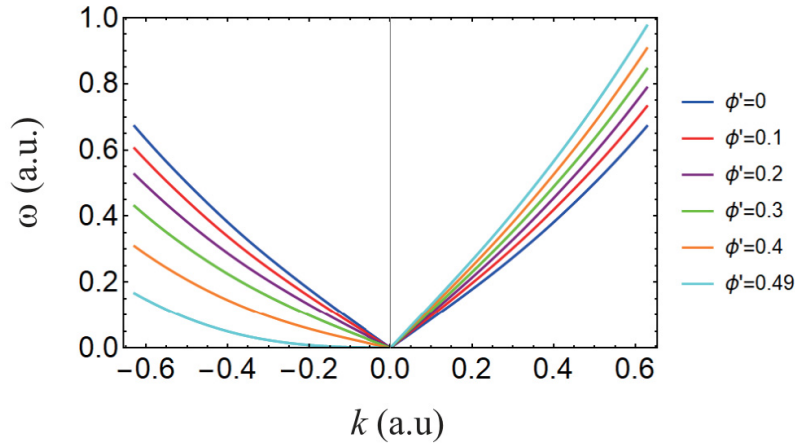


Fig. 1. Spin wave dispersion for different spin superfluid states parameterized by.

References

- [1] Y. Tokura and N. Nagaosa, Nat. Commun. **9**, 3740 (2018).
- [2] S. Seki, et al., Phys. Rev. B **93**, 235131 (2016).
- [3] S. Cheon, H.-W. Lee, and S.-W. Cheong, Phys. Rev. Lett. **98**, 184405 (2018).
- [4] G. Go and S. K. Kim, in preparation.

Long-range Spin Transport using Magnon Phonon Coupling

Kyongmo An^{1*}, Li Shi², Xiaoqin Li³, Olivier Klein⁴

¹Quantum Spin Team, Korea Research Institute of Standards and Science, Daejeon, Republic of Korea

²Department of Mechanical Engineering, The University of Texas at Austin, Austin, Texas 78712, USA

³Department of Physics, Center for Complex Quantum Systems, The University of Texas at Austin,
Austin, Texas 78712, USA

⁴Université Grenoble Alpes, CEA, CNRS, Grenoble INP, Spintec, 38054 Grenoble, France

In spintronics, this has revived interest for insulating materials and in particular garnets, which are the magnetic materials benefiting from the lowest magnetic damping. The sound wave attenuation coefficient in garnets is also exceptional, i.e. up to an order of magnitude lower than that in single crystalline quartz. In addition to the low damping of magnetic and sound waves, a strong coupling can be established between spin-waves (magnons) and lattice vibrations (phonons) through the magnetic anisotropy and strain dependence of the magnetocrystalline energy in magnetic garnets. The magnetoelasticity leads to new hybrid quasiparticles (“magnon polarons”) when spin wave and acoustic wave dispersions cross [1]. This coupling has been exploited in the past to produce microwave acoustic transducers [2]. The adiabatic conversion between magnons and phonons in magnetic field gradients proves their strong coupling in yttrium iron garnet (YIG) [3].

I will first demonstrate that the spin waves can be strongly coupled to coherent transverse sound waves that have very long characteristic decay length and propagate ballistically over millimetric distances [4]. The experiment was performed at room temperature with a magnetic field applied perpendicular to the film. Our sample consists of two 200 nm thick YIG layers deposited on both sides of a 0.5 mm thick gadolinium gallium garnet (GGG) substrate. The circularly polarized standing sound waves couple to the magnetization oscillations in both layers. An interference pattern is observed and it is explained as the strong coupling of the magnetization dynamics of the two YIG layers either in phase or out of phase by the standing transverse sound waves. This long range coherent transport of spin by phononic angular momentum can add new functionalities to insulator spintronic circuits and devices.

If time allows, I will also discuss my previous work on the nonequilibrium between magnons and phonons [5]. Here the local nonequilibrium is created optically within a focused laser spot and probed directly via micro-Brillouin light scattering. Through analyzing the deviation in the magnon number density from the local equilibrium value, we obtain the diffusion length of thermal magnons. By explicitly establishing and observing local nonequilibrium between magnons and phonons, this study represent an important step toward a quantitative understanding of various spin-heat coupling phenomena.

References

- [1] T. Kikkawa, K. Shen, B. Flebus et al., Phys. Rev. Lett. 117, 207203 (2016)
- [2] M. Pomerantz, Phys. Rev. Lett. 7, 312 (1961)
- [3] J. Holanda, D. S. Maior, A. Azevedo et al., Nat. Phys. 14, 500 (2018)
- [4] K. An, A.N. Litvinenko, R. Kohno et al., Phys. Rev. B 101, 060407(R) (2020)
- [5] K. An, K. S. Olsson, A. Weathers et al., Phys. Rev. Lett. 117, 107202 (2016)

Demonstration of Core Operations for Skyrmion Racetrack Memory Device

Seungmo Yang^{1*}, Kyoung-Woong Moon¹, Tae-Seong Ju¹, Changsoo Kim¹, Hyun-Joong Kim¹, Juran Kim¹, Bao Xuan Tran², Jung-Il Hong² and Chanyong Hwang^{1†}

¹Quantum Spin Team, Korea Research Institute of Standards and Science, Daejeon 34113, Republic of Korea

²Department of Emerging Materials Science, DGIST, Daegu 42988, Republic of Korea

Magnetic skyrmions, topological spin textures, have been intensively studied in spintronics as a prospective information carrier due to distinct topological features [1, 2]. Various skyrmion-related devices have been proposed including a logic device, a neuromorphic cell and a memory device. One of these proposals is a skyrmion racetrack memory, where information is encoded by magnetic skyrmions in a magnetic racetrack. Skyrmion racetrack memory device has attracted much attention as a promising alternative to the next-generation memory technology based on high density, high-speed and low power operation and topological stability. Skyrmion racetrack memory requires four core operations: electrical creation, deletion, shift and detection of isolated skyrmions. Therefore, the implementation of the four operations in a single device is the important experimental challenge for realizing skyrmion racetrack memory. Here, we demonstration of three core operations, skyrmion creation/deletion/shift, is a single three-terminal device and also present a proof-of-concept operation of skyrmion racetrack memory.

References

- [1] Nagaosa, N. et al., Nat. Nanotechnol. 8, 899-911 (2013).
- [2] Christian, H. B. et al., J. Phys. D Appl. phys. (2020).

Spin dependent light emission in organic light emitting diodes with single ferromagnetic electrode

Nyun Jong Lee^{1*}, Yu Jeong Bae², Heeyoung Jung³, Changhee Lee³ and Tae Hee Kim^{4†}

¹Department of Physics and Energy Harvest Storage Research Center, University of Ulsan, Ulsan, 44610 Korea

²Center for Quantum Nanoscience, Institute for Basic Science, Ewha Womans University, Seoul, 03760 Korea

³School of Electrical Engineering and Computer Science, Seoul National University, Seoul, 08826 Korea

⁴Department of Physics, Ewha Womans University, Seoul, 03760 Korea

We report an enhanced magneto-electroluminescence (MEL) in organic light-emitting diodes (OLEDs) consisting of a non-magnetic Al and a magnetic electrode of BCC-Fe(001)/MgO(001). A role of spin states of injected carrier from anode in the OLEDs was elucidated by employing different ferromagnetic (FM) anodes, such as polycrystalline-Fe, epitaxial Fe(001), and epitaxial Fe(001)/MgO(001). Organic layers consist of a traditional structure of CuPc/ α -NPD/Alq₃. The relatively larger MEL of $\sim 6\%$ was observed in the devices with Fe(001)/MgO(001) anode at room temperature in a low magnetic field of 0.1 T for an applied voltage in excess of ~ 5 volts, whereas these measurements revealed less than 3% for the non-fully spin polarized FM anodes. Our experimental results can be explained in terms of increasing the internal quantum efficiency during exciton formation in emission layer based on electron-hole pair model and clearly suggest the inserting of epitaxial MgO(001) layer improves spin-polarized hole injection resulting in enhanced MEL.

Reconfigurable spintronic physical unclonable functions based on spin-orbit torques in ferromagnet/nonmagnet/ferromagnet trilayer structures

Soogil Lee^{1*}, Jaimin Kang¹, Jeong-Mok Kim¹, Taek-Hyeon Lee², Sungjun Lee¹, Donghyeon Han¹, Sanghwa Lee¹, Kab-Jin Kim² and Byong-Guk Park¹

¹Department of Materials Science and Engineering, KAIST, Daejeon 34141, Korea

²Department of Physics, KAIST, Daejeon 34141, Korea

Entering the era of Inter of Things (IOT), diverse smart devices generate and transfer enormous digital information. In this IOT environment, information security is becoming a critical issue because conventional software-based security technology is vulnerable to adversarial machine learning attacks. Thus, hardware-based security technology has been proposed to overcome this vulnerability, receiving much attention as an alternative. Especially, randomness of nature serves as an essential ingredient for the hardware-based security technology. For example, manufacturing processes of complementary-metal-oxide-semiconductor (CMOS) involves inevitable tolerances. Therefore, every electronic device is physically not identical despite the identical manufacturing processes. Those distinguishable device characteristics under the identical manufacturing process, so called “physical unclonable function (PUF)”, can potentially create non-identical output (response) under the identical input (challenge) generating unique identification of each electronic devices [1].

In this presentation, we demonstrate the spintronic PUF utilizing bottom-ferromagnet (FM)/nonmagnet/top-FM trilayer structures. Here, bottom and top FMs exhibit in-plane and perpendicular magnetic anisotropy, respectively. In these trilayer structures, field-free magnetization switching of top-FM is achieved by out-of-plane polarized spin current injection due to the interfacial spin precession mechanism, and the switching polarity is controlled by the in-plane magnetization direction of bottom-FM [2]. Under the identical demagnetization process of the bottom-FM, distinct magnetic domain distributions are formed on each identical wafer, consisting of a number of Hall-bar devices with random magnetization direction of bottom-FM along the demagnetization axis. These randomly distributed domains of bottom-FM on each wafer are electrically detected through the current-induced field-free spin-orbit torque switching polarity relies on the direction of bottom-FM. Therefore, these spintronic PUF wafers with unique pattern of domain distributions manifests itself as the unique electrical identification which can also be integrated into magnetic random access memory. Furthermore, we also discuss the reconfigurability and reliability of this spintronic PUF, providing great potential to hardware-based security applications because it is compatible with current CMOS technology.

References

- [1] Yansong Gao, Said F. Al-Sawari, and Derek Abbott, “Physical unclonable functions” *Nature Electronics* **3**, 81 (2020).
- [2] S.-h. C. Baek et al, “Spin currents and spin-orbit torques in ferromagnetic trilayers” *Nature Materials* **17**, 509 (2018).

Tunable dynamics of exchange-biased domain wall via spin-current-induced antiferromagnet switching

Hyun-Joong Kim^{1*}, Soong-Geun Je², Jung-Il Hong³, Chanyong Hwang¹

¹Quantum Technology Institute, Korea Research Institute of Standards and Science, Daejeon 34113, Korea

²Department of Physics, Chonnam National University, Gwangju 61186, Korea

³Department of Emerging Materials Science, Daegu Gyeongbuk Institute of Science and Technology, Daegu 42988, Korea

Magnetic domain wall (DW) motion in ultrathin ferromagnetic (FM) film with Dzyaloshinskii-Moriya interaction (DMI) is drawing increased attention due to the prospect of developing new mechanism for information storage and processing technology. In order to augment functionalities of the DW motion-based devices, it is necessary

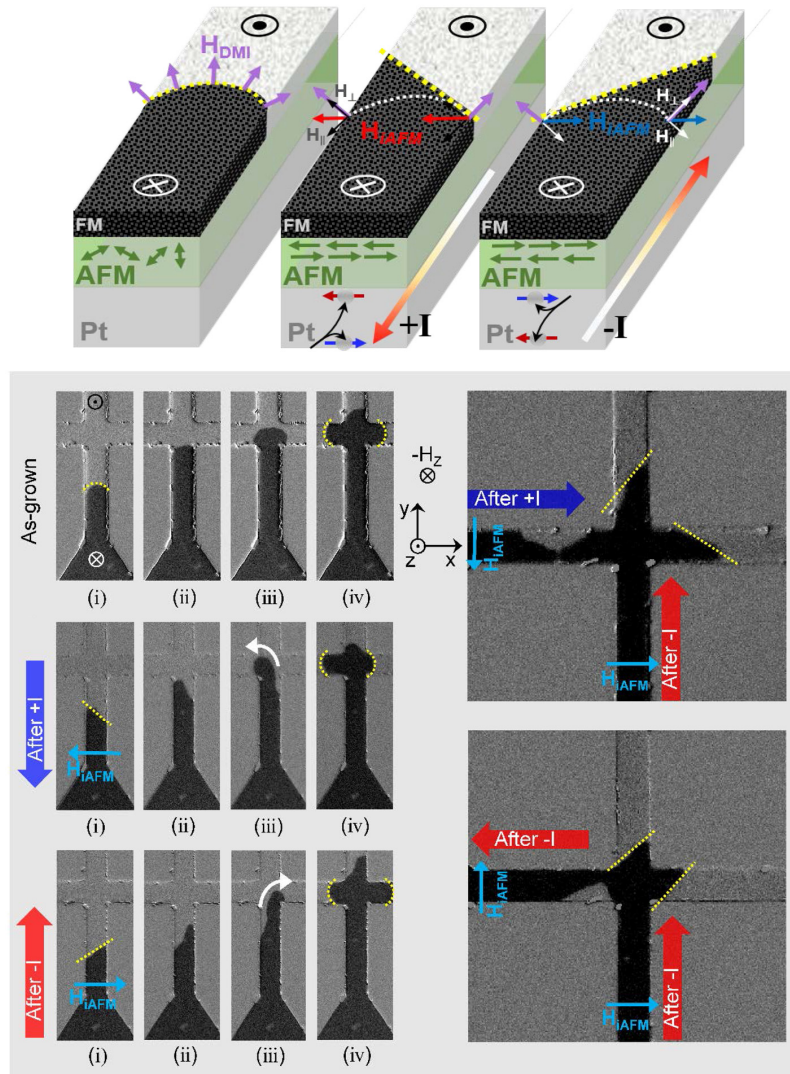


Fig. 1. In the crossbar-patterned sample, various behaviors of perpendicular field driven down-up DW motion without in-plane bias field can be generated depending on the configuration of AFM spins

to enhance controllability over the DW motion. Apart from electric currents, which leads to unidirectional shifting of a train of DWs, applying an in-plane magnetic field also enables controlling the DW dynamics by rotating the DW magnetization and consequently modulating the inherited chiral DW structure. However, applying the external bias field is not a viable approach to the miniaturization of the devices as the external field acts globally. Additionally, the DW motion of FM layer dependent on configuration of adjacent antiferromagnet (AFM) spins has not been studied although the exchange-bias phenomenon of exchange coupled AFM/FM system has been studied for a long time. In this report, we investigated field-driven DW motion of ultrathin FM films with perpendicular magnetic anisotropy (PMA) and DMI effect, in exchange-coupled with AFM IrMn layer. It was found that DW shows asymmetric propagation without an application of in-plane magnetic field due to the aid of an alignment of AFM spins. Interestingly, the direction of the exchange bias field can also be reconfigured by simply injecting spin currents through the device, enabling electrical and programmable operation of the device. Furthermore, our work suggests a prototype DW motion-based device based on the AFM/FM heterostructure, which could be utilized as a logic device.

Effect of post-sintering annealing temperature on the magnetic and microstructural properties of multi-main phase Nd-Ce-Fe-B with high Ce content

Kyoung-Hoon Bae^{1*}, Tae-Hoon Kim¹, Jung-Goo Lee¹, Sang-Hyup Lee², Dong-Hwan Kim²

¹Powder Materials Division, Korea Institute of Materials Science, Changwon, Korea

²R&D Center, Star Group, Daegu, Korea

Recently, the efficient usage of rare-earth (RE) element Ce, which possesses the merits of the low cost and high abundance, has attracted much attention in RE-Fe-B sintered magnet [1]. However, the coercivity (H_c) of magnets could be drastically deteriorated after replacing Nd with Ce due to the poor intrinsic magnetic properties of $Ce_2Fe_{14}B$ phase, compared with $Nd_2Fe_{14}B$ phase [2]. Developing the multi-main phase (MMP) microstructure by the dual alloy process a mixture of Ce-free and Ce-containing $RE_2Fe_{14}B$ powders is known to be the most effective way to enhance the H_c , and reduced the Nd required. However, the H_c of the MMP Nd-Ce-Fe-B sintered magnet with high Ce content (45 wt.% Ce substituting for Nd, 6.2 kOe) is remarkably low, which is a problem to be solved [1, 2]. The post-sintering annealing (PSA) enhanced the H_c , without changing the remanence (B_r), with previous results showing that there are critical changes in the microstructure of RE-rich triple junction phase (TJP) and grain boundary phase (GBP) [3]. However, the optimum PSA temperature for the MMP magnets with high Ce content have not yet been clarified. In this study, we investigated the effects of PSA conditions on the microstructural and the magnetic property changes of the MMP sintered Nd-Ce-Fe-B magnets with high Ce content and clarified the optimum PSA temperature for the MMP process. Ce-free and Ce-containing magnetic powders with nominal compositions of $(Pr,Nd)_{31.0}Fe_{bal.}M_{1.90}B_{1.0}$ and $[(Pr,Nd)_{19}Ce_{12}]_{31.0}Fe_{bal.}M_{1.90}B_{1.0}$ M(wt.%, M=Al, Ga, Nb, Cu, and Co) were prepared using the powder metallurgical method. Ce-free and Ce-containing powders, with a mean particle size of less than 3.0 μm , were mixed (ratio of 20:80 and 80:20). The green compacts were sintered at 1030°C for 2h. The PSA temperatures were varied from 850 to 600°C to optimize the PSA temperature. The microstructure, phase identify and magnetic properties of samples were investigated by using EPMA, HRTEM, DSC, and BH-tracer. When the magnet had a magnet with high Ce content (Ce-free : Ce-containing, 20 : 80), the H_c of the magnet increased as the PSA temperature decreased (from 850 to 650 °C). When the magnet had a low Ce content (Ce-free : Ce-containing, 80 : 20), the H_c was not changed with decreasing PSA temperature (from 850 to 650 °C). In the case of magnets with low Ce content, the $RE_1Fe_4B_4$ phase and the ferromagnetic GBP with high Fe content were formed. However, when the magnet had a high Ce content, the uniformity and continuity of the RE-rich GBP of the magnet with high Ce content was improved because the melting temperature of the RE-rich phase was decreased as the Ce content increased. In addition, the volume fraction of $REFe_2$ phase increased as the PSA temperature decreased (from 850 to 650 °C). The decrease in PSA temperature promoted the formation of MMP core-shell microstructures by limiting the RE diffusion behavior within the main phase. Consequently, the highest H_c of the magnet with high oxygen content was obtained when the magnets were PSA at 650 °C. The effect of the optimum PSA temperature on the

microstructure of the MMP magnet with high Ce content can be summarized as follows: the formation of $\text{RE}_1\text{Fe}_4\text{B}_4$ phase was suppressed, the REFe_2 phase and non-magnetic RE-rich GBP were formed and the MMP core-shell microstructure was effectively developed.

References

- [1] J.Y. Jin, Y.J. Zhang, G.H. Bai, Z.Y. Qian, C. Wu, T.Y. Ma, B.G. Shen, M. Yan, Sci. Rep., 6, (2016) 30194.
- [2] J. Y. Jin, M. Yan, Y. Liu, B.P. Peng, G. Bae, Acta. Mater., 169, (2019) 248-259.
- [3] K. H. Bae, S.R. Lee, H.J. Kim, M.W. Lee, T.S. Jang, J. Appl. Phys., 118, (2015) 203902.

Thermal Plasma Synthesis of $\text{Fe}_x\text{Co}_{1-x}$ Nano-Chained Particles with High Permeability for GHz-band Electromagnetic Wave Absorption

Min-Sun Jang^{1*}, Mi Se Chang¹, Young-tae Kwon¹, Sangsun Yang¹, Jina Gwak², Suk Jin Kwon³, Joonsik Lee³, Sang Bok Lee³, Byeongjin Park³, Jae Won Jeong¹

¹Metal Powder Department, Korea Institute of Materials Science (KIMS), 797 Changwondae-ro, Seongsan-gu, Changwon 51508, Korea

³Center for 3D Printing Materials, Korea Institute of Materials Science (KIMS), 797 Changwondae-ro, Seongsan-gu, Changwon 51508, Korea

⁴Functional Composites Department, Korea Institute of Materials Science (KIMS), 797 Changwondae-ro, Seongsan-gu, Changwon 51508, Korea

By the virtue of their convenience, wireless communications devices such as IoT (Internet of Things) home appliances, drones, and autonomous driving are also being widely spread, and the frequency band is closely diversified.^{1,2} As a result, electromagnetic interference or pollution has become a serious problem because it can cause malfunctions of devices and threaten human health.³ To deal with the problems, recently, the electromagnetic wave absorber has obtained noticeably improved absorption performance, reduced more the presence of waves than using reflections from electromagnetic shielding.^{4,5} Herein, we introduce novel 1-dimensional nano-chained FeCo particles with unusually-high permeability prepared by a highly-productive thermal plasma synthesis, and demonstrate an electromagnetic wave absorber with exceptionally low reflection loss in the high-frequency regime (1-26 GHz). During the thermal plasma synthesis, spherical FeCo nano-particles are first formed through nucleation and growth process; then, the high temperature zone of the thermal plasma accelerates diffusion of constituent elements, leading to surface-consolidation between particles at the moment of

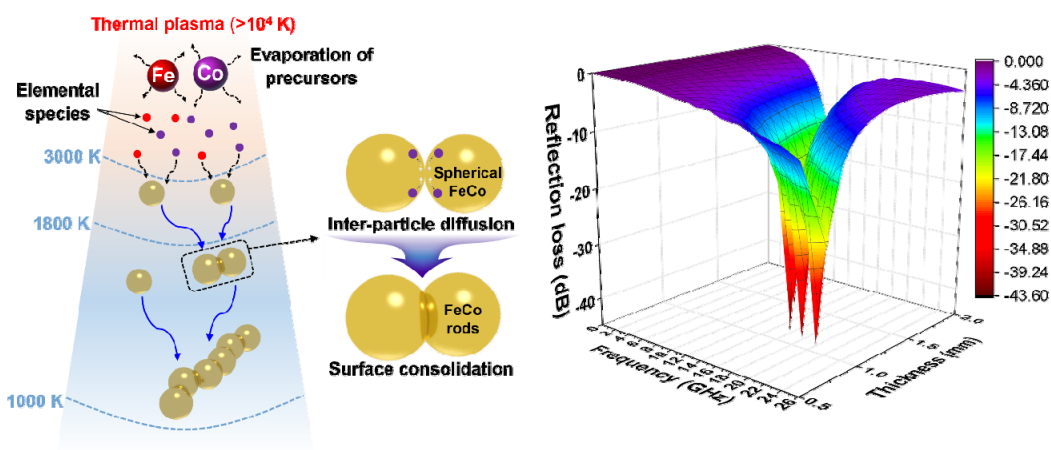


Fig. 1. (a) Schematic illustration of the thermal plasma preparation *via* RF-ITP (Radio-Frequency Inductively Coupled Plasma) synthesis of nano-chained FeCo composition. Diffusion occurs between the inter-particle to form a shaped like ‘rod’, below 1800 K. (b) 3-D mapping for the overall relationship between reflection loss and frequency (~ 26 GHz) for $\text{Fe}_{0.6}\text{Co}_{0.4}@\text{SiO}_2$.

collision, and 1-dimensional nano-chained particles are successfully fabricated without the need for templates or a complex directional growth process. Systematic control over composition and magnetic properties of $\text{Fe}_x\text{Co}_{1-x}$ nano-chained particles also has been accomplished by changing the mixing ratio of the Fe-to-Co precursors, *i.e.* from 7:3 to 3:7, leading to remarkably high saturation magnetization of 151-227 emu/g. In addition, precisely-controlled and uniform surface SiO_2 coating on the FeCo nano-chained particles was found to effectively modulate complex permittivity. Consequently, a composite electromagnetic wave absorber comprising $\text{Fe}_{0.6}\text{Co}_{0.4}$ nano-chained particles with 2.00-nm-thick SiO_2 surface insulation exhibits dramatically intensified permeability, thereby improving electromagnetic absorption performance with the lowest reflection loss of -43.49 dB and -10 dB (90% absorbance) bandwidth of 9.28 GHz, with a minimal thickness of 0.85 mm.

References

- [1] W. S. Chin and D. G. Lee, *Compos. Struct.*, 2007, **77**, 457-465.
- [2] Y. Wang, J. Li, L. Huang, Y. Jing, A. Georgakopoulos and P. Demestichas, *IEEE Veh. Technol. Mag.*, 2014, **9**, 39-46.
- [3] J. Hwang, T. Kang, J. Kwon and S. Park, *IEEE Trans. Electromagn. Compat.*, 2016, **59**, 48-57.
- [4] D. Chen, H. Quan, Z. Huang, S. Luo, X. Luo, F. Deng, H. Jiang and G. Zeng, *Compos. Sci. Technol.*, 2014, **102**, 126-131.
- [5] S.-E. Lee, W.-J. Lee, K.-S. Oh and C.-G. Kim, *Carbon*, 2016, **107**, 564-572.

Magnetic State Generation using Hamiltonian Guided Variational Autoencoder with Spin Structure Stabilization

H. Y. Kwon^{1*}, H. G. Yoon², S. M. Park², D. B. Lee², J. W. Choi¹ and C. Won²

¹Center for Spintronics, Korea Institute of Science and Technology, Seoul 02792, South Korea

²Department of Physics, Kyung Hee University, Seoul 02447, South Korea

Numerical generation of physical states has been an important task across all scientific research fields including magnetism not only to understand experimental results but also to predict or investigate the characteristics of the uncharted systems. We devised a variational autoencoder based machine learning model to generate magnetic states. In the model, the magnetic Hamiltonian calculation explicitly participates in the training process to generate magnetic states that is more energetically stable with less local noises and less deformation of magnetic structures compared to those without considering Hamiltonian. Another great benefit of this model is that the generator produces a ground state spin configuration when the influence of the Hamiltonian is increased, though the ground state is not included in the training process. Based on this study, we anticipate that the proposed Hamiltonian-guided generative model can bring about great advances in various scientific research fields conducted by numerical approaches.

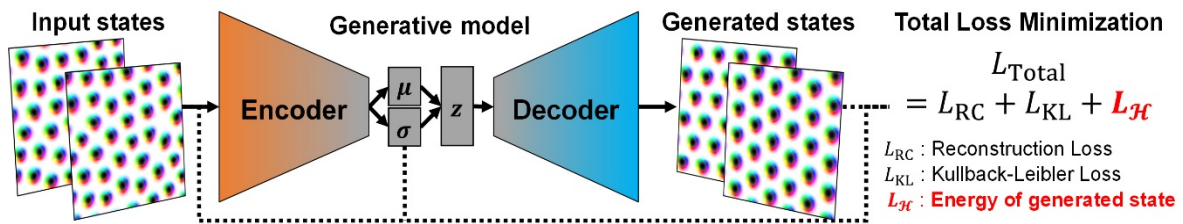


Fig. 1. Schematic process of the Energy-minimization Variational AutoEncoder (E-VAE) model

Role of Demagnetization Field on Permanent Magnet

Namkyu Kim^{1*}, Jihoon Park¹, Ki-Suk Lee², Chul-Jin Choi¹

¹Korea Institute of Materials Science (KIMS), Changwon 51508, Republic of Korea

²School of Materials Science and Engineering, Ulsan National Institute of Science and Technology, Ulsan 44919, Republic of Korea

With the rise of interest in electric vehicles and wind generators, the demand for high energy permanent magnet has been increased. To evaluate the performance of the permanent magnets, the figure-of-merit, the energy product BH is widely used. However, the BH is often used without clear understanding of its definition, despite being a basic concept widely known to relevant industry workers and researchers. Basically, the BH corresponds to the energy stored in the stray field produced by the magnet itself. Consequently, it should be measured from H_d and B at the remanent state, i.e., without any external field. Since the demagnetizing field depends on the shape of a magnet, the BH varies with the shape and thus, its value can be obtained from the remanent state in various shapes of magnets. The demagnetization factor in the saturation state is determined by the shape of the magnet, but in most cases both the magnetization and demagnetization field are not fully saturated in the remanent state.

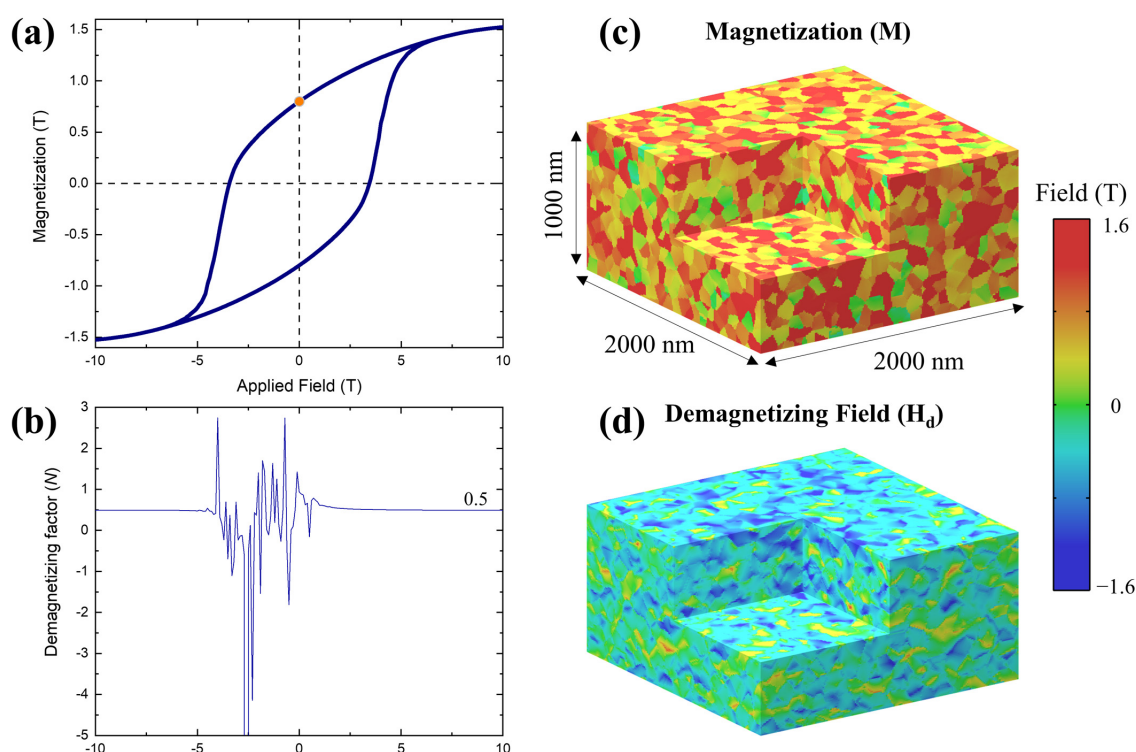


Fig. 1. (a) Magnetic hysteresis loop of the model system and the remanent state is expressed with orange circle. (b) Change of the demagnetizing factor when the applied field change from the positive value to the negative value. (c), (d) Simulated magnetization and demagnetizing field at remanent state ($H_{app} = 0$).

In this study, we investigated the demagnetizing field during the reversal process by a micromagnetic solver. As a model system, we adopted a $\text{Nd}_2\text{Fe}_{14}\text{B}$ magnet having $2000 \times 2000 \times 1000 \text{ nm}^3$ in dimension, which is composed of grains with a diameter of 100 nm, and assumed that the anisotropy directions of the grains were randomly distributed. As shown in Fig. 1. (b), the demagnetizing factor fluctuates during the reversal process. We will discuss the effect of this fluctuating demagnetizing field during magnetic switching on the energy product.

Higher-order Topological Magnons in Honeycomb Antiferromagnet

Moon Jip Park^{1*}, SungBin Lee², Yong Baek Kim³

¹Center of Theoretical Physics of Complex Systems, Institute for Basic Science (IBS) Daejeon 34126,
Republic of Korea

²Department of Physics, KAIST, Daejeon 34141, Republic of Korea

³Department of Physics, University of Toronto, Toronto, Ontario M5S 1A7, Canada

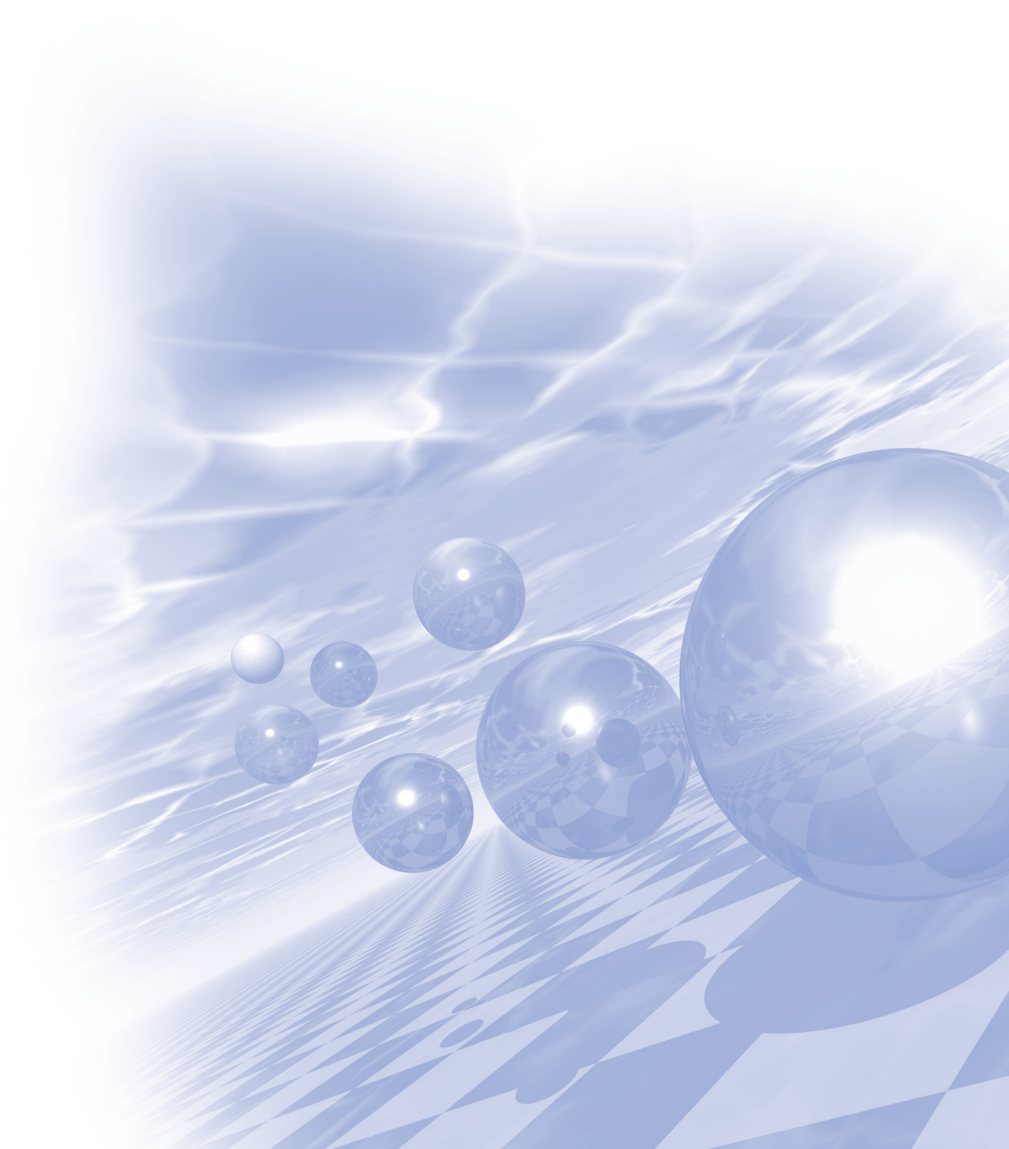
Topological phases of spin-wave excitations are the prominent area of research in quantum magnetism. In this work, we propose the non-collinearity induced higher-order topological magnon excitations. In three-dimensional honeycomb antiferromagnets, we consider the non-collinear order driven by the external magnetic field perpendicular to the easy axis. The corresponding magnon system is described by the non-Hermitian Hamiltonian. Interestingly, we show that the non-hermiticity of the Hamiltonian induces the higher-order topological phase transition, characterized by one-dimensional hinge magnon modes. As a concrete example, we discuss the case of van der Waals honeycomb antiferromagnet CrCl_3 , which we propose as the first promising material candidate of the higher-order topological magnon phase.



2021 KMS Summer Conference

Symposium 10

'Magnetics in Medical Science'



The Effect of Somatosensory Training in Combination with Low-Frequency Repetitive Transcranial Magnetic Stimulation on Functional Improvement in Stroke Patients

So-Young Han^{1*}, Byung Il Yang², Bo-Kyoung Song³

¹Dept. of Emergency Medical Rehabilitation, Graduate School of Kangwon National University, Korea

²Dept. of Physical Therapy, Sangji University, Wonju 26339, Republic of Korea

³Dept. of Occupational Therapy, Kangwon National University, Korea

Introduction

Stroke is a neurological lesion that causes damage to motor and sensory nerves due to vascular disorders, and 1/3 of hemiplegic patients suffer from upper extremity dysfunction accompanied by somatosensory impairment. According to a previous study, it is reported that the neurological recovery of hand function can be elicited even in chronic stroke patients by applying transcranial magnetic stimulation to control the cortical excitability of the hand region. Until recently, there have been many studies showing the recovery of upper extremity function by providing low-frequency magnetic stimulation to the non-injured hemisphere for stroke patients. Therefore, through this study, we intend to report functional changes of upper limb due to cerebral cortex reorganization.

Purpose

The purpose of this study was to investigate the effect of somatosensory training after low-frequency (1 Hz) repeated transcranial magnetic stimulation on upper extremity muscle activity and upper extremity function in patients with hemiplegia after stroke. Through this, we intend to prove the effectiveness of recovery of upper extremity function based on changes in the cerebral cortex of stroke patients.

Methods

The study group received somatosensory training after low frequency (1 Hz) rTMS 3 times a week, 40 minutes each, for 4 weeks, and the control group provided the same somatosensory training after sham rTMS. Somatosensory training was divided into training that directly stimulates the subject's shoulder and hand somatosensory through contact with the therapist's hand and upper limb task training. The evaluation of the upper limb muscle activity was performed by the anterior deltoid, biceps brachii, triceps brachii, and extensor carpi radialis longus muscles that are involved in performing reaching, surface EMG that can record compound action potentials from nerves and muscle fibers was used to measure EMG signals. For the evaluation of upper limb function, tests such as upper limb movement, grasping, and finger manipulation were performed using the stroke manual function test (MFT).

Results

As a result of comparing the changes in upper limb muscle activity and upper limb function before and after intervention within the study group, there was a statistically significant difference ($*p<.05$). As a result of comparing the changes in upper limb muscle activity and upper limb function before and after intervention within the control group, there was no statistically significant difference ($p>.05$). After the intervention, there was a statistically significant difference in upper limb muscle activity and upper limb function in the test of variation between groups ($*p<.05$).

Conclusion

As a result of this study, it was proved that somatosensory training in combination with low frequency rTMS is effective in improving the upper limb muscle activity and function of the affected side of stroke patients. In future research, it is thought that a comparative study on the results of somatosensory training according to frequency characteristics through more subjects is needed.

Scalability evaluation of resistor charge division circuit for PET detector based on GAPD

Jingyu Yang*, Hea Ryeong Lee and Jihoon Kang

Department of Biomedical Engineering, College of Engineering, Chonnam National University,
Jeonnam 59626, Korea

Performance evaluation was characterized the scalability of resistor charge division (RCD) circuit for positron emission tomography (PET) detector based on Geiger-mode avalanche photodiode (GAPD). PET detectors with different scales (4×4 , 4×8 , and 4×12 array) were consists of LYSO - GAPD array with a pixel pitch of 3.36 mm. All of signals from GAPD array were multiplexed by the RCD circuits to reduce the number of output channels from $N \times M$ to 4 for N by M array. Experimental measurements were performed by using a Na-22 point source placed 100 mm away from the top surface of the PET detector module for uniformly irradiation. The following four parameters were measured for analog output signals of different PET detectors: Amplitude, rise time, fall time, and pulse width. In addition, the following three investigations were performed for characterization of PET detector performance: Flood histogram, energy spectra and count rate. Experimental results show that rise time, fall time, and pulse width of waveforms were increased larger than 3-times as increasing scale of detector arrays. Although the considerable degradations were observed in spatial linearity including pincushion distortion (Fig. 1), the detector performances including position determination, energy resolution ($\sim 10.5\%$) and dead time loss were quite similar for the three types of PET detector module. This results revealed that RCD circuit could provide the extendibility for 4×12 array PET detector module with the moderate analog signal degradations and comparable PET detector performances.

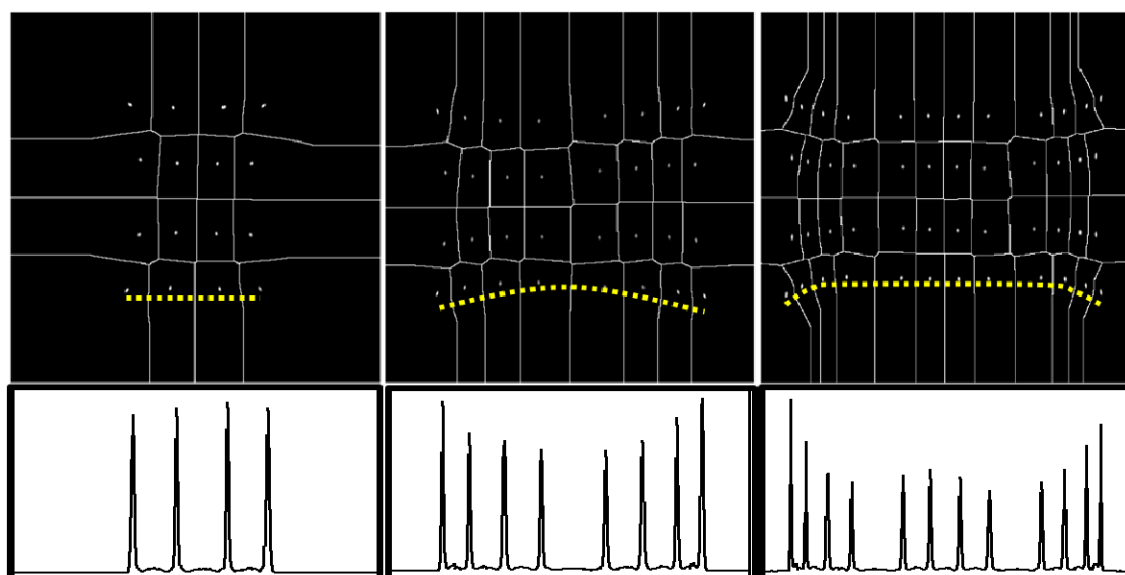


Fig. 1. Flood histograms (top) and line-profiles (bottom) for 4×4 (left), 4×8 (middle), and 4×12 (right) detector array. Pincushion distortion in the flood histogram was increased as the scale of GAPD array.

Optimization of Diverging Collimator for Radiation Monitoring Imaging using Monte Carlo Simulation

Dong-Hee Han^{1,3*}, Da-Eun Kwon^{1,3}, Kyung-Hwan Jung^{2,3}, Seung-Jae Lee⁴, Cheol-Ha Baek^{2,3†}

¹Department of Medical Health Science, Kangwon National University, Samcheok, Republic of Korea

²Department of Radiological Science, Kangwon National University, Samcheok, Republic of Korea

³Center for Radiological Science and Technology, Kangwon National University, Samcheok, Republic of Korea

⁴Department of Radiological Science, Dongseo University, Busan, Republic of Korea

Gamma imaging is used in nuclear facilities to maintain possible minimization of radiation exposure to radiation source. The quality of the gamma images depends on the performance of the collimator. A diverging collimator has been developed to improve the signal-to-noise ratio (SNR) while keeping the field of view of a pinhole collimator. The purpose of this study was to optimize a diverging collimator and to evaluate its possibility for nuclear accident monitoring by Monte Carlo simulation. An environmental monitoring gamma camera consists of a diverging collimator with a tungsten material and a GAGG scintillation crystal 3.5 mm thick and 50×50 mm² in area using GATE (Geant4 Application for Tomographic Emission). The sensitivity, spatial resolution, and peak signal-to-noise ratio (PSNR) were simulated and evaluated as a function of the diverging collimator. The optimal ranges of collimator height and diameter were determined through evaluation of the intrinsic resolution and PSNR trade-off curves. The simulation results allowed us to determine the optimal values of diverging diameter and height to be 1.5 mm and 70.0 mm, respectively. In this simulation study, the results indicated that wide field of view and high SNR of the environmental monitoring imaging are feasible using a diverging collimator camera.

Acknowledgement: This research was supported by the National Foundation of Korea (NRF) funded by the Ministry of Education, Science and Technology (No. 2020R1C1C1004584)

A Review on the Disposal of Radioactive Waste in the Radio-iodine Ward

Kim Jeong Ho*

Department of Radiology in Sunlin University, Korea

In the field of nuclear medicine, radioactive iodine treatment is performed only in a dedicated ward. The radioactive isotope used is ^{131}I -iodine, and trace amounts of other radioactive isotopes are mixed in the process of producing it. In particular, ^{129}I -iodine has a half-life of about 15 million years. Patients who ingested iodine generate radioactive waste in gaseous, drainage, and solid form while living in a dedicated ward for 3 to 5 days. The international standards for the treatment of radioactive waste are partially presented and the standards for each country are applied *mutatis mutandis*. In the case of domestic standards, in the case of solid waste, it is regulated by the absorbed dose at a 10 cm gap distance and the amount of radioactivity per area or capacity. In particular, in the case of domestic standards, in the case of ^{131}I -iodine, the acceptance standards of 1/26.7 to 1/4.5 of the international standards are applied. If only pure ^{131}I -iodine is used, it is not a big problem, but as ^{129}I -iodine is mixed, the difference in storage period according to domestic and international standards is large, and the points to be considered in the measurement standards are different. In particular, in the case of structures such as exhaust pipes and drain pipes, it can become a big problem in the follow-up management of the change of use of the hospital room and treatment. Therefore, the development of purification technology for pure ^{131}I -iodine should be considered as the top priority, and it is considered that follow-up measures according to the change of use and disposal are required as the next consideration.

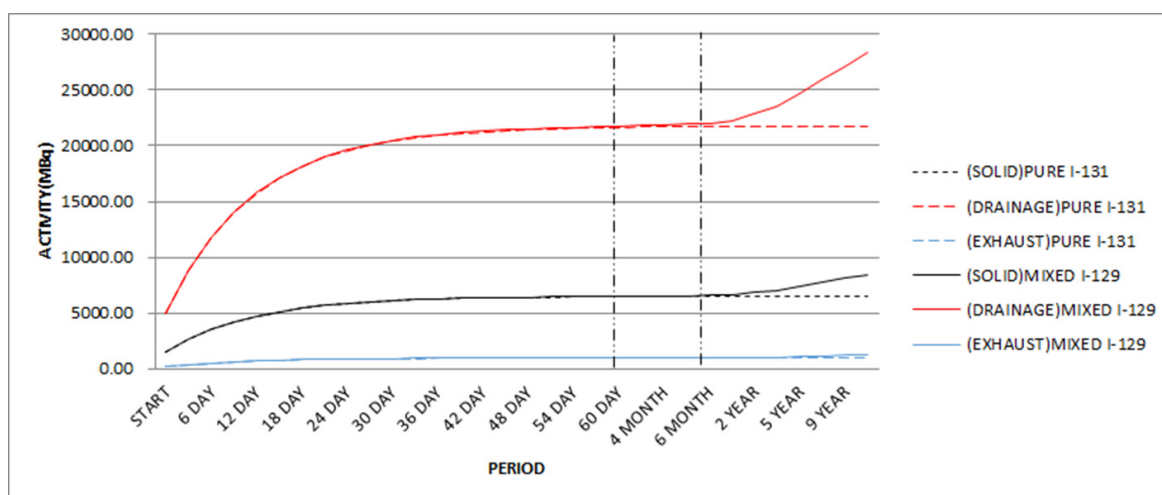


Fig. 1. The amount of radioactivity over time in the waste according to the purity of iodine

Monte Carlo project of carbon-ion radiation therapy at Yonsei Cancer Center: Present and future

Min Cheol Han*

Department of Radiation Oncology, Yonsei Cancer Center, Yonsei University College of Medicine,
Seoul, Republic of Korea

The new facility for carbon-ion radiation therapy (CIRT) is being assembled at Yonsei Cancer Center (YCC) for the first time in Korea. From Yonsei CIRT center, the particle beam energy delivered by synchrotron will be selected in the range between 56 to 430 MeV/u, and the selected beam will be injected into a fixed gantry and two of isocentric rotating gantries. The first treatment of Yonsei CIRT is scheduled in spring of 2023.

The major advantage of CIRT include the particle beam has a finite range, so called “Bragg peak,” and biological advantage due to high relative biological effectiveness (RBE) comparing with conventional X-ray treatment; hence, the reduced energy deposited in the patient comparing to conventional X-ray treatment. That is, reducing the uncertainties of beam range and RBE-weighted dose would a directly related to the quality assurance (QA) of CIRT dose delivery to a patient. For uncertainty quantification of CIRT, our research group is involved in various CIRT-related research projects with QST-NIRS, Kanagawa Cancer Center, and Yamagata University Faculty of Medicine (YUM); one project, called Monte Carlo project, is performing with YUM for patient-specific quality assurance, quantification of carbon-ion beam range uncertainty, and validation of RBE-weighted dose calculation. In the presentation, the current status of CIRT center at YCC and the Monte Carlo project will be introduced, and a future work will be reported about Monte Carlo project.

Review of the Task Group 284 Report: Magnetic Resonance Imaging Simulation in Radiotherapy

So Hyun Ahn*

Department of Radiation Oncology, Yonsei Cancer Center,
Yonsei University College of Medicine, Seoul, Republic of Korea

In the field of radiotherapy, MRI is used for the purpose of accurately segmenting the tumor and adjacent organs at risk for treatment planning, and this process is called MR simulation. In order to use the MR image for simulation of radiotherapy, there are several considerations such as co-registration with the existing CT sim image and consideration of the radiation therapy posture. The use of MR sim in radiotherapy planning can improve the treatment outcome by improving the location accuracy of the tumor, and reduce toxicity by increasing the segmentation accuracy of the oar. Despite these advantages, there are considerations to add MR sim to the current CT sim based radiation therapy workflow. As MRI technology is more actively used in the radiotherapy, appropriate recommendations on the installation and use of MR simulation equipment will be required. We reviewed the latest AAPM Task Group 284 provides general guidelines for special facility design for MR simulator, manpower operation, patient-specific, and device MR safety, protocol establishment related to RT-specific MR clinical workflows, respiratory management, periodic QA, etc.

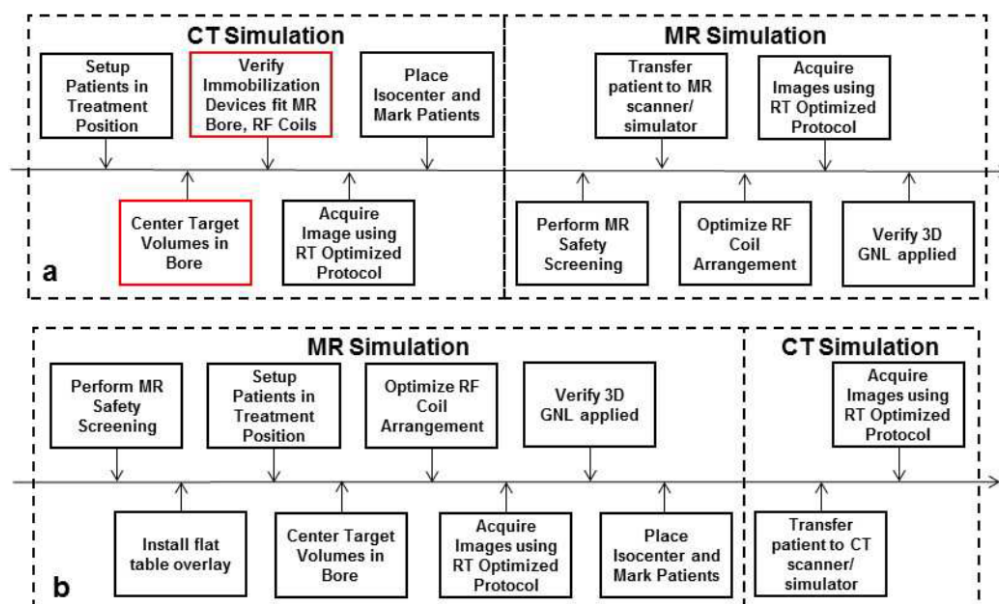


Fig. 1. Conventional (a) and reversed (b) simulation workflows. Processes denoted in red denote additional steps required to ensure compatibility with MR simulator equipment and high quality MR imaging.

Author Index

Name	Abstract ID	Page	Name	Abstract ID	Page
Ahn, Hyo-Bin	초S-2-9	191	Cha, Hee-Ryoung	PM08	98
Ahn, Hyo-Jun	PM11	103	Cha, In Ho	SS17	52
Ahn, So Hyun	초S-10-6	301	Cha, In Ho	SS24	62
Ahn, Su Yeon	PM06	95	Chang, Joonyeon	초S-9-1	267
Ahn, Su Yeon	PM09	99	Chang, Mi Se	초O-1-8	286
Ahn, Taehong	LM04	153	Chang, Seo Hyoung	QM01	146
Ain, Qurat ul	TC03	138	Chao, Weilun	LM15	165
Amin, Vivek	초S-2-2	183	Chao, Weilun	SM08	121
An, Kyongmo	초O-1-2	278	Chen, Gang	TC06	141
An, Subong	SM15	128	Chen, Lebing	초S-4-2	220
An, Suhyeok	MD03	70	Chen, Xianzhe	초S-2-4	185
An, Suhyeok	MD04	71	Chen, Yi	LM03	152
An, Suhyeok	SS10	45	Chérif, Salim M.	SS17	52
An, Suhyeok	SS22	59	Chin, Jun-Woo	EM01	19
Ardavan, Arzhang	SS28	67	Cho, Byeong Sun	SM14	127
Bae, Kyoung-Hoon	SM15	128	Cho, Franklin H.	SS28	67
Bae, Kyoung-Hoon	초O-1-7	284	Cho, In-Kui	초S-5-5	236
Bae, Yu Jeong	초O-1-4	280	Cho, Jaehun	MD10	78
Bae, Yujeong	LM03	152	Cho, Jaehun	MD12	81
Bae, Yujeong	LM04	153	Cho, Jaehun	SS09	43
Bae, Yujeong	LM08	157	Cho, Jaehun	초S-6-5	247
Baek, Cheol-Ha	MS01	21	Cho, Kyung Mox	PM09	99
Baek, Cheol-Ha	초S-10-3	298	Cho, Seunggho	LM06	155
Baek, Eunchong	MD03	70	Cho, SungJoon	PM15	107
Baek, Eunchong	MD04	71	Cho, Yong-Rae	PM10	101
Baek, Eunchong	SS10	45	Cho, Young-Hun	SS15	50
Baek, Seung-heon Chris	초S-6-3	245	Cho, Young-Jun	MD11	79
Baek, Youn-Kyoung	LM02	151	Choe, Sug-Bong	MD02	69
Baek, Youn-Kyung	PM03	91	Choe, Sug-Bong	MD10	78
Baik, Jae Sung	MM04	30	Choi, Chul-Jin	PM06	95
Baik, Jaeyoon	초S-9-2	268	Choi, Chul-Jin	PM07	96
Belmeguenai, Mohamed	SS17	52	Choi, Chul-Jin	PM09	99
Bhoi, Biswanath	MD08	75	Choi, Chul-Jin	PM10	101
Bhoi, Biswanath	MD09	77	Choi, Chul-Jin	PM11	103
Bhoi, Biswanath	MD13	83	Choi, Chul-Jin	초O-1-10	289
Boero, Giovanni	SS28	67	Choi, Chul-Jin	초S-3-13	211
Boukhvalov, Danil W.	초S-9-2	268	Choi, Deung-Jang	LM03	152
Brataas, Arne	초S-6-1	243	Choi, Gyung-Min	SD04	170
Bui, Thi Hong	LM03	152	Choi, Gyung-Min	SS11	46
Byun, Ik-Su	초S-9-2	268	Choi, Gyung-Min	SS12	47
Cha, Eunji	SM16	129	Choi, Gyung-Min	SS13	48
Cha, Eun-Ji	SM18	132	Choi, Hyeok-Cheol	MD10	78
Cha, Hee-Ryoung	PM05	93	Choi, Hyunkyoung	MM02	26

Name	Abstract ID	Page	Name	Abstract ID	Page
Choi, Hyunkyung	MM03	28	Galkin, Vitalii	PM16	108
Choi, Hyunkyung	MM04	30	Galkin, Vitalli	PM17	109
Choi, Hyunkyung	초S-7-4	254	Go, Dongwook	초S-6-1	243
Choi, J. W.	초O-1-9	288	Go, Gyungchoon	SS24	62
Choi, Jae-Young	PM03	91	Go, Gyungchoon	초O-1-1	277
Choi, Jang-Young	초S-3-14	212	Goo, Minseo	SD03	169
Choi, Jisu	초S-1-6	8	Gradhand, Martin	초S-6-1	243
Choi, Jong Woan	초S-7-3	253	Gwak, Jina	초O-1-8	286
Choi, Jong-Guk	SS19	55	Gweon, Hyung Keun	초S-9-3	269
Choi, Jong-Guk	SS27	65	Ha, Jae-Hyun	MD12	81
Choi, Joon Phil	초S-3-9	206	Ha, Taeho	초S-3-9	206
Choi, Joonyoung	SD05	171	Han, Dong-Hee	초S-10-3	298
Choi, Jun Woo	초S-9-1	267	Han, Donghyeon	LM12	162
Choi, Jun Woo	초S-9-3	269	Han, Donghyeon	초O-1-5	281
Choi, Kwangsu	SM05	118	Han, Guihyun	TC05	140
Choi, Minseok	TC01	136	Han, Guihyun	초S-8-2	262
Choi, Minseok	TC02	137	Han, Hee-Sung	LM14	164
Choi, SungJoon	PM14	106	Han, Hee-Sung	LM15	165
Choi, Sungjoon	SM07	120	Han, Hee-Sung	MD15	85
Choi, Sungkyun	초S-4-3	222	Han, Hee-Sung	MD16	86
Choi, Young-Gwan	SS11	46	Han, Hee-Sung	MD17	88
Choi, Young-Sin	SM18	132	Han, Hee-Sung	SM08	121
Choi-Yim, Haein	SM20	134	Han, Jung Hoon	초S-4-4	224
Choi-Yim, Haein	SM21	135	Han, Min Cheol	초S-10-5	300
Chongthanaphisit, Phunvira	SS16	51	Han, Seungyun	초S-2-8	190
Chongthanaphisit, Phunvira	SS18	54	Han, So-Young	초S-10-1	295
Chun, Dong Hyun	초S-7-1	251	Han, Woojoo	QM04	149
Chung, Jae-Ho	초S-4-2	220	Haney, Paul	초S-2-2	183
Chung, Jin-Seok	QM01	146	Haney, Paul	초S-2-6	188
Chung, Suk Bum	QM01	146	Heinrich, Andreas J.	LM03	152
Colazzo, Luciano	SS28	67	Heinrich, Andreas J.	LM04	153
Crosse, J. A.	OS03	176	Heinrich, Andreas J.	SS28	67
Cuong, D. D.	TC04	139	Heo, Jae-Hee	SM01	114
Cuong, Do Duc	SS23	60	Heo, Man Seung	MS02	22
Dai, Pengcheng	초S-4-2	220	Ho, Kim Jeong	초S-10-4	299
Delgado, Fernando	LM03	152	Ho, Thi H.	TC07	142
Denneulin, Thibaud	초S-6-1	243	Hoang, T. Thuy	SS23	60
Do, Thi-Nga	SS20	56	Hong, Ik-Sun	SS03	36
Dobrowolska, M.	SS16	51	Hong, Jisang	SS05	39
Dobrowolska, M.	SS18	54	Hong, Jisang	SS06	40
Donati, Fabio	SS28	67	Hong, Jung-Il	MD12	81
Duvjir, Ganbat	초S-2-9	191	Hong, Jung-Il	초O-1-3	279
Eom, Mingi	MM05	32	Hong, Jung-Il	초O-1-6	282
Fan, Xin	초S-2-10	192	Hong, S. C.	SS23	60
Fang, Lei	LM04	153	Hong, S. C.	TC04	139
Fukami, Shunsuke	초S-2-5	186	Hong, S. C.	TC07	142
Furdyna, J. K.	SS16	51	Hong, Soon Cheol	PM18	110
Furdyna, J. K.	SS18	54	Hong, Soon Cheol	PM20	113

Name	Abstract ID	Page
Hong, Soon Cheol	TC03	138
Hong, Soon Cheol	TC05	140
Hong, Soon Cheol	TC08	143
Hong, Soon Chul	PM06	95
Huh, Seok Hwan	LM05	154
Huh, Seok Hwan	SM06	119
Hwan, Huh Seok	LM07	156
Hwang, Chanyong	SS20	56
Hwang, Chanyong	초O-1-3	279
Hwang, Chanyong	초O-1-6	282
Hwang, Choongyu	초S-9-1	267
Hwang, Jinwoong	초S-9-1	267
Hwang, Jiyeon	LM04	153
Hwang, Kyusung	초S-4-6	226
Hwang, Seungchan	SD03	169
Im, Hyun Ah	SM15	128
Im, Mi-Young	LM15	165
Im, Mi-Young	SM08	121
Im, Pyung Won	MS02	22
Ipppei, Suzuki	LM12	162
Jang, Chaun	초S-9-1	267
Jang, Chaun	초S-9-3	269
Jang, Gang-Hyeon	초S-3-14	212
Jang, Jeongyun	초S-7-7	257
Jang, Kyuha	초S-2-9	191
Jang, Min-Sun	OS02	174
Jang, Min-Sun	초O-1-8	286
Jang, Moongyu	초S-1-6	8
Jang, Seung-Hun	MD09	77
Jang, Won-jun	LM03	152
Jang, Ye Ryeong	초S-3-15	213
Jang, Yu June	SS04	38
Je, Soong-Geun	LM15	165
Je, Soong-Geun	SM08	121
Je, Soong-Geun	초O-1-6	282
Jeon, Changyeop	초S-1-5	7
Jeon, Haechan	MD08	75
Jeon, Haechan	MD13	83
Jeon, Hankuk	PM09	99
Jeon, Hankuk	PM11	103
Jeon, Sungho	초S-1-6	8
Jeong, Jae Won	LM06	155
Jeong, Jae Won	SM15	128
Jeong, Jae Won	초O-1-8	286
Jeong, Jaehun	초S-1-6	8
Jeong, Jimin	SS14	49
Jeong, Jong-Ryul	LM16	166
Jeong, Jong-Ryul	SS21	57

Name	Abstract ID	Page
Jeong, Jong-Ryul	초S-6-6	248
Jeong, Myeong-Sik	초S-3-8	204
Jeong, Seyeop	SS22	59
Jeong, Suyeong	MD15	85
Jeong, Suyeong	MD16	86
Jeong, Suyeong	MD17	88
Jeong, Suyeong	PM19	112
Jeong, W.H.	SM11	124
Jeong, Yejin	SS28	67
Jin, Hosub	초S-9-6	272
Jin, Munsu	SS03	36
Jina, Liu	SD04	170
Jo, Gi-Ryeon	LM02	151
Jo, In Hyuk	SD05	171
Jo, Younghun	초S-2-9	191
Jo, Younjung	SD05	171
Ju, Tae-Seong	초O-1-3	279
Jung, Dae-Han	LM14	164
Jung, Dae-Han	MD15	85
Jung, Dae-Han	MD16	86
Jung, Dae-Han	MD17	88
Jung, Dae-Han	PM19	112
Jung, Daewon	SM16	129
Jung, Heeyoung	초O-1-4	280
Jung, Hyo Yun	SM05	118
Jung, Jin Gyo	MM02	26
Jung, Jin Gyo	MM03	28
Jung, Jinwon	SS09	43
Jung, Jinyong	MD10	78
Jung, Jinyong	MD12	81
Jung, Kyung-Hwan	초S-10-3	298
Jung, Myung Hwa	SS04	38
Jung, Myung Hwa	SS07	41
Jung, Seyeop	LM12	162
Jung, Young-Hoon	초S-3-6	201
Kang, Chang-Ki	MS03	23
Kang, Jaimin	SS27	65
Kang, Jaimin	초O-1-5	281
Kang, Jihoon	초S-10-2	297
Kang, Jun-Ho	SS08	42
Kang, Jun-Ho	SS15	50
Kang, Kyongho	초S-3-2	196
Kang, Min-Gu	SM03	116
Kang, Min-Gu	SS08	42
Kang, Min-Gu	SS14	49
Kang, Mingu	SS21	57
Kang, Myeonghwan	LM14	164
Kang, Myeonghwan	LM15	165

Name	Abstract ID	Page
Kang, Myeonghwan	SM08	121
Kang, Seong-Hyeon	MS03	23
Kang, Young-Min	PM01	89
Kang, Young-Min	SM01	114
Kang, Young-Min	SM02	115
Kang, Young-Min	SM03	116
Kim, Beom Hyun	초S-4-7	227
Kim, Bosung	MD08	75
Kim, Bosung	MD09	77
Kim, Bosung	MD11	79
Kim, Bosung	MD13	83
Kim, Bumseop	초S-8-4	264
Kim, Changsoo	초O-1-3	279
Kim, Changyoung	SS02	35
Kim, Cheol Gi	초S-1-5	7
Kim, Chul Sung	MM02	26
Kim, Chul Sung	MM03	28
Kim, Chul Sung	MM04	30
Kim, Chul Sung	초S-7-4	254
Kim, Chul Sung	초S-7-6	256
Kim, Dong Seob	초S-9-1	267
Kim, Dong-Hwan	초O-1-7	284
Kim, Dong-Hyun	초S-6-4	246
Kim, Dong-Hyun	초S-6-6	248
Kim, Dongryul	MD04	71
Kim, Dongryul	초S-1-4	6
Kim, Dongsoo	PM16	108
Kim, Dongsoo	PM17	109
Kim, Duck-Ho	SS03	36
Kim, G. Hye	TC08	143
Kim, Ganghwi	MD15	85
Kim, Ganghwi	MD16	86
Kim, Ganghwi	MD17	88
Kim, Ganghwi	PM19	112
Kim, Ga-Yeong	PM08	98
Kim, Gukcheon	SS09	43
Kim, Gyeonghye	TC03	138
Kim, Gyu Won	SS17	52
Kim, Gyu Won	SS24	62
Kim, Gyu Won	SS26	64
Kim, Heung-Sik	TC06	141
Kim, Hongjoon	QM02	147
Kim, Hwijun	SM16	129
Kim, Hwi-Jun	SM18	132
Kim, Hyun Ho	초S-2-3	184
Kim, Hyun Suk	초S-7-3	253
Kim, Hyung-jun	초S-9-1	267
Kim, Hyun-Joong	초O-1-3	279

Name	Abstract ID	Page
Kim, Hyun-Joong	초O-1-6	282
Kim, Inseo	TC01	136
Kim, Jae-Uk	SM02	115
Kim, Jae-Young	초S-9-1	267
Kim, Jang-Yeol	초S-5-5	236
Kim, Jeong Rae	QM02	147
Kim, Jeong Rae	QM03	148
Kim, Jeong Rae	SS02	35
Kim, Jeong-Mok	SS21	57
Kim, Jeong-Mok	초O-1-5	281
Kim, Jin-A	SS10	45
Kim, Jinhee	QM04	149
Kim, Jinkwon	QM01	146
Kim, Jinkwon	SS02	35
Kim, Jinkyung	LM03	152
Kim, Jisu	SS22	59
Kim, Ji-Wan	MD14	84
Kim, Ji-Wan	초S-6-6	248
Kim, Jong-Ryoul	SM18	132
Kim, Jong-Woo	PM06	95
Kim, Jong-Woo	PM07	96
Kim, Jong-Woo	PM09	99
Kim, Jong-Woo	초S-3-13	211
Kim, June-Seo	MD10	78
Kim, June-Seo	초S-6-5	247
Kim, Jungdae	초S-2-9	191
Kim, Jun-Su	SS09	43
Kim, Juran	초O-1-3	279
Kim, Kab-Jin	MD01	68
Kim, Kab-Jin	MD05	72
Kim, Kab-Jin	SD01	167
Kim, Kab-Jin	SS04	38
Kim, Kab-Jin	SS07	41
Kim, Kab-Jin	SS08	42
Kim, Kab-Jin	SS15	50
Kim, Kab-Jin	SS19	55
Kim, Kab-Jin	SS22	59
Kim, Kab-Jin	SS27	65
Kim, Kab-Jin	초O-1-5	281
Kim, Kitae	MD02	69
Kim, Kwangsu	초S-2-9	191
Kim, Kyoo	초S-2-9	191
Kim, Kyoung-Whan	SS13	48
Kim, Kyoung-Whan	초S-2-8	190
Kim, Kyoung-Whan	초S-9-3	269
Kim, Min-Ho	PM01	89
Kim, Miyoung	QM01	146
Kim, Miyoung	SS02	35

Name	Abstract ID	Page	Name	Abstract ID	Page
Kim, Namkyu	LM14	164	Kim, Yeyeon	초S-1-6	8
Kim, Namkyu	LM15	165	Kim, Yona	MS02	22
Kim, Namkyu	PM19	112	Kim, Yong Baek	초O-1-11	291
Kim, Namkyu	초O-1-10	289	Kim, Yong Jin	SS17	52
Kim, Sanghoon	LM12	162	Kim, Yong Jin	SS24	62
Kim, Sanghoon	MD01	68	Kim, Yongsub	MD07	74
Kim, Sanghoon	SS22	59	Kim, Young Duck	초S-9-5	271
Kim, Sanghoon	초S-2-9	191	Kim, Young Keun	LM11	160
Kim, Sanghoon	초S-6-2	244	Kim, Young Keun	SS17	52
Kim, Sang-Koog	MD06	73	Kim, Young Keun	SS24	62
Kim, Sang-Koog	MD07	74	Kim, Young Keun	SS25	63
Kim, Sang-Koog	MD08	75	Kim, Young Keun	SS26	64
Kim, Sang-Koog	MD09	77	Kim, Young Kuk	PM03	91
Kim, Sang-Koog	MD11	79	Kim, Youngdo	SS02	35
Kim, Sang-Koog	MD13	83	Kim, Younghak	초S-9-1	267
Kim, Sang-Koog	SM12	125	Kläui, Mathias	초S-2-1	181
Kim, Se Kwon	SS01	34	Kläui, Mathias	초S-6-1	243
Kim, Se Kwon	SS03	36	Klein, Olivier	초O-1-2	278
Kim, Se Kwon	SS04	38	Ko, Eun Kyo	QM01	146
Kim, Se Kwon	SS07	41	Ko, Han Seok	LM11	160
Kim, Se Kwon	초O-1-1	277	Ko, Kyun-Hun	SS12	47
Kim, Se Kwon	초S-2-9	191	Ko, San	SD01	167
Kim, Seong-Been	SS13	48	Koo, Bon Heun	LM05	154
Kim, Seunghyun	PM16	108	Koo, Bon Heun	LM07	156
Kim, Seunghyun	PM17	109	Koo, Bon Heun	SM06	119
Kim, Sung Hoon	SD03	169	Koo, Hyun Cheol	초S-9-1	267
Kim, Sung Hoon	초S-5-6	237	Koo, Hyun-Cheol	SS13	48
Kim, Sungmin	SM16	129	Kovács, András	초S-6-1	243
Kim, Tae Hee	SS20	56	Krylov, Denis	LM03	152
Kim, Tae Hee	초O-1-4	280	Krylov, Denis	LM04	153
Kim, Tae Heon	QM01	146	Kuchi, Rambabu	PM16	108
Kim, Tae-Hoon	PM05	93	Kuchi, Rambabu	PM17	109
Kim, Tae-Hoon	PM08	98	Kumar, Akshay	LM05	154
Kim, Tae-Hoon	초O-1-7	284	Kumar, Akshay	LM07	156
Kim, Tae-Hoon	초S-3-11	208	Kumar, Akshay	SM06	119
Kim, Taehyun	LM11	160	Kumari, Kavita	LM05	154
Kim, Taehyun	SS17	52	Kumari, Kavita	LM07	156
Kim, Taehyun	SS24	62	Kumari, Kavita	SM06	119
Kim, Taehyun	SS26	64	Kwak, Yongsu	QM04	149
Kim, Won Dong	LM13	163	Kwon, Da-Eun	초S-10-3	298
Kim, Wondong	초S-9-1	267	Kwon, Dohoon	SM16	129
Kim, Wondong	초S-9-2	268	Kwon, Do-Hun	SM18	132
Kim, Woo-Hyeon	초S-3-14	212	Kwon, H. Y.	초O-1-9	288
Kim, Woo-Yeong	MD03	70	Kwon, Hee Young	초S-9-3	269
Kim, Woo-Yeong	MD04	71	Kwon, Soon-O	초S-3-8	204
Kim, Woo-Yeong	SS09	43	Kwon, Suk Jin	초O-1-8	286
Kim, Yang-Do	PM05	93	Kwon, Young-tae	초O-1-8	286
Kim, Yang-Do	PM08	98	Lam, Nguyen Huu	초S-2-9	191

Name	Abstract ID	Page	Name	Abstract ID	Page
Lee, B.W.	SM11	124	Lee, Jung-Goo	PM05	93
Lee, Changgu	초S-2-9	191	Lee, Jung-Goo	PM08	98
Lee, Changhee	초O-1-4	280	Lee, Jung-Goo	초O-1-7	284
Lee, Changhoon	OS04	177	Lee, Jung-Goo	초S-3-11	208
Lee, D. B.	초O-1-9	288	Lee, Kanghyuk	PM14	106
Lee, Dae Sung	초S-5-8	239	Lee, Kang-Hyuk	PM15	107
Lee, Dal Ho	초S-5-8	239	Lee, Ki-Seung	MD03	70
Lee, Donghyeon	LM12	162	Lee, Ki-Seung	MD04	71
Lee, Donghyeon	SS22	59	Lee, Ki-Seung	SS10	45
Lee, Duk Hyun	LM13	163	Lee, Ki-Seung	SS22	59
Lee, Duk Hyun	초S-9-2	268	Lee, Ki-Suk	LM14	164
Lee, Eun Woo	초S-7-6	256	Lee, Ki-Suk	LM15	165
Lee, Eunjik	MM03	28	Lee, Ki-Suk	MD15	85
Lee, Eunjik	MM04	30	Lee, Ki-Suk	MD16	86
Lee, Eunjik	초S-7-7	257	Lee, Ki-Suk	MD17	88
Lee, Gayoung	초S-1-6	8	Lee, Ki-Suk	OS02	174
Lee, Geun-Hee	SD01	167	Lee, Ki-Suk	PM19	112
Lee, Gi-Ju	초S-3-8	204	Lee, Ki-Suk	SM08	121
Lee, Hakseung	초S-3-9	206	Lee, Ki-Suk	초O-1-10	289
Lee, Han Gyeol	QM01	146	Lee, Kwang Hyun	MD10	78
Lee, Hea Ryeong	초S-10-2	297	Lee, Kyujoon	초S-6-1	243
Lee, Hoon-Ki	초S-3-14	212	Lee, Kyung Jae	SS16	51
Lee, Ho-Young	초S-3-8	204	Lee, Kyung Jae	SS18	54
Lee, Hyun Joon	초S-5-5	236	Lee, Kyung-Jin	SS03	36
Lee, Hyungju	초S-3-5	200	Lee, Kyung-Jin	SS04	38
Lee, Hyungju	초S-3-15	213	Lee, Kyung-Jin	SS07	41
Lee, Hyungwoo	TC01	136	Lee, Kyung-Jin	SS13	48
Lee, Hyungwoo	TC02	137	Lee, Kyung-Jin	SS24	62
Lee, Hyun-Sook	초S-3-15	213	Lee, Kyung-Jin	T-2	16
Lee, Hyun-Woo	T-1	15	Lee, Mi Jung	LM10	159
Lee, Hyun-Woo	초S-2-8	190	Lee, Min Hyeok	SS24	62
Lee, Jaegi	MM05	32	Lee, Min Hyeok	SS25	63
Lee, Jaegi	초S-7-5	255	Lee, Minwoo	SM16	129
Lee, Jae-Ho	초S-5-5	236	Lee, Min-Woo	SM18	132
Lee, Jaehoon	초S-1-5	7	Lee, Nam Young	초S-5-8	239
Lee, Jae-Hyeok	MD07	74	Lee, Nyun Jong	초O-1-4	280
Lee, Jaeryung	초S-3-15	213	Lee, Nyun Jong	초S-2-9	191
Lee, Jeong Kyu	SS26	64	Lee, Nyunjong	LM12	162
Lee, Jeong-Min	PM03	91	Lee, Sang Bok	초O-1-8	286
Lee, Ji Hye	QM01	146	Lee, Sanghoon	SS16	51
Lee, Ji Hye	QM02	147	Lee, Sanghoon	SS18	54
Lee, Ji-Hye	PM01	89	Lee, Sanghwa	초O-1-5	281
Lee, Jiyoung	LM11	160	Lee, Sang-Hyup	초O-1-7	284
Lee, Jong Seok	QM03	148	Lee, Sangmin	QM01	146
Lee, Joonsik	초O-1-8	286	Lee, Sehee	SS20	56
Lee, Jun Han	LM06	155	Lee, Seong-Hyub	MD02	69
Lee, Jung Woo	SM15	128	Lee, Seungho	SS01	34
Lee, Jung-Goo	PM03	91	Lee, Seung-Jae	MS01	21

Name	Abstract ID	Page	Name	Abstract ID	Page
Lee, Seung-Jae	초S-10-3	298	Martin, Franziska	초S-6-1	243
Lee, Soogil	MD01	68	Millet, Loïc	MD08	75
Lee, Soogil	SS08	42	Min, Byoung-Chul	초S-9-1	267
Lee, Soogil	SS14	49	Mo, Sung-Kwan	초S-9-1	267
Lee, Soogil	SS15	50	Mokrousov, Yuriy	초S-6-1	243
Lee, Soogil	SS27	65	Moon, Dong Hyeok	초S-7-6	256
Lee, Soogil	초O-1-5	281	Moon, Joon	MD02	69
Lee, Soonhyeong	LM03	152	Moon, Kyoung-Woong	MD01	68
Lee, Sooseok	LM14	164	Moon, Kyoung-Woong	초O-1-3	279
Lee, Sooseok	LM15	165	Moon, Pilkyung	OS03	176
Lee, Sooseok	SM08	121	Mun, Junsik	QM01	146
Lee, Su-Mi	SM03	116	Mun, Junsik	SS02	35
Lee, SungBin	초O-1-11	291	Nahm, Ho-Hyun	TC01	136
Lee, SungBin	초S-4-5	225	Nam, Chunghee	SD06	172
Lee, Sungjun	초O-1-5	281	Nguyen, Quynh Anh T.	TC04	139
Lee, Sungmin	LM10	159	Noh, Kyungju	LM04	153
Lee, Sungwon	초S-1-3	5	Noh, Tae Won	QM01	146
Lee, Taekhyeon	SS07	41	Noh, Tae Won	QM02	147
Lee, Taekhyeon	SS22	59	Noh, Tae Won	QM03	148
Lee, Taekhyeon	SS27	65	Noh, Tae Won	SS02	35
Lee, Taek-Hyeon	초O-1-5	281	Ochirkhuyag, Tumentsereg	PM18	110
Lee, Won-Bin	SS13	48	Ochirkhuyag, Tumentsereg	PM20	113
Lee, Wooyoung	초S-3-15	213	Odkhuu, Dorj	PM18	110
Lee, Yeonjoo	SM16	129	Odkhuu, Dorj	PM20	113
Lee, Youngjin	MS03	23	Oh, DaYea	LM13	163
Li, Oi Lun	PM07	96	Oh, Gwang Taek	LM13	163
Li, Xiaojin	초O-1-2	278	Oh, Gwangtak	LM10	159
Liedtke, Anna	초S-6-1	243	Oh, Inseon	OS02	174
Lim, byeonghwa	초S-1-5	7	Oh, Jung Hoon	초S-5-5	236
Lim, Jung Tae	PM06	95	Oh, Yoon Seok	LM06	155
Lim, Jung Tae	PM07	96	Ok, Hye-Jin	LM14	164
Lim, Jung Tae	PM09	99	Ok, Hye-Jin	LM15	165
Lim, Jung Tae	PM11	103	Ok, Hye-Jin	OS02	174
Lim, Jung Tae	초S-3-13	211	Ok, Hye-Jin	SM08	121
Lim, Jun-Pyo	PM01	89	Okay, Mahmut Sait	초S-8-4	264
Lim, Myung-Seop	EM01	19	Paek, Sun Ha	MS02	22
Lim, Myung-Seop	초S-3-6	201	Pan, Feng	초S-2-4	185
Liu, Junjie	SS28	67	Park, Bae Ho	LM13	163
Liu, X.	SS16	51	Park, Bae Ho	초S-9-2	268
Liu, X.	SS18	54	Park, Bea Ho	LM10	159
Liu, Yu	초S-9-1	267	Park, Byeongjin	초O-1-8	286
Lotsch, Bettina	초S-6-1	243	Park, Byong-Guk	SD01	167
Low, Tony	초S-2-6	188	Park, Byong-Guk	SS08	42
Lutz, Christopher P.	LM03	152	Park, Byong-Guk	SS14	49
Ly, Pham Ngoc Luu	SS12	47	Park, Byong-Guk	SS15	50
Ly, Trinh Thi	초S-2-9	191	Park, Byong-Guk	SS19	55
Marfoua, Brahim	SS05	39	Park, Byong-Guk	SS21	57
Marfoua, Brahim	SS06	40	Park, Byong-Guk	SS27	65

Name	Abstract ID	Page
Park, Byong-Guk	초O-1-5	281
Park, Gu-Gon	MM03	28
Park, Gu-Gon	MM04	30
Park, Gu-Gon	초S-7-7	257
Park, Gyuyoung	SM12	125
Park, Hyeon-Kyu	MD06	73
Park, Hyung Woo	MS02	22
Park, Hyun-Uk	MM03	28
Park, Hyun-Uk	MM04	30
Park, Hyun-Uk	초S-7-7	257
Park, Jaehyeon	SS19	55
Park, Jaehyeon	SS27	65
Park, Jaeyoung	MS03	23
Park, Je-Geun	LM10	159
Park, Je-Geun	초S-4-1	219
Park, Ji-Ho	SS04	38
Park, Jihoon	PM06	95
Park, Jihoon	PM07	96
Park, Jihoon	PM09	99
Park, Jihoon	PM10	101
Park, Jihoon	PM11	103
Park, Jihoon	초O-1-10	289
Park, Jihoon	초S-3-13	211
Park, Jin Jae	TC08	143
Park, Jin-Cheol	EM01	19
Park, Jin-Cheol	초S-3-6	201
Park, Jong Hwan	SM14	127
Park, Jungmin	초S-2-9	191
Park, Junho	PM14	106
Park, Juyoung	SS28	67
Park, Kwonjin	MD12	81
Park, Min Gyu	MD01	68
Park, Min Gyu	MD05	72
Park, Min Tae	SS04	38
Park, Min Tae	SS07	41
Park, Minkyu	SS23	60
Park, Minkyu	TC05	140
Park, Minkyu	초S-8-2	262
Park, Moon Jip	초O-1-11	291
Park, Noejung	초S-8-4	264
Park, S. M.	초O-1-9	288
Park, Se Young	초S-9-1	267
Park, Seongjin	SS16	51
Park, Seongjin	SS18	54
Park, Seung-Young	SM07	120
Park, Su Jeong	SM06	119
Park, Tae-Eon	초S-2-9	191
Park, Taesu	OS04	177

Name	Abstract ID	Page
Park, Yeong Jun	SM14	127
Petrovic, Cedomir	초S-9-1	267
Phouc, Cao-Van	SS21	57
Pyo, Min-Ji	LM02	151
Qian, Hui-Dong	PM07	96
Qian, Hui-Dong	PM09	99
Qian, Hui-Dong	PM10	101
Qian, Hui-Dong	PM11	103
Qian, Hui-Dong	초S-3-13	211
Qiu, Zi Qiang	초S-9-3	269
Rhee, Eunjun	초S-3-2	196
Rhim, S. H.	SS23	60
Rhim, S. H.	TC03	138
Rhim, S. H.	TC05	140
Rhim, S. H.	TC08	143
Rhim, S. H.	초S-8-2	262
Rhim, Sonny H.	TC04	139
Rhim, Sonny H.	TC07	142
Roh, Chang Jae	QM03	148
Roussigné, Yves	SS17	52
Rubio, Angel	초S-8-3	263
Ryu, Hyejin	초S-9-1	267
Ryu, Hyejin	초S-9-3	269
Ryu, Jeongchun	SS27	65
Ryu, Woo Hyeon	LM13	163
Ryu, Woohyeon	LM10	159
Samanta, Subhasis	TC06	141
Samardak, Alexander S.	SS17	52
Saunderson, Tom G.	초S-6-1	243
Schmitt, Maurice	초S-6-1	243
Scholz, Tanja	초S-6-1	243
Sebastian, Armando Ramos	SD03	169
Seo, Min Ho	초S-7-7	257
Shahee, Aga	초S-6-1	243
Shi, Li	초O-1-2	278
Shim, In-Bo	MM02	26
Shim, Ji Hoon	OS04	177
Shin, Dongbin	초S-8-3	263
Shin, Hyun-Joon	초S-9-2	268
Shin, Jin-Yeong	초S-3-8	204
Shin, Kyung-Hun	초S-3-14	212
Shin, Min Ji	SM06	119
Shin, Mincheol	MD01	68
Shin, Minjeong	LM10	159
Shin, Minji	LM05	154
Shin, MinJi	LM07	156
Shin, Sooyong	초S-1-6	8
Shin, Sun-Yong	EM01	19

Name	Abstract ID	Page
Shin, Yooleemi	MD14	84
Shin, Yooleemi	초S-6-6	248
Simensen, Haakon Thømt	초S-6-1	243
Son, Hyunsol	SM20	134
Son, Hyunsol	SM21	135
Son, Jong Wan	LM13	163
Son, Young-Guk	LM02	151
Son, Young-Woo	초S-8-1	261
Son, Young-Woo	초S-9-2	268
Song, Bo-Kyoung	초S-10-1	295
Song, Cheng	초S-2-4	185
Song, Jaejung	LM06	155
Song, Jonghyun	QM04	149
Song, Moojune	MD05	72
Sousa, Duarte Pereira de	초S-2-6	188
Stashkevich, Andrey	SS17	52
Stiles, Mark	초S-2-2	183
Suh, Su Jeong	SM14	127
Sun, Gwang-Min	MM05	32
Sun, Gwang-Min	초S-7-5	255
Sur, Jung Chul	초S-7-3	253
Thi, Trinh Nguyen	LM16	166
Tran, Bao Xuan	초O-1-3	279
Tran, N.	SM11	124
Tuvshin, Dorjsuren	PM20	113
Uhm, Young Rang	MM05	32
Uhm, Young Rang	초S-7-5	255
Uhm, Young Rang	초S-7-6	256
Van, Phuoc Cao	LM16	166
Van, Phuoc Cao	초S-6-6	248
Vomir, Mircea	초S-6-6	248
Wang, Jian-Ping	초S-2-6	188
Wang, Kaiyou	초S-2-7	189
Wolf, Christoph	LM03	152
Won, C.	초O-1-9	288
Won, Woon-Jae	SS08	42
Won, Woon-Jae	SS15	50
Xue, Fei	초S-2-2	183
Xue, Fei	초S-2-6	188
Yang, Byung Il	초S-10-1	295
Yang, Heejun	초S-9-4	270
Yang, Hyunsoo	초S-2-4	185
Yang, Jingyu	초S-10-2	297
Yang, Jiseok	MD01	68
Yang, Sangsun	SM15	128
Yang, Sangsun	초O-1-8	286
Yang, Seungmo	MD05	72
Yang, Seungmo	초O-1-3	279

Name	Abstract ID	Page
Yang, Yang	PM06	95
Yang, Yang	PM07	96
Yang, Yang	PM09	99
Yi, Seonghoon	SM05	118
Yim, Sung-Dae	MM03	28
Yim, Sung-Dae	MM04	30
Yoo, Jae-Gyeong	PM05	93
Yoo, Jung-Woo	OS02	174
Yoo, Jung-Woo	초S-9-7	273
Yoo, Sang-Im	PM14	106
Yoo, Sang-Im	PM15	107
Yoo, Sang-Im	SM07	120
Yoon, Chansoo	LM10	159
Yoon, H. G.	초O-1-9	288
Yoon, Jaesung	MD02	69
Yoon, Ji Hyeon	초S-7-6	256
Yoon, Sangwon	LM03	152
Yoon, Seok In	SS25	63
Yoon, Seungha	LM01	150
Yoon, Seungha	SD02	168
Yoon, Seungha	SM04	117
Yoon, Seung-Young	초S-3-8	204
You, Chun-Yeol	MD03	70
You, Chun-Yeol	MD04	71
You, Chun-Yeol	MD10	78
You, Chun-Yeol	MD12	81
You, Chun-Yeol	SS09	43
You, Chun-Yeol	SS10	45
You, Chun-Yeol	SS22	59
You, Chun-Yeol	초S-1-4	6
You, Chun-Yeol	초S-2-9	191
You, Jin-Young	PM01	89
You, Mujin	MD05	72
Yu, Changho	SD03	169
Yu, Jisoo	SS28	67
Yu, Young-Sang	SM08	121
Yukiko, Takahashi	LM12	162
Zhou, Tian Hong	PM09	99
Zhou, Tianhong	PM10	101
Zhou, Xiaofeng	초S-2-4	185
강윤식	초S-7-2	252
구본옥	SM17	130
권영태	SM17	130
권영태	초S-3-1	195
권해웅	PM04	92
김갑진	O-1	11
김대원	초S-5-7	238
김대유	SM13	126

Name	Abstract ID	Page
김동영	LM09	158
김동영	초S-5-1	231
김동환	PM13	105
김동환	초S-3-3	197
김미진	초S-1-2	4
김부안	PM04	92
김상우	SM10	123
김상우	SM19	133
김상욱	OS05	178
김석환	초S-3-4	198
김성기	초S-1-2	4
김성민	초S-7-2	252
김성훈	OS01	173
김양도	PM02	90
김예래	SM09	122
김용진	초S-3-1	195
김은애	초S-5-3	233
김인호	OS05	178
김재민	초S-5-2	232
김철기	초S-1-2	4
김철성	MM01	24
김태훈	PM02	90
김태훈	초S-3-1	195
김형욱	초S-3-4	198
김혜란	SM17	130
나현민	PM13	105
노태성	PM02	90
류권상	초S-5-3	233
박구곤	초S-7-2	252
박덕근	초S-5-2	232
박민로	초S-3-12	209
박봉태	SM13	126
박석희	초S-7-2	252
박종민	SM17	130
박종민	초S-5-7	238
박진철	초S-3-12	209
박현욱	초S-7-2	252
배기웅	초S-5-4	234
배석	PM13	105
백재성	MM01	24
서호건	초S-5-2	232
손대락	초S-5-3	233
손성우	PM04	92
송원일	OS01	173
송창빈	OS05	178
신선용	초S-3-12	209
심인보	MM01	24
안종빈	PM12	104

Name	Abstract ID	Page
안종빈	초S-3-7	203
안지훈	SM09	122
안지훈	SM13	126
양상선	SM17	130
양상선	초S-3-1	195
양창섭	초S-5-4	234
오선종	초S-1-2	4
우승희	초S-7-2	252
우혁준	SM13	126
우혁준	SM19	133
웬 티 꾸인 안	TC09	144
유성초	SM10	123
윤명환	초S-3-10	207
윤석수	초S-5-1	231
윤석수	LM09	158
이기택	초S-3-10	207
이민영	SM09	122
이민영	SM10	123
이민영	SM19	133
이보람	초S-1-1	3
이보연	초S-1-2	4
이보화	SM10	123
이보화	SM09	122
이보화	SM13	126
이보화	SM19	133
이상규	초S-5-4	234
이상석	초S-1-1	3
이수경	초S-3-12	209
이은직	초S-7-2	252
이정구	PM02	90
이정구	PM04	92
이정구	초S-3-1	195
이정우	SM17	130
이정종	초S-3-10	207
이준규	TC09	144
이진이	초S-5-2	232
이철희	PM13	105
이현숙	초S-1-1	3
이훈기	초S-3-16	215
이희성	초S-5-7	238
임명섭	초S-3-12	209
임성대	초S-7-2	252
임성현	TC09	144
임현석	PM13	105
장민선	SM17	130
정영도	초S-1-2	4
정우현	SM10	123
정재원	SM17	130

Name	Abstract ID	Page
정재원	초S-3-1	195
정현주	초S-5-4	234
조영식	초S-3-4	198
조준호	초S-5-7	238
지동민	OS01	173
차희령	PM02	90
차희령	초S-3-1	195
최상현	초S-1-1	3
최유경	초S-1-1	3

Name	Abstract ID	Page
최장영	초S-3-16	215
최재영	PM04	92
최판규	PM12	104
최판규	초S-3-7	203
호 후인 티	TC09	144
홍순철	TC09	144
황병봉	초S-5-7	238
황진성	PM12	104
황진성	초S-3-7	203



Digests of the 2021 KMS Summer Conference
The Korean Magnetics Society
사단법인 한국자기학회

2021년 하계학술대회 논문개요집

제 31권 1호

(06130) 서울특별시 강남구 테헤란로 7길 22(역삼동635-4) 한국과학기술회관 신관 905호

TEL. (02)3452-7363, **FAX.** (02)3452-7364

E-mail. office@magnetics.or.kr, **Home-page.** www.magnetics.or.kr